Mitochondrial dynamics in the radiation response of cancer cells

by

Michelle Parker

PRKMIC010

SUBMITTED TO THE UNIVERSITY OF CAPE TOWN
In fulfilment of the requirements for the degree

DOCTOR OF PHILOSOPHY
(Radiotherapy)

Faculty of Health Sciences

UNIVERSITY OF CAPE TOWN

August 2017

Dedicated to those who
have battled a giant

DECLARATION

I, *Michelle Parker*, hereby declare that the work on which this dissertation/thesis is based is my original work (except where acknowledgements indicate otherwise) and that neither the whole work nor any part of it has been, is being, or is to be submitted for another degree in this or any other university.

I empower the university to reproduce for the purpose of research either the whole or any portion of the contents in any manner whatsoever.

Signature: Signed by candidate

Date: 11 August 2017

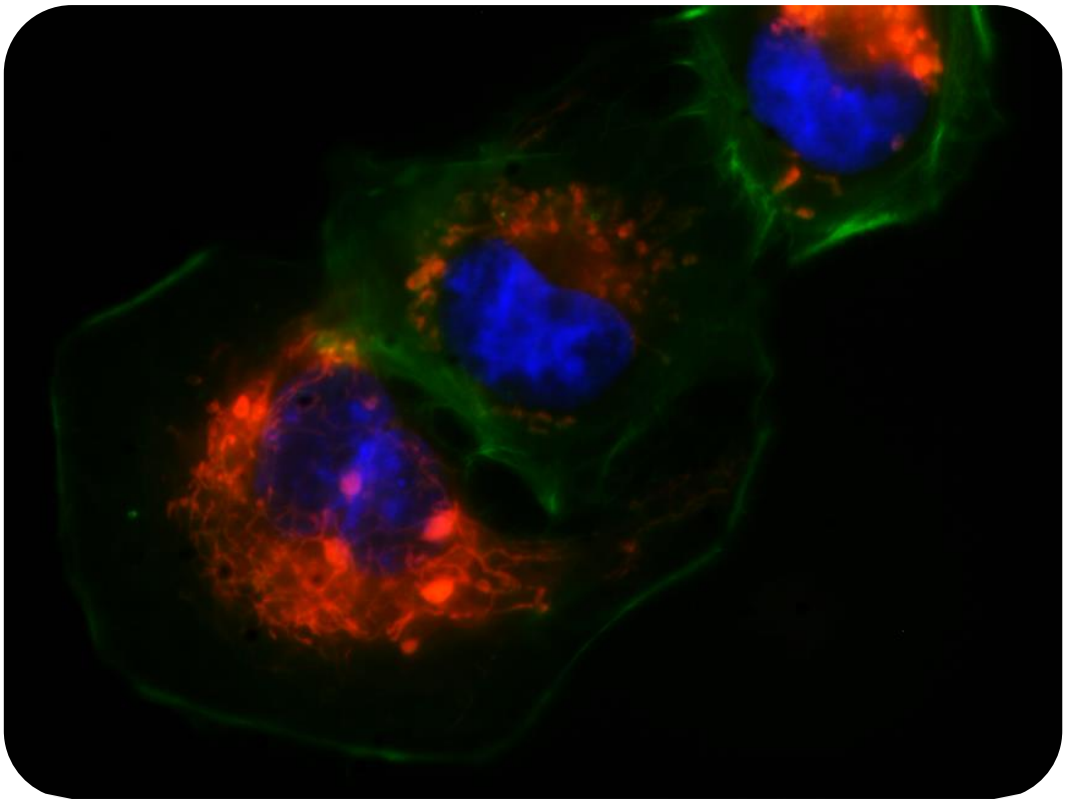

Mitochondrial localisation in A549 cells (MitoTracker® Red).
Nuclei and cytoskeleton are shown in blue and green, respectively.
(from the present work)

ACKNOWLEDGEMENTS

I would like to acknowledge Alistair Hunter for supervision of this project. His guidance, wisdom and enduring patience is greatly appreciated. Thank you for making this work possible.

I would like to acknowledge Michael Renan for his encouragement and the endless supply of biscuits to boost energy levels. Thank you for the advice and helpful comments on my dissertation.

I would like to acknowledge Andre Hendrikse for help with the experimental aspects of my project and Elijah Dyani for his effort to ensure that the lab is stocked with liquid N_2 and sterilised supplies.

A special thank you to my colleagues at UCT and GSH for support, as well as, institutions and individuals who have assisted with experimental advice and equipment.

In particular, I would like to thank:

- The Division of Exercise Science and Sports Medicine, Department of Human Biology, UCT and Gerald Maarman for assistance with polarographic measurements.
- The UCT flow cytometry core facility and Ronnie Dreyer for assistance with flow cytometry.
- iThemba LABS and Philip Beukes for assistance with metaphase analysis.
- The UCT Lennox Eales Porphyria laboratory and Division of Human Genetics for assistance with protein isolation and analysis.
- The UCT Confocal and Light Microscope Imaging Facility for imaging of mitochondria

I acknowledge crucial financial support received including;

- ✧ The German Academic Exchange Service (DAAD)
- ✧ National Research Foundation (NRF)
- ✧ Medical Research Council (MRC)
- ✧ University of Cape Town (UCT)
- ✧ Vlaamse Interuniversitaire Raad (VLIR) and Ithemba LABS
- ✧ Department of Radiation Medicine and Radiation Oncology Division GSH

I would especially like to thank friends and family who have been my support in so many ways and have held up my arms in prayer; Janet and Ian Hardie, Fiona McCutcheon, Kevin Boyd, Rosalie and Julian Laughton, Julie and Barry Coltham, Hugh and Heather James, Anne Corrigall, Alet Prinsloo, Alvera Vorster, Janet Roodman and all the family and Wesley, Maureen and Sharon Parker, my mom, dad and sister. And most importantly;

I owe a huge debt of gratitude to my Lord and Saviour,

Jesus Christ; when I am weak He is strong.

TABLE OF CONTENTS

LIST OF TABLES

LIST OF FIGURES

LIST OF SUPPLIERS

Atomic Energy of Canada Ltd, Ottawa, Canada

BD Biosciences, Franklin Lakes, NJ, USA

BDH Laboratory supplies, Poole, England UK

Canon Inc. Tokyo, Japan

Carl Zeiss, Göttingen, Germany

Difco Laboratories, Michigan, USA

European Collection of Authenticated Cell Cultures, Porton Down, Salisbury, UK

Fisher Scientific, Pittsburgh, PA, USA

FMH Instruments, Labotec, Midrand, SA

Gibco, Massachusetts, USA

GraphPad Software, Inc. San Diego, CA, USA

Greiner Bio-One GmbH, Frickenhausen, Germany

Highveld Biological, Johannesburg, SA

Lasec, Cape Town, SA

Martin Microscope Company, Easley, USA

Merck, NJ, USA

Metasystems Group Inc., Watertown, MA

Microsoft, Redmond, WA, USA

Molecular Probes® Inc, Invitrogen, Carlsbad, CA, USA

Motic Deutschland GmbH, Wetzlar, Germany

Olympus, Shinjuku-ku, Tokyo, Japan

OROBOROS Instruments Corp. Innsbruck, Austria

Santa-Cruz Biotechnology, Dallas, TX, USA

Sigma-Aldrich, St. Louis, Mo, USA

Vector Laboratories Inc., Burlingame, CA, USA

Verity Software House, Topsham ME, USA

Wild, Heerbrugg, Switzerland

ABBREVIATIONS AND SYMBOLS

Abbreviations

α-TOS: alpha-tocopheryl succinate

AB: antibiotics

ADP: adenosine diphosphate

AIF: apoptosis initiating factor

AKT: protein kinase B

AMP: adenosine monophosphate

AMPK: AMP-activated protein kinase

APC: anaphase promoting complex

ATM: ataxia telangiectasia mutated

ATP: adenosine triphosphate

ATR: ataxia telangiectasia and rad3-related

BER: base excision repair

bp: base pairs

BSA: Bovine serum albumin

BTIC: brain tumour initiating cell

CCD: charge coupled device

Cdc: cell division cyclin

Cdk: cyclin-dependent kinase

cGy: centigray

Chk: checkpoint protein

CO_2: carbon dioxide

CT: computed tomography

D: dose

DAPI: 4',6-diamidino-2-phenylindole

ddH_2O: double-distilled water

$DiOC_6$: 3,3'-dihexyloxacarbocyanine Iodide

DMEM: Dulbecco's Modified Eagle Medium

DMSO: dimethyl sulfoxide

DNA: deoxyribonucleic acid

DPP: digital photo professional

DRP1: dynamin-related protein 1

DSB: double-strand breaks

dUTP: deoxyuridine triphosphate

E': maximal O_2 consumption (ETS)

E_{abs}: Absolute maximal respiratory capacity

ECACC: European Collection of Animal Cell Cultures

ER: endoplasmic reticulum

ETC: electron transport chain

ETS: electron transport system

F-I8 FDG: 2-[^{I8}F] fluoro-2-deoxy-D glucose

$FADH_2$: flavin adenine dinucleotide (reduced)

FCCP: carbonyl cyanide-4-(trifluoromethoxy) phenylhydrazone

FCR: flux control ratio

FCS: fetal calf serum

FITC: fluorescein isothiocyanate

FRAP: fluorescence recovery after photobleaching

GTP: guanine triphosphate

Gy: Gray

HIF-1: hypoxia-inducible factor 1

HR: homologous recombination

ICGEB: International Centre for Genetic Engineering and Biotechnology

IMM: Inner mitochondrial membrane

ISO: International Standards Organization

JC-1: 5,5',6,6'-tetrachloro-1,1',3,3'-tetraethylbenzimidazolylcarbocyanine iodide

kV: kilovolt

L': phosphorylation-independent respiration (LEAK)

L_{abs}: Absolute phosphorylation-independent respiration

LET: linear energy transfer

LQ: linear quadratic

LSCM: laser scanning confocal microscopy

MAPK: mitogen-activated protein kinase

MCC: mitotic checkpoint complex

Mdivi-1: mitochondrial division inhibitor 1

MDM2: mouse double minute 2 homolog

MEF: mouse embryonic fibroblasts

MeV: megaelectron volt

MFN1 and 2: mitofusins 1 and 2

MN: micronuclei

MNNG: N-methyl-N'-nitro-N-nitrosoguanidine

MnSOD: manganese superoxide dismutase

MOMP: mitochondrial outer membrane permeabilisation

MPF: mitosis promoting factor

mPTP: mitochondrial permeability transition pore

mtDNA: mitochondrial DNA

MTT: methyl-thiazolyl-tetrazolium

NADH: nicotinamide adenine dinucleotide reduced

NER: nucleotide excision repair

NHEJ (alt-NHEJ): non-homologous end-joining (alternative-NHEJ)

NOX: NAD(P)H oxidases

O_2: oxygen

OCR: O_2 consumption rate

OECD: Organisation for Economic Co-operation and Development

OMM: outer mitochondrial membrane

OPA1: optic atrophy 1

OXPHOS: oxidative phosphorylation

p-H3: phospho-histone H3 staining

PARP: poly(ADP-ribose) polymerase

PCP: phosphorylation control protocol

PBS: phosphate buffered saline

PDH: pyruvate dehydrogenase

PDK: pyruvate dehydrogenase kinase

PE: plating efficiency

PET: positron emission tomography

PI: propidium iodide

PLD: potentially lethal damage

r: linear correlation coefficient

r^2: coefficient of determination

R': physiological, cellular respiration rate (ROUTINE)

R_{abs}: Absolute total oxygen consumption

RCF: relative centrifugal force

RCR: respiratory control ratio

Redox: reduction-oxidation

RFP: red fluorescent protein

Rho0: mtDNA-depleted

Rho+: mtDNA-containing

ROI: region of interest

ROS: reactive oxygen species

ROX: Residual (non-mitochondrial) respiration

RPMI: Roswell Park Memorial Institute

rRNA: ribosomal ribonucleic acid

S: surviving fraction

SAC: spindle assembly checkpoint

SAE: small airway epithelial

SD: standard deviation

SEM: standard error of the mean

SF2/SF4: surviving fraction at 2/4 Gy

siRNA: small interfering RNA

SLD: sub-lethal damage

SNP: single nucleotide polymorphism

SOD: superoxide dismutase

SSD: source to surface distance

STS: staurosporine

tiff: tagged image file format

TMRM/TMRE: tetramethylrhodamine methyl/ethyl ester

TUNEL: terminal deoxy transferase transferase-mediated dUTP nick end labelling

UCP2: uncoupling protein-2

UCR: uncoupling control ratio

UCT: University of Cape Town

UV: ultraviolet

VSMC: vascular smooth muscle cell

Symbols

^{60}Co: 60-Cobalt

α: alpha coefficient from LQ model

β: beta coefficient from LQ model

D_{10}: dose required to give a surviving fraction of 0.1

$\bar{D}$: mean inactivation dose

ΔΨm: mitochondrial membrane potential

γ: gamma

γ-H2AX: phosphorylated Histone 2AX

ABSTRACT

Mitochondria are involved in the regulation of key cellular processes that determine the response of cells to damage. Mitochondrial fission and fusion are associated with cell cycle regulation, apoptosis, cellular bioenergetics and redox status, which contribute to cellular homeostasis and damage response. The study aimed to describe and correlate cancer cell mitochondrial features and inherent radiosensitivity, and to determine the effect of modulation of mitochondrial dynamics on radiation response using a fission inhibitor, Mdivi-1.

Methods: Mitochondrial status in a number of cancer cell lines was characterised by assessment of mitochondrial morphology, respiration and membrane potential using MitoTracker® Red staining, respirometry and JC-1 ratiometric staining, respectively. Correlations with radiation sensitivity were performed. Radiation- and Mdivi-1-induced changes in mitochondrial morphology were also examined. Responses to various schedules of radiation and Mdivi-1 treatment were assessed using clonogenic survival. Microscopy was used to quantify apoptosis, micronuclei and mitotic features, while cell cycle dynamics were analysed using flow cytometry.

Results: Notably, modulation of mitochondrial fission using Mdivi-1 significantly increased radiation response in A549 cancer cells. Mdivi-1 reduced fragmentation, increased membrane potential and induced cytotoxicity, cytogenetic damage, apoptosis and G2/M cell cycle arrest. However, with the exception of survival, sub-additive responses were consistently observed when Mdivi-1 was combined with radiation. Sub-lethal damage repair was unaffected by Mdivi-1. Characterisation of cancer cell lines revealed inherent diversity in radiation response and mitochondrial morphology, membrane potential and respiration, and several correlations were identified.

Discussion and conclusions: Inhibition of mitochondrial fission was shown for the first time to enhance radiosensitivity in cancer cells, and to induce cytotoxicity. Mitochondrial modulators may therefore have therapeutic application. However, the sub-additive responses observed with Mdivi-1-radiation interactions suggest that optimisation of treatment scheduling may be important. The Mdivi-1-induced mitotic arrest may, in part, be responsible for the observed radiosensitisation, as cells accumulate in a radiosensitive cell cycle phase. In addition, the finding that Mdivi-1 treatment induced micronuclei, suggested that the radiosensitisation may result from the interaction of cytogenetic damage induced by each agent. Overall, mitochondrial dynamics and the modulation thereof appear to significantly influence radiation response.

CHAPTER 1

INTRODUCTION

The ability of cells to respond to radiation damage is a key determinant of radiotherapy outcome and may be influenced by mitochondrial function. A variety of factors including the extent of damage incurred, repair capacity, apoptosis induction and cell cycle checkpoint integrity determine radiation response. In addition, cell signalling and the ability to manage oxidative stress are important. Mitochondrial dynamics are regulated according to the conditions and needs of the cell and serve an integral function in cellular physiology and damage response. Therapeutic modulation of basic aspects of cellular function has the potential to increase radiation sensitivity of tumours and thereby enhance the efficacy of radiotherapy. While current radiotherapeutic strategies are partly effective, many tumours are resistant to treatment. It is therefore important to develop approaches that identify novel cellular targets and that incorporate the application of new anti-cancer agents, radiosensitisers and potential normal tissue radioprotectors.

Current treatments aim to induce effects on DNA, interfere with spindle formation or target signalling pathways that are primarily associated with cell growth and survival. Since mitochondria are involved in the regulation of many cellular processes that determine the response of cells to damage, they may be considered rational candidates for therapeutic-targeting. Mitochondrial dysfunction is frequently observed in tumours and has been proposed as a factor determining treatment outcome[1-4]. In addition, a number of agents have recently been identified that disrupt mitochondrial function[5-8]. Aspects of mitochondrial function that may be targeted include apoptotic mechanisms[9], mitochondrial metabolism[10], redox status[11], mitochondrial membrane homeostasis[12] and mitochondrial DNA[13].

Mitochondrial number, size, localisation and content, described collectively as *mitochondrial dynamics*, are in constant flux. These dynamic processes are often reflected in the mitochondrial morphology and may influence functional aspects including mitochondrial membrane potential and respiration. Mitochondrial morphology is largely determined by fission and fusion processes, which have been associated with cellular homeostasis and damage response. The net effects of fission and fusion contribute to many aspects of cellular function, including cell cycle regulation, apoptosis, cellular bioenergetics and redox status.

Increased mitochondrial fusion has been shown to inhibit drug-induced apoptosis[14-16], a process frequently associated with mitochondrial fission[17-20]. Such involvement in cell death processes suggests that a highly fused mitochondrial network may be protective against radiation-induced apoptosis. However, inhibition of fission has also been shown to induce cytotoxicity in cancer cells[21-24] and enhance the effects of certain cytotoxic agents[23, 25, 26]. This paradox indicates that further elucidation is warranted.

In addition, functionally active mitochondria may be more efficient at inducing a stress response or initiating cell death processes. Furthermore, energy metabolism is frequently altered in cancer cells[27] and an increased dependence on glycolysis has been associated with radiation-resistance[28-30]. Functional and respiratory parameters of cancer cells may correlate with radiation responsiveness. However, the effects of inherent mitochondrial status or modulation of mitochondrial fission and fusion processes on radiation response have not been established. Agents that alter mitochondrial function, such as Metformin, have been associated with increased radiotherapy efficiency[2] and thus are of great interest as clinical adjuncts. The current work represents a novel approach that elucidates and exploits mitochondrial status, and that may hold potential for significant clinical benefit.

In this study, it was proposed that mitochondrial status may be associated with radiation sensitivity and that modulation of mitochondrial dynamics may alter radiation response in cancer cells. While this chapter provides a brief introduction to the thesis, the following two chapters will provide a review of the relevant literature and a presentation of the study hypotheses and aims, respectively. Experimental work is described in Chapters 4, 5 and 6. Chapter 4 describes the inherent status of mitochondria in relation to the intrinsic radiation responsiveness of cancer cells. Chapter 5 addresses the effect of modulation of mitochondrial fission, using the inhibitor Mdivi-1, on radiation response. Chapter 6 details the cellular effects of Mdivi-1 that may be related to altered radiosensitivity.
A brief final discussion of the overall findings is presented in Chapter 7.

CHAPTER 2

LITERATURE REVIEW

Ionising radiation is an important modality in cancer therapy with more than 50 % of cancer patients receiving radiotherapy during their treatment[31-34]. Radiotherapy is unique in that it exploits both physical radiation dosimetric and radiobiological differentials for therapeutic advantage. However, further improvements and optimisation are required. While improvements in physical dose delivery appear to be reaching saturation, there is potential for further radiobiological improvements.

A new and relatively un-researched area involves the role of mitochondrial dynamics in the response of cells to cancer therapy. Furthermore, the involvement of mitochondria in several key cellular processes suggests that they may be important in the modulation of radiation response. An understanding of the role of mitochondrial dynamics in radiation response has the potential to lead to the development of new treatment paradigms.

This chapter provides an overview of the roles of mitochondria in cancer and radiation therapy. Radiation effects on cells and mitochondria, the role of mitochondria in response to radiation-induced damage, mitochondrial physiology and function in tumour cells and modulation of mitochondrial dynamics and cancer therapy are discussed.

2.1. Mitochondria in radiation research

Established biological targets of radiation include chromosomal DNA, proteins and lipids. In the therapeutic dose range, the nucleus is considered to be a primary target although membrane damage may also elicit cell death signalling[35, 36].

Mitochondria may be subjected to radiation energy depositions that may influence both their structure and function. While the effect of radiation on mitochondria was not the focus of this study, discussion of potential radiation-induced mitochondrial sequelae may give insight into how modulation of mitochondrial status could influence radiation response.

2.1.1. Could mitochondria be targets of radiation?

Mitochondrial dysfunction incurred as a consequence of radiation may be a significant factor in the response of cells to therapy. An early study proposed that *Abraxas grossulariata* mitochondria were more radiosensitive than the nucleus as cytoplasmic constituents appeared to be preferentially damaged[37]. The relatively higher level of radiation-induced damage observed in mitochondrial DNA (mtDNA) compared to nuclear DNA, in later studies[38, 39], is consistent with such a finding. More recent studies report changes in mitochondrial function, gene expression and ATP production following irradiation, which support a role for mitochondria in the response to damage[40-42]. Microbeam irradiation of cytoplasmic components, excluding irradiation of the nucleus, resulted in mitochondrial fragmentation, reduced respiratory chain activity and increased autophagy including mitophagy[43, 44].

While not all studies have found effects on mitochondria after irradiation, a large number of studies spanning almost 100 years have demonstrated changes[37, 42-63]. Such studies have reported a range of structural changes to both mitochondria and cristae, as well as altered mitochondrial biogenesis after irradiation. Swollen mitochondria and changes in mass and number have frequently been described. Mitochondrial changes, including functional defects, are variable and may be apparent hours to days after irradiation. Overall, there appears to be significant variation in radiation-induced mitochondrial damage among cell and tissue types[64, 65].

Direct radiation damage to mtDNA has been reported[66-68], including mtDNA point mutations[55] and induction of the *Common deletion* of 4977bp[69], which disrupts complex I, IV and V of the electron transport chain, as well as, structural changes to mtDNA (‘*supercoiling formation changes’*)[70].

2.2. Cellular interactions with radiation

A complex array of biological processes form the radiation damage response, which may involve cell death, cell cycle regulation, DNA repair and cell signalling. It is important to understand such cellular interactions to identify the scope for mitochondrial involvement.

Cellular damage after irradiation arises from both direct and indirect interactions[71, 72]. Indirect damage results from the production of free radicals mostly from interactions between radiation and water within the cell and is the predominant mode of action with sparsely ionising radiation.

While the representation of direct and indirect effects is commonly illustrated using nuclear DNA, an important radiation target, mitochondrial DNA would be similarly affected, as shown in Figure 2.1.

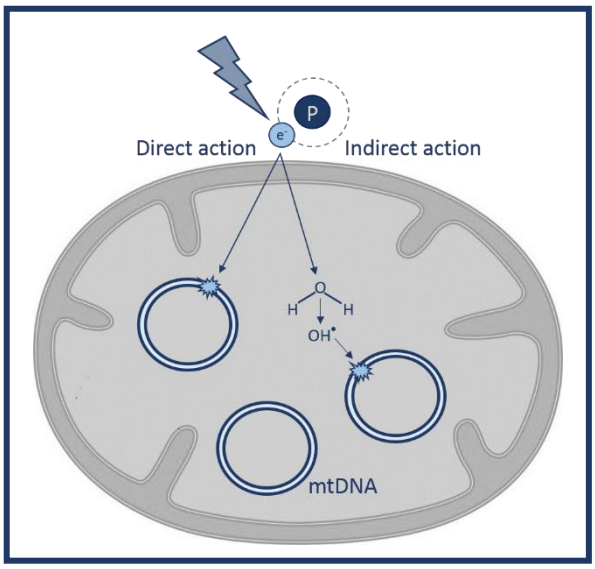

Figure 2.1. Schematic representation of the direct and indirect effects of radiation on mitochondrial DNA (own diagram).

Certain cellular sites will receive more-compound damage. Clustered damage, which includes the formation of multiple different lesions including strand breaks, base oxidation and abasic sites within a few helical turns of DNA, may be induced by a track of ionising radiation[73, 74]. Such complex lesions may constitute critical DNA damage that can lead to double-strand breaks[75]. The consequence of mtDNA strand breaks after irradiation on cellular integrity has not been fully investigated.

2.2.1. Radiation targets

DNA double-strand breaks are considered to be the primary genotoxic lesions after irradiation. In addition, radiation causes single strand breaks, base and sugar damage, DNA-DNA crosslinks[76, 77], as well as cross-links with proteins and other cellular components [78, 79]. Other targets include lipids, membranes and metabolites, which may undergo oxidative damage.

Aberrations, evident as changes in chromosome structure, number or morphology occur as a consequence of breaking and re-joining of chromosomal DNA[80, 81]. Chromosome aberrations result in unbalanced segregation of chromosomes to daughter cells or mitotic catastrophe. The interaction of two unrepaired DNA double strand breaks may induce serious cellular consequences, however, if repaired, double strand breaks may not constitute critical lesions[81]. Lethal chromosome aberrations include dicentrics, fragments, large deletions and ring chromosomes[71]. In contrast, cells can tolerate milder aberrations such as aneuploidy, small deletions and minor reciprocal translocations[71, 82].

2.2.2. Cellular damage response

DNA damage initiates a damage response process that consists of damage recognition and signalling (Figure 2.2). This response includes the activation of cell cycle checkpoints, as well as the initiation of repair mechanisms, cell death and processes that allow damage tolerance[83, 84]. Thus, the efficiency of the DNA damage response determines the fate of damaged cells. Excessive damage or ineffective repair may result in apoptosis or senescence[85].

Mitochondria are integral to the damage response in that they have roles in the intrinsic apoptosis pathway[86, 87] and have been implicated in the regulation of cell cycle progression[88, 89].

Mitochondria also provide reactive oxygen species (ROS) for signalling[90] and are a source of cellular energy that indirectly drives cellular processes[91]. Cell death after irradiation, while largely as a result of direct nuclear damage may arise partly through indirect damage from ROS generated by mitochondrial dysfunction following irradiation[92, 93].

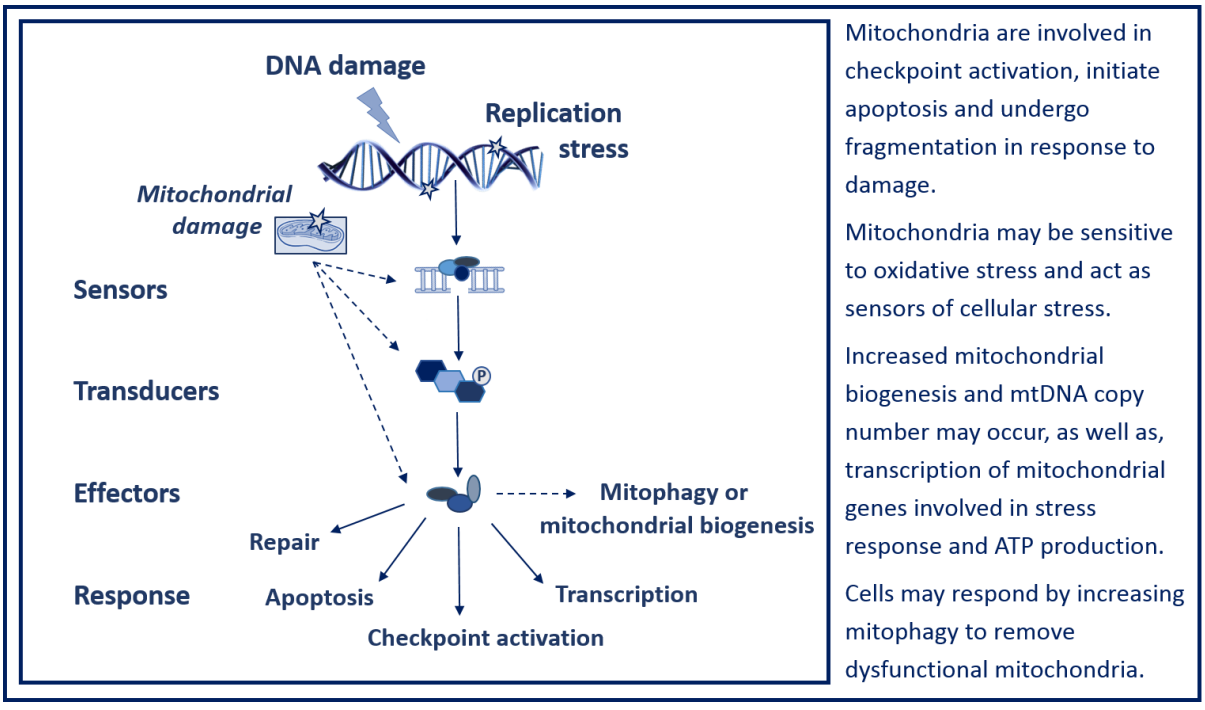

Figure 2.2. Schematic representation of the DNA damage response pathway (own diagram). Damage to mtDNA may elicit similar responses as described in the accompanying narrative.

Cellular responses to radiation-induced damage are characterised by successive stages that include detection of the damage by sensor molecules, transduction of the signal and finally execution of the response (Figure 2.2). Multiple DNA damage response proteins are involved in signal transduction and repair[85], however, only a selection of role players will be discussed here.

After damage has occurred, cell cycle arrest may be induced to facilitate repair, the nature and extent of which is dependent on the cell cycle phase[94, 95]. In attempting mitosis, cells may succumb to mitotic catastrophe at division as a result of unrepaired damage. In addition, interphase death by apoptosis may occur[96].

2.2.3. Cell cycle arrest

Radiation-induced cell cycle arrest is critical to allow damaged cells time for repair and to prevent cell division or DNA replication while damage is present[97]. Whereas extended cell cycle arrest may increase time for repair and thus enhance survival, persistent radiation-induced damage may result in permanent arrest and cell senescence[98-100]. The cell cycle position at the time of irradiation partly determines the checkpoint at which cells may arrest. DNA maintenance checkpoints include the G1 and G2 checkpoints that prevent entry into S-phase and mitosis, respectively, and the intra S-phase checkpoint, which arrests cells that have entered S-phase (Figure 2.3). Modulation of mitochondrial dynamics may potentially affect cell cycle progression and thereby influence cell cycle arrest following irradiation.

2.2.3.1. G1 and G2 checkpoints

Activation of cell cycle arrest as part of the DNA damage response involves complex phosphorylation-dependent protein cascades that ultimately influence the individual cyclins responsible for cell cycle phase transition. Briefly, DNA damage activates sensor proteins, ATR and ATM kinases that phosphorylate Chk1 and Chk2 transducers[101, 102], respectively, leading to p53 phosphorylation and stabilisation[103, 104]. p53 activates p21, a cyclin-dependent kinase (Cdk) inhibitor[105], causing repression of the cyclin E-Cdk2 complex, which is necessary for G1-S transition[98, 106]. This results in a p53-dependent G1 checkpoint activation and arrest[107-109]. Similarly, p53 stabilisation and inactivation of the cyclin B-Cdk1 complex, by p21 or Cdc25C inhibition[101], activates the G2 checkpoint and prevents entry into mitosis[110, 111]. In addition, p53-independent arrest occurs via p-Chk1 and p-Chk2 leading to ubiquitination and degradation of Cdc25A[112, 113], a protein involved in activation of both the cyclin E-Cdk2 and the cyclin B-Cdk1 complexes[114, 115].

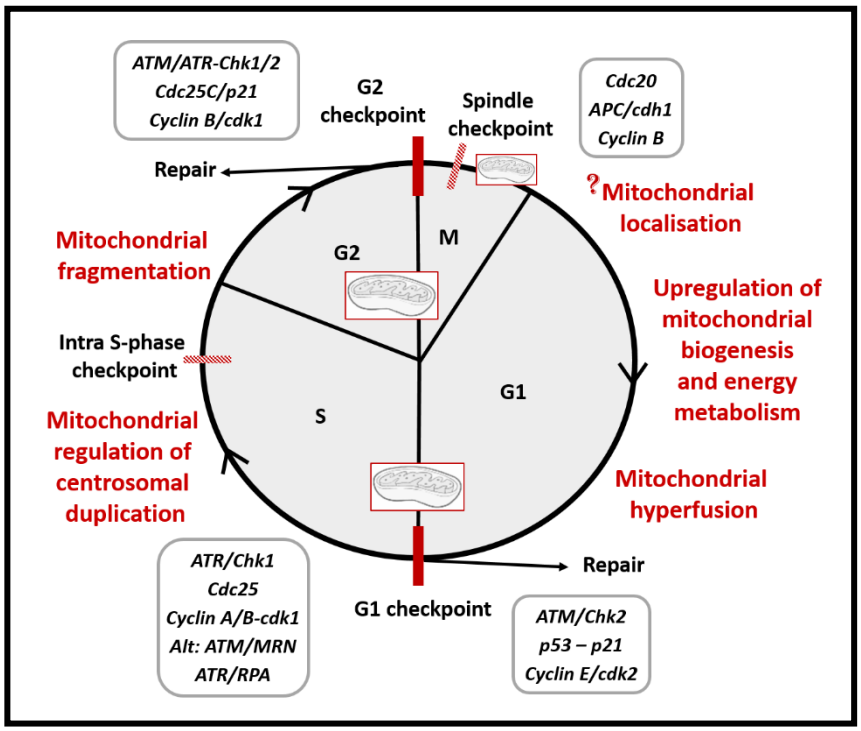

Figure 2.3. Cell cycle checkpoints with potential points of mitochondrial involvement in cell cycle progression.

2.2.3.2. S-phase checkpoints

An S-M checkpoint exists that is activated in response to replication stress and prevents mitosis in the presence of stalled replication forks[116]. In addition, an intra-S phase arrest caused by DNA strand breaks occurs and has been observed in cells exposed to ionising radiation[115, 117]. Arrest is activated by ATM or Chk2-mediated phosphorylation of Cdc25A and requires the Mre11 recombinational protein in humans[112, 118, 119]. The ATM–MDC1–MRN–SMC1 acts as an alternative pathway[120]. The intra-S phase checkpoint slows DNA replication rather than preventing cell cycle progression completely and residual damage invokes a G2-checkpoint[118]. Additional S-phase checkpoints, mediated by the ATR through the RPA complex, that may be induced by replication stress or incomplete replication[121-123] have also been distinguished from the intra-S phase arrest.

2.2.3.3. Spindle checkpoint

The spindle checkpoint guards the integrity of mitosis and is responsible for ensuring proper alignment of chromosomes prior to their separation in anaphase. It was first observed that cells in metaphase were prevented from entering anaphase if kinetochores were not properly positioned on the metaphase plate[124]. The presence of numerous DNA double-strand breaks during mitosis may elicit a strong mitotic arrest in response to lack of kinetochore attachment[125].

The spindle assembly checkpoint, which senses spindle position and integrity, is constitutively active, in contrast to other cell cycle checkpoints that become activated in response to damage. High Cdk activity is thus maintained but requires suppression for mitotic exit[126]. The spindle assembly checkpoint regulates mitosis by inhibition of cell division cyclin 20 (Cdc20), suppression of the anaphase promoting complex cyclosome (APC/C) and prevention of securin- and cyclin B degradation for cell cycle progression[127, 128]. Securin is an inhibitor of separase, an enzyme required for cleavage of the cohesion complex that holds two sister chromatids together while cyclin B degradation inactivates Cdk1 allowing mitotic exit[129]. APC/C, an E3 ubiquitin ligase, is inhibited by the mitotic checkpoint complex (MCC) that includes the MAD (*mitotic arrest deficient*) and Bub (*budding uninhibited by benzimidazole*) proteins, Aurora B and Cdc20 among others and is associated with the chromatid (kinetochore) cohesion complex[126, 130, 131]. Prolonged mitotic arrest frequently results in cell death, however, Cdc20 release from the MCC[132] or direct inhibition of Cdk1[133] may occur and result in mitotic slippage[126]. Mitotic slippage is suggested as a mitotic cell death avoidance mechanism and premature mitotic exit results in polyploidy.

2.2.4. Mitochondria and the cell cycle

Mitochondria are important in the cell's adaptive response to stress or damage[134, 135]. In particular, mitochondria regulate cellular ATP levels[136] and indirectly modulate cell cycle progression[137, 138] and apoptosis[139]. For example, in Drosophila, distinct mutations in respiratory chain complexes I and IV caused increased ROS and reduced ATP, respectively[140, 141]. ROS signalling in the mutant complex I clones induced activation of the G1/S checkpoint via upregulation of the cyclin E-Cdk2 inhibitor, Dacapo[141]. Reduced ATP was shown to activate AMP-activated protein kinase leading to activation of p53 and reduction in cyclin E with an associated G1/S arrest[140]. In addition, studies using respiratory chain inhibitors have provided evidence for a link between ATP levels and cell cycle arrest in malignant cells. For example, reduced ATP levels in HL-60 cells caused cell cycle arrest at both G1/S and G2/M[142].

As mitochondrial dysfunction was associated with cell cycle arrest, it is likely that there is some mitochondrial influence over cell cycle progression. Of note, the cyclin B-Cdk1 complex and mitochondrial matrix proteins have been shown to interact to upregulate respiration[143], thus satisfying energy requirements for G2/M transition. Cyclical regulation of OXPHOS throughout the cell cycle may also influence cell cycle progression and may be controlled by mitochondrial dynamics. Differences in ATP levels have been observed throughout the cell cycle.

An increase in ATP production was shown in cells at the G1/S boundary and was associated with mitochondrial hyperfusion[144]. ATP production was reduced in S-phase and was lowest in cells in mitosis, which is frequently associated with mitochondrial fragmentation. Furthermore, cyclin D1, which is increased in S-phase, has been shown to inhibit mitochondrial function and size[145] and repress nuclear respiratory factor 1[146], which results in reduced respiratory capacity. Thus, during S-phase and G2/M (reductive phases), cells rely mainly on glycolysis, which protects vulnerable, replicating DNA from damaging ROS produced by OXPHOS[147, 148]. In addition, mitochondrial protein import and mitochondrial membrane potential (ΔΨm) was lower in S-phase than in G1-phase in proliferating fibroblasts[149]. Another study, however, reported increasing ΔΨm from G1 to G2/M although they maintained that ΔΨm was not fully developed until mitosis[150].

Mitochondrial fission and fusion status show variation through the cell cycle (Figures 2.3 and 2.8). This will be described in more detail in subsequent sections that describe mechanisms of mitochondrial fusion and fission.

2.2.5. Is there a mitochondrial damage-induced checkpoint?

The concept of a mitochondrial damage checkpoint, termed a *mitocheckpoint*, was first proposed by Singh in 2004[92], whereby mitochondria signal changes in gene expression to repair damaged mitochondria. Detection of mtDNA damage is important as mitochondrial dysfunction has been found to lead to loss of nuclear DNA integrity after radiation exposure[151-153].

Similar to nuclear DNA damage, mtDNA damage has been shown to initiate cell cycle arrest and repair of mtDNA[138]. Drug-induced mtDNA damage was shown to result in an S-phase arrest in HeLa cells and was associated with an increase in Chk2 phosphorylation[138]. In addition, persistent mtDNA damage was shown to induce permanent arrest through the induction of p21[154].

G2/M checkpoint activation was suppressed in mtDNA depleted cells[155, 156] indicating that damage signalling from mtDNA rather than the loss of mitochondrial function per se may be required for checkpoint induction. While mtDNA damage may influence cell cycling, other studies have reported that mtDNA depletion had no effect on the cell cycle[157, 158].

Cancer cells are often characterised by mitochondrial dysfunction that influences cellular metabolism, which may impact on the way in which cancer cells sense and respond to damage. However, checkpoint-related mechanisms are frequently altered in cancer cells and thus certain cell cycle regulatory processes may be less active or absent[108, 159].

2.2.6. Repair of radiation-induced damage

Radiation induces pro-survival signalling pathways that include cell cycle arrest, suppression of apoptosis and repair[160]. DNA single- and double strand breaks activate the phosphatidylinositol 3-kinase-like protein kinases Ataxia Telangiectasia and Rad3-related protein (ATR) or ataxia telangiectasia mutated (ATM)[161, 162], respectively. ATR is frequently involved in repair of breaks that result from replication stress while ATM is more important in the context of DNA damaging agents including ionising radiation. ATM and ATR initiate signals that are transmitted by phosphorylation, sumoylation and ubiqitination of a variety of transducers and effectors [85, 163].

Phosphorylation and stabilisation of the key regulatory protein, p53[103] is an important step in the process that allows cell cycle arrest for repair. p53 phosphorylation prevents MDM2 binding[164] thereby blocking its degradation[165]. In addition, the poly(ADP-ribose) polymerase (PARP) proteins, PARP1 and 2 are activated by single and double-strand DNA breaks, respectively, and catalyse the addition of poly(ADP-ribose) chains on proteins to facilitate repair[166].

Auto phosphorylation and activation of ATM is facilitated by binding of the MRN complex to double-strand breaks with subsequent phosphorylation of chromatin-associated proteins[161, 167]. The histone H2AX, one of the first proteins marking a double-strand break, is called γ-H2AX when phosphorylated[168]. MDC1 amplifies H2AX phosphorylation and recruits other DNA damage response proteins that form foci, which can be detected by immunocytochemical staining[84, 169].

Repair of single strand DNA breaks occurs via either the nucleotide excision repair (NER) or base excision repair (BER) pathways that rely on copying information from a complementary template DNA strand[83]. However, more complex repair mechanisms are required for DNA double-strand breaks[170]. The two major pathways of DNA double-strand break repair are non-homologous end-joining (NHEJ) and homologous recombination (HR). Alternative-NHEJ (alt-NHEJ) and single strand annealing are two further repair pathways that have been identified for double-strand break repair[85]. The choice of pathway depends on the complexity of the double-strand break, the position in the cell cycle and the chromatin conformation.

HR makes use of a complementary sister chromatid for repair and is therefore only active during late S- and G2-phase once the DNA has been replicated[171]. NHEJ, which is active throughout the cell cycle, requires processing of the damaged ends of the strands prior to ligation. Binding of the Ku70/Ku80 heterodimer[172] facilitates recruitment of the core NHEJ complex[173] that includes, the XRCC4/DNA Ligase IV (X4LIG4) complex, as well as, DNA-dependent protein kinase catalytic subunit (DNA-PKcs) and XLF[83].

The DNA-dependent protein kinases are important for activation of end-processing nucleases while the XRCC4/LIG4 complex is responsible for the ligation reaction[85, 174]. NHEJ represents an error-prone type of DNA repair as a result of DNA strand end-processing. Alt-NHEJ involves PARP proteins that sense DNA double-strand breaks and serves as a backup for the NHEJ pathway[175]. Here, the MRN complex is recruited in an MDC1/γ-H2AX-independent manner[176] and LIG3/XRCC1-dependent DNA end ligation occurs.

In contrast, HR relies on the sister chromatid sequence and provides a more efficient type of repair. The MRN complex together with CtIP initiate a resection reaction that involves EXO1 and DNA2 nucleases and Sgs1/BLM helicase[85, 177]. In addition, BRCA1 in complex with CtIP can cause resection[178]. Synapsis involves homology searching and DNA strand invasion and D-loop formation that requires formation of the RAD51 nucleofilament[179]. The RPA-complex at resected ends facilitates binding of RAD51 and RAD52 proteins that are important for regulation of homologous cross-over and re-annealing of resected strands. Holliday junctions formed from cross-over events are resolved by the activity of GEN1 and SLX1/4 nucleases[85, 179].

2.2.7. Importance of repair in radiotherapy

Mechanisms of repair are relevant to radiotherapy, which is often delivered using multiple fractions or altered dose rates. Radiotherapy generally exploits the repair differentials between tumour and normal tissue for therapeutic advantage. Cancer cells frequently display aberrant signalling and repair pathways and may thus be less repair proficient[180, 181].

In addition to sub-lethal damage, which is repaired between fractions, the post-irradiation conditions are important and may determine the outcome of repair of potentially lethal damage. It is possible that modulation of mitochondrial dynamics that influence cellular damage response mechanisms may conceivably affect that ability of cells to repair.

2.2.8. Mitochondrial DNA repair

As mentioned previously, mitochondria may influence the cell cycle to facilitate repair of mtDNA damage[138]. Such repair is necessary, particularly as mtDNA is in close proximity to the site of ROS production and is therefore susceptible to oxidative damage[182, 183]. Mitochondria have mechanisms for BER[184], mismatch repair[185] and HR[186]. Recognition of base damage occurs by DNA glycosylases. Of note, p53 has been shown to translocate to mitochondria when ROS production is increased[187] and has 3'-5' exonuclease activity, which is able to excise oxidised bases[188].

Double-strand break repair has been described in mitochondria after treatment with a restriction enzyme, *ScaI*, and loss of the intervening mtDNA sequence suggested NHEJ repair[189]. Although mechanisms of HR have also been described for mitochondria[186], such repair may be restricted by limited contact between separate mtDNA molecules[183, 190].

2.2.9. Mitochondrial role in repair after irradiation

While the role for mitochondrial dynamics in radiation repair remains to be fully elucidated, other aspects of mitochondrial involvement in the ability of cells to repair damage have been suggested from a range of different studies. For example, a recent report described the translocation of Cdk1 to the mitochondria and subsequent increase in ATP production after irradiation. Knockdown of Cdk1 caused inhibition of post-irradiation repair likely as a result of inadequate ATP production[191]. Loss of a mitochondrial tumour suppressor protein, Fus1, which is regulated by oxidative stress was also shown to influence repair of radiation-induced damage. Fus1 knock-out in normal tissue resulted in premature release from cell cycle arrest, with early reduction in γ-H2AX in irradiated cells without sufficient time for repair resulting in increased radiation-induced apoptosis[192].

Mitochondrial function has been shown to be decreased in a number of radiosensitive cell lines that were thought to be repair deficient[193]. Mutations or deficiencies in mtDNA are also associated with reduced repair. The loss of mtDNA has been shown to downregulate HR repair protein BRCA2, leading to an increase in unrepaired DNA double-strand breaks and genomic instability[194]. Cell lines from ataxia telangiectasia patients, who have ATM gene mutations and associated DNA repair deficiency, have been observed to display mitochondrial dysfunction and oxidative stress[195]. Cells from patients with the mitochondrial diseases, Leigh syndrome and Leber's optic atrophy, showed differences in gene expression related to regulation of energy and response to DNA damage from ionising radiation. Mutant cells showed reduced induction of repair proteins and an increased expression of apoptosis-related genes suggesting that mitochondrial dysfunction may limit the ability of cells to repair damage and preferentially induce apoptosis[196]. The same authors showed previously, that both Leigh and Leber's cells were radiosensitive relative to normal cells with respect to the initial radiation damage. However, Leber's cells were able to repair more efficiently relative to Leigh's cells and ultimately displayed reduced radiation response[41]. Furthermore, work using Rho0 fibroblasts, which lack mtDNA, indicated that such cells were also more radioresistant with lower apoptosis rates than their normal counterparts[158].

2.2.10. Radiation-induced cell death

Initiation and execution of the DNA damage response ultimately results in cell survival, senescence or death. Cell death may occur as a result of certain critical damage in the absence of cell cycle arrest or failure of repair mechanisms. Necrosis[197], autophagy[198] and apoptosis[199], as well as other forms of programmed cell death, may be induced in response to damage. Autophagy, which is a normal degradation of cells to recycle cellular constituents, as well as being a form of programmed cell death, is relevant in the cellular radiation response and is receiving increased attention. Interestingly, there may be an interplay between autophagy and other types of cell death such as apoptosis[736].

The major form of cell death induced by radiation is mitotic cell death, which occurs as cells attempt division[71]. Cell death that is independent of mitosis, classically known as interphase death, may occur via apoptosis depending on the sensitivity of the cells to this mode of cell death[200]. In systems where apoptosis is the primary mode of cell death, apoptosis following irradiation has been described as, either *early* apoptosis, defined as apoptosis that occurs within 4 to 6 hours after irradiation and generally happens at doses below 5 Gy, or *secondary* apoptosis, which occurs after the first cell division, requires higher doses and may partly reflect reproductive cell death[201, 202]. In general, cells of haematological origin predominantly undergo early apoptosis while epithelial cells primarily undergo secondary apoptosis[201, 203]. Early and late radiation-induced apoptosis has also been described for high and low doses[203, 204]. Apoptosis in U937 cells, assessed by DNA fragmentation was shown to be significant only from 36 h after 5 Gy, while higher doses of 20 and 40 Gy elicited a significant response from 6 hours. Interestingly, the S-phase cells were found to be the most sensitive to radiation-induced apoptosis [205]. Cellular radiosensitivity has been associated with the induction of a high level of early apoptosis[71, 206].

Mitochondria play a central role in apoptosis induced by both the intrinsic and extrinsic pathways and apoptogenic factors reside in the intermembrane space. Bcl-2, Bcl-xl and Mcl1, among others, are anti-apoptotic proteins, able to inhibit mitochondrial outer membrane permeabilisation (MOMP) and are able to form heterodimers with apoptosis-initiating proteins[207]. Pro-apoptotic Bax and Bak, activated by BH3 only proteins, such as Bid, Bim, Noxa and Puma[207], mediate MOMP and release of cytochrome C[208], Smac (*second mitochondria-derived activator of apoptosis*)/DIABLO (*direct AIP-binding protein with low PI*) and Omi/HtrA2 (*high temperature requirement protein A2*) that leads to caspase activation through the intrinsic mechanism[209]. Initiator and executioner caspases exist that transduce a death signal and cleave diverse cellular substrates, respectively[210].

In the cytoplasm, cytochrome C interacts with Apaf-1, to form the apoptosome that facilitates recruitment and activation of procaspase 9[211], which then activates effector caspases 3, 6 and 7. Smac/DIABLO and Omi/HtrA2 function to neutralise the inhibitor of apoptosis proteins. The extrinsic apoptotic pathway involves binding of ligands, for example, Fas to a death receptor on the cell surface that activates initiator procaspase 8 leading to activation of other caspases[212].

An amplification loop exists between the extrinsic and intrinsic pathways via bid cleavage to enhance the apoptotic signal. In addition, release of apoptosis initiating factor and endonuclease G from the mitochondrial intermembrane space induces a caspase independent form of cell death that results in direct nuclear cleavage[213].

2.2.10.1. Mitochondrial dynamics and apoptosis

Evasion of apoptosis has been found to be associated with mitochondrial dysfunction[92] and mtDNA-depleted cells may be resistant to cell death[214]. Mitochondria are therefore important in the induction of apoptosis.

Mitochondrial fission, which will be described in detail later, has been shown to be associated with apoptosis[215-217]. Modulation of mitochondrial dynamics can influence MOMP through the interaction of DRP1, a fission protein, with Bax on the outer mitochondrial membrane[218, 219]. In addition, overexpression of fusion proteins, MFN1 and 2[19], and OPA1[220], that reside on the outer and inner mitochondrial membranes, respectively, inhibit MOMP. Both DRP1[221] and MFN1 and 2[222] have been found to interact with Bax[218] and OPA1 has been associated with release of cristae-bound cytochrome C[223, 224]. Thus, there appears to be a significant link between mitochondrial dynamics and apoptosis. Although radiation-induced apoptosis in cancer cells in culture has been well documented, the contribution of apoptosis to tumour cell kill *in vivo* varies considerably[71, 201]. In general, solid tumours are thought to be resistant to apoptosis[225]. Mitochondrial dysfunction in tumours may to some extent reflect apoptotic dysfunction.

2.3. Determination of cellular radiosensitivity

The response of cells to irradiation may be affected by the extent of the initial damage incurred, the capacity of cells to initiate a DNA damage response and repair[226]. Factors that determine the extent of critical biological damage include, the cell type[227], cell cycle phase[228], anti-oxidant status[229] and possibly metabolic status, among others. Many of the factors that influence radiation response may be influenced by mitochondrial status and cellular bioenergetic capacity. In addition, certain physical factors influence cellular radiosensitivity including dose rate, fractionation and radiation quality.

The initial damage incurred by the cell after irradiation reflects the inherent radiosensitivity[230, 231]. While the terms radiosensitivity and radiation responsiveness are often used interchangeably, it is strictly-speaking important to draw a distinction between them. Radiosensitivity depends on the inherent sensitivity of the cells, while radiation responsiveness is dependent on the net result of initial damage as well as repair.

2.3.1. *In vitro* radiobiological endpoints: Assays

In the present study, certain tumour cell lines were used to assess radiobiological endpoints, as well as factors determining radiation response. A brief discussion of these endpoints is included below.

Early studies suggested that cultured cells may reflect the radioresponsiveness of tumours[227, 232]. In one study, the radiosensitivity of 70 % of the 29 tumour-derived cell lines investigated was shown to be similar to that of normal fibroblasts[233]. The remaining 30 % of the cell lines from the same study derived from "radio-incurable" tumours, were inherently radioresistant. This suggests that tumour cell lines may reflect, to some extent, the inherent radioresponsiveness of a parent tumour. Intrinsic radiosensitivity may be a determinant of tumour cell response to radiotherapy[234].

A number of *in vitro* assays have been developed for quantifying the cellular effects of radiation, for example assessment of clonogenic cell survival, cell proliferation, genetic alterations and immunocytochemical markers.

For clonogenic assays, individual cells are assessed for their ability to form colonies after irradiation. Cell proliferation can be assessed using colorimetric MTT (methyl-thiazolyl-tetrazolium)-type assays, which assess cellular metabolic activity and depend on dehydrogenase -induced reduction of tetrazolium salts to formazan. Alternatively, direct quantification of cellular proliferation markers, such as Ki-67 and proliferating cell nuclear antigen can be undertaken. DNA damage may be assessed by the determination of γ-H2AX focus formation, chromosome aberrations, micronuclei and single cell gel electrophoresis (comet assay), amongst others. Apoptosis may be routinely assessed using a multitude of different techniques based on morphological or biochemical criteria. Necrosis is frequently assessed by the uptake of vital dyes such as trypan blue or propidium iodide, which can traverse compromised cell membranes. Cell cycle analysis is conducted using flow cytometry, immunocytochemical staining of histones and morphological quantification of the mitotic index.

2.3.1.1. Cell Survival

The clonogenic survival assay, introduced by Puck and Marcus (1956)[235], provides a measure of the reproductive integrity of cells after treatment and is a valuable tool for the assessment of radiation survival *in vitro* [236]. This technique is suited to studying the modulation of radiation effects including the influence of agents that modify mitochondrial dynamics. Survival assays are considered to be more informative than cellular proliferation assays, which can reflect cytostatic- in addition to cytotoxic responses.

The assay can be adapted for assessment of non-adherent cells, with the use of a gel matrix for colony formation. However, the assay requires up to 3 weeks depending on cell proliferation rate and relatively large numbers of cells to assess particularly toxic treatments.

The mechanistic Linear-quadratic (LQ) model of radiation interaction is commonly used to describe the dose response (Figure 2.4)[237-239]. This relationship between survival and dose is thought to be determined by the interaction of two separate chromosomal breaks that may recombine to yield aberrations. The equation is as follows:

$$S = e^{-(\alpha D+\beta D^2)}$$

Where S is the cell surviving fraction, D represents dose, and α and β are constants relating to the contribution of non-repairable and repairable damage, respectively.

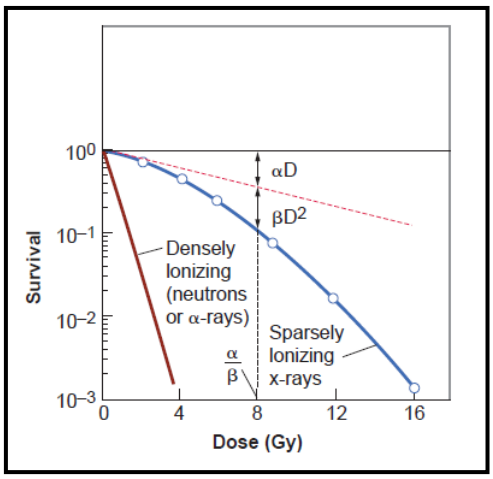

Figure 2.4. Graphical representation of a radiation survival curve fitted using the linear quadratic equation as a means to model the biological response to radiation. Densely ionising radiation produces a straight line while x- and γ-rays produce a curved shape with an initial linear portion[71].

Alpha damage may result when two chromosome breaks occur simultaneously as a result of a single ionising track, while beta-type damage occurs when breaks are separated by time and are therefore amenable to repair. The initial slope of the curve is dominated by the linear alpha component while beta determines the quadratic component of the survival curve. The ratio of alpha to beta (α/β) gives the dose at which the linear and quadratic components of cell kill are equal, and defines the shape of the survival curve. Radiosensitivity is sometimes estimated from the initial slope of the radiation survival curve, determined by alpha. However, overall responsiveness, which also takes into account beta, is a function of the full curve.

Other descriptors of radiation responsiveness that have been used include D_{10}, $\bar{D}$, SF2 and SF4. D_{10} is the dose required to give 10 % survival. The mean inactivation dose, $\bar{D}$, represents the overall cellular radiation responsiveness over the whole dose range considered. This value can be estimated from the area under the survival curve and has been used as a measure of radiosensitivity[240-243]. The surviving fractions of cells after doses of 2 and 4 Gy, namely SF2 and SF4, are also used for comparison of survival.

2.3.1.2. Micronuclei

The cytokinesis-block micronucleus assay was developed for assessment of DNA damaging agents including radiation[244, 245]. Micronuclei are small, additional nuclei that are formed during mitosis (Figure 2.5). Radiation-induced chromosomal breaks or mis-alignment at metaphase and the resulting inadequate spindle attachment may lead to micronucleus formation. Whole or acentric chromosomes, or chromatid fragments may be left stranded during anaphase[246, 247] and become bound within their own nuclear membranes. Micronuclei are either lost during cytokinesis or maintained in the cell as extra-nuclear genetic material[248].

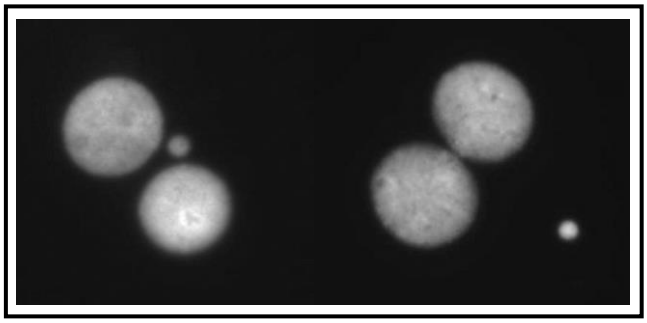

Figure 2.5. Two binucleate U937 cells each containing a single micronucleus (present work). 1000x magnification.

The assay allows quantification of micronuclei in cells that have undergone a single division. Such binucleate cells can be obtained using cytochalasin B to inhibit cytoplasmic division while permitting nuclear division. The frequency of micronuclei for a given cell number is routinely determined as a measure of the DNA damaging capability of a cytotoxic agent. Alternatively, the frequency of binucleate cells containing micronuclei can be scored to give an indication of the proportion of cells expressing cytogenetic damage[249-252]. The OECD (Organisation for Economic Co-operation and Development) Guidelines for the Testing of Chemicals, *in vitro* Mammalian Cell Micronucleus Test[253] describe the frequency of micronucleated cells as their method of choice.

A linear relationship has been shown to exist between radiation dose and micronuclei frequency[244]. The sensitivity of cells to radiation-induced micronuclei has been proposed to correlate with clonogenic survival[254, 255].

2.3.1.3. Apoptosis

Apoptosis[256] may not be a major consequence of radiation therapy in tumour cells, which characteristically exhibit defects in the apoptotic machinery[257-259]. However, it would be beneficial to identify agents that are able to stimulate apoptosis or modulate radiation-induced apoptosis.

Methods to quantify apoptosis are based on the characteristic morphological and biochemical features associated with this type of programmed cell death. Fluorescence microscopic evaluation of cells undergoing apoptosis (Figure 2.6) reveals condensed chromatin (pyknosis), spherical or ovoid cytoplasmic fragments and cell shrinkage[260]. Several assays based on morphological assessment have been developed. Manual scoring of apoptosis that assesses the above features is a simple and reliable way to quantify apoptotic cells. Cells displaying such features are generally in an advanced stage of apoptosis[260, 261]. Other manual scoring methods include assays that allow discrimination between viable, necrotic and apoptotic cells, for example, double staining with Hoechst 33342 and propidium iodide (PI). While Hoechst 33342 intercalates with the DNA double helix and stains all cells allowing identification of apoptosis, PI is used as a vital stain to distinguish necrotic cells as a result of loss of membrane integrity[262].

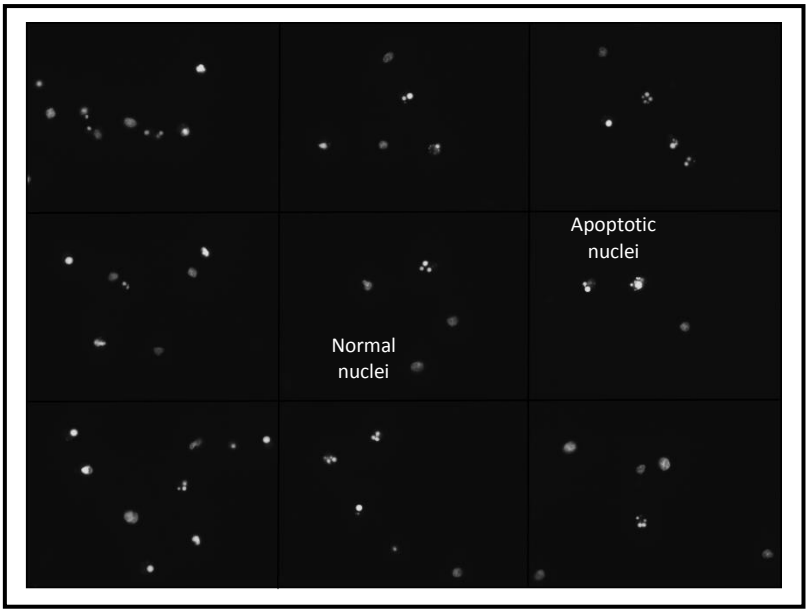

Figure 2.6. Representative images of apoptotic U937 cells stained with Hoechst 33342 (present work). 100x magnification.

A widely utilised method of apoptotic cell detection using flow cytometry combines the use of Annexin V and PI to effectively distinguish late and early apoptosis[263, 264]. Annexin V binds to phosphatidylserine that is exposed on the surface of cells during apoptosis[264]. The ability of PI to stain cells is dependent on membrane permeability[263]. Live cells and early apoptotic cells exclude PI and this allows them to be distinguished from necrotic cells where membranes become compromised[263]. In early apoptosis, cells are stained primarily with Annexin V but late apoptotic cells are stained with PI and Annexin V[264]. In addition, using flow cytometry, apoptosis may be detected by means of fragmented, hypo-diploid cells that appear as a sub-G1 peak on a DNA histogram[265, 266].

Gel electrophoresis of isolated DNA from apoptotic cells can be used to detect DNA fragmentation that forms a characteristic ladder pattern. Similarly, the comet assay can be performed at a single cell level where lysed cells are subjected to electrophoresis on a microscope slide and degraded DNA is visualised as a *tail* attached to a *head* consisting of intact DNA following staining with ethidium bromide or PI. The amount of DNA in the tail is proportional to the amount of damage induced. Although both necrosis and apoptosis can be detected using the comet assay, it has been shown that the tail moment (the product of the tail length and total DNA content) can effectively distinguish the two types of cell death[267].

The terminal deoxy transferase-mediated dUTP nick end labelling (TUNEL) method[268, 269] exploits the characteristic DNA fragmentation that occurs during apoptosis to detect cell death. TUNEL uses a terminal transferase to label single and double-strand DNA breaks with, for example, fluorescently labelled or biotinylated 2'-deoxyuridine 5'-triphosphate.

This method can distinguish early apoptotic cells as DNA breaks occur before a change in morphology of the cell can be detected. A similar assay, the *in situ* 3'-end labelling method, which relies on DNA polymerase I and thus only labels single-strand breaks, may be used but is less sensitive than TUNEL.

Immunohistochemistry and Western blotting can be used to examine apoptosis by using antibodies against proteins such as caspases and the Bcl-2 family[270]. Apoptosis can also be quantified by measuring release of cytochrome C and other apoptotic factors from the mitochondria[271].

As mentioned previously, radiation may induce both early and secondary apoptosis that is dose, cell type and cell cycle phase dependent. The time course of apoptosis following irradiation is therefore an important consideration when assessing apoptosis[201, 272]. In addition, the differences in the kinetics of apoptosis in cultured cells should be considered as apoptotic cells are not eliminated by phagocytes in the same way as they would be in *in vivo* systems[202]. This lack of elimination of apoptotic cells as well as the proliferation of unaffected cells in culture may influence quantification of apoptosis. In general, the apoptotic index may be expected to increase initially after treatment, saturate, and then be reduced, as proliferation of unaffected cells occurs.

2.4. Mitochondrial physiology

Mitochondria are multifaceted organelles that display a high degree of functional diversity. Differences in the environmental conditions and tissue of origin may dictate mitochondrial physiology. In addition, mitochondria derived from tumour or normal tissue may have significantly altered function.

- Historical interest -

Discovery of mitochondria and their function

The role of mitochondria in the generation of cellular energy in the form of ATP has been well established since the 1940's. At this time, a newly developed method of tissue fractionation enabled Albert Claude to isolate mitochondria and determine that enzymes, known to be responsible for respiration ("cytochrome-linked enzymes") resided in these organelles[273]. Although cellular structures referred to as "granules" were observed in the 1840's, it is believed that mitochondria, were first recognised and named "bioblasts" in 1890 by Richard Altmann[274].

The popularised term "*powerhouse of the cell*", coined by Philip Siekevitz in 1957[275], encapsulated the contemporary knowledge of mitochondria and highlighted the central role of this organelle in cellular bioenergetics. Important research that contributed to this knowledge included observations by Otto Warburg. He linked mitochondria to cellular respiration by studying extracts of guinea-pig liver and concluded that structures he termed "grana" are associated with the activity of "*atmungsferment*" (cytochrome C oxidase)[274]. This foundational work and his interest in the metabolism of tumours culminated in his belief that "*the prime cause of cancer is the replacement of the respiration of oxygen in normal body cells by a fermentation of sugar*" [276, 277]. The observation that tumours preferentially use glycolysis even in the presence of oxygen[278] led Warburg and his contemporaries to suggest that altered metabolism was necessitated by a dysfunction in mitochondrial respiration[278, 279].

2.4.1. Altered metabolism and mitochondrial function in tumour cells

2.4.1.1. Metabolic reprogramming as a hallmark of cancer

2.4.1.1.1. Warburg effect

A shift from respiration to aerobic glycolysis in tumours is a trait that is characteristic of a large proportion of tumours and is exploited in the field of functional imaging of tumours[280, 281].
A radioactive glucose analog 2-[^{I8}F] fluoro-2-deoxy-D glucose (F-I8 FDG) is taken up by cells with a high rate of glycolysis and is used with positron emission tomography (PET) scanning to provide spatial information on the metabolic and biochemical activity of tissues. In combination with a computed tomography (CT) scan for anatomical information, a PET/CT provides a 3-D image that includes more precise localisation of diseased tissue than is achieved with PET scanning alone. The widespread use of this technique in cancer diagnostics and management attests to the prevalence of this alteration in tumour metabolism that has been referred to as "the Warburg effect".

Support for a role of upregulated glycolysis in cancer initiation or progression is highlighted by an emerging hallmark, *"metabolic reprogramming"*, described by Hanahan and Weinberg[225, 282]. The status of an emerging rather than a core hallmark results from uncertainty over whether this phenotype should be regarded a consequence of enhanced proliferation, as many of the genes involved overlap or as a fundamental change in tumour development.

A related publication provides a review supporting the inclusion of altered metabolism as a core hallmark of cancer[283]. The primary focus of their discussion addressed the apparent paradox behind a shift in metabolism to increased glycolysis, a less efficient energy producing process, in cancer cells that are proliferating rapidly and therefore, presumably, require increased amounts of energy. They refer to fundamental differences in metabolism between quiescent cells and those that are proliferating in situations where growth factor stimulation is abundant. A shift from catabolic to anabolic metabolism under these conditions supports lipid, protein and nucleotide biosynthesis needed for cell division[284, 285].

Specifically, cellular growth requires NADPH for fatty acid and cholesterol biosynthesis, and recycled carbon and nitrogen for nucleic and amino acid synthesis[286, 287]. In addition, NADPH is important for modulating oxidative stress by reducing glutathione, converting H_2O_2 to H_2O in the process, and preventing hydroxyl radical formation[288].

A glycolytic phenotype may give cancer cells a survival advantage in a microenvironment characterised by intermittent hypoxia[290, 291]. Mitochondrial respiration, which regulates glycolysis via ATP feedback[289], is often downregulated accordingly[286, 291].

2.4.1.2. Mitochondrial respiration in tumour cells

Despite the observed dependence of tumours on glycolysis, cancer cells have been shown to be metabolically heterogeneous with a proportion of cells reliant on mitochondrial respiration[292, 293]. A subset of cells may exist that maintain stem cell-like characteristics and are dependent on OXPHOS with low basal levels of glycolysis. Such a sub-population was reportedly unable to upregulate glycolysis and was therefore particularly sensitive to OXPHOS-inhibiting drugs[293].

Cellular respiration involves a series of biochemical reactions culminating in ATP production. Glycolysis, the first stage in cellular respiration, produces ATP but also supplies pyruvate and NADH for pyruvate oxidation and OXPHOS, respectively. Acetyl Co-A produced by pyruvate oxidation, in the mitochondria, is oxidised by the citric acid cycle yielding NADH and $FADH_2$. During OXPHOS, NADH and $FADH_2$ deliver electrons to be transported by the electron transport chain (ETC), which consists of respiratory complexes that pump protons from the mitochondrial matrix into the intermembrane space to form a proton gradient. ATP generation by ATP synthase is driven by the exchange of protons across the inner mitochondrial membrane and oxygen acts as the final electron acceptor[294].

2.4.1.2.1. Mitochondrial function and dysfunction

Paradoxically, it appears that cancer cells need some degree of both functional mitochondria and mitochondrial dysfunction for transformation and maintenance of tumour growth[295]. Several factors may account for differences in mitochondrial respiration between cancer and normal cells. Metabolic changes in tumour cells are frequently the result of changes in expression or regulation of proteins involved in respiration.

The downregulation of OXPHOS is a common feature in cancer cells even in the context of an intact ETC. A particularly informative parameter of respiration, in the analysis of cancer cells, is the LEAK state respiration which describes mitochondrial dysfunction linked to ATP synthesis and provides a measure of the efficiency of electron transport. In addition, proton leak is regulated by oxidative stress through a feedback loop and is increased in the presence of excess ROS[296-298]. Cells displaying high proton leak, as a consequence of oxidative stress, may upregulate additional anti-oxidant defences, e.g. intracellular superoxide dismutase (SOD) and glutathione [299].

As anti-oxidant capability influences the effectiveness of radiation[300-303], it may be expected that cells displaying increased LEAK state respiration would have increased radioresistance.

Studies regarding the reduction of oxidative stress, and increased radioprotection, using mitochondrial-targeted anti-oxidants support this notion. For example, administration of ROS scavengers or synthesised antioxidants, were shown to reduce radiation-induced damage and mortality using mouse models[304, 305]. In a cell culture model, the use of a mitochondrial ROS suppressor, uncoupling protein-2 (UCP2) reduced UV-induced apoptosis in colon cancer cells[306]. Conversely, suppression of MnSOD that leads to increased ROS levels, augmented sensitivity to ionising radiation in colon cancer cells[307].

Alternatively, oxidative stress from reduced mitochondrial function could generate DNA damage and activate a DNA damage response[308]. Cells that are primed to detect and respond to DNA damage may have increased radioresistance as a result of their greater capacity to counter radiation-induced DNA damage. This mechanism is suggested for the radio-adaptive response where low doses of ionising radiation prime cells to respond more efficiently to subsequent higher doses[309]. Similar adaptations to those described above have been observed when analysing cancer stem cell radioresistance as they display increased antioxidant mechanisms and DNA damage response activation[310, 311].

2.4.1.2.2. Alterations in ATP synthase function

ATP, among other factors, suppresses glycolysis through feedback inhibition of phosphofructokinase[287]. Reducing ATP production by downregulation of ATP synthase would therefore be advantageous for cell proliferation. ATP synthase inhibition by oligomycin in mammalian cells was also shown to reduce mitochondrially-induced apoptosis[312]. ATP synthase dysfunction thus serves to increase cellular resistance and may be responsible for increased resistance to radiation-induced apoptosis.

Maintenance of ΔΨm under situations of downregulated OXPHOS, with functional ATP synthase, has been suggested to be a result of ATP synthase reversal where ATP is cleaved to reduce cellular ATP levels[313, 314]. Under induction of cell death, ATP synthase reversal may be a result of Bax-induced proton leak. The extrusion of protons from the matrix then leads to matrix alkalinity which has been known to cause permeability transition. This observation may explain some of the conflicting reports regarding an association between apoptosis and loss of ΔΨm. ATP synthase reversal would cause a transient increase in ΔΨm which would dissipate on opening of the permeability transition pores.

Inhibition or dysregulation of ATP synthase is common in tumours and results in ETC inhibition and increased ROS and ΔΨm[295]. ROS may activate hypoxia inducible factors (HIF) through HIFα stabilisation, which allows adaptation to oxygen-poor environments[315]. HIF1α increases glycolytic flux by increasing expression of enzymes and transporters involved in glycolysis, as well as, pyruvate dehydrogenase kinase (PDK) 1 that regulates PDH[316]. Phosphorylation inhibits PDH, an enzyme that catalyses the oxidative decarboxylation of pyruvate, thereby downregulating aerobic respiration. Upregulation of glycolysis further inhibits OXPHOS as a result of competition for phosphates and ADP (Crabtree effect). Increased glycolysis in tumours frequently occurs through PI3K–PTEN–AKT pathway activation, which increases cell surface nutrient transporters e.g. glucose. ROS can inactivate PTEN or activate AKT both leading to activation of the PI3K pathway[311].

2.4.1.2.3. Spare respiratory capacity

The bioenergetic reserve capacity is the difference between maximum respiratory capacity and ATP-linked respiration[317]. In cardiomyocytes exposed to oxidative stress, an initial increase in oxygen consumption was followed by decreased respiration as mitochondria became damaged[318].
It was proposed that assessing mitochondrial reserve function may predict cellular stress response. Cells with higher reserve function may have more potential to adapt to their environment[319]. In support of this finding, spare respiratory capacity has been suggested as a major determinant in cellular stress response and survival in neuronal[320, 321], endothelial[322] and memory T-cells[323].

2.4.1.2.4. mtDNA mutation

Although mtDNA mutations have been found in cancer cells[295, 324], consistent associations with altered respiratory function have not been determined[325]. Increased ROS production is both a consequence and inducer of mtDNA mutation, however, such increased levels are important for tumour growth and remain below that required for extensive damage[311]. Specific mtDNA haplotypes or single nucleotide polymorphisms (SNP) are associated with increased risk (~2-2.5 fold) for certain cancers[2]. In addition, changes to nuclear-encoded mitochondrial genes may lead to alterations in respiratory function.

2.4.1.2.5. Description of respiratory parameters determined by polarographic measurements

Reliable measurements of oxygen consumption and metabolites in cancer cells are needed[326]. Optimal protocols for assessment have only recently been developed. High resolution respirometry provides a simple and sensitive approach for collection of such data[327].

Several methods have been developed for measuring energy metabolism in cultured cells using either permeabilised cells, isolated mitochondria or intact cells. These methods include polarography using O_2 sensors, for example the Clarke-type O_2 electrode[328], O_2-sensing fluorophores or fibre optic O_2 sensors. Bioluminescent or fluorescent complementary methods that detect ATP concentrations or ΔΨm are also available. A summary can be found in an article by Zhang et al. (2012)[329]. For simplicity, only the oxygraph-type apparatus, a traditional method for measuring mitochondrial respiration, will be described, as this technique is the basis for measurements in this thesis.

Using the oxygraph apparatus, O_2 consumption is determined by recording changes in dissolved O_2 detected by a Clarke-type O_2 electrode. Cells or isolated mitochondria in a physiological solution are stirred constantly to ensure homogeneity of the solution. The O_2 facilitates the flow of electrons from a silver anode to a platinum cathode to create a current which is directly proportional to the O_2 concentration. The O_2 consumption rate is a measure of the reduction of total O_2 in the chamber.

Respiratory states have been defined for isolated mitochondria[330]. State 1 respiration refers to the initial OXPHOS activity, state 2 and state 3 refer to respiration at depleted and saturating levels of ADP, respectively. State 4 is a measure of the O_2 flux at rest when the added ADP is depleted and state 5 is respiration during anoxia or in the presence of a complex III inhibitor that abolishes mitochondrial respiration. A common index for mitochondrial function, the respiratory control ratio (RCR), is defined as the O_2 consumption in state 3/state 4[331]. This value is highly variable as it depends on many factors, including the preparation of the mitochondrial isolate[332].

Respiration cannot be determined under saturating ADP conditions in intact cells and respiratory states specifically for evaluation in intact cells have therefore been defined[327]. Oxygen consumption for each respiratory state is determined in the presence of a mitochondrial uncoupler or inhibitor. A detailed description of the protocol is provided in Chapter 4.

ROUTINE respiration can be considered equivalent to state 1 while *ETS* is the maximum mitochondrial respiratory capacity, which is similar to state 3. *LEAK* state respiration is similar to state 4 respiration, however, instead of ADP depletion, this state is induced by inhibition of ATP synthase by oligomycin. *ROX*, a measure of the non-mitochondrial respiration is equivalent to state 5 when induced by a complex III inhibitor. RCR for intact cells, namely ETS/LEAK, is a measure of mitochondrial efficiency that determines the capacity for ATP generation. Flux control ratios, which will be described in Chapter 4, are useful indicators of mitochondrial function that allow comparison of respiration states between cells independent of cell size and mitochondrial content[327].

2.4.1.3. Mitochondrial membrane potential in cancer cells

Functional analysis of mitochondria frequently includes both assessment of respiratory capacity and ΔΨm. The difference in electric potential across the inner mitochondrial membrane, or ΔΨm, is the result of a net positive charge created by the pumping of protons into the intermembrane space during electron transport.

In general, cancer cells have been reported to display hyperpolarised mitochondria[333-336], which, rather than representing increased mitochondrial function, is commonly associated with defective electron transport or ATP synthesis. For example, the hyperpolarised membrane may arise from the accumulation of protons in the intermembrane space as a result of ATP synthase dysfunction as described above [337, 338].

Cancer cells often display increased ΔΨm in the absence of increased respiration[333]. Subtle differences in intrinsic ΔΨm have been linked to altered cellular function in cancer cells[339]. This reflects the heterogeneity in energetic status of tumour mitochondria and may be linked to therapeutic response[340].

A hyperpolarised ΔΨm has been associated with tumour progression[282, 293, 341] and may therefore possibly confer a survival advantage. Neurons displaying a hyperpolarised ΔΨm were found to be resistant to excitotoxic injury[342]. Similarly, Bcl-2 overexpression, which is common in tumours and which was associated with elevated ΔΨm, resulted in increased survival of mouse fibrosarcoid cells after exposure to tumour necrosis factor[343]. Conversely, tumour cells with induced resistance to cisplatin showed increasing ΔΨm with increasing resistance[344]. It has been suggested that cells with high ΔΨm may be rationally targeted in cancer therapy[345].

2.4.1.3.1. Measurement of ΔΨm with JC-1

The lipophilic fluorescent stain, JC-1 (5,5',6,6'-tetrachloro-1,1',3,3'-tetraethylbenzimidazolylcarbocyanine iodide) can be used to determine ΔΨm in live cells[346, 347]. JC-1 has a broad excitation spectrum and an emission maximum at 590 nm. It diffuses through cell and mitochondrial membranes and, being cationic, accumulates in the negatively charged matrix of mitochondria with intact ΔΨm to form red fluorescent j-aggregates[348]. At lower concentrations JC-1 monomers are green and may be distributed throughout the cytoplasm. JC-1 is a ratiometric dye and thus the red to green (R:G) fluorescence ratio is an indication of ΔΨm[347]. In addition, the red fluorescence value (j-aggregate formation) as a measure of the abundance of polarised mitochondria per cell, can also be used independently as a measure of the functionality of the mitochondria[346, 349].

Measurement of ΔΨm in isolation may be a poor assessment of mitochondrial function, given the inconsistencies between ΔΨm and mitochondrial respiration. The inclusion of specific measures of OXPHOS and respiratory capacity give a more holistic assessment[350]. For example, polarographic measurement of O_2 consumption allows effective measurement of mitochondrial function, which can be analysed in conjunction with ΔΨm.

2.4.1.4. Radiation-induced effects on mitochondrial function

Numerous effects on mitochondrial function have been described after irradiation. The influence of ionising radiation on respiration includes alterations in oxygen consumption[42, 63, 351], OXPHOS enzyme activities[56, 153, 352, 353] and ATP production[40, 42]. Similarly, observations of altered ΔΨm[57, 149, 354] and mitochondrial biogenesis[352] including mtDNA copy number [55, 67, 355, 356] have been documented.

Local heart irradiation in a rat model reduced ΔΨm, basal O_2 consumption and LEAK state respiration although the RCR remained constant[63]. In addition, mitochondrial mass increased and a heightened sensitivity to swelling and mitochondrial permeability transition was observed[63]. Similarly, mitochondria in mouse hearts after 2 Gy (x-ray, 200 kV) appeared intact and healthy, however, functional defects, including increased ROS, decreased respiration and enhanced oxidation of mitochondrial proteins were observed[61]. Transformed small airway epithelial cells showed reduced O_2 consumption and ATP production and increased ROS after alpha particle irradiation[353].

It has been reported that the OXPHOS complex IV was particularly sensitive to both direct irradiation and exposure to irradiated cell conditioned medium[56]. In another study by the same investigators, recovery from an initial decrease in respiration was associated with an increase in mitochondrial mass, suggesting compensatory mitochondrial biogenesis[352]. In A549 cells, an increase in ΔΨm occurred after 10 Gy irradiation and was followed by an increase in O_2 consumption and ATP production, as well as mitochondrial biogenesis[42]. In addition, radiation-induced effects were observed in a highly radioresistant glioblastoma cell line, including increased ΔΨm and upregulated expression of three mitochondrially-encoded genes necessary for OXPHOS[40]. Similarly, an increased expression of mitochondrial proteins of heart cells after 3 Gy whole body irradiation of mice was observed[357]. These investigators suggested that mitochondrial proteins were particularly sensitive to ionising radiation.

Increased mtDNA copy number, which may also be compensatory, has been shown after irradiation of cells in culture[353], mice[355, 356] and humans[67]. The mtDNA common deletion (4977bp) has been observed after irradiation and occurred frequently in radiosensitive fibroblasts[68].

Interestingly, low dose irradiation of 10 cGy caused an increase in mitochondrial protein import while 4 Gy decreased mitochondrial protein import, thus altering mitochondrial function and indicating differential effects depending on radiation dose[149]. Although variable, these observations suggest that cellular response to radiation damage involves adaptation of mitochondrial functionality.

2.4.1.5. Does inherent mitochondrial functionality influence radiosensitivity?

The influence of mitochondrial function on radiosensitivity has been investigated using cells that have been depleted of mtDNA or that contain mtDNA mutations, however, the results have been inconclusive. Rho0 (mtDNA-depleted) cells appeared to be more radioresistant as assessed by clonogenic survival[156, 158] and micronuclei analysis[358-360]. However, no difference in clonogenic survival was found between irradiated Rho0 cells and those containing mtDNA (Rho+)[157, 358-360]. Rho0 cells also displayed reduced apoptosis[155, 158] and $\Delta\Psi m$[155]. Rho+ cells, cells with mutant mtDNA and Rho0 cells had high, intermediate and low radiation sensitivity, respectively, which correlated with ATP level[358, 359]. In general, differences in cell cycle regulation were also found after mtDNA depletion. A decrease in the number of cells in S-phase was observed in Rho0 cells[156]. In addition, mtDNA depletion suppressed the radiation-induced G2-checkpoint activation[155, 156]. However, other studies have reported no cell cycle effects[157, 158].

The radiosensitivity of certain mouse strains has been associated with mtDNA copy number[356]. Increased sensitivity to mitochondrial permeability transition pore opening was found specifically in radiosensitive mouse strains and offspring from radioresistant mouse strains displayed mitochondria that were resistant to swelling by calcium[356].

Mitochondrial membrane hyperpolarisation has been linked to increased radiation sensitivity in MCF7 breast cancer cells[361]. In addition, irradiated immortalised human lymphocytes (10 Gy) were shown to undergo loss of $\Delta\Psi m$ after an initial hyperpolarisation and maintained a population of cells with hyperpolarised $\Delta\Psi m$ for up to 36 hours[362], which was consistent with previous work[363].

2.4.1.5.1. Evidence from mitochondrial diseases

Cells from patients with mitochondrial diseases, such as Leigh's syndrome and Leber's optic atrophy, showed differences in gene expression related to regulation of energy and DNA damage response to ionising radiation. Such patients were shown to be hypersensitive to radiation with increased induction of chromosomal aberrations and a reduced mitotic index, which suggests an enhanced G2/M checkpoint arrest[364], as well as an increased tendency towards apoptosis[196].

However, although Leigh's cells also showed increased radiosensitivity as determined by clonogenic survival, Leber's cells were more radioresistant, potentially as a result of an observed greater repair capacity[41]. In this study, Leigh's cells were characterised by an ATP6 gene mutation and reduced ATP levels, which may affect repair capacity. Mutant cells showed reduced induction of repair proteins and an increased expression of apoptosis-related genes suggesting that mitochondrial dysfunction may limit the ability of cells to repair damage and preferentially induce apoptosis[41, 196]. Leber's cells were able to repair more efficiently relative to Leigh's cells and ultimately displayed reduced radiation response[41].

2.5. Mitochondria as dynamic organelles

Mitochondria constantly adapt to their environment and cellular conditions through changes in distribution and morphology. Accordingly, cells tend to maintain a predominantly fused or fragmented state depending on factors such as energy requirements[365-368], microenvironmental conditions[369, 370] and cell cycle phase[137, 144, 371].

- Historical interest -

Discovery of mitochondrial dynamics

Depictions of mitochondria as individual, oval-shaped structures, commonly found in textbooks, came from an inability to observe 3-D structure within 2-D electron micrographs. These images relied on thin sections of tissue and scientists were observing cross-sections through tubular mitochondria, which in reality would form part of a network of interconnected mitochondrial filaments (Figure 2.7). It is interesting that, despite this misconception, the name 'mitochondria', derived by Benda in 1898, accurately describes this organelle[274]. Derived from the two Greek words "mitos" (thread) and "chondros" (granule) which together describe granules forming threads, the term 'mitochondria' hints at the dynamic nature of this organelle.

Mitochondrial dynamics includes the processes of fusion and fission of mitochondria that result in fused networks and fragmented structures, respectively. The concept of a dynamic organelle was later strengthened when Lewis and Lewis (1914)[372] reported not only filaments and granules but also "anastomosing threads and networks". They noted that mitochondria were constantly changing shape and position, and reported that granules were able to fuse together to form "rods or chains", elongate into threads and networks, and then "break down into threads, rods, loops and rings" again[372]. Other observations of rod- or thread-like and branched organelle structures also suggested plasticity of mitochondrial morphology[373-375]. With the invention of the phase contrast microscope in the 1930's[376], phase cinematography allowed the visualisation of movement and change in living cells. Bereiter-Hahn et al. (1990)[377] reported on numerous studies that commented on the mobility of mitochondria and their ability to fuse and divide including studies by Zollinger, Frederic & Chevremont, Pomerat, Lefeber & Smith, Gey, Tobioka & Biesele and Rose between 1950 and 1960. A defining paper by Hoffman and Avers (1973)[378] introduced the concept of the mitochondrion as a single organelle made up of branches. Improved microscopy techniques and the visualisation of cellular structures using fluorescent staining and live cell imaging, brought new understanding of the dynamic nature of the mitochondrion[52, 379-381]. Rather than the static organelles observed in electron micrographs, mitochondria were shown to form a network that constantly changes shape and connectivity to meet metabolic requirements[52]. The processes of mitochondrial fusion and fission were thus established as integral to cellular physiology.

2.5.1. Mitochondrial proteins regulating fission and fusion

Mitochondrial homeostasis is governed by proteins that allow fragmentation (fission) and fusion of mitochondrial segments[382, 383]. A number of GTPase-containing proteins, including dynamin-related protein 1 (DRP1), hFis1, mitofusins (MFN) 1 and 2 and OPA1 have been identified as regulators of mitochondrial fission and fusion, respectively. A brief description of these proteins follows with a focus on the primary protein involved in mitochondrial fission, namely DRP1.

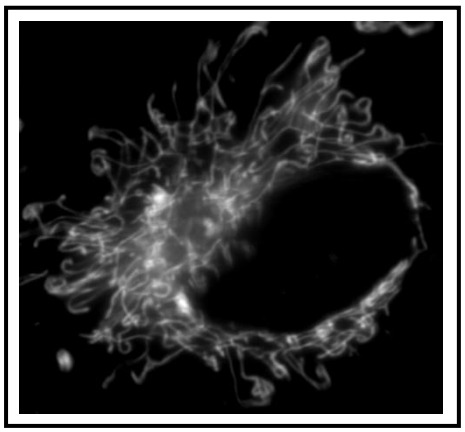

Figure 2.7. Fluorescence image of a filamentous mitochondrial network. A549 lung cancer cell stained with MitoTracker® Red (present work). 1000x magnification.

2.5.1.1. Outer membrane fusion proteins: MFN1 and 2

Mitochondrial fusion is required to balance the ongoing opposing process of mitochondrial fission and is regulated by two mitofusins, MFN1 and 2[382, 384-386]. A fusion-related gene, *fzo* ("fuzzy onions") was first described in *Drosophila melanogaster*[387]. The name relates to the appearance of mitochondrial aggregates during meiosis that form a "spherical *Nebenkern*" resembling an onion slice[387] before elongating during flagellum formation. Drosophila mutants for *fzo* are sterile and showed defects in *Nebenkern* formation. The yeast "*fzo"* ortholog was shown to be similarly involved in mitochondrial fusion[388]. The *fzo* protein, a large GTPase, was the first of a novel family of transmembrane GTPases to be assigned a function[387].

Overexpression of MFN1 or 2, the human homologs of the *fzo* proteins, results in elongated mitochondria[384]. Complete deficiencies of either MFN1 or 2 in developing zygotes lead to embryonic lethality, however, there is some redundancy present, with overexpression of one mitofusin compensating partially for deficiency of the other[389, 390]. The two fusion proteins have distinct roles in the fusion process. MFN1 has the role of tethering two opposing mitochondrial membranes while MFN2 appears to be important at later steps in the fusion process and have a regulatory function[20, 391-393] (Figure 2.8). A role for MFN2 in tethering the endoplasmic reticulum (ER) to the mitochondrion has also been proposed[394, 395].

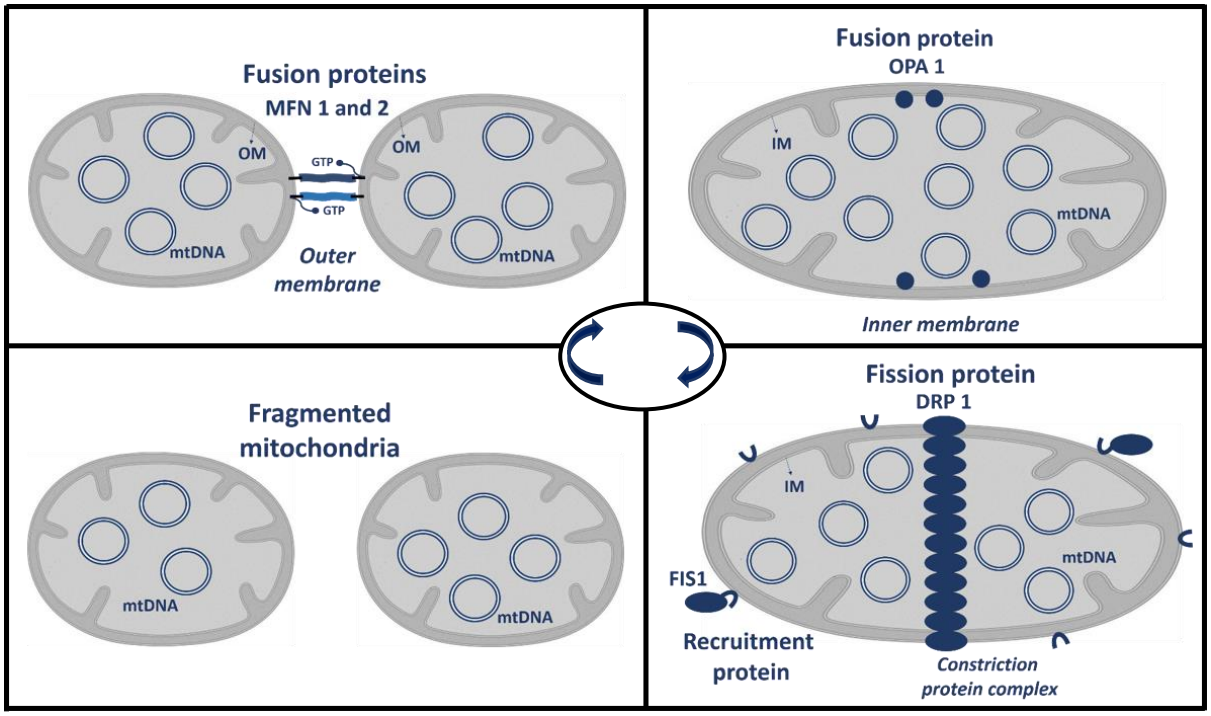

Figure 2.8. Schematic representation of mitochondrial fusion and fission (own illustration). Fragmented mitochondria become fused by mitofusins MFN1 and 2 and OPA1. Fission of mitochondria occurs by DRP1 and FIS1. OM = outer membrane. IM = inner membrane.

Mutant MFN1 cells display spherical, fragmented mitochondria of uniform size while, in contrast, MFN2 mutants have mitochondria of variable size and increased diameter[386, 389]. MFN2 mutants also display alterations in mobility showing random, Brownian-type movement instead of the typical directed movement along microtubule tracks[396, 397]. Interestingly, overexpression of mitofusin proteins leads to mitochondrial fragmentation and clumping after an initial increase in fusion. This suggests a threshold level of mitofusin activity[398].

The fusion process is sensitive to mitochondrial function. Fusion of the outer membrane is insensitive to the metabolic status of mitochondria, however, inner membrane fusion is related to OXPHOS activity[399, 400]. Reduction in mitochondrial fusion in mammalian cells was not found to translate into any associated defect in respiration or the loss of mtDNA. A subset of mitochondria, however, displayed associated loss of ΔΨm and various authors have suggested that an intact ΔΨm is required for membrane fusion[401-403], although this requirement may be limited to inner mitochondrial membrane fusion[404, 405].

2.5.1.2. Inner membrane fusion protein: OPA1

The mitofusins are responsible for outer membrane fusion while OPA1 (optic atrophy type 1) gene, the human homolog of yeast mgm1p, enables fusion of the inner membrane[406, 407]. OPA1 exists in eight different isoforms[408-412] consisting of both long (l-OPA1) and short (s-OPA1) forms and mutations in this gene cause autosomal dominant optic atrophy[413, 414].

Cells with OPA1 insufficiency display fragmented mitochondria with loss of ΔΨm and altered cristae morphology. Knockdown of OPA1 using siRNA resulted in cytochrome C release and spontaneous apoptosis, supporting the notion that cristae remodelling is necessary for cytochrome C release[220, 415].

OPA1 was able to protect against apoptotic cell death even in the absence of MFN1, suggesting that the protective effect of OPA1 is not related to its role in fusion[220]. Moreover, a number of additional studies have suggested that mitochondrial fusion is a protective mechanism[20, 416-419]. It appears that regulation of the release of cytochrome C can be linked to mitochondrial fusion via involvement of ATP-synthase. The F1F0-ATP synthase has been shown to be involved in regulation of cristae morphology[420] and Mgm1p stabilises Tim11p, a protein necessary for assembly of F1F0-ATP synthase subunits[421].

2.5.1.3. Fission protein: DRP1

Dynamin-related protein 1 (DRP1) is the primary mammalian fission-related protein that was identified and characterised by Imoto et al. (1998)[422] as being similar to the yeast vsp1p, a protein present in the Golgi apparatus to aid vacuolar protein sorting. DRP1 was initially described as a protein that affected mitochondrial distribution in mammals[423]. Dynamin-like proteins responsible for the maintenance of mitochondrial morphology and distribution have been described by a number of investigators, who each provided a synonym for DRP1, namely DNM1p in yeast[424], DVLP[425], DLP1 in mice[426] and DYMPLE in a scleroderma patient[427].

DRP1 belongs to the dynamin superfamily, which are large GTPase proteins responsible for endocytosis and protein trafficking at various cellular locations[428]. In addition to mitochondrial fission, DRP1 was shown to be involved in peroxisomal division[429]. DRP1 is regulated through S-nitrosylation, ubiquitination, phosphorylation and SUMOylation[430]. Overexpression of DRP1 in *C. elegans* caused increased mitochondrial fission and DRP1 was shown to be responsible for outer membrane but not inner membrane fragmentation[431].

Additional evidence in cultured mammalian cells showed that DRP1 can tubulate and constrict membranes in a similar fashion to dynamin proteins[432]. Mutant proteins were shown to result in increased fusion in Cos7 mammalian cells despite no alteration in the rate of fusion[433].

DRP1 mutation has been shown to induce senescence[434]. The loss of DRP1, and associated loss of fission, may not necessarily result in the loss of mitochondrial function, as the import of mitochondrial proteins has been shown to be maintained in *dnm1-null* yeast[424]. However, extended periods without mitochondrial division may lead to an accumulation of mutant mtDNA clones, eventually leading to loss of function[435, 436]. Mitochondrial membrane potential has been shown to be attenuated on DRP1 depletion[24] but, in contrast, ΔΨm may also be increased[437].

2.5.1.3.1. DRP1 is associated with apoptosis

Frank et al. (2001)[15] described a novel role for dynamin proteins by implicating DRP1 in the regulation of cell death. They showed that staurosporine (STS)-induced DRP1-dependent fission was reduced in cells with mutant DRP1. The loss of ΔΨm observed during STS-induced apoptosis was also shown to require DRP1.

Radiation-induced apoptosis in normal and tumour cells was similarly reduced after high doses (200 Gy). Mitochondria became enlarged and retained both their tubular morphology and ΔΨm, whereas cells with wildtype DRP1 displayed fragmented mitochondria that excluded a ΔΨm dependent dye[15]. In addition, in DRP1 mutated cells that were treated with STS, cytochrome C showed punctate staining, suggesting a lack of apoptotic response. In contrast, diffuse staining was observed in wildtype cells corresponding to the release of cytochrome C. Reduction in cytochrome C release with loss of DRP1 was confirmed by other investigators[217], however, apoptosis was delayed but not completely abolished, suggesting that mitochondrial fragmentation was not necessarily required for apoptosis[217, 438].

DRP1, primarily a cytoplasmic protein, was shown to associate with the outer mitochondrial membrane after apoptosis induction at discrete foci that correspond to scission points[431]. Both Bax and Bcl2, important proteins involved in the regulation of apoptosis, have also been shown to interact with DRP1[218, 221] suggesting a role for DRP1 in apoptosis. In addition, the involvement of Bax in membrane scission was suggested[218] and overexpression of Bax alone was shown to induce apoptosis and the formation of punctate mitochondria[15].

A role for DRP1 in cristae remodelling to allow cytochrome C release has been proposed[439]. Bid or Bik-induced cell death that results in release of cytochrome C through the activation of Bax or Bak[440], caused recruitment of DRP1 to the mitochondria with subsequent cristae remodelling[415, 439]. It is interesting to note that bid-induced cell death could be prevented by DRP1 knockdown[438, 441].

2.5.1.3.2. ER-DRP1 association

There is evidence for ER and DRP1 interaction. The ER has been shown to facilitate DRP1 constriction of membranes at mitochondrial fragmentation scission sites[442, 443] and therefore is also important in mitochondrial dynamics.

Staining of the ER with Rab1, a Golgi- and ER-associated membrane protein, in conjunction with DRP1 staining gave a pattern of DRP1 foci interspersed with Rab1 proteins[426]. Other associations between DRP1 and the ER have been proposed and may be significant in the cellular stress response[442, 444], given the prominent role of the ER in this regard. The release of Ca^{2+} from the ER, which may act as a signal for apoptosis, was associated with the recruitment of DRP1 to mitochondria[17, 445].

2.5.1.3.3. Additional fission-related proteins

In yeast, three mitochondrial-associated proteins regulate fission, namely Dnml1, Mdv1p and Fis1p. Mdv1p was shown to form a complex with Dnml1[446] however only Fis1p was shown to be directly involved in the assembly and function of DRP1 as mutant Fis1p inhibits fragmentation[447].

Structural characterisation of the first mammalian homolog, hFis1, suggested that this protein was a molecular adaptor for DRP1[448]. Although not localised to scission sites, hFis1 encompassed the mitochondrial outer membrane and formed a scaffold for protein-protein interactions[218, 448].

Reduced expression of hFis1 has been associated with elongated mitochondria and cellular senescence[449-451]. Decreased fission leading to increasingly fused mitochondria and interaction with DRP1 suggest a role for hFis1 in DRP1 recruitment[452].

When expressed in cells in culture, hFis1, was shown to induce fragmentation with associated cytochrome C release and apoptosis, in the absence of an increase in DRP1[453]. In addition, downregulation of hFis1 inhibited apoptosis to a greater extent than downregulation of DRP1[454]. Further, spontaneous apoptosis in HeLa cells, induced by loss of OPA1, was shown to require hFis1[454]. Additional proteins that have been associated with mitochondrial fission include Endophilin B1[455], mitochondrial fission factor[456, 457] and adaptor proteins, miD49 and miD51[458, 459].

2.5.2. Techniques used to study mitochondrial fusion and fission dynamics

2.5.2.1. Membrane potential-dependent dyes

The examination of dyes that rely on differences in $\Delta\Psi m$[460] led to the development of useful fluorescent lipophilic cationic stains for assessment of mitochondrial morphology, including Rhodamine 123[461], TMRM/TMRE (tetramethylrhodamine methyl/ethyl ester)[462], $DiOC_6$ (3,3'-dihexyloxacarbocyanine Iodide)[463] and the more photostable rosamine CMXRos stains[379]. As a result of their indirect dependence on respiration, these stains are useful for assessment of mitochondrial function in addition to morphology[464].

Morphological assessment of mitochondria using MitoTracker® Red, a rosamine stain, has been used extensively for the investigation of mitochondrial dynamics. MitoTracker® Red vital staining, which was used in this study, requires live cells for uptake but remains well-retained after fixation[379]. Various methods have been described for determination of the proportions of fusion and fission in a population of cells, for example, the identification of the proportions of cells with fused, intermediate or fragmented mitochondria[465-467]; image thresholding analysis to determine the level of fusion or fission[221]; quantification of morphology based on mitochondrial length[468] and analysis of shifts towards either fusion or fission[469].

Such dyes are commonly used for live staining of mitochondria, however, careful handling is required to maintain mitochondrial integrity. Staining and imaging should be conducted at physiological temperature and the overall processing time should be minimised to avoid artifacts. Excessive exposure of cells to these dyes may damage mitochondria leading to structural and morphological changes such as fragmentation.

Fluorescence imaging of live cells is useful as it allows detection of fine mitochondrial structure, however, excessive exposures may lead to photo-toxicity. The use of fluorophores of longer wavelengths or two-photon excitation microscopy may decrease photo-toxicity allowing continuous imaging of cells for extended periods.

Laser scanning confocal microscopy (LSCM) is often used to obtain sharp images that display superior detail than obtained using conventional fluorescence microscopy. LSCM allows the collection of serial optical sections that are assembled into a single, clear image, which is particularly important for objects with a significant depth of focus. In addition, spatial arrangement of mitochondria can be observed using 3-D image construction.

In conventional microscopy for imaging mitochondria, the use of flattened, adherent cells, which have a narrow depth of focus, can produce good quality images. Stain- and illumination damage-induced artifacts can be avoided by prompt fixing of cells after staining. However, photobleaching remains an important factor that limits imaging time. The type of fixative used and the tonicity of the incubation solutions are important to maintain native mitochondrial morphology. Paraformaldehyde fixation has been shown to be the most reliable as glutaraldehyde fixation leads to shrinkage of mitochondria and methanol has a precipitatory effect on membranes[470].

2.5.2.2. Morphological analysis based on detection of mitochondrial proteins

Mitochondria can be visualised by immunocytochemistry using labelled antibodies to mitochondrial membrane proteins, for example, TOM20, an outer mitochondrial membrane receptor protein. In addition, transfection of mitochondrially-targeted fluorescent proteins, such as DsRed2 and mitoGFP, has been used to label mitochondria[471, 472]. Labelled mitochondria can then be followed over multiple passages using this technique, however, the transfection rate is frequently less than 90 % implying that a proportion of cells will not be available for microscopic evaluation. Techniques using stable, rather than transient expression of marker proteins are recommended due to stress-related factors that may influence mitochondrial morphology[473].

Fluorescence recovery after photobleaching is a technique that uses fluorescent stains or labelled mitochondrial markers to measure mitochondrial continuity as an indication of the extent of fusion. The method involves localised photobleaching of an area of the mitochondria and subsequent observation of the re-establishment of fluorescence that would suggest movement of molecules from connected regions.

2.5.3. Mitochondrial dynamics and cellular function

The mitochondrial morphological phenotype, which reflects mitochondrial dynamics, may be a valuable indicator of cellular physiological status[474-476]. Characterisation of fusion and fission has the potential to provide insight into the metabolic and functional status of different cancers.

Mitochondrial dynamics, cellular function and radiosensitivity may be interrelated. In addition to factors that influence intrinsic radiosensitivity generally[477] differences in the response of tumours to therapy are known to be affected by several factors that have significant effects on mitochondrial status. Such factors include microenvironmental features such as hypoxia[478, 479], as well as position in the cell cycle[480], tumour pH[481], respiratory capacity[482] and other underlying physiological conditions[483].

In accordance with the mitochondrion's role to provide energy through OXPHOS, mitochondrial morphology is closely linked with cellular respiration[484]. Highly fused mitochondria generally have a higher OXPHOS capacity[399, 475, 485] and inhibition of respiration has been shown to cause fragmentation of the mitochondrial network[486, 487].

In addition to respiratory function, ΔΨm, another functional measure, has been associated with mitochondrial morphological status. From initial studies, it was shown that electrically polarised mitochondrial membranes are required for mitochondrial fusion[403, 488, 489], however, some authors suggest that the association is indirect[396, 400].

Inhibitors and uncouplers of the respiratory chain, mutations in respiratory complexes and loss of mtDNA have been shown to cause a loss of ΔΨm and fragmentation of the mitochondrial network[474, 490]. In contrast, the use of oligomycin, also induced fragmentation, in spite of an associated increase in ΔΨm[491, 492]. This fragmentation was suggested to be a result of OPA1 inactivation by decreased ATP levels and shows that an intact ΔΨm alone is not sufficient to maintain mitochondrial fusion[396, 493]. Decreased ΔΨm, generally observed during apoptosis, is also associated with mitochondrial fragmentation[18, 494]. It is generally acknowledged that healthy respiring cells typically display an intact ΔΨm of 150-180 mV[495], while cellular stress[496], respiratory dysfunction[497] and cell death[498] processes lead to loss of ΔΨm. Thus, measurement of ΔΨm may provide an indication of mitochondrial and cellular fitness.

In general, cell death and mitosis have been associated with mitochondrial fragmentation. Cellular stress resistance or damage, in particular the ER-initiated cellular stress response has been linked to fusion. It has been observed that a shift in the balance of mitochondrial dynamics towards mitochondrial fusion in different cell types increases stress resistance[19, 416, 434, 454]. For example, senescent cells, which typically display networked, fused mitochondria[434, 449, 450], are resistant to cytotoxic agents including radiation[449, 499]. Despite the fused state senescent cells have been shown to display reduced ΔΨm and reduced respiration suggesting this fusion may not be metabolically-induced[500].

Hypoxia has been shown to enlarge tubular mitochondria in a reversible, Hif-1-independent manner in a range of cancer cells and normal fibroblasts[419]. Enlarged mitochondria maintained both respiratory function and ΔΨm. Apoptosis resistance observed in colon cancer cells was linked to MFN1 induction, suggesting that the enlarged mitochondria were a consequence of increased or atypical fusion[419]. Stress-induced hyperfusion also protected against UV-irradiation- and actinomycin D-induced apoptosis[501].

2.5.3.1. Variation of mitochondrial fusion and fission through the cell cycle

The cell cycle is controlled by differential expression of regulatory cyclins and the activation and inactivation of cyclin-dependent kinases. Mitochondria also appear to be influenced by such processes. Dynamic changes in mitochondrial morphology are evident during the cell cycle (Figure 2.9). In general, mitochondrial fusion has been associated with interphase, while fission has been proposed as a requirement during mitosis[150, 502-504]. However, filamentous mitochondria have been observed in all phases of the cell cycle, becoming condensed and localised to the perinuclear region at prophase[505].

Proteins involved in mitochondrial fusion and fission, including MFN1 and 2 and DRP1, have been shown to be regulated by proteins that govern cell cycle progression (Figure 2.9). Importantly, mitotic fission is coordinated with the cell cycle and may be considered a cell cycle checkpoint itself[443, 503]. During interphase, APC/C-Cdh1 facilitates ubiquitination of DRP1 thereby inhibiting mitochondrial fission. DRP1 levels rise at G1/S following inhibition of APC/C-Cdh1 by cyclin D/E complexes and activation of DRP1 occurs by cyclin B-Cdk1-mediated phosphorylation in mitosis. In contrast, MFN1 is inhibited by cyclin A/B-Cdk1 as cells prepare for mitosis.

Besides changes in fission and fusion, relocation of mitochondria to the cell periphery prior to cytokinesis occurs to ensure proper segregation of mitochondria to daughter cells[506]. Such redistribution of mitochondria is supported by observations of mitochondria being excluded from the metaphase plate during chromosome alignment but allowed re-entry into the region by telophase[150].

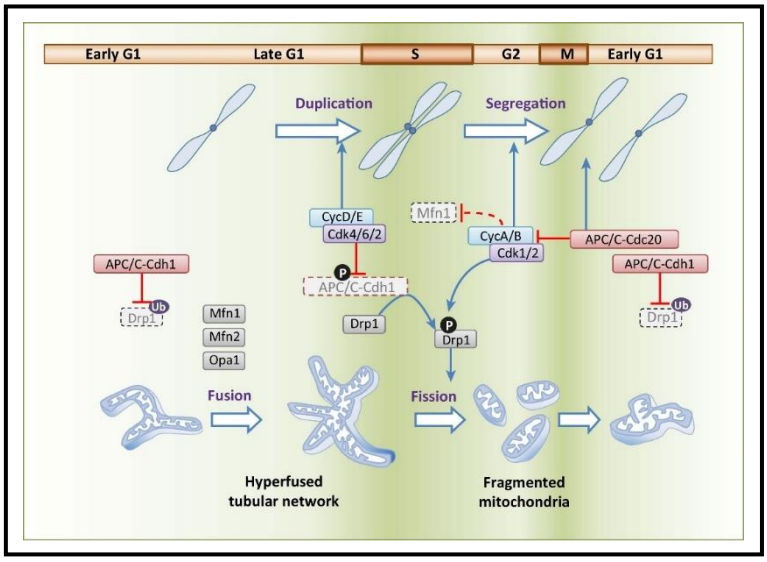

Figure 2.9. Cell cycle related changes in mitochondrial dynamics and interaction of fusion and fission proteins with cell cycle regulatory proteins. [From: "Fueling the Cell Division Cycle, Salazar-Roa and Malumbres (2017)[503]-used with permission].

Proliferation of vascular smooth muscle cells (VSMC) was reported to be dependent on mitochondrial dynamics. Cell division was inhibited when mitochondrial fusion or fission was reduced[507]. Higher expression of the mitochondrial fusion protein, MFN2 and netlike mitochondria has been found in G0/G1 relative to S-phase[144, 508], suggesting cyclical changes in mitochondrial dynamics. Overexpression of MFN2 caused G1 cell cycle arrest while knockdown of MFN2 caused S-phase arrest. The investigators suggested that MFN2 controls VSMC proliferation through mitochondrial remodelling.

Normal rat kidney cells at the G1-S border were found to form a transient hyperpolarised network of mitochondria distinct from the mixture of fused and fragmented mitochondria that were observed within the individual phases[137]. Increased connectivity at the G1-S border may be consistent with the increased oxygen usage reported from early to late G1 and reflect the increased ATP requirement for initiation of S-phase[509]. However, increased mitochondrial fusion was also associated with increased cyclin E, a requirement for G1-S transition[144]. Mitochondrial fusion may therefore be required for such transition to provide the necessary increase in ΔΨm and upregulation of cyclin E. Such a hyperfused mitochondrial network, however, was found to be transient[137].

In contrast, maintaining a fused morphology prevents cell cycle progression in a manner that mimics the effects of cyclin E overexpression[144, 510]. Mitochondrial hyperfusion at the G1-S border may, therefore also be considered a mitochondrial checkpoint. In addition, damage-induced mitochondrial fragmentation may be a mechanism used to reinforce the G1/S checkpoint by opposing the formation of such a hyperfused state required for transition.

Mitochondrial cycling, although related to cell cycle transition, appears to be largely an independent process[371]. Mitochondrial turnover includes biogenesis and a type of programmed organellar death, mitophagy[371, 511]. Biogenesis occurs primarily in G1[502], however, morphology and content are modified throughout the cell cycle in response to the metabolic needs of the cell (Figure 2.10)[371]. A drastic reduction in mitochondrial content has been described following mitosis[502].

There appears to be both cellular and organellar control of fission[371]. From G1 to M-phase, ΔΨm was found to be gradually increased with a reduction in ΔΨm following division[502] which may be related to mitosis-associated fission. Fragmentation of the mitochondrial network which occurs as a result of the dynamic nature of mitochondrial morphology may also act as a quality control mechanism. Mitochondria that are depolarised and are unable to recover their ΔΨm do not fuse with polarised mitochondria and are eliminated by mitophagy[401, 512].

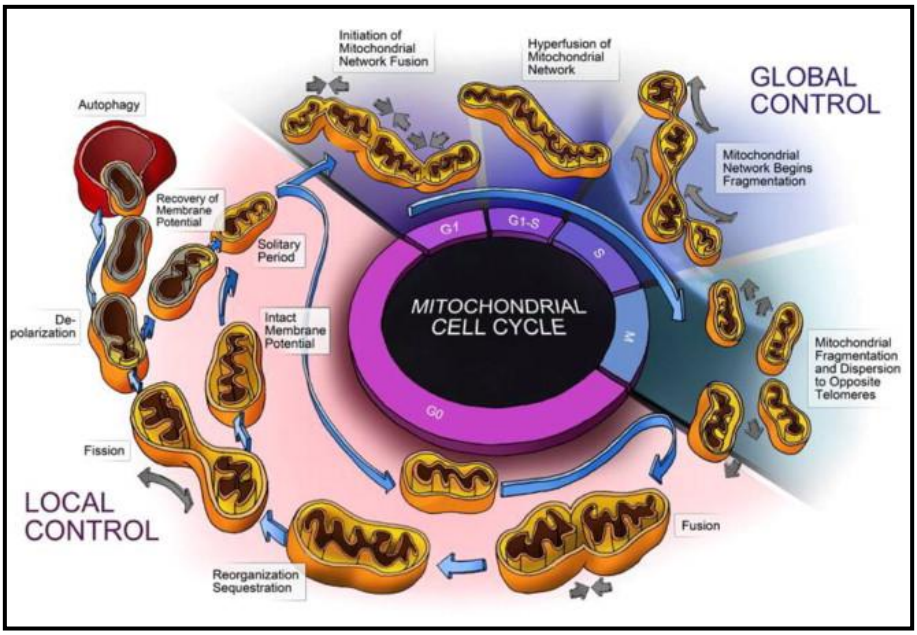

Figure 2.10. Regulation of mitochondrial biogenesis and autophagic elimination requires cell cycle independent fission in addition to mitosis-associated fragmentation. [From: "Organellar vs cellular control of mitochondrial dynamics, Hyde B, et al. (2010)[371]-used with permission].

2.5.4. Mitochondrial dynamics in tumours

Dysfunctional mitochondria and mtDNA mutations are commonly described in cancer[295, 513-515], however few studies report on the role of fission and fusion in tumour cells. It was suggested almost 100 years ago[516] that, in general, tumour tissue contained more fragmented mitochondria while filaments were associated with normal tissue. In a review of recent literature, Srinivasan et al. (2017)[1] suggested that fission was pro-tumorigenic and that inhibition of fragmentation reversed specific tumour properties. However, there is no consensus as to whether fission or fusion predominates in cancer cells. It is likely that mitochondrial dynamics is cancer type specific.

2.5.4.1. Ultrastructural changes

Mitochondria from cancer cells have been reported to display ultrastructural changes[369, 517] although these may reflect metabolic rather than innate differences.

Hurthle cell and other thyroid adenomas were shown to contain abundant, irregularly-shaped mitochondria[518-520]. Oncocytic tumours of the thyroid displayed large, swollen, densely-packed mitochondria[521]. Shape, size and structural anomalies have also been described in mesotheliomas[522] and leukaemia cells, which were found to be respiration deficient[523].

Malignant papillary cystadenoma lymphomatosum (Warthin's tumour) displayed large, swollen, densely-packed mitochondria with abnormal cristae that formed concentric rings of cup-shaped mitochondria[524]. A low level of fission was reported in astrocytomas and gliomas that were found to display heterogeneous mitochondrial morphology, often swollen with disorganised cristae[525]. Similarly, extensive mitochondrial pleomorphism was observed in tumour-derived cell lines, where mitochondria were more abundant and enlarged with abnormal cristae structure[520].

2.5.4.2. Biogenesis, localisation and protein expression

Reports describing mitochondrial dynamics in cancer also include those that assess mitochondrial biogenesis, localisation and expression of proteins related to fission and fusion.

Mitochondrial dysfunction in cancer may, in certain cases, result from defective expression of oncogenes[3]. Differences in mitochondrial mass have been observed in various cancers and between individual tumours and regulation of mitochondrial biogenesis by c-Myc, a known oncogene, has been described[526]. Immunohistochemical staining demonstrated variable mitochondrial staining of a range of primary human breast cancer tissues[3, 521], indicating differences in mitochondrial biogenesis and therefore content.

A reduced mitochondrial content was observed in carcinomas of the liver[527]. In hypoxic tumours, activation of HIF-1 induced Mxi-1, a c-Myc repressor protein resulting in reduced mitochondrial biogenesis[526, 528]. In pancreatic cancer, expression of Ras or activation of the mitogen-activated protein kinase pathway results in Erk2 phosphorylation of DRP1 leading to increased fission[529]. Inhibiting DRP1 phosphorylation in this model prevented tumour growth. Besides oncogene expression, dysregulation of genes involved in mitochondrial function occurs in cancer.

2.5.4.3. mtDNA copy number

Abnormal mtDNA copy number and mutations in both mtDNA and nuclear-encoded mitochondrial genes have been described in cancer studies. Mutations that reduce cytochrome C oxidase activity have been associated with tumours of the breast, colon, pancreas and prostate[324, 530-534]. Similarly, low mtDNA copy number has been associated with cancers of the breast[535], prostate[536] and kidney[537]. In addition, mtDNA mutations have been shown to promote cancer metastasis[538].

2.5.4.4. Cause or effect?

Mitochondrial dysfunction may be either a cause or consequence of tumour development[539]. The protein kinase B (AKT) survival pathway is beneficial to cancer cells and is activated in the presence of mitochondrial respiration defects[482]. Similarly, a respiratory complex 1 deficiency promotes tumourigenesis through activation of the AKT pathway and induction of oxidative stress[540, 541] or inhibition of apoptosis[514]. Depleted mtDNA in C2C12 cells has been shown to cause mitochondrial retrograde signalling and lead to cellular transformation. Cellular morphological changes that are characteristic of tumours were accompanied by an increase in DRP1 localisation to the mitochondria and decreased OPA1 expression resulting in an increase in fragmentation[1]. In addition, either the prevention of fusion or forced fusion may result in reduced respiration and O_2 consumption[474, 475].

2.5.4.5. Apoptosis-related proteins

Apoptosis-associated proteins were also found to influence mitochondrial dynamics in tumours. The apoptotic-resistance protein, survivin is situated in the mitochondrion and is highly expressed in many tumours[542]. In neuroblastoma cells, survivin was shown to recruit DRP1 to the mitochondria and induce fragmentation[543]. The loss of DRP1 has been associated with apoptosis in colon cancer cells[24]. Deregulated expression and phosphorylation of DRP1 and decreased MFN2 leading to increased fission was observed in lung cancer cells[21].

2.5.5. Radiation-induced effects on mitochondrial morphology

As mentioned previously, mitochondrial structural changes in response to radiation, including ultrastructural damage, swelling, vacuolation and fragmentation of the membranes, have been reported[53]. A large proportion of the studies, however, were conducted prior to the identification of specific, reliable mitochondrial morphological stains, which came into use in the 1980s.

Many of these early descriptions of irradiated mitochondria, however, described mitochondrial morphological features, which likely reflect mitochondrial dynamics. For example, morphological changes including, longitudinal branching and the formation of clubbed ends and loops, as well as the observation of enlarged and giant mitochondria may indicate increased fusion[544].

More recent studies described changes in mitochondrial morphology assessed using fluorescence microscopy. In BJ-hTERT fibroblasts and murine mammary gland cells, progressive mitochondrial fragmentation occurred in a dose- and time-dependent manner after irradiation with the greatest fragmentation occurring 3 days post-irradiation in fibroblasts[57, 60]. Similarly, cytoplasmic microbeam irradiation using high linear energy transfer (LET) particles led to increased fission[43, 44]. UV-irradiation and irradiation using green light (0.3 J/cm^2) emitted by a microscope mercury lamp, also resulted in fragmentation, as well as perinuclear collapse of the mitochondria[219, 221, 449]. Mitochondrial movement and DRP1 translocation to the mitochondria was also shown to be stimulated after irradiation[57].

Changes to mitochondria may not only be the result of direct irradiation. Evidence of a bystander effect comes from studies using conditioned medium from previously irradiated immortalised keratinocytes. An increase in mitochondrial mass and perinuclear localisation was observed following incubation in medium from cells irradiated with 0.5 Gy. Interestingly, these changes were not observed using the higher radiation dose of 5 Gy[545].

Alterations in functionality were not consistently associated with changes in morphology. Despite an increase in ΔΨm and ATP levels, irradiated (4 Gy) glioblastoma cells did not show an increase in mitochondrial mass[40]. Notably, changes in mitochondria after irradiation have been reported to be reversible[60].

In addition, upregulation of mitochondrial biogenesis[42, 59] and increases in mtDNA copy number[54] after irradiation have been reported. An augmented oncocytic phenotype, characterised by increased mitochondrial biogenesis, and large, irregular mitochondria in patient rectal adenocarcinoma samples after radiochemotherapy was observed[546].

2.5.6. Targeting mitochondria for cancer therapy

Poor response of cancer cells to many current targeted agents has prompted the development of drugs that target alternate pathways[8, 547]. Mitochondria may provide such novel targets for cytotoxic therapy or modulation of other agents.

2.5.6.1. Mitochondrial targeted agents

The differences between tumour and normal cell mitochondria may provide an opportunity to increase selectivity and reduce side effects of cancer therapy. While current targeted therapies tend to be highly pathway-specific, diverse tumour heterogeneity may be more substantially addressed using therapies that target mitochondria[548, 549].

The mitocans are a class of therapeutic agents that result in destabilisation of mitochondrial function and can be regarded as mitochondrial poisons[7]. Eight distinct classes of mitocans have been proposed[8], which include; Hexokinase II inhibitors e.g. 2-deoxyglucose[10]; BH3 mimetics e.g. gossypol[9]; thiol redox inhibitors e.g. arsenic trioxide or isothiocyanates, e.g. phenylethyl isothiocyanate[11]; VDAC/ANT targeting e.g. ionidamine[12]; ETC-targeting e.g. tamoxifen[550] and α-tocopheryl succinate (α-TOS)[551]; lipophilic cations targeting the mitochondrial inner membrane e.g. rhodamine-123[552]; drugs targeting the citric acid cycle e.g. dichloroacetate[553] and those that target mtDNA e.g. vitamin K3[13]. A number of chemotherapeutic agents have been shown to damage mtDNA, including cisplatin, doxorubicin and DNA damaging anthracycline derivatives.

Certain antibiotics, such as the aminoglycosides, target bacterial ribosomes and can be regarded as tissue-specific mitochondrial poisons. It is thought that the cochlea is particularly sensitive to reduced mitochondrial function as these antibiotics can cause ototoxicity[554]. The similarity between bacteria and mitochondria (endosymbiotic theory) may partly account for the off-target effects on mitochondria and toxicity. Mutations in mtDNA, e.g. the 12S rRNA gene[555], which increases structural similarity between bacteria and mitochondria, have been shown to increase susceptibility to aminoglycoside toxicity[554, 556].

In general, mitocans act by disrupting mitochondrial function, which leads to apoptosis[8]. It is possible that, in general, the toxicity induced by agents that target mitochondria occurs as a result of increased oxidative stress. This mechanism has been reported for the induction of apoptosis by α-TOS[557] and aminoglycoside ototoxicity[558], among others. Cancer cells may be specifically vulnerable to drugs that cause higher intrinsic levels of ROS as these cells often have elevated base-line ROS levels[311].

2.5.7. Modulators of mitochondrial dynamics

The morphological make-up of the mitochondrion is the net result of fission and fusion processes in the cell in response to intra- and extracellular conditions and stimuli. Mitochondrial morphology therefore, not only reflects the physical connectedness of the mitochondria, but is also an indication of cellular function. In addition, modulation of mitochondrial morphology has the potential to influence cellular functioning, for example, by altering bioenergetic capacity or redox status.

Modulation of mitochondrial dynamics is a relatively new area of study and few agents have been identified that specifically regulate fission and fusion proteins. The inhibition of DRP1 has been accomplished most successfully using the mitochondrial division inhibitor, Mdivi-1[559]. A number of other inhibitors of DRP1 or mitochondrial fission have also been investigated. These include, Mdivi-1 analogues[560, 561], calcineurin[562, 563], overexpression of dominant-negative (K38A) Drp1 [22, 564] and P110, a molecule that primarily prevents the interaction between DRP1 and Fis1[437].

Indirect inhibition of mitochondrial fusion and fission has been accomplished using siRNA-mediated knockdown of fission and fusion proteins including DRP1, Fis1, MFN1 and 2 and OPA1. Mitochondrial morphology can also be altered by stress[565], hypoxia[566, 567] and certain respiratory inhibitors[568], among others, which are however, non-specific and often toxic, thus limiting their application.

2.5.7.1. Mitochondrial division inhibitor-1 (Mdivi-1)

Mdivi-1 (3-(2,4-dichloro-5-methoxyphenyl)-2-sulfanyl-4(3H)-quinazolinone) is a quinazolinone compound (Figure 2.11), which was first described by Cassidy-Stone et al. (2008)[559]. This compound prevents polymerisation of the mitochondrial DRP1 subunits into a spiralled filament that is necessary for mitochondrial fragmentation. Mdivi-1 is therefore a useful tool for modulation of mitochondrial morphology and examination of the effects of inhibition of fission on cellular responses.

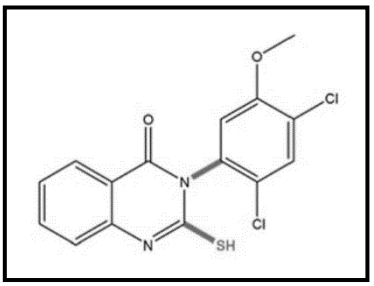

Figure 2.11. Chemical structure of Mdivi-1
[From Cassidy-Stone et al. (2008)[559], used with permission].

2.5.8. Cellular responses to Mdivi-1

2.5.8.1. Effects on mitosis and the cell cycle

A number of studies have identified Mdivi-1-related cell cycle effects and specific abnormalities in mitosis[21, 144, 466, 507, 569-573]. Cyclin E levels became elevated in normal NRK cells and colon cancer cells after short Mdivi-1 exposures with a concomitant increase in S-phase cells[144]. The same authors described mis-alignment of chromosomes during metaphase in colon cancer cells treated with Mdivi-1. In contrast, Mdivi-1 inhibition of mitochondrial dynamics in artery smooth muscle cells led to a decrease in S-phase cells and an increased G0/G1 population, possibly indicating a G1 arrest[507]. However, this study used a longer (48 h) Mdivi-1 treatment than that described above. Cells previously arrested in S-phase may have been released and contribute to the increase in the G1 population. Consistent with these results, 48 h of hyperfusion induced by overexpression of DRP1 also resulted in a decrease in cell cycle progression[144]. In a study by Wang et al. (2015)[573], an increase in the G2/M population of cells after 30 µM Mdivi-1 treatment was reported for cancer cells, however, normal dermal fibroblasts did not display a G2/M arrest.

Mdivi-1 prevents the inactivation of Cdk1, an important cell cycle regulatory protein, by cyclin B1 degradation[571]. In association with cyclin B, Cdk1 controls the G2/M transition, allowing entry of cells into mitosis[574, 575]. Cdk1 partly facilitates this transition by upregulating mitochondrial respiration thereby ensuring sufficient energy for cell cycle progression[143]. Initiation of DNA replication, and therefore S-phase transition, has also been linked to Cdk1, particularly in cells lacking Cdk2[576].

Related to this, modulation of the centrosome cycle, in particular centrosome duplication[576] and separation[577, 578] and spindle formation[355], have also been linked to Cdk1 activity. In addition, chromosome condensation and separation of chromosomes after alignment at the metaphase plate relies on inactivation of Cdk1[579, 580]. Cdk1 also regulates mitotic microtubule dynamics, which are related to chromosome separation[581].

2.5.8.2. Cytotoxic effects of Mdivi-1

Direct cytotoxic effects of Mdivi-1 have been reported for both cancer and normal cells. Increased cell death was observed in colon cancer cells with 50 µM Mdivi-1 treatments longer than 5 hours[144]. Similarly, knockdown of DRP1 led to increased apoptosis in colon cancer cells and Mdivi-1 was suggested to be useful as a chemotherapeutic agent in colon cancer[24]. A549 lung cancer cells treated with Mdivi-1 showed reduced proliferation and increased apoptosis[21, 23, 582].

Similarly, decreased survival after Mdivi-1 treatment of breast (MDA-MB-231 and MCF7) and ovarian cancer cells (A2780), among others, was observed[25, 573, 582, 583]. However, reported results for cancer cells are variable. For example, no Mdivi-1 toxicity was reported in HL-60 leukaemia cells[584], however, limited effects were demonstrated in A549 lung cancer, melanoma and osteosarcoma cells[468].

There is some evidence of Mdivi-1-induced effects in normal cells. Mdivi-1 reduced survival of small airway epithelial cells using doses greater than 50 µM for 6 h or 30 µM for 12 h[353]. Apoptosis was observed in mouse embryonic fibroblasts treated with Mdivi-1[469, 585]. In addition, toxicity was induced in hippocampal and primary neurons with concentrations above 75 and 25 µM, respectively[441]. Primary myoblasts and C2C12 cells also showed increased apoptosis after Mdivi-1 treatment[22].

There are a number of studies, however, reporting no Mdivi-1 toxicity in normal cells. The cell types include vascular smooth muscle cells (VSMC)[586], SH-SY-5Y cells[587], BV-2 cells[588], rat aortic VSMC[569], spinal cord neurons[589, 590] and hESC-human embryonic stem cell-derived neurons[591]. Some of the studies used low doses (1 - 25 µM) or short Mdivi-1 exposures (15 minutes - 1 hour). However, minimal toxicity was demonstrated in normal dermal fibroblast cells and melanocytes, even using a higher dose of 50 µM[468, 583].

Additional effects of Mdivi-1 include increased function, reduced mobility and transformation potential in a range of models. Mdivi-1 enhanced functional recovery after traumatic brain injury in mice[592]. Reduced migration of MDA-MB-436 and -231 breast cancer cells[593] and mtDNA-depleted C2C12 myocytes[1], as well as, attenuated migration of glioblastoma cells[564] was shown with Mdivi-1. Despite having only a minimal effect on apoptosis in normal and transformed cells, Mdivi-1 prevented E1A+RAS^{G12V}-mediated transformation and reduced clonogenic survival, as well as, SV-40-mediated transformation of mouse embryonic fibroblasts[469].

2.5.9. Mdivi-1 as a modulator of cytotoxic agents

The frequently observed association between mitochondrial fragmentation and apoptosis[15, 19, 20] suggests that inhibition of mitochondrial fission may be protective after cellular injury under certain circumstances. Mdivi-1 was found to prevent STS-induced apoptosis as well as Bax-dependent cytochrome C release from isolated mitochondria[559].

Protection by Mdivi-1 against cytotoxic challenge has been demonstrated in a number of *in vitro* and *in vivo* models. Mdivi-1 was found to reduce or abolish drug-induced cytotoxicity in human ovarian[594, 595], lung[596] and breast[597] cancer cell lines as well as a rat astrocytoma cell line[598]. The growth of brain tumour initiating cells (BTIC) from glioblastoma patients in a mouse model was inhibited using Mdivi-1 and survival of mice was increased. In addition, Mdivi-1 induced apoptosis in BTIC cells but not in non-BTIC cells[599]. Non-tumorigenic cells were similarly protected against cytotoxic agents.

Protection against ischaemia-reperfusion injury by Mdivi-1 has also been observed *in vivo* in mammalian heart failure models where reduced cardiotoxicity[584, 600], smaller infarct size[601, 602] and improved function[603] have been described[604].

Pifithrin-μ-[605] and STS-induced[585] cell death were reduced by Mdivi-1 in mouse embryonic fibroblasts but no effect was observed on BH3-induced cell death[585]. Other *in vivo* experiments showed reduced pilocarpine-induced seizures[606, 607] and reduced neuropathic pain[608] in rats. Other systems showing similar responses to Mdivi-1 treatment include reduced renal tubular damage[609], reduced apoptosis in ischaemic retina[610], reduced injury from cerebral ocular occlusion and ischaemic injury[611-613], reduced neuronal injury after acute spinal cord injury[589, 614], reduced infarct size, ischaemia-reperfusion injury and cytotoxicity in neuronal tissue[441, 587, 588, 591, 615, 616].

In contrast to the protective effects detailed above, Mdivi-1 has been shown to enhance the toxic effects of certain cytotoxic agents. Combining Mdivi-1 with a range of chemotherapeutic agents led to increased efficacy of these compounds. Exposure of breast cancer cells to the combination of Mdivi-1 (50 μM) and cisplatin for 2 hours reduced cell number by 70 % when compared to cisplatin alone[582]. The same investigators showed that improved efficacy of a range of chemotherapeutic agents was obtained using extended Mdivi-1 exposure times (20 hours)[582]. In addition, Mdivi-1 exposure enhanced sensitivity to TRAIL-induced apoptosis in cancer cells[23, 583] while sparing normal fibroblasts[23]. Increased loss of ΔΨm and mitochondrial permeability transition pore opening induced by ionomycin was observed in mouse embryonic fibroblasts after Mdivi-1 treatment[26].

2.5.9.1. Does modulation of mitochondrial dynamics affect radiation response?

The Mdivi-1-induced effects on the cellular response to cytotoxic agents described above suggest that modulation of mitochondria dynamics may influence cellular response to other cytotoxic agents, such as radiation. Some evidence exists that directly implicates mitochondrial fission in radiation response.

Apoptosis induced by high radiation doses was shown to be significantly less in both a normal and a colon adenocarcinoma cell line transfected with a mutant form of DRP1 compared to wildtype cells[15].

Radiation-induced apoptosis is an important mechanism that contributes to cellular sensitivity to irradiation. The ability of Mdivi-1 to protect against drug-induced apoptosis and apoptosis induced by hostile environmental conditions, as described above, may suggest potential for radioprotection by Mdivi-1. However, protective effects have generally been observed for low doses of Mdivi-1 or short exposure times. At higher Mdivi-1 concentrations, toxicity was often demonstrated, particularly in cancer cells. Additional cytotoxic effects from Mdivi-1 may contribute to therapeutic efficacy. Synergistic effects of radiation with Mdivi-1 may also be possible.

As described above, Mdivi-1 has been shown to be associated with rapid progression of cells into S-phase[144], a more radioresistant phase of the cell cycle. In addition, as mentioned previously, initiation of DNA replication is associated with Cdk1 activation[576] and Mdivi-1 has been reported to activate Cdk1[571]. Pre-treatment of cells with Mdivi-1 prior to irradiation may therefore be protective. However, diverse roles for Cdk1 and the Cdk1-cyclin B complex have been identified[143], primarily related to progression into mitosis, a radiosensitive phase. Activation of Cdk1 leads to DRP1 phosphorylation (and activation) inducing mitochondrial fragmentation that is characteristic of mitosis[503, 504].

Cyclin B-Cdk1 phosphorylation and activation of respiratory complex 1 with an accompanying increase in ATP production is important for cell cycle progression[143]. This mechanism has recently also been associated with radiation-induced damage repair leading to increased survival[191]. In addition, in the context of radiation-induced DNA damage, Cdk1 phosphorylates mitochondrial p53 thus blocking apoptosis[617, 618]. Active Cdk1, in contrast, phosphorylates BRCA2[619] and 53BP1[617, 620] inhibiting DNA damage repair during G2/M transition. These observations would suggest that Mdivi-1 activation of Cdk1 might sensitise cells to radiation damage by promoting cell cycle progression into mitosis and prevent an efficient DNA damage response although there is evidence that Mdivi-1 can activate ATM pathways[572]. However, Cdk1 is able to phosphorylate and activate MnSOD[618], which would be expected to have a protective effect by reducing radiation-induced ROS. Indeed, MnSOD has been shown to enhance repair of mtDNA[134, 621]. Together, activation of cyclin B-Cdk1 by Mdivi-1 may thus potentially sensitise or protect cells against radiation-induced damage.

2.5.9.2. Evidence for modulation of sensitivity to radiation and other cytotoxic agents by modulation of mitochondrial dynamics

Little is known about the effects of mitochondrial dynamics on radiosensitivity. The mitochondrial morphological status at the time of irradiation may determine either the ability of cells to resist initial damage or respond to damage incurred.

Knockdown of DRP1 expression prior to irradiation of fibroblast cells was shown to reduce the number of ionising radiation-induced DNA double-strand breaks that persisted 3 days after irradiation[58] and prevent radiation-induced fragmentation and loss of $\Delta\Psi m$[57]. In addition, DRP1-deficient cells were demonstrated to be more radioresistant than normal cells[58]. Similarly, knockdown of DRP1 was shown to decrease UV-induced apoptosis in Drosophila embryos[622].

Modulation of fusion and fission proteins has been shown to influence the response of cells to a range of cytotoxic agents. Many of these interactions may potentially be similar to those with ionising radiation. During apoptosis, Bak has been shown to have a role in regulating mitochondrial dynamics through interaction with the mitofusins[623]. Loss of Bak in normal fibroblasts reduced apoptosis induced by STS, cisplatin and azide. In the same study, dominant-negative DRP1 expressed in HeLa cells suppressed apoptosis induced by the cytotoxic treatments. It was also shown that cells containing fragmented mitochondria were more sensitive to MOMP and apoptosis[624]. Overexpression of mitofusins rendered HeLa cells resistant to azide and cisplatin-induced apoptosis[19].

Brief summation

Mitochondria are indispensable for proper cellular functioning and have been proposed as useful targets for cancer therapy. Tumour mitochondria are frequently found to be different both in function and content, which may present an opportunity for therapeutic gain. They have important roles in cell cycle regulation and in the response of cells to damage, particularly in the initiation of apoptosis. Radiation has effects on mitochondrial function and morphology and there is evidence that inherent mitochondrial function may influence cellular radiosensitivity. Mitochondrial dynamics may have roles in many of the abovementioned processes. Mdivi-1, a mitochondrial fission inhibitor, can affect cellular integrity and modulate cellular response. Thus, modulation of fusion and fission proteins may significantly affect cellular response to cytotoxic therapy.

CHAPTER 3

FORMULATION OF HYPOTHESES

Mitochondria are prominent role-players in an array of cellular processes including those involved in the response of cells to radiation. In this study, it was hypothesised that the inherent mitochondrial status may influence cellular radiosensitivity. In addition, we hypothesised that modulation of mitochondrial dynamics may have the potential to alter cellular radiosensitivity. While there is some evidence that mitochondrial dynamics and inherent mitochondrial status, in general, may influence radiation response, the relevance of fusion and fission specifically has yet to be elucidated.

General aims

1) To characterise and correlate the inherent radiation responsiveness and certain mitochondrial characteristics of a range of cancer cell lines

2) To modulate mitochondrial dynamics and investigate the influence thereof on radiation response

3) To investigate the effects of Mdivi-1 that may be associated with modulation of radiation response

Research Questions

3.1. Is the radiation responsiveness of cancer cells associated with mitochondrial morphology or function?

We sought to determine the role of mitochondrial dynamics in the radiation responsiveness of cancer cells and examined correlations between mitochondrial status, including morphological and functional features, and inherent radiation sensitivity. It was hypothesised that the extent of mitochondrial fragmentation would correlate with radiation responsiveness. In addition, mitochondrial function was hypothesised to correlate with radiation responsiveness.

3.2. Does modulation of mitochondrial dynamics influence cellular integrity or response to radiation?

Modulation of mitochondrial dynamics using an inhibitor of mitochondrial fission, Mdivi-1, was used to investigate the role of mitochondrial dynamics in cellular radiation response. It has been reported that apoptosis is associated with DRP1-mediated mitochondrial fragmentation[503, 504] and mutant DRP1 protected cells from apoptosis induced by cytotoxic agents[15]. It was therefore initially hypothesised that increased fusion would protect cells against radiation-induced cell death.

3.2.1. Does Mdivi-1 induce mitochondrial fusion?

Mdivi-1 has previously been demonstrated to inhibit mitochondrial fission[559] and it was hypothesised that Mdivi-1 would increase fusion in our cancer cell lines.

3.2.2. Does inhibition of mitochondrial fission alter survival of cancer cells?

Having demonstrated inhibition of fission by Mdivi-1 in the experimental model used, the consequences of these effects were examined. Given that disruption of mitochondrial dynamics affects cellular physiology, it was hypothesised that Mdivi-1 would be cytotoxic.

3.2.3. Does inhibition of mitochondrial fission influence radiation survival of cancer cells?

Mdivi-1 has been reported to display both protective[595-597] and sensitising[23, 582, 583] effects when combined with cytotoxic agents. It was therefore hypothesised that Mdivi-1 would similarly modulate radiation sensitivity.

3.2.4. Does inhibition of mitochondrial fission influence repair of radiation-induced damage?

Radiation treatment seeks to exploit differences in repair capacity between tumour and normal tissue. It is therefore important to establish the influence of inhibition of fission on cellular repair capability in the event that such approaches are applied clinically. It was hypothesised that Mdivi-1 would alter sub-lethal or potentially-lethal damage repair.

3.2.5. Does inhibition of mitochondrial fission influence cell cycle dynamics and/or radiation-induced cell cycle arrest in cancer cells?

Given the reported cyclical nature of mitochondrial fragmentation during the cell cycle[371, 503], it was hypothesised that Mdivi-1 would influence cell cycle dynamics in our model. Specifically, a G2/M arrest was hypothesised as mitochondrial fission, which is inhibited by Mdivi-1, is typically required for distribution of mitochondria to daughter cells during mitosis. Similarly, it was hypothesised that the presence of Mdivi-1 would influence the radiation-induced cell cycle arrest.

3.3. How does Mdivi-1 alter radiation response?

In our investigations, it was found that Mdivi-1 had cytotoxic and radiosensitising properties. Further investigations of Mdivi-1 effects on specific processes that may be related to radiation response were therefore undertaken to provide mechanistic insight. Certain processes known to be involved in radiation response include apoptosis, cytogenetic damage-induction and cell cycle delay and therefore we investigated these aspects.

3.3.1. Does Mdivi-1 delay cells in mitosis?

Mitochondrial fragmentation is required for mitosis and therefore prolonged inhibition of fission may affect cell proliferation and division. Cell cycle analysis of cells exposed to Mdivi-1 showed a G2/M arrest and suggested an effect of Mdivi-1 on the passage of cells through mitosis. In addition, misalignment of mitotic chromosomes has been reported as a consequence of Mdivi-1 treatment[144]. It was thus hypothesised that Mdivi-1 would arrest cells in mitosis.

3.3.2. Does Mdivi-1 influence the level of mitosis after irradiation?

Having demonstrated an Mdivi-1-induced mitotic arrest, it was hypothesised that the proportion of mitotic cells would be altered when Mdivi-1 was combined with radiation, which induces a G2/M arrest.

3.3.3. Does Mdivi-1 cause apoptosis in cancer cells?

It was established in initial experiments that Mdivi-1 reduced clonogenic survival. Since apoptosis frequently contributes to cell death after exposure to cytotoxic agents, it was hypothesised that Mdivi-1 would cause an increase in apoptosis.

3.3.4. Does Mdivi-1 modulate radiation-induced apoptosis in cancer cells?

Mdivi-1 has been reported to modulate apoptosis induced by adverse cellular conditions and cytotoxic agents. It was hypothesised that Mdivi-1 would modulate radiation-induced apoptosis.

3.3.5. Does Mdivi-1 induce cytogenetic damage?

Chromosomal aberrations induced by Mdivi-1 have been reported in other studies[466, 572, 573].
In addition, the observation that Mdivi-1 results in a cell cycle delay and cell death suggests that significant damage to the cell has occurred. Thus, it was hypothesised that Mdivi-1 treatment would result in cytogenetic damage.

3.3.6. Does Mdivi-1 modulate the induction of radiation-induced cytogenetic damage?

Micronuclei induction, as a result of chromosomal breaks, is a consequence of radiation treatment. It was hypothesised that Mdivi-1 treatment, which was demonstrated to induce cytogenetic damage alone, would augment the cytogenetic damage induced by radiation.

CHAPTER 4

MITOCHONDRIAL MORPHOLOGICAL AND FUNCTIONAL STATUS IN CANCER CELLS AND RADIATION RESPONSE

Mitochondrial dysfunction has been implicated in cancer initiation and growth and may be involved in therapeutic response. Radiation sensitivity is determined by an array of biological and environmental factors many of which are associated with mitochondrial function.

Studies into the role of inherent mitochondrial status in radiation response are lacking and additional research is required. We postulated that the morphological classification of mitochondria according to their fragmentation status, and specific parameters of mitochondrial function are associated with inherent radiosensitivity.

In this chapter, the radiation response of several cancer cell lines is correlated with mitochondrial morphology and functional measures of inherent mitochondrial activity, including respiration and mitochondrial membrane potential.

4.1. Aim and objectives

To identify potential correlations between the inherent radiation-responsiveness of selected cancer cell lines and their mitochondrial morphological and functional characteristics.

The specific objectives include:

a) To determine the inherent radiation-responsiveness of a selection of established tumour cell lines representing a range of different cancer types
b) To characterise the mitochondrial morphological characteristics of a subset of these cell lines
c) To determine the relative mitochondrial membrane potential in each of the selected cells lines
d) To determine the inherent respiratory capability of each cell line
e) To determine whether the inherent radiation-responsiveness of these tumour cell lines is associated with mitochondrial status.

4.2. Methods

4.2.1. Cancer cell lines

A selection of available tumour cell lines, described in detail in Appendix A and listed in Table 4.1, were characterised according to their radiosensitivity and mitochondrial status. Cells were cultured in the appropriate culture medium for each cell type supplemented with 10 % fetal calf serum (FCS) and antibiotics (AB) and were incubated under standard culture conditions of 37°C, 100 % humidity and 5 % CO_2/95 % O_2 (please see Appendix A for full details).

Table 4.1. Cancer cell lines selected for characterisation of inherent radiosensitivity

Cell Line	Tumour cell type
A549	Lung adenocarcinoma
T47D	Breast ductal carcinoma
U937	Leukemic monocyte lymphoma
MDA-MB-231	Breast adenocarcinoma
DU145	Prostate carcinoma
HeLa	Cervical carcinoma

4.2.2. Cellular radiation responsiveness

4.2.2.1. Clonogenic cell survival assay

The surviving fraction after irradiation of the adherent A549, MDA-MB-231, T47D, DU145 and HeLa cell lines, was assessed using the clonogenic cell survival assay[235]. Experimental details are provided in Appendix B1. The survival curves for each cell line were determined for doses ranging from 1 to 10 Gy ^{60}Co γ-radiation. Unirradiated controls were mock treated. The radiation setup is shown in Appendix B2. Cells were irradiated in culture medium with full build-up at a dose rate of approximately 1 Gy/min. At the end of the assessment period, cell survival was determined by the number of colonies containing more than 50 cells. At least two separate experiments were performed for clonogenic assays.

For the U937 suspension cell line, the clonogenic assay was modified because these cells do not form adherent colonies. These cells were plated into culture medium containing agarose which provided a semi-solid matrix for colony formation (Appendix B1.2). Colonies were assessed microscopically using a grid for orientation and the number of colonies, representing more than 50 cells was determined.

4.2.2.2. Data processing and analysis

Data from the clonogenic assays was used to construct survival curves followed by derivation of certain parameters of radiation response, namely SF4, SF2, $\bar{D}$, alpha (α) and D_{10}, as defined in Chapter 2.

The surviving fraction (S) was determined according to the equation,

S = colonies counted / (cells plated x PE)

Where plating efficiency (PE) = colonies counted/cells plated in untreated cells.

Radiation survival curves were constructed using the GraphPad Prism software v6.05 (GraphPad Software, Inc. San Diego, California). Survival curves were fitted to the data according to the Linear Quadratic model using the equation,

$$S = e^{-(\alpha D+\beta D^2)}$$

where D represents dose, and α and β are constants relating to the contribution of non-repairable and repairable damage, respectively.

Values for SF2 and SF4 were determined from surviving fractions after 2 and 4 Gy, respectively. The α and D_{10} values were determined from the fitted curves. In addition, the mean inactivation dose, $\bar{D}$, was approximated by calculating the area under the curve for the region 0-6 Gy using the midpoint method.

4.2.3. Characterisation of mitochondrial morphology

4.2.3.1. MitoTracker® Red staining protocol

Mitochondria were stained using the fluorescent dye, MitoTracker® Red CMXRos (Molecular Probes® Inc., Invitrogen, Carlsbad, CA, USA) in live cells. The dye diffuses through the plasma membrane and accumulates in actively respiring mitochondria. MitoTracker® Red reacts with protein surface thiols and is maintained within mitochondria after fixation and permeabilisation of cells[379, 464].

The six cell lines described above were divided into three groups on the basis of their response to radiation (section 4.3.1). One cell line from each group was selected for evaluation of mitochondrial morphology. For analysis, cells were kept under physiological conditions before being stained with MitoTracker® Red and the morphology was assessed microscopically.

The MitoTracker® Red staining protocol is detailed in Appendix C1. Briefly, cells were plated onto glass coverslips and incubated overnight for cells to adhere. The following day cells were stained with MitoTracker® Red at 37°C, washed and then either fixed for scoring or mounted immediately for live cell imaging using glycerol mounting medium as an antifade agent (Appendix D). Fixed cells were stored at 4°C until visualisation.

Representative samples from each cell line were assessed using live cell imaging to confirm that live and fixed cells had comparable mitochondrial morphology (Appendix C2.1). Cells were maintained at 37°C in the appropriate culture medium before visualisation and were observed promptly within 10 minutes of mounting. Noticeable signs of deterioration, such as swollen mitochondria, defined previously[567] were only evident after 30 minutes.

In addition, A549 cells were transfected with a red fluorescent protein construct to allow visualisation of mitochondria (CellLight® Mitochondria-RFP, BacMam 2.0; Molecular Probes Inc). To confirm that MitoTracker® Red did not induce obvious morphological changes, the mitochondrial morphologies were compared (Appendix C2.2). The transfection method was not used generally for mitochondrial classification in experiments due to sub-total transfection rates and dilution of the proportion of labelled cells with cell division. The use of MitoTracker® Red was selected as the method of choice.

4.2.3.2. Visualisation and scoring of morphological subtypes

Microscopic visualisation of mitochondria stained with MitoTracker® Red (ex: 579 nm, em: 599 nm) was carried out with a BX41 Olympus fluorescence microscope (Olympus, Shinjuku-ku, Tokyo, Japan) using the Olympus WG (green light) filter. Samples were observed at 1000x magnification using the MPLAPON-Oil Plan Apochromat oil immersion objective (Olympus). A detailed description can be found in Appendix D.

Mitochondrial morphology was classified using adaptations of the methods used by Margineantu et al. (2002)[625] and Lutz et al. (2009)[626]. Cells were assessed manually. Criteria for classification, as shown in Table 4.2, were similar to those used in previously published studies.

Table 4.2. Morphological categories used for scoring the mitochondrial population in each cell line

Morphological category	Description	Examples described in the literature
Predominantly fused		
Filamentous	Thin, interconnected filaments, reticular	Margineantu et al. 2002[625]; Taguchi et al. 2007[504], Das et al. 2012[627]; Chen et al. 2003[389]; Barni et al. 1996[628]; Ishihara et al. 2006[629]; Park et al. 2008[630]; Brooks et al. 2007[623]; McCarron et al. 2013[565]; Plecita-Hlavata et al. 2008[476]; Jendrach et al. 2008[631]; Duvezin-Caubet et al. 2006[411]; Winter et al. 2008[632]
Transitional	A combination of long filaments with a few short tubules	Margineantu et al. 2002[625]; Ishihara et al. 2006[629]; Benard and Rossignol 2008[366]; Jendrach et al. 2008[631]; Duvezin-Caubet et al. 2006[411]; Winter et al. 2008[632]; Lee et al. 2007[502]
Enlarged	Enlarged or augmented filaments (often accompanied by a few oval structures)	Das et al. 2012[627]; Mattiolo et al. 2014[605]; Rossignol et al. 2004[485]; Plecita-Hlavata et al. 2008[476]; Mai et al. 2010[449]; Chiche et al. 2010[419]
Predominantly fragmented		
Ovoid	Enlarged, round or oval structures	Liu and Hajnocsky 2011[567]; Benard et al. 2007[474]; Chen et al. 2003[389]; Brooks et al. 2007[623]; McCarron et al. 2013[565]; Jendrach et al. 2008[631]
Fragmented	Short, separated tubules or small bright speckles	Margineantu et al. 2002[625]; Chen et al. 2003[418]; Das et al. 2012[627]; Mattiolo et al. 2014[605]; Ishihara et al. 2006[629]; Brooks et al. 2007[623]; Jendrach et al. 2008[631]; Duvezin-Caubet et al. 2006[411]; Winter et al. 2008[632]; Yu et al. 2005[633]

Ultimately, cells were divided into *predominantly fused* and *predominantly fragmented* categories. To increase objectivity, cells were first allocated to one of the five defined descriptive morphologies. The *filamentous*, *transitional* and *enlarged* sub-groups were combined to form the *predominantly fused* category while the *predominantly fragmented* category included the *ovoid* and *fragmented* sub-groups. At least 200 cells per slide (n = 5) were scored. Representative images of the morphological categories are shown in Figure 4.1 and Appendix E.

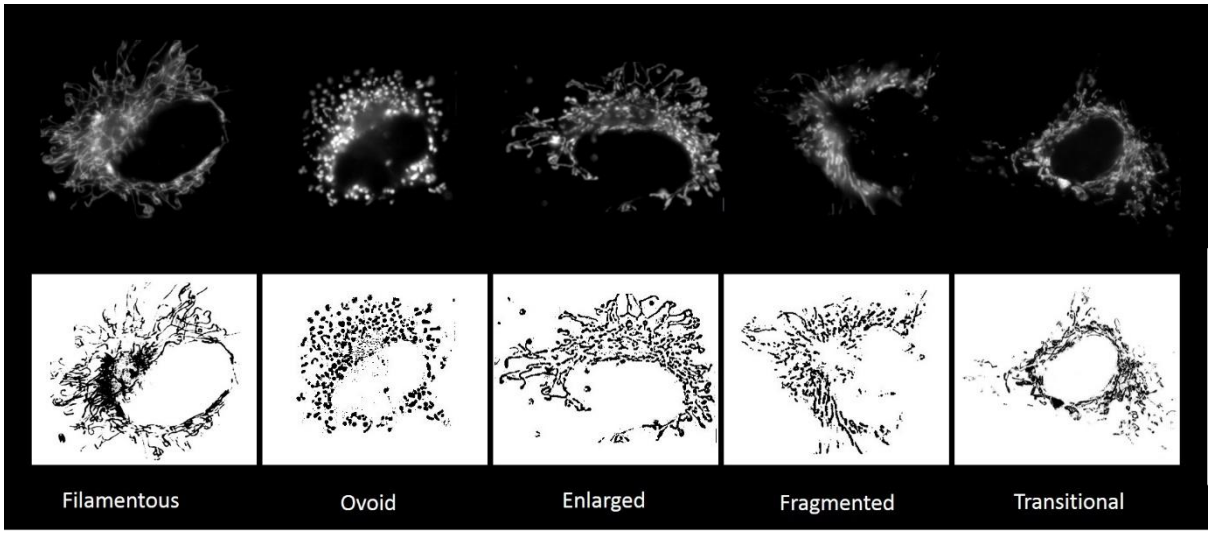

Figure 4.1. Representative images of the different morphological sub-groups. The lower panels represent contrast enhanced versions of each of the images created using Image J (NIH)[634] to highlight differences for demonstration purposes only and were not used for scoring. A 5x5 spatial convolution filter was applied to enhance edges of the image followed by binarisation.

4.2.4. Mitochondrial membrane potential

4.2.4.1. JC-1 assay

As described in Chapter 2, JC-1 is a ratiometric dye and the red to green (R:G) fluorescence ratio is an indication of $\Delta\Psi m$[347]. The red fluorescence value (j-aggregate formation), may also be used independently as a measure of mitochondrial function[346, 349]. Both R:G ratio and j-aggregate formation were determined in experiments using fluorescence cytometry[635].

Characterisation of $\Delta\Psi m$ was carried out in all cell lines selected for sub-analysis (A549, T47D, DU145 and U937). Comprehensive methodology can be found in Appendix C3. Briefly, exponentially growing cells from each cell line were stained with JC-1 dye for 15 minutes under physiological conditions and images of cells were captured for analysis using fluorescence microscopy (Appendix D). Samples were stained and imaged in suspension. A sample from each cell type was processed concurrently to ensure comparative staining conditions. Images were acquired using identical camera settings.

4.2.4.2. Validation of the JC-1 assay in selected cell lines

To confirm that the JC-1 assay was able to detect differences in ΔΨm in our cells, mitochondrial depolarisation was induced using sodium azide, a mitochondrial inhibitor[636, 637], in each cell line. Briefly, cells were incubated in 20 mM sodium azide (Sigma-Aldrich, St. Louis, Mo, USA) for 1 to 2 hours, depending on the cell line, prior to staining with JC-1. Observation and image analysis of unstained cells from each cell line indicated the absence of cellular autofluorescence. In addition, a sample from each cell line was evaluated using the trypan blue viability assay (Appendix A2.3) to confirm that loss of ΔΨm was not attributed to cell death.

4.2.4.3. Visualisation of cells and image acquisition

Prepared samples, which were kept in the dark, were imaged within 20 minutes of mounting. Samples were visualised using a BX41 Olympus fluorescence microscope (Olympus). The green fluorescence, of the monomeric JC-1 units, and the red fluorescence, of JC-1 aggregates, were imaged using the Olympus WB filter (max ex: 488 nm) and the Olympus WG filter (max ex: 590 nm), respectively (Appendix D, Table D1). Images for quantification were obtained using the UPlanFl 40x/0.75 objective (Olympus). In addition, a subset of samples were imaged with the UPlanFl 100x/1.30 oil immersion objective (Olympus) to document differences in JC-1 aggregate distribution within the mitochondria of individual cells and between cell types.

Images for analysis of ΔΨm were captured using a Canon EOS 1000D colour camera (Canon Inc. Tokyo, Japan) mounted onto the microscope with a MDSLR-BX 1.38x Widefield T-mount adapter for Olympus BX (Martin Microscope Company, Easley, USA). Camera exposure and illumination settings were kept constant between images and the aperture was fixed. The exposure time was set to 0.3s (1/3) and the ISO setting was 400 for green fluorescence capture and 100 for red fluorescence imaging. The green fluorescence capture is more sensitive because of the lower intensity of the monomeric form of the JC-1 stain.

Care was taken to prevent unnecessary exposure of the slide to fluorescent light prior to image acquisition. Once positioning and focus had been set, the image was captured immediately following illumination of the field to avoid bleaching. RAW image files (.CR2) were converted to "Tagged Image File Format" (.tiff) using Digital Photo Professional v3.4 for compatibility with Image J.

4.2.4.4. Quantification of mitochondrial membrane potential

Quantification of the green and red fluorescence intensity was carried out by measuring the mean grey value per cell using the image analysis application, Image J v1.48 (NIH)[634] (Appendix C3.2). All values were corrected for background staining by subtracting the average grey value for five random regions containing no cells. The fluorescence intensity for both the red and green channels was determined for a minimum of 200 cells per sample (n = 3). The R:G fluorescence ratio per cell was calculated to determine the ΔΨm spectrum for each cell line.

4.2.5. Mitochondrial respiratory capacity

The decrease in oxygen concentration in a closed system was used as a measure of cellular respiration. Differences in mitochondrial oxygen consumption can be determined by uncoupling OXPHOS from ATP-synthesis, depolarising the inner mitochondrial membrane and by inhibiting complexes of the electron transport chain with specific mitochondrial inhibitors and uncouplers. The relative O_2 consumption rates under these conditions provide a measure of both the maximal and physiological function of mitochondria in a population of cells.

4.2.5.1. High resolution respirometry

Preparation of cells for high resolution respirometry is detailed in Appendix G. Cellular oxygen consumption rates were determined using the OROBOROS Oxygraph-2k for high resolution respirometry (OROBOROS Instruments corp. Innsbruck, Austria). Prior to data collection, the oxygen sensor was calibrated using solutions of known oxygen partial pressures. For experiments, polarographic measurements were taken of intact cells in suspension at a density of 0.8 million cells/ml. Cells were continuously stirred in a chamber containing 2 ml of the appropriate cell culture medium at 37°C. Care was taken when inserting the stopper to ensure elimination of air bubbles. Samples were initially aerated to approximately 200 µM oxygen at 102 kPa barometric pressure by allowing 2 minutes of contact with air for oxygenation under agitation. In addition, a sample from each cell line was evaluated using the trypan blue viability assay (Appendix A2.3) both before and after oxygraph analysis to confirm the integrity of the cells assessed.

4.2.5.2. Phosphorylation control protocol

The phosphorylation control protocol for OXPHOS analysis provided a method for determining the general, *ROUTINE* state respiration of the cells under physiological conditions as well as specific parameters of mitochondrial function in each cell line. These included *LEAK* state respiration, which is a measure of O_2 consumption independent of ATP synthesis; *ETS* uncoupled state respiration, which determines the maximal capacity of the mitochondria for respiration and *ROX* respiration state, which denotes the cellular O_2 consumption independent of mitochondrial utilisation.

Initial measurements of O_2 flux denote ROUTINE respiration supported by exogenous substrates in the cell culture medium. Each subsequent respiratory state was induced by administration of either a mitochondrial inhibitor or uncoupler that did not require permeabilisation of cell membranes. Addition of an ATP-synthase inhibitor, oligomycin (1 µl; 2.5 µM), allowed determination of LEAK state respiration. Stabilisation of this state was restricted to 5 minutes. The subsequent, step-wise, titration of an uncoupler, FCCP [carbonyl cyanide-4-(trifluoromethoxy) phenylhydrazone] in 4 µl (20 µM) steps increased membrane depolarisation until the maximum ETS capacity was determined. Finally, the addition of a complex I inhibitor, rotenone (1 µl; 0.5 µM) and a complex III inhibitor, antimycin A (1 µl; 2.5 µM), abolished mitochondrial respiration which allowed extra-mitochondrial oxygen consumption (ROX) to be assessed. At each stage, respiratory flux rates were allowed to reach a steady state. Total O_2 consumption (R_{abs}) for each cell line, which is comparable to oxygen consumption rate (OCR), was determined for seven samples while values for additional respiration states were determined in triplicate.

4.2.5.3. Interpretation of respirometry measurements

The polarographic measurements were analysed using Oroboros DatLab 4.3 v6.0.1.7 software. An example of a trace of O_2 consumption for the A549 cell line is given in Figure 4.2. The perpendicular blue markers indicate the time points for addition of respiration inhibitors and uncouplers as described above. The red markers indicate regions of stable flux for each respiratory state measured. Average values for the selected regions are exported from DatLab to the Oxygraph-2k Microsoft Excel 2010 (Microsoft, Redmond, WA, USA) template for analysis. Mitochondrial O_2 flux was corrected for ROX and values were normalised to ETS capacity.

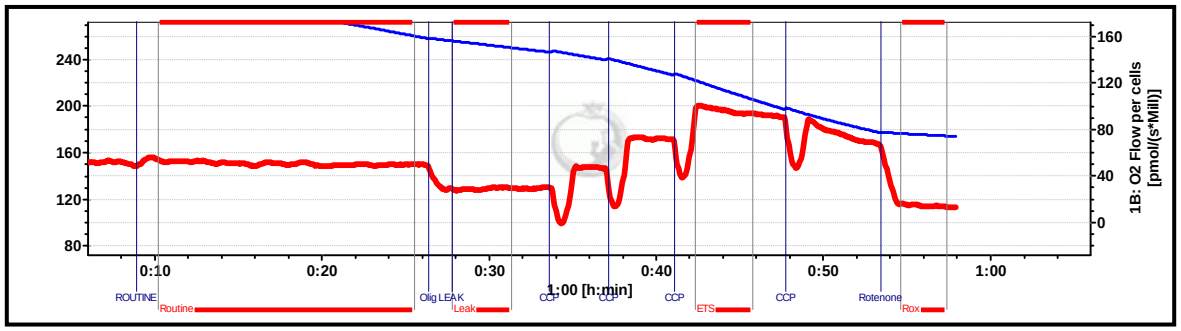

Figure 4.2. O_2 flux over time for a sample of A549 cells showing the regions selected (red bars) for determination of O_2 consumption during different respiration states. Data was sampled every 2s.

4.2.6. Correlation of morphological and functional mitochondrial characteristics with inherent radiation responsiveness

Potential associations between the degree of mitochondrial fragmentation, ΔΨm, cellular O_2 consumption and response to radiation were examined by correlation analysis as described in statistical analyses below.

4.2.7. Statistical analyses

GraphPad PRISM v6.05 (GraphPad software) was used for construction of graphs and for statistical analyses and error bars represent SEM unless otherwise indicated. Groups were considered to be statistically significantly different if a p-value smaller than 0.05 was determined.

Clonogenic survival

Parameters used to describe radiation sensitivity, namely, SF2, SF4, $\bar{D}$, D_{10} and α, were correlated using Pearson's correlation analysis. Linear regression analysis of correlated parameters was conducted using Microsoft Excel 2010 (Microsoft).

Morphology

The fragmentation index from morphological categorisation of the three cell lines was compared using ANOVA with the Fisher's LSD test for multiple comparisons.

ΔΨm

JC-1 ratio and red fluorescence values were evaluated for normality using the D'Agostino-Pearson normality test. Histograms and scatterplots were constructed displaying the distribution of ratio and red and green values, respectively for comparison of untreated and azide-treated samples. The Kruskal-Wallis nonparametric test with Dunn's multiple comparison's test was used for ΔΨm comparisons between cell lines. The range of ΔΨm determined from the fluorescence values calculated for each cell line was represented using box and whisker plots. Regression analyses were performed for median R:G ratio and red fluorescence values.

Respirometry

Oxygen consumption rates and flux control ratios for each of the cell lines were compared using ANOVA with the Fisher's LSD test for multiple comparisons.

Correlation

Radiation responsiveness and mitochondrial characteristics including morphology, ΔΨm and respiration were correlated using Pearson's correlation analysis. Correlation descriptors including the linear correlation coefficient (r) and the coefficient of determination (r^2) were determined. Three groups defining the linear correlation coefficient were identified: weak (r = 0.4-0.59), moderate (r = 0.6-0.79) and strong (r = 0.8-0.99) correlations.

4.3. Results

4.3.1. Inherent radiation responsiveness

The relative response of a range of cancer cell lines to radiation treatment was investigated using clonogenic cell survival assays. Survival curves demonstrating the fraction of cells surviving in the different cell lines with each dose of radiation are shown in Figure 4.3.

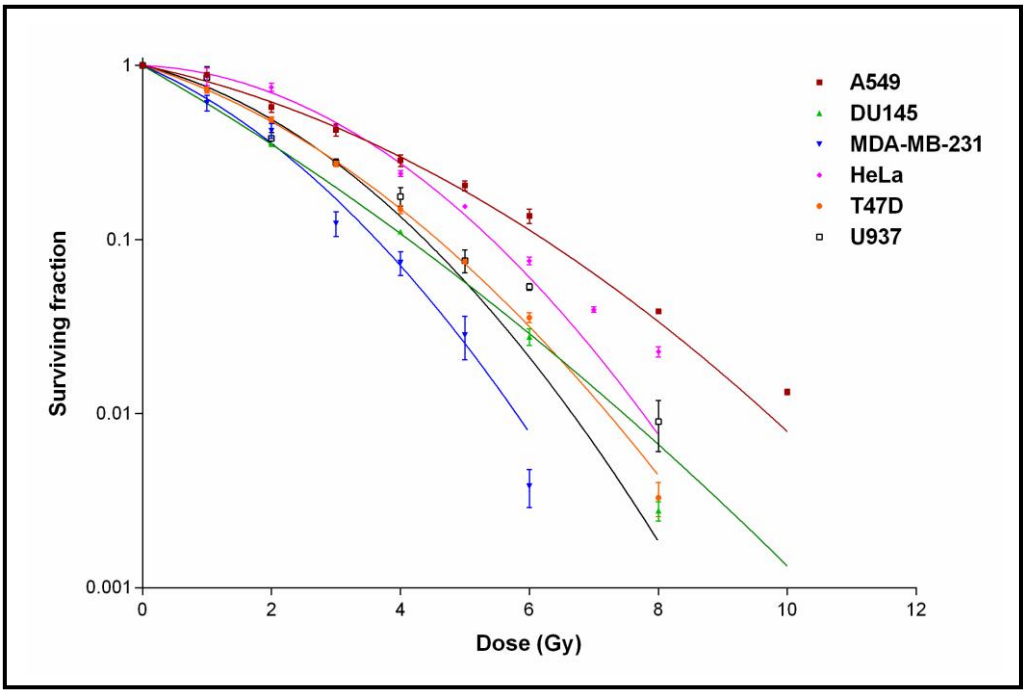

Figure 4.3. Radiation survival curves for six cancer cell lines fitted using the Linear Quadratic equation. Data are shown as mean ± SEM and represent at least 5 replicate samples.

Inherent radiation responsiveness of the cell lines was described in terms of a number of different measures of radiosensitivity, as summarised in Table 4.3. Cell responses represent a spectrum of radiosensitivity as defined by SF2, SF4, D_{10} and $\bar{D}$.

Table 4.3. Cell survival parameters indicating indices of radiation responsiveness. The alpha and beta coefficients, and the R^2 values are derived from the curves fitted using the LQ equation.

	SF2	SF4	$\bar{D}$	D_{10}	α	β	R^2
A549	0.575 ± 0.097	0.284 ± 0.057	2.941	6.2	0.181 ± 0.033	0.03 ± 0.009	0.9919
HeLa	0.749 ± 0.067	0.239 ± 0.015	2.999	5.4	0.037 ± 0.03	0.072 ± 0.009	0.9947
U937	0.381 ± 0.07	0.177 ± 0.047	2.307	4.4	0.212 ± 0.098	0.072 ± 0.037	0.9743
T47D	0.488 ± 0.039	0.149 ± 0.018	2.222	4.6	0.269 ± 0.01	0.051 ± 0.004	0.9997
DU145	0.352 ± 0.023	0.111 ± 0.005	1.954	4.1	0.485 ± 0.008	0.018 ± 0.003	0.99
MDA-MB-231	0.422 ± 0.118	0.074 ± 0.032	1.759	3.6	0.367 ± 0.082	0.074 ± 0.036	0.9908

$\bar{D}$: The area under the curve between 0 and 6 Gy

D_{10}: Dose required to give a surviving fraction of 0.1 according to a best-fit curve

Errors shown are standard deviations

The clonogenic survival assays established the A549 cell line as the most resistant line examined and the MDA-MB-231 cell line as the most sensitive, indicated by SF4 values of 0.28 and 0.074, respectively. A relative change in sensitivity of approximately 1.7 times was found for these cell lines when comparing D_{10} values. As expected, SF4 correlated strongly with $\bar{D}$ ($r^2 = 0.946$; $p = 0.001$) and relative sensitivity at D_{10} ($r^2 = 0.943$; $p = 0.001$). SF2 values were moderately but not significantly correlated with SF4 ($r = 0.713$). Linear quadratic parameters, alpha (α) and beta (β), are included in Table 4.3. Low α values were observed with the more resistant A549 and HeLa cell lines, and higher α values were associated with increasing radiation responsiveness. Alpha values correlated strongly with SF2 ($r = -0.849$; $p = 0.03$) but only moderately with SF4 ($r = -0.794$; $p = 0.06$). The β values did not correlate with any measure of radiosensitivity assessed.

4.3.2. Mitochondrial characteristics

The six cell lines analysed for radiation response were divided into three groups representing low, intermediate and high radiation responsiveness. One cell line from each of these groups, namely A549, T47D and DU145 cells, respectively, was selected for characterisation of mitochondrial status. In addition, the U937 cell line was included for analysis of $\Delta\Psi m$ and O_2 consumption but was excluded from morphological classification because of limitations in visualisation of the morphology of rounded suspension cells.

4.3.2.1. Characterisation of mitochondrial morphology

The range of different morphological subtypes observed for each of the three cell lines is shown in Figure E3 (Appendix E). Each cell line was defined in terms of their mitochondrial phenotype by categorising cells into two morphological groups representing *predominantly fused* and *predominantly fragmented* cells. A graphical representation of the mitochondrial fragmentation index observed for the three cell lines is given in Figure 4.4.

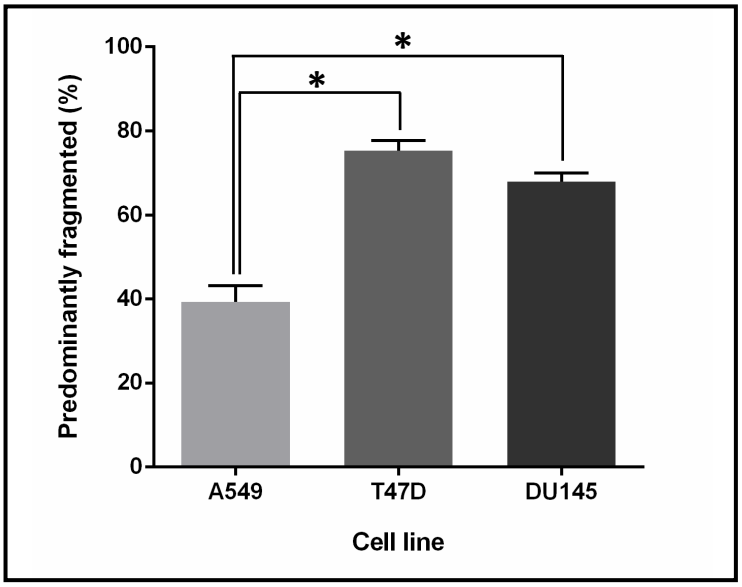

Figure 4.4. The proportion of cells displaying predominantly fragmented mitochondria in three cancer cell lines determined using MitoTracker® Red staining. Data are shown as mean ± SEM and represent 5 replicate samples. *$P < 0.05$.

The A549 cell line displayed the highest level of mitochondrial fusion (60 %) while both the T47D and the DU145 cell lines were predominantly fragmented (> 60 %). The A549 fragmentation index was significantly different from that of the other cell lines ($p < 0.001$) while the more fragmented cell lines were not found to be statistically different from each other.

4.3.2.2. Mitochondrial membrane potential

The ΔΨm of four cancer cell lines was assessed (Figure 4.5). Red:Green (R:G) ratio, as well as, red (j-aggregate) fluorescence values alone were analysed and compared (Figure 4.6A and B). Cell populations reflected similar maximum and minimum red values indicating a comparable range in functionality of mitochondria. In general, ΔΨm values were not considered to be normally distributed as determined using the D'Agostino-Pearson normality test. The median j-aggregate and R:G ratio values correlated strongly ($r^2 = 0.93$, $p = 0.035$) (Figure 4.6C).

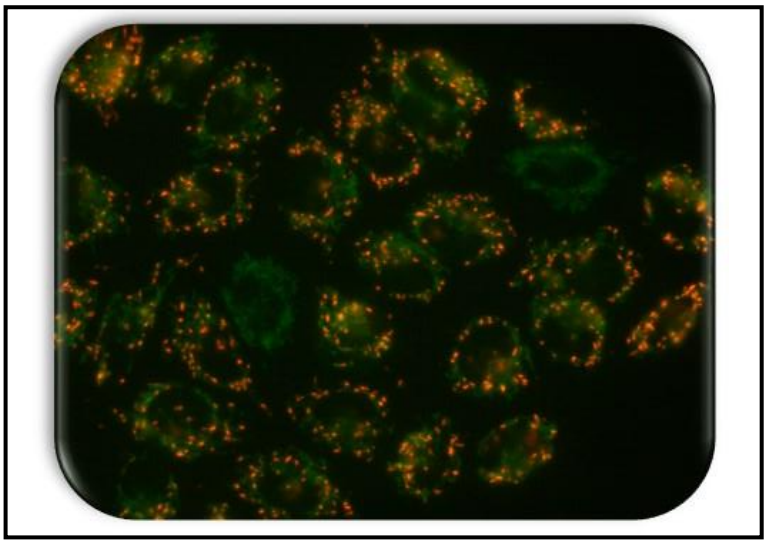

Figure 4.5. JC-1 staining of mitochondria for ΔΨm determination (present work). 1000x magnification.

The U937 cells yielded the highest average ΔΨm while A549 cells yielded the lowest, with a 10-fold difference in median j-aggregate values and an 8-fold difference in median R:G ratio values.
In Figure 4.6A, the R:G ratios for cell lines were found to be significantly different from each other ($p < 0.001$). However, when using j-aggregate values to quantify ΔΨm (Figure 4.6B), no significant difference was observed between the T47D and DU145 cell lines.

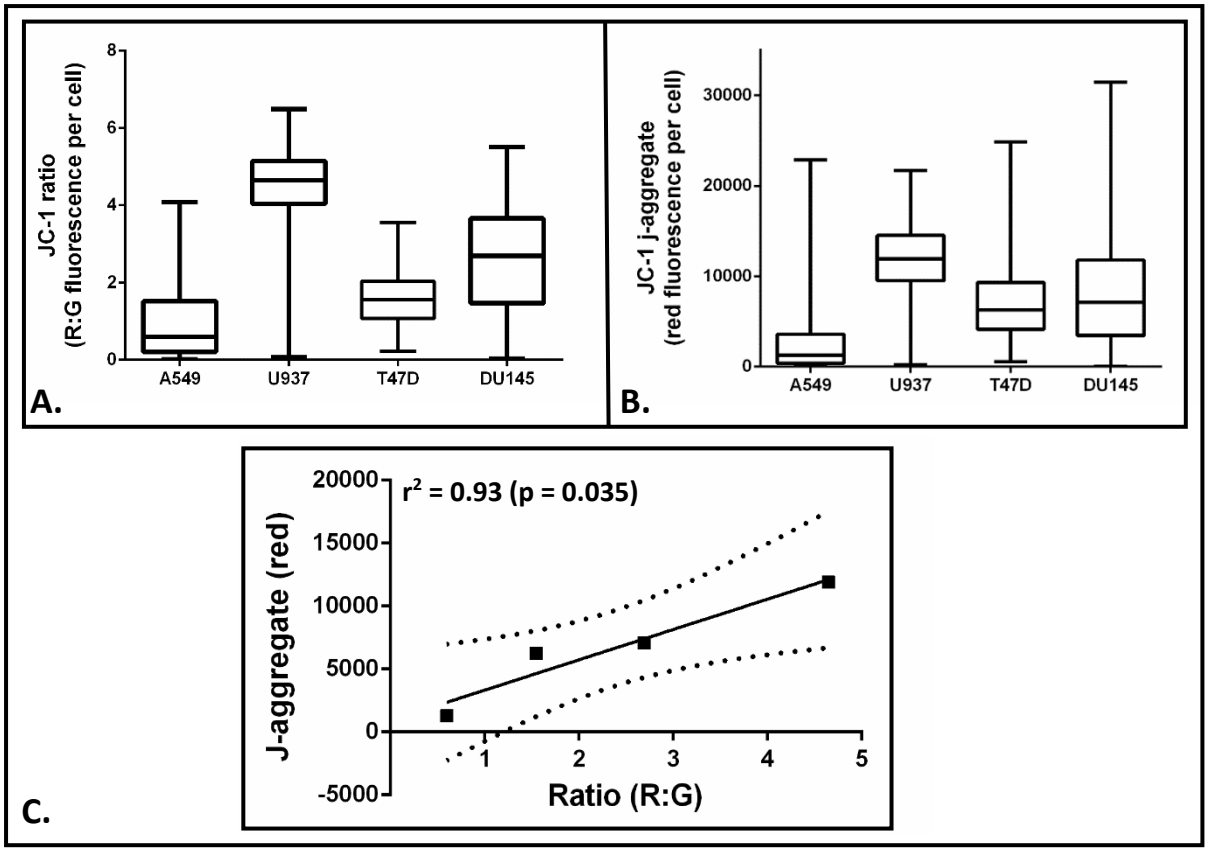

Figure 4.6. Comparison of ΔΨm measurements for cancer cell lines. **A)** JC-1 R:G fluorescence ratios and **B)** J-aggregate (red) fluorescence values. Box and whisker plots illustrate the median values obtained for each cell line as well as the interquartile range and minimum and maximum values for each set of data. Data represent 3 replicate samples per cell line. **C)** Linear regression analysis of JC-1 R:G ratio and j-aggregate (red) values. The 95 % confidence interval is shown.

JC-1 sensitivity

The sensitivity of the JC-1 assay to detect small differences in ΔΨm was assessed using an inhibitor of mitochondrial respiration. Figure 4.7A shows the reduction in ΔΨm in sodium azide-treated cells relative to controls. All cell lines responded to sodium azide treatment, which reduces mitochondrial function by inhibiting complex IV of the electron transport chain. Unlike FCCP, which rapidly depolarises mitochondrial membranes and is commonly used as a positive control, sodium azide has a milder effect on ΔΨm and was used at a time and dose that did not completely dissipate the ΔΨm. In addition the influence of sodium azide treatment on ΔΨm for the U937 cells is illustrated in Figure 4.7B and C, as shown by a scatterplot and a histogram, respectively.

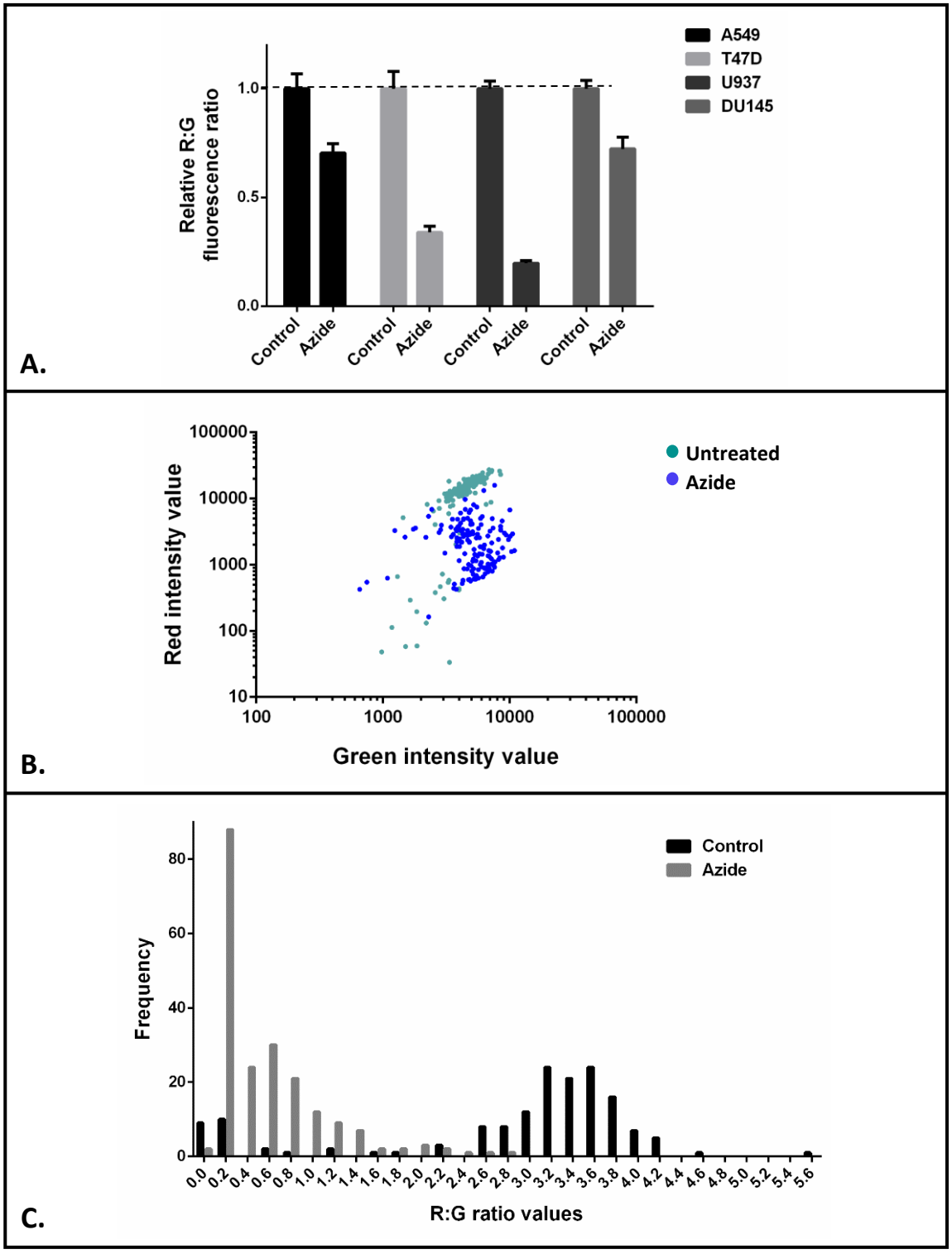

Figure 4.7. Modulation of ΔΨm using a respiratory inhibitor. **A)** Relative reduction in JC-1 R:G fluorescence ratios observed for each cell line after sodium azide-treatment (respective control values were normalised to 1). **B)** Shift in ΔΨm observed for U937 cells after sodium azide treatment. Untreated cells are represented in blue while sodium azide-treated cells are represented in teal. **C)** Histogram showing the distribution of R:G ratio values for U937 untreated and sodium azide-treated samples. Data are shown as mean ± SEM and represent 3 replicate samples.

4.3.2.3. Mitochondrial respiration

The respiratory competence of four cancer cell lines, as estimated by cellular O_2 consumption rate, was compared using high resolution respirometry. An oxygraph trace of O_2 flux through A549 cells over time obtained from experiments is given as a representative example in Figure 4.8. Markers, shown in blue, indicate the addition of mitochondrial modulators, oligomycin, FCCP and rotenone. The accompanying respiration states are designated R', L', E' and ROX and represent physiological, phosphorylation-independent, maximal O_2 consumption and residual O_2 consumption, respectively.

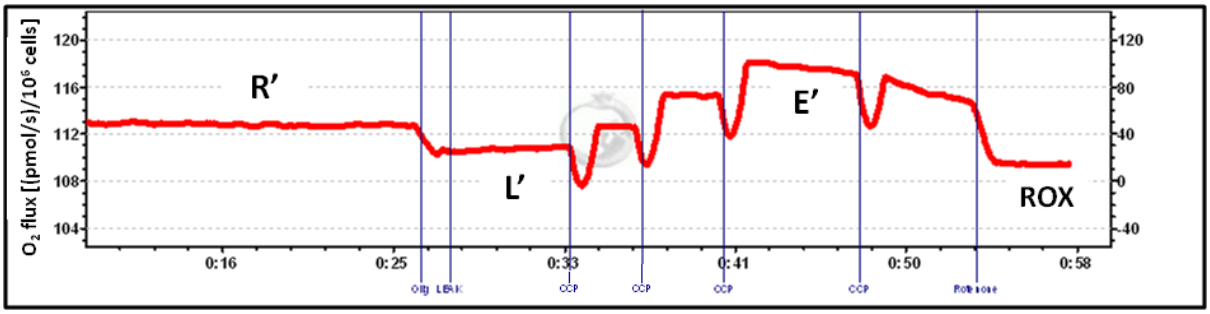

Figure 4.8. Oxygraph trace showing O_2 flux for a sample of A549 cells. R', L' and E' indicate regions representing physiological, phosphorylation-independent and maximal O_2 consumption. The residual O_2 consumption (ROX) for these cells is also shown.

Graphs depicting absolute values of O_2 consumption are presented initially in Figure 4.9, while the results presented thereafter (Figure 4.10) are values normalised to the maximal O_2 consumption rate for each cell line, namely the flux control ratios (FCRs). The former allows comparison of the overall O_2 usage of the cells in each respiration state, namely routine, phosphorylation-independent and uncoupled, while the latter provided a means to compare the efficiency of the respiration between cell lines.

Figure 4.9A depicts the cellular respiration rate (R'), which includes both mitochondrial and non-mitochondrial O_2 consumption, for the cell lines. The T47D and A549 cellular respiration rates under routine cell culture were comparable (48±6.83 and 45±2.66 (pmol/s)/10^6 cells, respectively) and were approximately 15 and 20 % lower, respectively, than the DU145 respiration rate (56.70±6.59 (pmol/s)/10^6 cells). In contrast, the cellular respiration rate of the U937 cell line (21.75±3.8 (pmol/s)/10^6 cells) was less than half the rate of the other cell lines ($p < 0.001$).

The absolute mitochondrial O_2 consumption rates for each respiration state, namely, R_{abs}, L_{abs} and E_{abs}, are presented in Figure 4.9B. These values were derived from R', L' and E' respectively, after correcting for non-mitochondrial (residual) O_2 consumption (ROX). The relatively high ROX value (36.26±9.86 (pmol/s)/10^6 cells) for the DU145 cell line resulted in a lower R_{abs} (24.67±2.68 (pmol/s)/10^6 cells) despite the high cellular respiration rate (56.70±6.59 (pmol/s)/10^6 cells). The T47D and U937 cell lines differed by more than 30 %, displaying the highest (38.21±4.8 (pmol/s)/10^6 cells) and lowest (13.99±1.84 (pmol/s)/10^6 cells) mitochondrial O_2 consumption rates, respectively. The absolute spare respiratory capacities (E_{abs} - R_{abs}) for each cell line were 43.7, 25.1, 34.9 and 25.66 for the A549, T47D, DU145 and U937 cells, respectively.

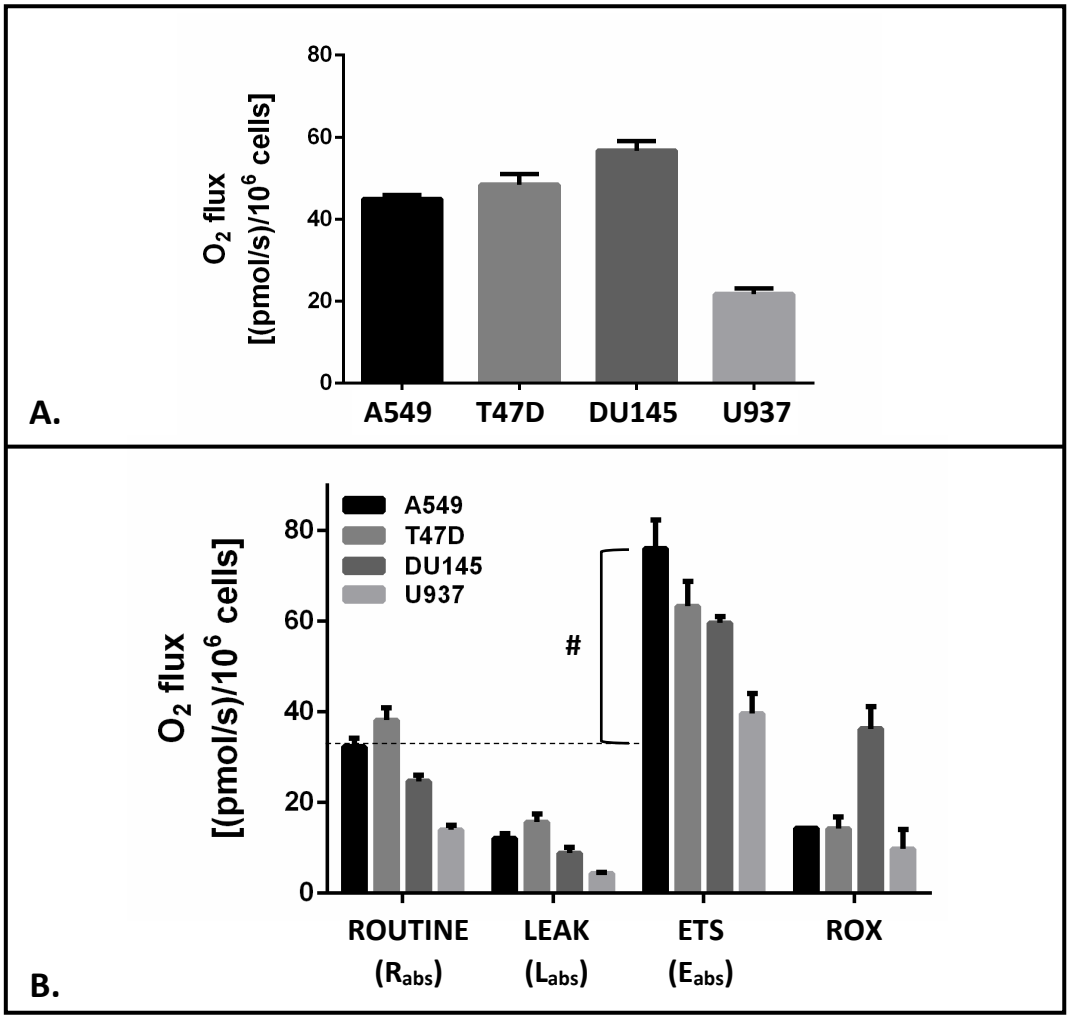

Figure 4.9. Absolute O_2 consumption rates for four cancer cell lines. **A)** Cellular respiration rate (R'), which includes mitochondrial and non-mitochondrial O_2 consumption. **B)** Mitochondrial O_2 consumption rate for three respiration states, R_{abs}, L_{abs} and E_{abs}, representing physiological, phosphorylation-independent and maximal respiration, respectively, and ROX values used for adjustment. O_2 consumption rate was measured per million cells in culture medium [(pmol/s)/10^6 cells]. # = spare respiratory capacity for the A549 cell line. Data are shown as mean ± SEM and represent at least 3 independent experiments.

Comparison of the respiration states, for phosphorylation-independent, L_{abs} and maximal ETS capacity, E_{abs}, for each of the cell lines are shown in Figure 4.9B. As observed for R_{abs}, the T47D cells (15.704±3.11 (pmol/s)/10^6 cells) and the U937 cells (4.36±0.53 (pmol/s)/10^6 cells) showed the greatest difference (72 %) between mitochondrial O_2 consumption rates that are independent of ATP synthesis (L_{abs}). A549 and DU145 L_{abs} values were similar (12.12±1.73 and 8.86±2.45 (pmol/s)/10^6 cells). The highest E_{abs} was determined for the A549 cell line (76.09±10.85 (pmol/s)/10^6 cells) and the U937 E_{abs} was approximately 50 % lower (39.65±7.64 (pmol/s)/10^6 cells). T47D and DU145 cells showed comparable E_{abs} (63.324±9.46 and 59.66±2.69 (pmol/s)/10^6 cells).

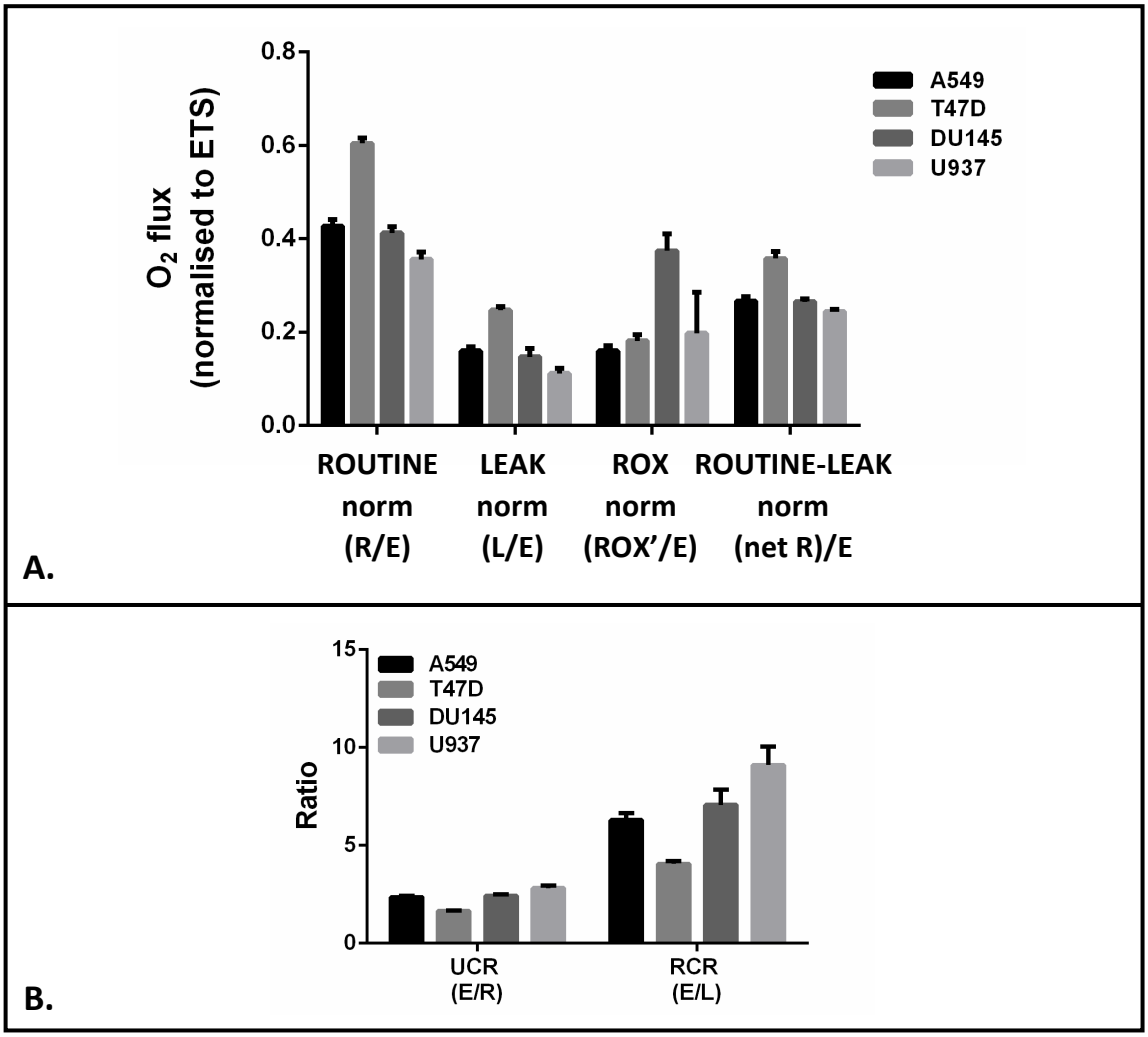

Figure 4.10. Flux control ratios for comparison of respiratory parameters of four cancer cell lines. The ratios of absolute values, R/E, L/E and ROX/E', represent ROUTINE, LEAK and non-mitochondrial O_2 consumption, respectively, normalised to maximal respiratory capacity for each cell line. The respiration related to phosphorylation (R-L = net R) and normalised to maximal respiratory capacity is given by (net R)/E. The respiratory control ratio (RCR = E/L) and the uncoupling control ratio (UCR = E/R) are reciprocal ratios that indicate mitochondrial efficiency and excess respiratory capacity. Data are shown as mean ± SEM and represent at least 3 independent experiments.

Calculated FCRs used to describe respiratory function relative to E_{abs} are presented in Figure 4.10. The ROUTINE control ratio (R/E) describes coupled respiration in terms of the proportion of ETS capacity used. The T47D cells were observed to use 60 % ETS capacity (0.61±0.02) which was at least 20 % more than used by the other cell lines ($p < 0.001$). Reciprocally, the T47D had a lower UCR (1.65±0.05) indicating reduced excess respiratory capacity than the other cell lines. The range of LEAK control ratios (L/E) determined, namely, 0.11-0.25 are comparable to those reported previously[327]. The T47D cell line was shown to be significantly different from the other cell lines in terms of proton leak (L/E = 0.25±0.014; A549: $p = 0.002$, DU145: $p < 0.001$, U937: $p < 0.001$). The net ROUTINE respiration describes the phosphorylation-related respiration as a proportion of ETS capacity. The T47D cell line displayed a significantly higher net ROUTINE respiration (0.36±0.025) compared to the other cell lines suggesting greater ETS capacity is used for ATP generation ($p < 0.001$). The DU145 cells, as mentioned previously, consume 37 % more O_2 than utilised by the mitochondria (ROX_{norm}: 0.37±0.07) compared to the other cell lines where approximately 20 % of the O_2 consumption is non-mitochondrial (A549: $p = 0.01$, T47D: $p = 0.016$, U937: $p = 0.024$).

4.3.3. Correlation analyses

We have hypothesised that mitochondrial status is associated with intrinsic cellular radiosensitivity. Therefore, in this thesis, both measures of mitochondrial structure and function have been correlated with radiosensitivity. Tables 4.4 – 4.6 list the outcomes of the correlation analyses.

4.3.3.1. Correlation of cellular radiation-responsiveness with mitochondrial characteristics

The radiation response for the four cell lines, represented by SF2, SF4, $\bar{D}$ and alpha were correlated with the mitochondrial characteristics investigated (Table 4.4). Correlations of factors with SF4 or were comparable. Strong negative correlations were found between both SF4 and $\bar{D}$, and the fragmentation index ($r = -0.919$ and -0.896, respectively), however, the relationships were not statistically significant.

SF2 correlated strongly with both JC-1 ratiometric (median: $r = -0.822$) and j-aggregate (mean: $r = -0.857$ and median: $r = -0.820$) measures of mitochondrial $\Delta\Psi m$ however, with the small data set, the correlations were not significantly non-zero. None of the parameters of radiation-responsiveness correlated strongly with measures of respiration, however the following moderate correlations were observed. SF2 was positively correlated with E_{abs} ($r = 0.771$, $p = 0.23$) and mitochondrial respiration (R_{abs}) ($r = 0.69$, $p = 0.31$). Alpha correlated positively with cellular respiration rate (R'), which includes mitochondrial and non-mitochondrial O_2 consumption ($r = 0.650$, $p = 0.35$).

Table 4.4. Correlation coefficients for measures of radiosensitivity versus mitochondrial morphology and function**.** p-values are shown in brackets.

	SF4		$\bar{D}$		SF2		alpha (α)	
Fragmentation index	**-0.919**	(0.258)	**-0.896**	(0.293)	-0.665	(0.537)	0.577	(0.609)
JC-1 R:G ratio (mean)	-0.407	(0.593)	-0.459	(0.541)	-0.777	(0.223)	0.056	(0.944)
JC-1 R:G ratio (median)	-0.485	(0.515)	-0.535	(0.465)	**-0.822**	(0.178)	0.128	(0.872)
JC-1 j-aggregate (mean)	-0.666	(0.334)	-0.700	(0.300)	**-0.857**	(0.143)	0.227	(0.773)
JC-1 j-aggregate (median)	-0.622	(0.378)	-0.655	(0.345)	**-0.820**	(0.180)	0.159	(0.841)
R' (cellular respiration)	-0.255	(0.745)	-0.217	(0.783)	0.124	(0.876)	0.650	(0.350)
R_{abs} (corrected for ROX)	0.173	(0.827)	0.242	(0.758)	0.690	(0.310)	0.058	(0.942)
E_{abs} (max ETS capacity)	0.492	(0.508)	0.534	(0.466)	0.771	(0.229)	0.049	(0.951)
UCR (E/R)	0.136	(0.864)	0.062	(0.938)	-0.449	(0.551)	-0.034	(0.966)
RCR (E/L)	0.017	(0.983)	-0.056	(0.944)	-0.551	(0.449)	-0.021	(0.979)
ROUTINE (R/E)	-0.183	(0.817)	-0.110	(0.890)	0.396	(0.604)	-0.014	(0.986)
(Net R)/E	-0.237	(0.763)	-0.165	(0.835)	0.337	(0.663)	-0.010	(0.990)
LEAK (L/E)	-0.134	(0.866)	-0.061	(0.939)	0.446	(0.554)	-0.018	(0.982)
Spare respiratory capacity	0.635	(0.365)	0.624	(0.376)	0.500	(0.500)	-0.016	(0.984)

4.3.3.2. Correlation of mitochondrial morphology, ΔΨm and respiratory parameters

Correlations between measures of mitochondrial structure and function were subsequently examined (Table 4.5). Strong, positive correlations were observed between the fragmentation index and JC-1 j-aggregate values (mean: r = 0.926 and median: r = 0.95). The fragmentation index correlated negatively with E_{abs} (r = -0.918). These correlations were, however, not significantly non-zero. As reported previously in section 4.3.2.2, the four different JC-1 measures of mitochondrial ΔΨm (R:G ratio and j-aggregate values) were strongly correlated.

Strong, negative correlations (r = -0.915 and -0.892) were obtained between JC-1 R:G ratio values and mitochondrial respiration (R_{abs}). In addition, the mean JC-1 R:G ratio value was positively correlated with RCR (r = 0.809; p = 0.19). All JC-1 measures also showed strong, negative correlation with E_{abs} (Ratio mean: r = -0.981; p = 0.019 and median: r = -0.987; p = 0.013; j-aggregate mean: r = -0.977; p = 0.023 and median: -0.986; 0.014).

Table 4.5. Correlation coefficients for mitochondrial morphology versus function**.**
p-values are shown in brackets.

	Morphology (fragmentation index)		JC-1 (ratio) mean		JC-1 (ratio) median		JC-1 (j-aggregate) mean		JC-1 (j-aggregate) median	
Fragmentation index										
JC-1 (ratio) mean	0.674	(0.529)								
JC-1 (ratio) median	0.734	(0.475)	**0.996**	**(0.004)**						
JC-1 (j-agg) mean	**0.926**	(0.247)	**0.938**	(0.062)	**0.962**	**(0.038)**				
JC-1 (j-agg) median	**0.950**	(0.202)	**0.945**	(0.055)	**0.964**	**(0.036)**	**0.998**	**(0.002)**		
R' (cellular)	0.586	(0.602)	-0.721	(0.279)	-0.666	(0.334)	-0.543	(0.457)	-0.595	(0.405)
R_{abs} (corrected)	0.120	(0.924)	**-0.915**	(0.085)	**-0.892**	(0.108)	-0.739	(0.261)	-0.740	(0.260)
E_{abs} (max ETS)	**-0.918**	(0.260)	**-0.981**	**(0.019)**	**-0.987**	**(0.013)**	**-0.977**	**(0.023)**	**-0.986**	**(0.014)**
UCR (E/R)	-0.584	(0.603)	0.693	(0.307)	0.650	(0.350)	0.424	(0.576)	0.425	(0.575)
RCR (E/L)	-0.453	(0.701)	**0.809**	(0.191)	0.772	(0.228)	0.573	(0.427)	0.576	(0.424)
ROUTINE (R/E)	0.608	(0.584)	-0.589	(0.411)	-0.545	(0.455)	-0.309	(0.691)	-0.304	(0.696)
(Net R)/E	0.647	(0.552)	-0.517	(0.483)	-0.471	(0.529)	-0.227	(0.773)	-0.221	(0.779)
LEAK (L/E)	0.567	(0.616)	-0.649	(0.351)	-0.608	(0.392)	-0.379	(0.621)	-0.376	(0.624)

Table 4.6 shows the correlation analysis between various respiratory measures. A strong, significant correlation (r = 0.996; p = 0.004) was observed between ROUTINE respiration and ATP-coupled respiration (netR/E). The UCR and RCR, as inverse functions of the ROUTINE and LEAK state respiratory ratios, respectively, also show strong correlations (r = -0.989 and -0.970; p = 0.011 and 0.03). Cellular respiration (R'), which includes ROX, did not correlate strongly with the other respiratory measures while, in contrast, strong correlations were observed with all respiratory measures when ROX was subtracted (R_{abs}). Maximal respiratory capacity (E_{abs}), as determined by complete uncoupling of respiration correlated weakly with the additional measures of respiration. Excess respiratory capacity (UCR) correlated strongly (r = 0.984; p = 0.016) with the measure of mitochondrial function, RCR, and consequently with other measures determined by LEAK or ROUTINE state respiration.

Table 4.6. Correlation coefficients comparing measures of cellular and mitochondrial respiration**.** p-values are shown in brackets.

	R' (cellular)		R_{abs} (R'- ROX)		E_{abs} (E'- ROX)		UCR (E/R)		RCR (E/L)		ROUTINE (R/E)		(Net R)/E	
R'														
R_{abs}	0.673	(0.327)												
E_{abs}	0.703	(0.297)	**0.821**	(0.179)										
UCR	-0.581	(0.419)	**-0.923**	(0.077)	-0.543	(0.457)								
RCR	-0.655	(0.345)	**-0.975**	**(0.025)**	-0.682	(0.318)	**0.984**	**(0.016)**						
ROUTINE	0.473	(0.527)	**0.865**	(0.135)	0.423	(0.577)	**-0.989**	**(0.011)**	**-0.950**	**(0.050)**				
(Net R)/E	0.423	(0.577)	**0.818**	(0.182)	0.343	(0.657)	**-0.973**	**(0.027)**	**-0.919**	(0.081)	**0.996**	**(0.004)**		
LEAK	0.513	(0.487)	**0.901**	(0.099)	0.491	(0.509)	**-0.997**	**(0.003)**	**-0.970**	**(0.030)**	**0.997**	**(0.003)**	**0.987**	**(0.013)**

Overall, besides the expected, significant correlations observed between different measures of respiration, few strong, significant correlations were observed with other measures of mitochondrial function. The individual measures of ΔΨm and radiation sensitivity correlated strongly with each other and these correlations were found to be significant. In addition, strong, significant correlations were obtained between ΔΨm and maximum respiratory capacity. Although statistical significance was not reached for correlations with mitochondrial morphology, the strong correlation observed between radiation sensitivity (SF4) and the fragmentation index is notable and may be shown to be significant in a larger study.

4.4. Discussion

It was the intention of the current work to characterise the mitochondrial status of cancer cell lines and to determine whether such features correlated with cellular radiation sensitivity.

4.4.1. Radiation response in the cancer cell lines

The tumour cell lines used in this study were divided into three groups based on the relative radiation sensitivities determined. Parameters of radiosensitivity correlated well with each other. Within the range of clonogenic survival observed, cell lines were classified as exhibiting relatively high, intermediate or low response to radiation. SF2 values, and to a lesser extent $\bar{D}$ values, are commonly used to describe sensitivity of cell lines[240, 242]. SF2 values in the current study ranged from 0.35 - 0.75, which reflect the middle to upper end of the range observed for tumour cell lines (0.08 – 0.79) in several previously reported studies[40, 206, 230, 231, 638-640]. This suggests that the cell lines selected represented a significant spectrum of radiation-responsiveness. The mean inactivation dose ($\bar{D}$), in our cell lines, ranged from 1.75 to 2.99 Gy. This was comparable to a large study of 70 fibroblast cell lines, where the sensitivity ($\bar{D}$) ranged from 0.78 to 2.5 Gy[641]. Similarly, from a selection of previous studies, a range of 0.81 to 2.4 Gy in normal fibroblasts has been determined[642]. Thus, the radiosensitivities of our cell lines, based on SF2 values or $\bar{D}$, are similar to published ranges for cancer and normal cells[234].

A representative cell line from each of the three groups identified was chosen for characterisation of mitochondrial morphology and function. A brief discussion of the selected cell lines is presented below.

Least radioresponsive cell lines

In this study, the A549 and HeLa cell lines were the most resistant to radiation, approximately 2-fold more resistant than the MDA-MB-231 cell line. Although the HeLa cell line showed greater resistance than the A549 cell line at low doses (up to 3 Gy), sensitivity was increased at higher doses and $\bar{D}$ values were similar (2.941 and 2.999, respectively). Hence, the A549 cell line was selected to represent the least radiation-responsive group for characterisation of mitochondrial structure and function.

Evidence suggests that non-small cell lung cancer cell lines are radioresistant[639]. The reduced radiation responsiveness of A549 cells is consistent with clinical observations of therapeutic resistance in non-small cell lung cancer that is often associated with tumour heterogeneity and acquired mutations[643-645]. Investigations into the mechanisms behind the radiation resistance of non-small cell lung cancers have implicated, among others, dysregulation of signalling pathways[646, 647], altered p53-related pathways[648, 649] and inhibition of apoptotic mechanisms[650, 651].

Most radioresponsive cell lines

The DU145 and MDA-MB-231 cell lines were the most responsive to radiation treatment. In addition, the DU145 cells had the lowest SF2 and were thus chosen to represent the group with low radiation-responsiveness. The sensitivity displayed by our DU145 cell line is similar to that published by Love et al. (2003)[652]. It has been shown that, after irradiation, purified DNA from these cells appears fragmented on electrophoresis suggesting sensitivity to radiation-induced apoptosis[206, 228, 653]. Other investigators have reported variants of this cell line expressing greater resistance[231, 654, 655].

In the clinic, prostate tumours are often considered to be slow growing with low α/β ratios[656, 657]. In contrast, our DU145 cell line was fast growing and appeared to have a high α/β ratio (approximately 27 Gy^{-1}). The low β-component and relatively high α-component of our DU145 survival curve suggests that these cells may be repair-deficient or have higher intrinsic radiation sensitivity. DU145 cells are known to be mismatch repair deficient[658] and loss of this type of repair has been shown to influence activation of S-phase arrest in response to radiation[659], although other investigators report no effect on radiosensitivity[660, 661]. Mismatch repair deficient cells are likely to display a mutator phenotype suggesting that other repair pathways may be affected over time. Differences in radiation sensitivity may thus occur as a result. Nevertheless, the DU145 cell line used in the present study was useful in our context as it provided a model with low radiation-responsiveness for correlation with mitochondrial status.

Cell lines displaying intermediate radiation-responsiveness

The U937 monocytic leukaemia and T47D breast cancer cell lines formed the third group with intermediate radiation-responsiveness. Both cell lines from this group were investigated for mitochondrial functional parameters. While the mitochondrial morphology of T47D cells was documented for correlation analysis, morphology was not quantified for the U937 cell line due to technical limitations of scoring morphology in suspension cells.

Characterisation of mitochondrial features and correlation with radiation-responsiveness

Functional aspects of mitochondria, including the fragmentation index, $\Delta\Psi m$ and O_2 utilisation, were investigated with the ultimate goal of determining the strength of correlation between these characteristics and the radiation-responsiveness of the four selected cell lines. Additional correlation analysis of individual aspects of mitochondrial functional was included for completeness.
The parameters analysed that gave favourable correlations are highlighted in Tables 4.4 – 4.6.

To our knowledge, no formal correlation analysis between cellular radiosensitivity and the inherent cellular characteristics of mitochondrial structure and function, as investigated in this study, has been reported previously. However, an early study using tumour tissue did correlate similar aspects of mitochondrial structure and function with radiosensitivity of tumour samples using isolated mitochondria and electron microscopy[50]. The investigators determined that radiosensitivity was associated with reduced OXPHOS and ATP production and mitochondrial content, as well as, mitochondria that contained fewer cristae. In addition, radiosensitive tumours showed increased damage to mitochondria after irradiation. Although the techniques used were different, our respiratory results were consistent with these findings in that the more sensitive cell lines displayed reduced or inefficient mitochondrial O_2 consumption.

Correlations with inherent radiation-responsiveness

Radiation-responsiveness, as defined by SF4 or $\bar{D}$, and the fragmentation index were negatively correlated ($r = -0.919$ and -0.896, respectively). However, the correlations, although strong, were not statistically significant ($p = 0.26$ and 0.29). SF2, however, correlated only moderately. It should be noted that of the three cell lines analysed for mitochondrial morphology, only the A549 cell line displayed a significantly different fragmentation index.

The predominantly fused mitochondrial morphology of the A549 cell line was associated with reduced radiation-responsiveness. Evidence exists that supports such an association. For example, stress-induced mitochondrial hyperfusion has been shown to protect against apoptosis caused by UV-irradiation in HeLa cells and mouse embryonic fibroblasts[501]. Similarly, inhibition of mitochondrial fission was reported to be protective against apoptosis in many cases[15, 365, 454] suggesting that fusion may contribute to resistance. However, induced changes in mitochondrial fragmentation may not necessarily be equivalent to inherent mitochondrial fragmentation.

SF4 correlated moderately with ΔΨm while, SF2, which may more closely reflect intrinsic radiosensitivity than SF4, was found to correlate negatively (r = approximately -0.8 for all measures of ΔΨm). This suggests that increased ΔΨm may be associated with enhanced radiation response. Alpha, another estimate of radiosensitivity, did not correlate notably with ΔΨm. Since α was determined from fitted survival curves with limited data points in the shoulder region, which determines the accuracy of fit, the uncertainty in α may account for the weak correlations observed.

Mitochondrial function, given its association with intrinsic apoptosis, is thought to be important for radiation-induced cell kill. It should be noted, however, that high ΔΨm may not necessarily reflect increased mitochondrial function, particularly in cancer cells, where ATP synthase function is frequently aberrant. We have shown inverse relationships between ΔΨm and measures of respiratory function (Table 4.5), suggesting that a higher ΔΨm in our cancer cell lines is associated with poorer mitochondrial function. Thus, defining mitochondrial functionality in terms of ΔΨm alone may be misleading. This will be examined later in the discussion of additional correlations with ΔΨm. The interplay between radiation response, ΔΨm and respiration is likely to be complex in the context of cancer cells and it may be important to consider defining factors collectively rather than single determinants in isolation.

Both SF2 and α correlated moderately with the respiratory parameters, E_{abs} and R_{abs}, and R', respectively. Notably, the sensitive DU145 line had the greatest alpha, approximately twice that of the other lines, the smallest SF2 value and the greatest total cellular respiration (R') of the group. As mentioned previously, maximal ETS capacity (E_{abs}) is a measure of mitochondrial O_2 consumption in a fully uncoupled state and may be an indication of the potential of cells to respond to a cellular stressor such as ionising radiation. In our investigations, the more resistant A549 cells had both the highest E_{abs} and greatest spare respiratory capacity, supporting this relationship. Interestingly, the apoptosis-sensitive U937 cells had the lowest E_{abs}. Spare respiratory capacity has been shown previously to be an important determinant in the ability of cells to respond to stress[318, 320, 322].

Correlations were observed between measures of radiosensitivity and respiration, determined under ideal physiological conditions where O_2 was not limited. *In vivo*, due to the oxygen effect, tumour hypoxia reduces the radiosensitivity of solid tumours. Differences in the respiration rate of tumour cells might be expected to influence tumour O_2 concentration and influence the extent of tumour hypoxia, particularly when blood supply is limited.

A positive correlation between intrinsic radiosensitivity and mitochondrial respiration (R_{abs}) in this *in vitro* model, despite the absence of hypoxia, may suggest that inherent respiratory function may also affect radiation response more directly.

Correlations observed between respiratory parameters and radiosensitivity may relate to oxidative stress, which is often evident in cancer cells as a result of mitochondrial dysfunction[299, 662]. Adaptive measures that aid cells in coping with oxidative stress include increased anti-oxidant defences[663, 664] such as upregulation of MnSOD[301] or increased mitochondrial proton leak[298, 306]. Increased mitochondrial O_2 consumption with higher accompanying proton leak, in our cells, may indicate up-regulation of anti-oxidant defences. The more resistant A549 and T47D cells had a higher LEAK respiration (L_{abs}) and, given the role of ROS in radiation damage, such higher LEAK respiration could indicate an increased ability to scavenge radiation-induced ROS and induce radiation resistance. It has been established that the upregulation of anti-oxidant defences protects against radiation damage by neutralising ROS[300, 302, 303, 310].

4.4.2. Mitochondrial morphology

Mitochondrial fission and fusion status was assessed by categorisation of cells depending on the relevant predominant morphology.

Integrity of mitochondrial morphology assessment

Mitochondrial morphology was effectively classified using fluorescence microscopy in the three adherent cell lines selected for characterisation. The reliability of morphological quantitation was optimised by processing cells under physiological conditions and by viewing cells attached to coverslips to attain clear images given the shallow depth of focus. In addition, it was verified that the fixation process did not affect the appearance of mitochondria (Appendix C, Figure C2). Further, confocal microscopic images for A549 cells were found to be practically identical to images obtained using conventional fluorescence microscopy (Appendix C, Figure C4).

Correlations with mitochondrial morphology

The strong correlation between the fragmentation index and inherent radiation-responsiveness supported our hypothesis that increased mitochondrial fusion can protect against ionising radiation. The A549 cell line displayed the highest level of fusion and had the lowest radiation response.

Increased fusion has been linked with increased electron transport capacity, which is consistent with the negative correlation found between the fragmentation index and the respiratory parameter, ETS ($r = -0.918$). Moderate negative correlations with O_2 consumption as a proportion of maximum capacity (R/E and netR/E) are also in agreement, as mitochondrial fusion is generally increased to meet respiratory demands, leading to an increase in utilised capacity.

The A549 model displayed a greater proportion of cells with fused mitochondria, high respiratory capacity and increased resistance to radiation, however, these factors cannot be unequivocally linked.

Wide variation in mitochondrial morphology was particularly evident for the A549 cell population. Mitochondrial morphology is dynamic, and allows constant adaptation to cellular circumstances. Diverse morphological features in a population of cells are also indicative of a proliferative state[507]. In addition, mitochondrial morphology varies through the cell cycle[371, 503, 504] and assessment of morphology in an asynchronous population would likely reflect the distribution of cells in the cell cycle. Given the variability in radiosensitivity of cells in different phases of the cell cycle, the proportion of cells in each phase for the different cell lines may influence their respective radiosensitivity. For example, a cell line that is highly proliferating would have an increased proportion of cells in mitosis, a particularly radiosensitive phase. In this case, the cell line may display an increase in fragmentation as fission occurs in preparation for mitosis. Associations between morphology and radiation response may therefore partly indicate differences in cell cycle distribution between cell lines. In our experiments, survival, ΔΨm and respiration analyses for each cell line were performed in an asynchronous state. While correlation analysis of the inherent characteristics of the cell populations as a whole may reflect radiosensitivity, potential cell cycle effects cannot be discounted.

4.4.3. Mitochondrial membrane potential

Sensitivity of the JC-1 assay used for ΔΨm assessment

Correlation analyses with measures of ΔΨm were carried out for the four selected cell lines. JC-1 is commonly used to detect relatively large differences in ΔΨm that occur during apoptosis. It was therefore important to show that this assay could be effectively used to detect smaller changes in ΔΨm. The assay effectively resolved the reduction in ΔΨm induced by non-toxic concentrations of sodium azide indicating that sensitivity was sufficient to detect potentially small differences between the cell lines.

Subtle differences in ΔΨm amongst cells within a tumour could be demonstrated using a similar technique[339]. Of note, despite heterogeneity in ΔΨm, no differences in cell viability or growth were observed[339]. Similar variability in ΔΨm was demonstrated in our cell lines as evidenced by the wide range of ΔΨm values determined for individual cells.

While mitochondrial dyes have been shown to affect cellular metabolism by, for example, inhibiting ATP synthase activity[665], the JC-1 stain was shown not affect respiratory control ratios at 0.37 µg/ml[349]. Moreover, routine use in flow cytometry assays has demonstrated no significant cellular effects for concentrations up to 10 µg/ml yielding a cell viability in excess of 95 %[347, 666]. In our experiments, a concentration of 1 µg/ml JC-1 was applied and we did not observe any adverse effects on the cell shape or membrane integrity.

Correlations with ΔΨm

JC-1 ratio and j-aggregate values, were strongly correlated ($r^2 = 0.93$; $p = 0.035$) with each other (Figure 4.6). JC-1 j-aggregate values gave greater consistency between experiments, however, the correlations suggest that R:G ratio values also described relative differences between cell lines well.

ΔΨm and radiation response

As discussed above, a strong, negative correlation between ΔΨm and intrinsic radiation-responsiveness was demonstrated. High ΔΨm in cancer cells has been associated with both sensitivity and resistance to chemotherapeutic agents. For example, a study investigating the intrinsic ΔΨm in cells from colonic and mammary tumours showed an association between chemoresistance and cells with higher ΔΨm[667]. The investigators suggested that mtDNA mutations may be responsible for increased ΔΨm in certain clones and reported a common heteroplasmic mtDNA mutation in clones with elevated ΔΨm that was absent in those with lower ΔΨm.

Similarly, cisplatin-resistant human adenocarcinoma and hepatoma cells displayed higher ΔΨm along with a reduced O_2 consumption and a disordered mitochondrial morphology, when compared to parent cells[344]. A high ΔΨm, therefore, is not always associated with functional integrity in tumour cells, despite enabling resistance to therapy.

ΔΨm and mitochondrial fragmentation

Mitochondrial membrane potential correlated strongly with the fragmentation index (median: $r = 0.95$; $p = 0.20$) in contrast to reports that decreased ΔΨm is associated with increased fragmentation in normal and cancer cells[569, 668, 669]. Mitochondrial fusion is frequently associated with increased respiration and therefore an increase in ΔΨm.

However, cells with fragmented mitochondria may show increased ΔΨm in the context of respiratory dysfunction. For example, the highly fragmented DU145 cell line has been shown to have aberrant mitochondrial metabolism, displaying a low affinity of complex 1 for NADH and a reliance on glutamate as a substrate[670].

Electrogenic transport provided by a high ΔΨm is necessary for glutamate transport into the mitochondrial matrix. Upregulation of proton import into the matrix, in spite of the fragmented state, would then be required and would be consistent with the observed correlations. The underlying reasons for a high ΔΨm in DU145 and U937 cells may be multifaceted. However, this finding is consistent with the tendency for many cancer cells to display hyperpolarised ΔΨm[334].

ΔΨm and respiration

In keeping with the inverse relationship between ΔΨm and respiration mentioned previously, negative correlations were observed between ΔΨm and mitochondrial O_2 consumption (R_{abs}).
In the context of aberrant respiratory function, these correlations are consistent with the phenomenon where ΔΨm is increased as a result of ATP synthase dysfunction or reversal[313, 314].
Another explanation may be related to the "leakiness" of the mitochondrial membrane. Cells that have a high O_2 consumption may display low ΔΨm as a result of proton leak from the intermembrane space. Both the A549 and T47D cells showed higher LEAK respiration (L_{abs}) and had relatively low ΔΨm. UCP2, a mitochondrial membrane uncoupling protein has been shown to be increased in cancer cells leading to increased proton leak[306], which is thought to be an adaptation to manage oxidative stress[671-673]. In one study, a similar JC-1 value to that obtained for the T47D cells was determined for MFN2-mutant cells that displayed uncoupling of respiration and a reduced RCR[674].

In contrast, the U937 respiration is relatively more efficient and less O_2 consumption is attributed to LEAK respiration. These cells may therefore maintain a higher ΔΨm than cells with increased LEAK respiration despite reduced overall capacity.

Strong, significant correlations between ΔΨm and ETS capacity (E_{abs}), as found in this study, are interesting although may be difficult to interpret. Maximal respiration was measured during complete uncoupling whereas ΔΨm was measured under conditions of routine respiration.
ΔΨm has been shown to be dissipated in the presence of FCCP, a respiratory uncoupler[675, 676].
Maximal stimulation of respiration during increased ATP demand, however, would presumably require an intact ΔΨm.

In addition, the ETS capacity value, although useful for normalising mitochondrial function for comparison of cell lines, is dependent on mitochondrial content and ΔΨm values may therefore reflect differences in mtDNA copy number.

Nevertheless, the possibility that respiratory capacity may be reflected by ΔΨm under routine conditions is worth considering. Deficiencies in electron transport may be reflected by low ΔΨm[677], however, reduced ΔΨm may not necessarily indicate a deficiency in maximal respiratory capability[678]. Notably, A549 cells displayed the highest E_{abs} despite having a reduced ΔΨm.

A549 cells preferentially rely on glycolysis for energy metabolism. This may be due to inhibition of pyruvate dehydrogenase (PDH) through dysregulation of PDH kinase[679]. The metabolic targeting agent, dichloroacetic acid, which enables PDH activation, increased OCR by 60 %, thus normalising glucose oxidation in these cells[553, 680]. Likewise, the addition of succinate, the substrate for complex II, to A549 cells in culture increased O_2 consumption[681]. This potential to upregulate OXPHOS suggests that low ΔΨm in A549 cells may reflect the restricted use rather than lack of respiratory capacity.

The mitochondrial efficiency, represented by RCR, correlated positively with ΔΨm. The leakiness of the membranes which, in turn, influences ΔΨm determines, in part, the efficiency of mitochondrial respiration. Therefore, such an association is plausible.

The U937 cells displayed the highest RCR (9.1) while the lowest value was determined for the T47D cell line (4.1). Healthy, respiring cells were indicated to have RCR values of 10 or higher[682]. Similarly in a study of human fibroblasts, RCR was approximately 12[674]. Several studies that included both normal and tumour cells have shown RCR values ranging from 3 to 10 in isolated mitochondria[683]. It would appear therefore, that the mitochondrial efficiency of U937 cells was similar to that of normal cells. This high efficiency was in spite of a lower mitochondrial respiration rate. In contrast, the T47D mitochondrial respiration rate was higher.

T47D cells have a high LEAK state respiration which corresponds with their relatively lower ΔΨm, and may be responsible for their low mitochondrial efficiency. In a study comparing breast cancer cell lines, it was reported that T47D cells have a low mitochondrial efficiency relative to MCF7 cells[292]. The increased radiation-responsiveness of the T47D cells may reflect differences in respiratory function and reserve capacity when compared to the A549 cell lines.

Correlations between respiratory parameters

As expected, strong correlations between different measures of respiratory function were found. Similarly, minimal correlation of measures of mitochondrial function with maximal respiratory capacity (E_{abs}) and total cellular respiration (R'), was probable as these parameters include non-mitochondrial respiration.

It has been reported in a diverse group of cancer cell lines that non-mitochondrial O_2 consumption is frequently approximately 10 %, but can vary significantly between 1 and 90 % of total O_2 consumption[684]. The proportion of maximal O_2 consumption (ROX/E') in each of our cell lines was generally higher than previously reported[327]. In particular, the DU145 cell line showed higher non-mitochondrial O_2 consumption than the other cell lines. Non-mitochondrial O_2 consumption is mainly due to oxidase enzymes including NAD(P)H oxidases (NOX) and peroxidases.

DU145 cells, that displayed the highest ROX, have been shown to have high expression of NOX enzymes[685, 686]. In addition, extracellular acidification of the culture medium has been associated with cell surface O_2 consumption[684]. The DU145 cells were observed to acidify the culture medium more rapidly than the other cell lines, which may be related to this process.

4.4.4. Limitations of correlation analysis

The present work selected a subgroup of available cell lines on the basis of observed radiosensitivity. Thus, a limited number of cell lines was analysed, which may provide selective information that would need to be expanded for wider generalisation and increased statistical power. In addition, only three parameters of mitochondrial structure and function were investigated. It may be necessary to describe mitochondrial function more comprehensively. No clear associations between radiosensitivity and the factors investigated in this study have been described previously. The correlations observed were, therefore, useful to identify trends that could be elucidated in future studies using a multifactorial approach.

4.5. Conclusions

Characterisation and investigation of radiation sensitivity and mitochondrial structural and functional features in a range of tumour cell lines has provided a complex, yet informative picture of cellular status and radiation response.

- The six cell lines assessed provided a range of cellular responses to radiation.
- Strong, negative correlations were displayed between measures of radiation-responsiveness and both mitochondrial morphology and ΔΨm, although the associations were not statistically significant.
- Heterogeneous mitochondrial morphology and ΔΨm within and between cell populations was observed suggesting functional differences. The relatively high ΔΨm values overall support the notion that cancer cells have hyperpolarised inner mitochondrial membranes.
- Respiratory parameters examined were similar between cell types, however, the A549 cells had the greatest reserve respiratory capacity and the DU145 cells had significantly higher non-mitochondrial O_2 consumption.
- Strong correlation of ΔΨm with respiratory capacity and RCR, an index of mitochondrial function, suggested that ΔΨm may reflect mitochondrial efficiency.

Overall, the mitochondrial status of cancer cells may be a factor contributing to cellular radiation response. This work highlights the application of modern mitochondrial assessment techniques to examine novel aspects of the radiosensitivity of cancer cells. Future studies, that include an increased number of cell lines and a multifactorial approach, may yield further insights.

CHAPTER 5

DO MITOCHONDRIAL DYNAMICS AFFECT CELL SURVIVAL AND RADIATION RESPONSE?

Since mitochondria indirectly support many aspects of cellular damage response, including repair, cell cycle arrest and apoptosis, it is conceivable that mitochondrial modulation may influence radiation response. Changes in mitochondrial dynamics have been found to affect cellular response to cytotoxic agents other than radiation[14, 596, 597]. In addition, cellular bioenergetic and redox status, which are largely determined by mitochondrial function, have been shown to modulate radiation sensitivity[300, 687, 688]. Alteration of mitochondrial fission and fusion processes, which may critically affect mitochondrial function, may influence response to radiation.

The mitochondrial division inhibitor, Mdivi-1, has been shown to cause increased fusion, and was thus used to examine the influence of modulation of such processes on radiation response and cytotoxicity in the current work. This chapter considers inhibition of mitochondrial fission in combination with radiation therapy in terms of cell survival, cell cycle arrest and repair.

5.1. Aims

1) To investigate the influence of inhibition of mitochondrial fission on cancer cell survival.
2) To investigate the potential for inhibition of fission to modulate the radiosensitivity of cancer cells.

The specific objectives were:

a) To demonstrate an Mdivi-1-induced shift in mitochondrial morphology and determine the appropriate concentrations for combination with radiation treatment.
b) To determine the effect of Mdivi-1 treatment on clonogenic cell survival.
c) To determine the effect of Mdivi-1 treatment on clonogenic survival after irradiation.
d) To determine the effect of Mdivi-1 treatment on repair of radiation-induced damage.
e) To determine the effect of Mdivi-1 on radiation-induced cell cycle arrest.

5.2. Methods

The A549 cell line was selected for modulation of mitochondrial dynamics using Mdivi-1 and for the investigation of the effect of Mdivi-1 on radiation response. This cell line was an established model that yields clear mitochondrial morphology and has been used extensively for testing of cytotoxic agents *in vitro*. For radiation survival assays, cells were γ-irradiated using a ^{60}Co-teletherapy unit as described in Appendix B2.

5.2.1. Effect of Mdivi-1 on mitochondrial dynamics

5.2.1.1. Assessment of the Mdivi-1-induced shift in mitochondrial dynamics

Mdivi-1 (Sigma-Aldrich) was reconstituted in DMSO to a stock concentration of 57 mM. Working solutions were diluted in RPMI medium supplemented with 10 % FCS and 1 % AB and maintained a DMSO concentration below 0.1 %.

Categorical approach based on morphological sub-types

Adherent A549 cells were plated at a density of 10 000 cells per cm^2 onto 22 x 22 mm glass coverslips (Lasec) placed in 35 x 10 mm CELLSTAR® cell culture dishes (Greiner Bio-One) and incubated in RPMI culture medium (with FCS and AB) at 37°C for 12 h to adhere. Dilutions of Mdivi-1 were prepared to final concentrations of 5, 10, 20, 30, 50 and 100 µM. Samples were incubated in 1 ml of the respective Mdivi-1 concentration for 3 h under physiological conditions. Controls containing equivalent concentrations of the vehicle (DMSO) to those of experimental samples were included. In addition, untreated samples were included for comparison with the control samples.

After the required treatment time, Mdivi-1-containing medium was removed and cells were washed once with pre-warmed RPMI medium prior to staining of mitochondria. The MitoTracker® Red staining protocol was outlined in section 4.2.3.1. Briefly, samples were stained with 100 nM MitoTracker® Red (Molecular Probes® Inc) for 15 minutes at 37°C, fixed with 4 % paraformaldehyde in culture medium (Appendix D2.3.1) and stored at 4°C in 1 ml PBS until assessment.

The visualisation and quantification of morphological subtypes was described in Chapter 4.
A minimum of 200 cells per sample (n = 11), from three separate experiments, were classified microscopically using the mitochondrial morphology categorisation system described previously (section 4.2.3.2, Table 4.2).

Control and untreated samples (n = 7), with and without DMSO respectively, were scored in parallel to confirm that the DMSO did not affect mitochondrial morphology and classification.

Small-fragment analysis for the quantification of mitochondrial fragmentation

Methods for quantifying mitochondrial morphology are varied and not standardised for application in different laboratories. Observational approaches for classifying mitochondrial morphology, as used above, are limited by the subjective components of assessment. In an attempt to develop a more objective technique for assessing induced changes in fragmentation, a method based on the technique of Farrand et al. (2013)[689] was applied. The method involves the identification of the minimum number of small (< 3 µm) mitochondrial fragments in individual cells and a diagram illustrating the principle of the technique is shown in Appendix E1.4.

Mdivi-1 treatment and analysis for Small-fragment analysis

The method of Farrand et al. (2013)[689] was modified to quantify mitochondrial fragmentation induced by Mdivi-1. The criteria for distinguishing cells based on fragment number were adapted to account for inherent differences in the extent of fragmentation in our cell lines.

Cells were cultured as described previously and were treated with 30 µM Mdivi-1 for 2 h prior to staining (Appendix C1). MitoTracker® Red-stained cells were divided into groups based on the number of small (< 3 µM) mitochondrial fragments per cell.

Initially, 4 categories, namely, 0-5, 6-11, 12-20 and > 20 fragments were selected arbitrarily to determine the critical level of fragmentation required to distinguish untreated cells from Mdivi-1 treated cells. At least 50 cells were classified per category from 3 replicate samples. The results of this initial experiment to establish suitable criteria are shown in Figure 5.6 in the results section. Further categorisation was then possible to determine the number of fragments required to detect a difference between groups. This pilot analysis set the criteria for subsequent experiments.

An additional analysis of the abovementioned Mdivi-1 treated and untreated samples using a small-fragment threshold of 40 fragments was included. At least 100 cells per group (n = 3) were analysed and categorised as containing either ≤ 40 or > 40 small fragments.

Based on initial preparative experiments, Mdivi-1-induced fusion in A549 cells following a 6 h treatment was evaluated for both 10 and 30 µM Mdivi-1 concentrations. The cells were divided into two categories, namely, ≤ 10 and > 10 mitochondrial fragments.

5.2.2. Effect of Mdivi-1 on mitochondrial membrane potential

Mdivi-1-induced changes in ΔΨm were investigated using A549 cells. The protocol for JC-1 staining was similar to that described in section 4.2.4.1 and detailed in Appendix C3. Cells were plated at a density of 500 000 cells/ml and were incubated in 1 ml Mdivi-1 (30 µM) for 3 h under physiological conditions. Control samples were mock-treated. Samples were washed twice with RPMI and incubated in JC-1 dye for 15 minutes at 37°C. As described previously, images of cells were captured for quantification using fluorescence microscopy (Appendix D).

5.2.3. Effect of Mdivi-1 on clonogenic survival

The toxicity of Mdivi-1 in the A549 cell line was determined initially. Thereafter, the role of mitochondrial dynamics in radiation response was examined using Mdivi-1.

The cytotoxicity of 0, 10, 20, 30 and 50 µM Mdivi-1 in A549 cells was assessed using the clonogenic cell survival assay. Analyses of cell survival with Mdivi-1 were carried out using post-plated assays, as detailed in Appendix B1.3. Briefly, equal numbers of cells for each concentration were seeded and incubated for 20 h prior to treatment. The cells were treated with Mdivi-1 for a total of 6 and 16 h, respectively, at 37°C. After the required exposure time, the Mdivi-1 incubation medium, PBS washes and trypsinised cells were collected to ensure that no cells were discarded. After the appropriate dilutions were made, cells were plated out and incubated at 37°C for 10 days for colony formation. At least 5 replicate samples were included for each dose point. Stained colonies were counted manually and the surviving fraction was calculated as described in section 4.2.2.1.

5.2.4. Effect of Mdivi-1 on cellular radiation response

The potential modulation of radiation response by Mdivi-1 was investigated in the A549 cells using two different Mdivi-1 doses, as determined from initial morphology and survival experiments. The lowest dose that resulted in a significant change in mitochondrial morphology was selected for initial experiments. Subsequent experiments explored the modulation of radiation response using Mdivi-1 doses that showed evidence of cytotoxicity as well as a shift in mitochondrial morphology.

5.2.4.1. Effect of Mdivi-1 on radiation survival

Treatment with doses of Mdivi-1 that induce fusion without cytotoxicity

The lowest Mdivi-1 dose that was shown to alter mitochondrial dynamics in A549 cells was initially used to investigate the modulation of radiation response. In this way, the effect of increased mitochondrial fusion, in the absence of toxicity, on cellular response to irradiation could be assessed. Clonogenic survival after Mdivi-1 treatment for 6 h either prior to or post-irradiation was determined.

As mentioned, cell survival analyses with Mdivi-1 were carried out using post-plated clonogenic assays. Mdivi-1 and radiation treatments were applied in two different schedules that are represented schematically in Figure 5.1. Four experimental groups were included, namely, a control, 5 Gy, 10 µM Mdivi-1 (6 h) and 5 Gy with Mdivi-1. Briefly, cells were either treated with 10 µM Mdivi-1 for 6 h followed by 5 Gy irradiation (immediate plating) or irradiated and then treated with Mdivi-1 for 6 h (delayed plating after irradiation). After the required exposure time, Mdivi-1 incubation medium, PBS washes and trypsinised cells were collected and plated out for colony formation.

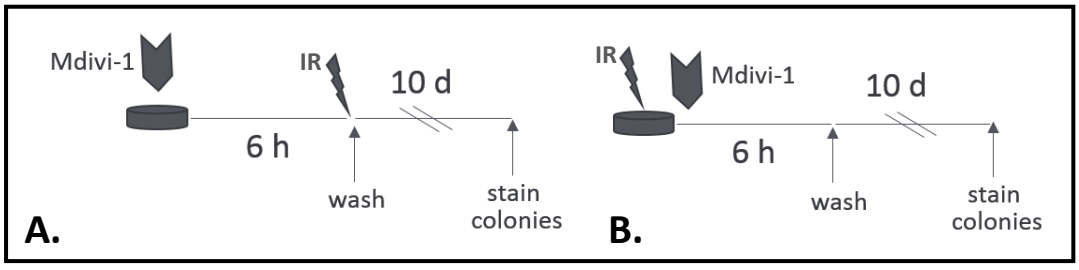

Figure 5.1. Two different treatment schedules for the combination of Mdivi-1 and 5 Gy for examination of the effect of Mdivi-1 on radiation response. **A)** Mdivi-1 treatment for 6 h pre-irradiation and **B)** Mdivi-1 treatment for 6 h post-irradiation.

For Mdivi-1 pre-treatment, cells were irradiated in the presence of Mdivi-1 or the vehicle. Surviving fractions were calculated as described in section 4.2.2.2. To determine Mdivi-1 effects on radiation response, Mdivi-1-induced reduction in survival was taken into account by using the plating efficiency of cells exposed to Mdivi-1 alone. Surviving fractions were determined from 8 replicates collected from two separate experiments.

Treatment with doses of Mdivi-1 that induce fusion and cytotoxicity

Clonogenic cell survival assays were also used to examine the effects of higher doses of Mdivi-1. Briefly, cells were incubated in 30 µM Mdivi-1 for 6 or 16 h, prior to 5 Gy irradiation. The groups included, an untreated control, Mdivi-1 (30 µM), 5 Gy and 5 Gy with Mdivi-1. Cells were pre-incubated with Mdivi-1 for the required time, as depicted in the irradiation schedule illustrated in Figure 5.2. Cells were irradiated in the presence of Mdivi-1 or the vehicle and were washed before plating. The effects of 16 h Mdivi-1 treatment were investigated with doses of 2, 5 and 8 Gy. Surviving fractions were calculated as described previously for at least 10 replicate samples. Again, for determining Mdivi-1 effects on radiation response, Mdivi-1-induced toxicity was taken into account.

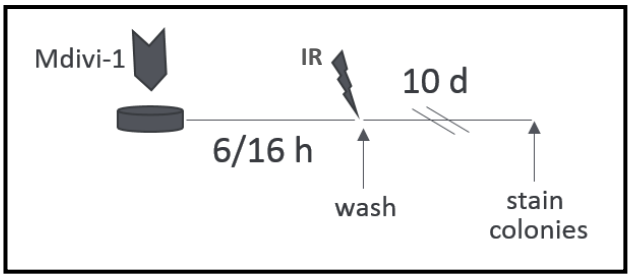

Figure 5.2. Irradiation schedules for different Mdivi-1 exposure times pre-irradiation.

5.2.4.2. Effect of Mdivi-1 on split dose repair in A549 cells

The effect of Mdivi-1 on sub-lethal damage repair after irradiation, was investigated using a split-dose experiment.

Split-dose repair assay

A pre-plated clonogenic assay (Appendix B1) was used to assess radiation survival after delivering two fractions separated by different time intervals. Cells were plated into 35 x 10 mm CELLSTAR® cell culture dishes (Greiner Bio-One) for a yield of at least 100 colonies after treatment. Cells were incubated overnight at 37°C to adhere before irradiation.

Cells were treated in triplicate with 30 µM Mdivi-1 or the vehicle for 1 h and then irradiated. A dose of 6 Gy was given in a single fraction or in two separate fractions of 3 Gy each, with up to 6 h between fractions, as shown in Figure 5.3. After each treatment, dishes were washed with 2 ml RPMI to remove Mdivi-1 and samples were incubated for colony formation. Unirradiated controls were mock treated. Recovery ratios were calculated by determining the ratio between the surviving fraction obtained for a split dose and the value obtained for 6 Gy.

To assess any potential radio-modulating effects of Mdivi-1 exposure prior to irradiation, survival at 1 and 7 h were compared. Corresponding unirradiated control samples were included.

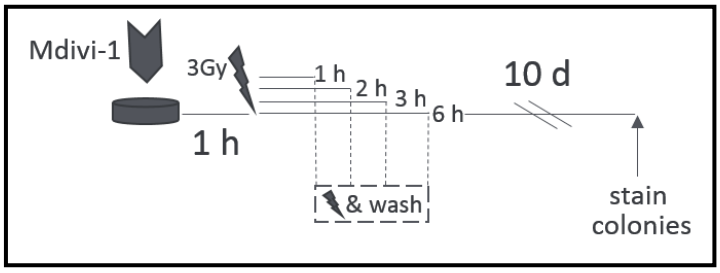

Figure 5.3. Irradiation schedules for examination of the effect of Mdivi-1 on split dose repair.

5.2.4.3. Effect of Mdivi-1 on the cell cycle

The cell cycle distributions for A549 cells were assessed following treatments with combinations of Mdivi-1 and radiation. The groups included, an unirradiated control, Mdivi-1 (30 µM), 5 Gy and 5 Gy with Mdivi-1. The irradiation schedule for the combined group is depicted in Figure 5.4. Briefly, cells were exposed to Mdivi-1 for 1 h, irradiated with 5 Gy and incubated at 37°C for a further 5 h in Mdivi-1. The cells were washed and incubated for an additional time, as necessary, for collection at 5, 12, 24, and 48 h after irradiation. The control groups were mock treated and collected at the respective time points.

Flow cytometry

The flow cytometry protocol is detailed in Appendix G. Briefly, following the required treatment and incubation schedules, cells were trypsinised and pelleted by centrifugation for 10 minutes and resuspended in 2 ml PBS supplemented with 2 % FCS. Samples were washed twice and resuspended in 1 ml PBS (with 2 % FCS). While vortexing, 3 ml ice cold absolute ethanol was added dropwise and cells were incubated at 4°C for 1 h and stored at -20°C.

Cells were stained 24 h prior to analysis. Samples were washed with PBS and resuspended in 500 µl RNAse A solution (1 mg/ml). After incubation at 37°C for 30 minutes, 50 µl propidium iodide (500 µg/ml) was added directly to the RNAse A-containing samples to give a final concentration of 50 µg/ml. Samples were stored in the dark at 4°C until analysis.

Flow cytometry and cell cycle profile analysis were carried out with the assistance of the UCT Flow Cytometry Core Facility (IDM, UCT) using a Beckton-Dickinson (BD) FACSCalibur™ flow cytometer (BD Biosciences, Franklin Lakes, NJ, US) and the ModFit LT™ v3.3.11 data analysis program (Verity Software House, Topsham, ME, US). At the time of sample acquisition, each sample was filtered using a 5 ml Falcon round bottom polystyrene test tube with cell strainer cap (Fisher Scientific, Pittsburgh, PA, USA).

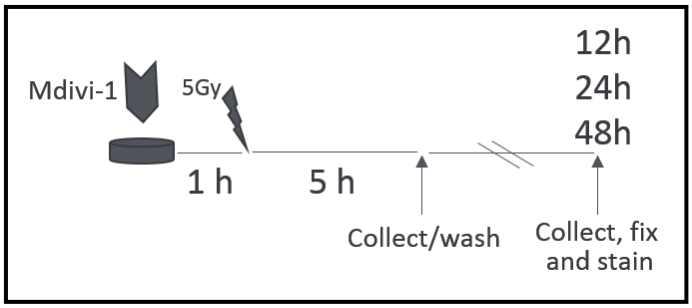

Figure 5.4. Mdivi-1 and 5 Gy irradiation schedule for A549 cell cycle analysis.

5.2.5. Statistical analyses

GraphPad PRISM v6.05 (GraphPad software) was used for all analyses. A p-value smaller than 0.05 was considered statistically significant and error bars in the figures represent SEM.

Mdivi-1-treated and control groups from the Categorical morphological analysis, and Mdivi-1-treated and irradiated groups from clonogenic survival analyses, were compared using ANOVA and the Fisher's LSD test. The Student's T-test (two-tailed, unpaired, equal variance) was used for pairwise comparisons to evaluate differences between Mdivi-1-treated and control groups for Small-fragment and survival analyses. JC-1 ratio values, for quantification of changes in ΔΨm after Mdivi-1 treatment, were compared using the Mann-Whitney U nonparametric test.

Recovery ratios determined for the split-dose repair experiment, for Mdivi-1 treated and untreated samples, and differences in cell cycle distributions were compared for each time-point using the Student's T-test.

5.3. Results

5.3.1. Effect of Mdivi-1 on mitochondrial dynamics

5.3.1.1. Mdivi-1-induced shift in mitochondrial morphology

Categorical approach based on morphological sub-types

The effect of Mdivi-1 on mitochondrial fission and fusion was determined by categorisation of mitochondrial morphology. The overall proportion of cells representing a predominantly fragmented phenotype for each concentration of Mdivi-1 was determined (Figure 5.5). The proportion of cells with fragmented mitochondria (fragmentation index) decreased from approximately 42 to 32 % following exposure to Mdivi-1 concentrations of 10 μM ($p = 0.011$), 30 μM ($p = 0.015$) or 50 μM ($p = 0.015$). The trend towards a decrease in fragmentation was also observed with 100 μM but was not statistically different from controls ($p = 0.381$). At this higher concentration, there was no noticeable swelling of mitochondria, which might indicate stress or cytotoxicity. In addition, comparison of control and untreated samples indicated that the DMSO vehicle did not have a significant effect on mitochondrial dynamics in these cells.

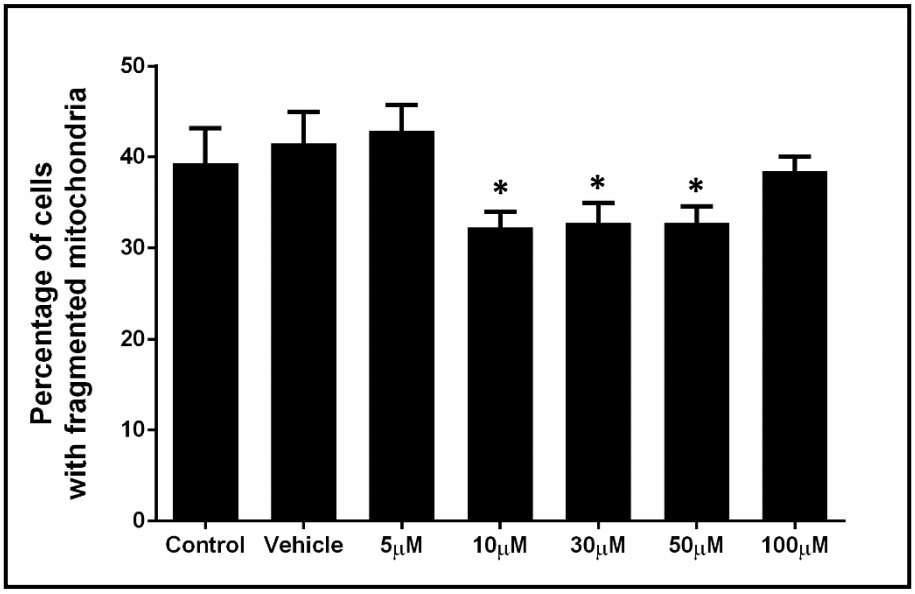

Figure 5.5. Mdivi-1 induced mitochondrial fusion in A549 cells. Cells were categorised using MitoTracker® Red staining following Mdivi-1 treatment. Data are shown as mean ± SEM and represent 11 replicate samples from 3 independent experiments. *$P < 0.05$ versus vehicle.

Effect of Mdivi-1 on ΔΨm

After 3 h Mdivi-1 (30 µM) treatment, the ΔΨm as determined from the mean R:G ratio was significantly increased by 48 % relative to controls ($p < 0.01$).

Small-fragment analysis for the quantification of mitochondrial fragmentation

Figure 5.6A shows the effect of Mdivi-1 on the proportion of cells displaying specific numbers of small mitochondrial fragments, namely, 0-5, 6-11, 12-20 and > 20 fragments. The difference between Mdivi-1 treated and control cells was most evident in the 0-5 fragment category ($p < 0.001$), indicating an increased number of cells containing only a few small mitochondrial fragments for the Mdivi-1-treated group. Conversely, a decrease in the number of Mdivi-1-treated cells displaying a larger number (12-20) of small fragments, was observed, however this was not significant.

Cumulative totals of the proportion of cells displaying up to a certain threshold fragment number are shown in Figure 5.6B. At a threshold number of 10 fragments (≤ 10), the Mdivi-1 treated group was again significantly different from untreated cells ($p < 0.01$). However, while there was a trend towards an increase in the number of cells with ≤ 20 small fragments, this disappeared when a threshold of 40 fragments was used and neither was found to be statistically significantly different.

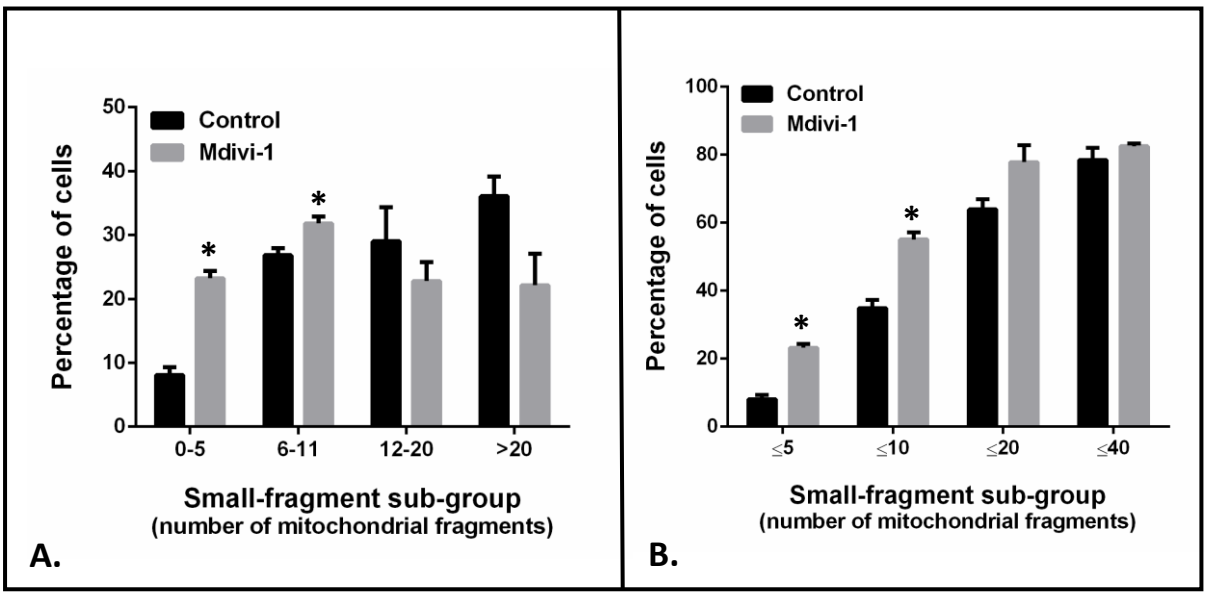

Figure 5.6. A shift in mitochondrial fragmentation induced by Mdivi-1. **A)** Cells displaying specific numbers of small mitochondrial fragments for each category. **B)** Cumulative totals of cells displaying up to a certain threshold fragment number. Data are shown as mean ± SEM and represent 3 replicate samples. *$P < 0.05$ versus control.

The determined threshold value of 10 fragments was then applied to the analysis of 10 and 30 µM Mdivi-1 treatments for 6 h. The method was unable to detect a difference from untreated cells for 10 µM but did show an approximately 30 % change relative to controls for cells treated with 30 µM ($p < 0.01$) (Figure 5.7).

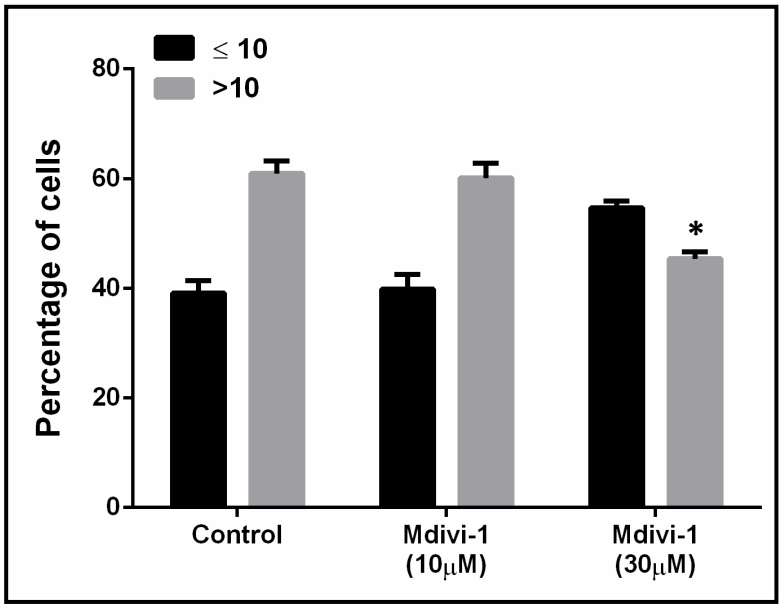

Figure 5.7. Small-fragment analysis of cells treated for 6 h with 10 and 30 µM Mdivi-1, respectively. Dark bars represent the ≤ 10 fragment sub-group while light bars represent cells with > 10 mitochondrial fragments per cell. Data are shown as mean ± SEM and represent 3 replicate samples. *$P < 0.05$ versus control.

5.3.2. Effect of Mdivi-1 on clonogenic survival

The cellular dose response for 6 and 16 h Mdivi-1 treatment is given in Figure 5.8. Mdivi-1 was cytotoxic at concentrations of 20 µM and above for 16 h treatments, with a maximum toxicity of approximately 65 % at 30 µM. The 6 h, 30 µM Mdivi-1 treatments induced minimal toxicity (15 %), however this was not significant. In addition, the 20 and 50 µM survival fractions for the 6 h treatments were similar to that of control samples. The 10 µM Mdivi-1 treatment did not induce a decrease in survival for either treatment time. Additional cell proliferation assays using quantification of crystal violet nuclear staining confirmed that 10 µM Mdivi-1 had no toxicity in the A549 cell line (data not shown).

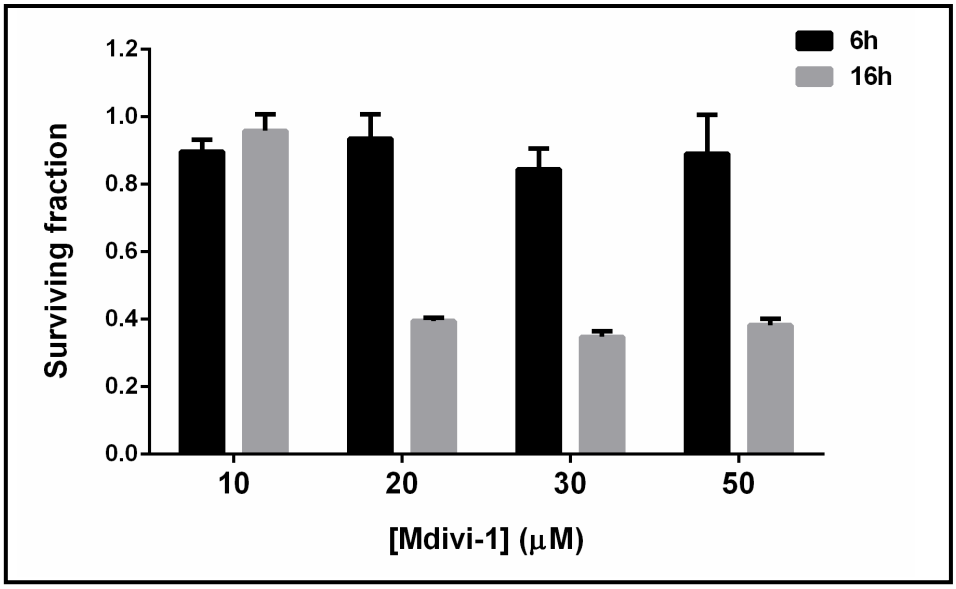

Figure 5.8. Mdivi-1-induced cytotoxicity in A549 cells was dose- and time-dependent. Surviving fractions were normalised to control samples. Data are shown as mean ± SEM and represent at least 5 replicate samples from multiple experiments.

5.3.3. Effect of Mdivi-1 on cellular radiation response

5.3.3.1. Treatment with doses of Mdivi-1 that induced fusion without cytotoxicity

The effect of a low, minimally toxic dose of Mdivi-1 (10 μM) on A549 radiation responsiveness was investigated using clonogenic survival assays. Figure 5.9 illustrates the surviving fraction of cells exposed to Mdivi-1 either before or after irradiation. In these experiments, Mdivi-1 induced minimal toxicity, which was not significantly different from controls. No significant difference was observed between groups for either pre-treatment or post-treatment with 10 μM Mdivi-1. A difference in survival after 5 Gy between the immediate and delayed plating experiments was demonstrated (0.13 versus 0.29, $p < 0.001$).

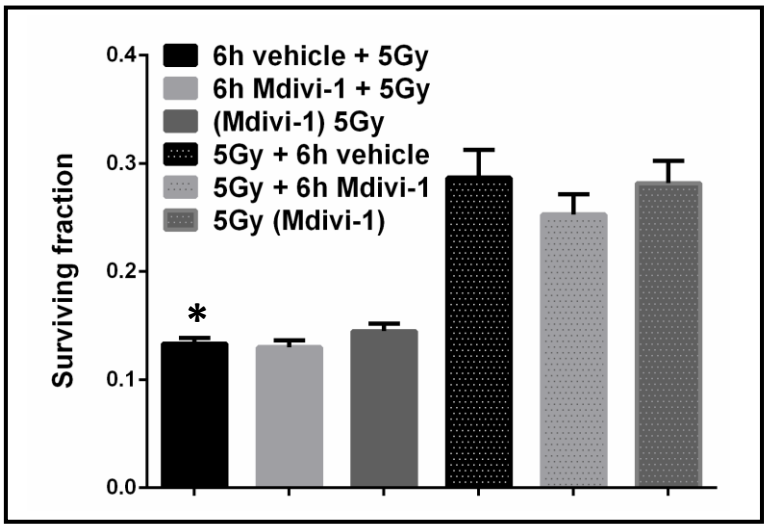

Figure 5.9. Mdivi-1 (10 µM) treatments did not influence radiation response. Cells were pre-treated with Mdivi-1 for 6 h then irradiated (immediate plating) or irradiated and then treated with Mdivi-1 for 6 h (delayed plating). Data are shown as mean ± SEM and represent 8 replicate samples from 2 independent experiments. *$P < 0.05$ versus 5 Gy + 6 h vehicle. The right-hand bar in each set represents the survival after irradiation corrected for Mdivi-1 toxicity.

5.3.3.2. Treatment with Mdivi-1 doses that induce fusion and cytotoxicity

The effect of 30 µM Mdivi-1 (6 h) in combination with 5 Gy was assessed and the survival shown in Figure 5.10. The combined effect of Mdivi-1 and radiation did not significantly reduce survival compared to irradiation alone (0.13 versus 0.10, p = 0.17). The presence of Mdivi-1 also did not influence radiation efficacy as surviving fractions were equal when corrected for Mdivi-1 toxicity. Similarly, no effect on radiation survival was found for 50 µM Mdivi-1 (results not shown).

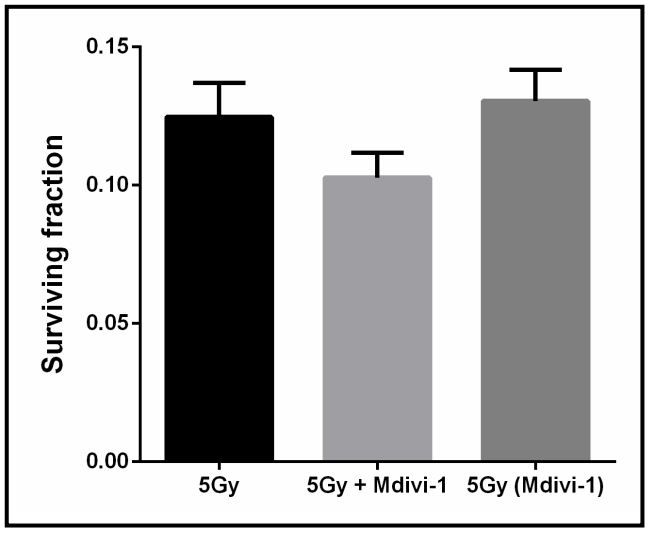

Figure 5.10. Short exposure (6 h) to 30 µM Mdivi-1 did not influence the A549 radiation response. Data are shown as mean ± SEM and represent 10 replicate samples from 3 independent experiments. The bar labelled '5 Gy (Mdivi-1)' represents the survival after irradiation corrected for Mdivi-1 toxicity.

As reported, treatment of cells with 30 µM Mdivi-1 for 16 h reduced survival by approximately 60 %. Moreover, radiation cell kill and radiation efficacy were enhanced with the addition of Mdivi-1 (Figure 5.11). Mdivi-1 when added to 5 Gy resulted in a 5-fold (80 %) decrease in survival relative to radiation alone ($p < 0.001$). Notably, as shown in the right-hand bar, Mdivi-1 sensitised cells to 5 Gy yielding an approximately 40 % reduction in radiation survival ($p < 0.001$).

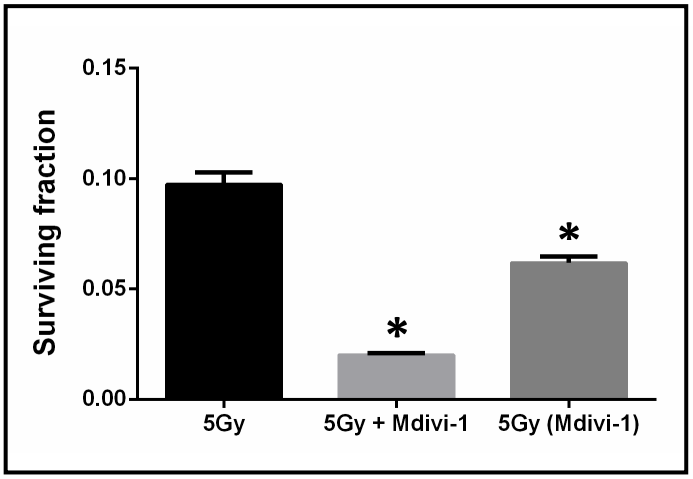

Figure 5.11. Extended exposure (16 h) to Mdivi-1 enhanced the A549 radiation response. The effect of Mdivi-1 on radiation response corrected for Mdivi-1 toxicity is shown on the right. Data are shown as mean ± SEM and represent 10 replicate samples from 3 independent experiments. *P < 0.05 versus 5 Gy.

Modulation of radiation response by Mdivi-1 is also shown in Figure 5.12. Mdivi-1 significantly reduced survival by 40 % ($p < 0.001$) and 25 % ($p < 0.001$) for 5 and 8 Gy, respectively. Mdivi-1 did not modulate radiation survival after 2 Gy.

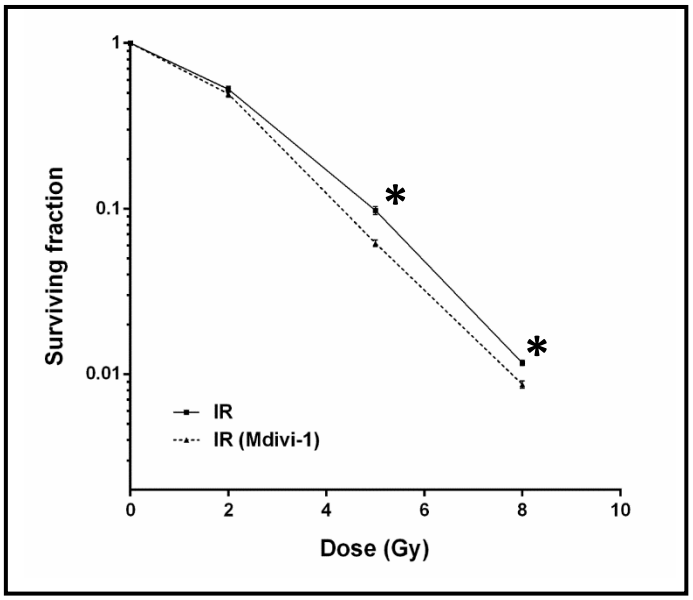

Figure 5.12. Mdivi-1 modulates the radiation response of A549 cells. Cells were pre-treated with Mdivi-1 for 16 h followed by irradiation. Data are shown as mean ± SEM and represent 10 replicate samples from 3 independent experiments. *P < 0.05.

5.3.3.3. Effect of Mdivi-1 on split dose repair

The split dose repair experiment compared the survival after two separate 3 Gy fractions separated by up to 6 h in the presence and absence of Mdivi-1. Figure 5.13 shows the influence of Mdivi-1 on repair of radiation-induced sub-lethal damage. Recovery ratios for samples irradiated alone or in the presence of Mdivi-1, plotted against the time between fractions, are compared. Significant repair was demonstrated when time was allowed between fractions in both the presence and absence of Mdivi-1. Similar repair was observed for both treatments.

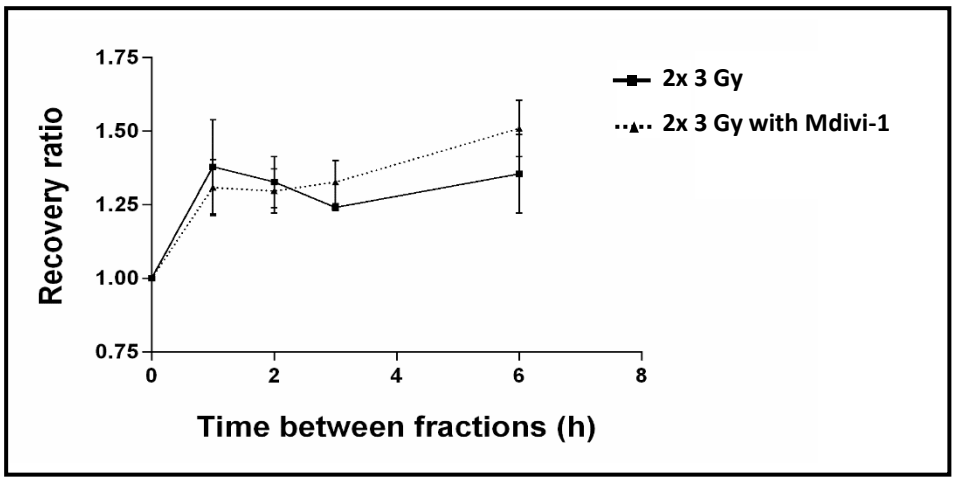

Figure 5.13. Mdivi-1 did not influence radiation-induced damage repair. Recovery ratios indicate the surviving fractions after a split dose relative to surviving fractions obtained using a single fraction. Data are shown as mean ± SEM and represent 3 replicate samples.

5.3.3.4. Effect of Mdivi-1 on the cell cycle

The effect of Mdivi-1 treatment on the A549 cell cycle was investigated using flow cytometry. In addition, Mdivi-1 treatment was combined with 5 Gy irradiation to determine the potential for Mdivi-1 to modulate cell cycle distributions (Figures 5.14 and 5.15).

As illustrated in Figure 5.15, after Mdivi-1 treatment (6 h), a 10 % increase in the proportion of cells in S-phase ($p = 0.01$) was observed with a parallel reduction in the proportion of cells in G1 ($p = 0.01$) relative to controls. After a further 6 h incubation without Mdivi-1, an 80 % increase in the proportion of cells in G2/M ($p < 0.01$) was observed and a 20 % decrease in the proportion of cells in S-phase ($p < 0.01$) relative to controls. At longer times, cycle distributions for Mdivi-1 treated cells were similar to those of controls, however the S-phase population showed a 10 % increase at 24 h, relative to controls with a concomitant decrease in G1 cells.

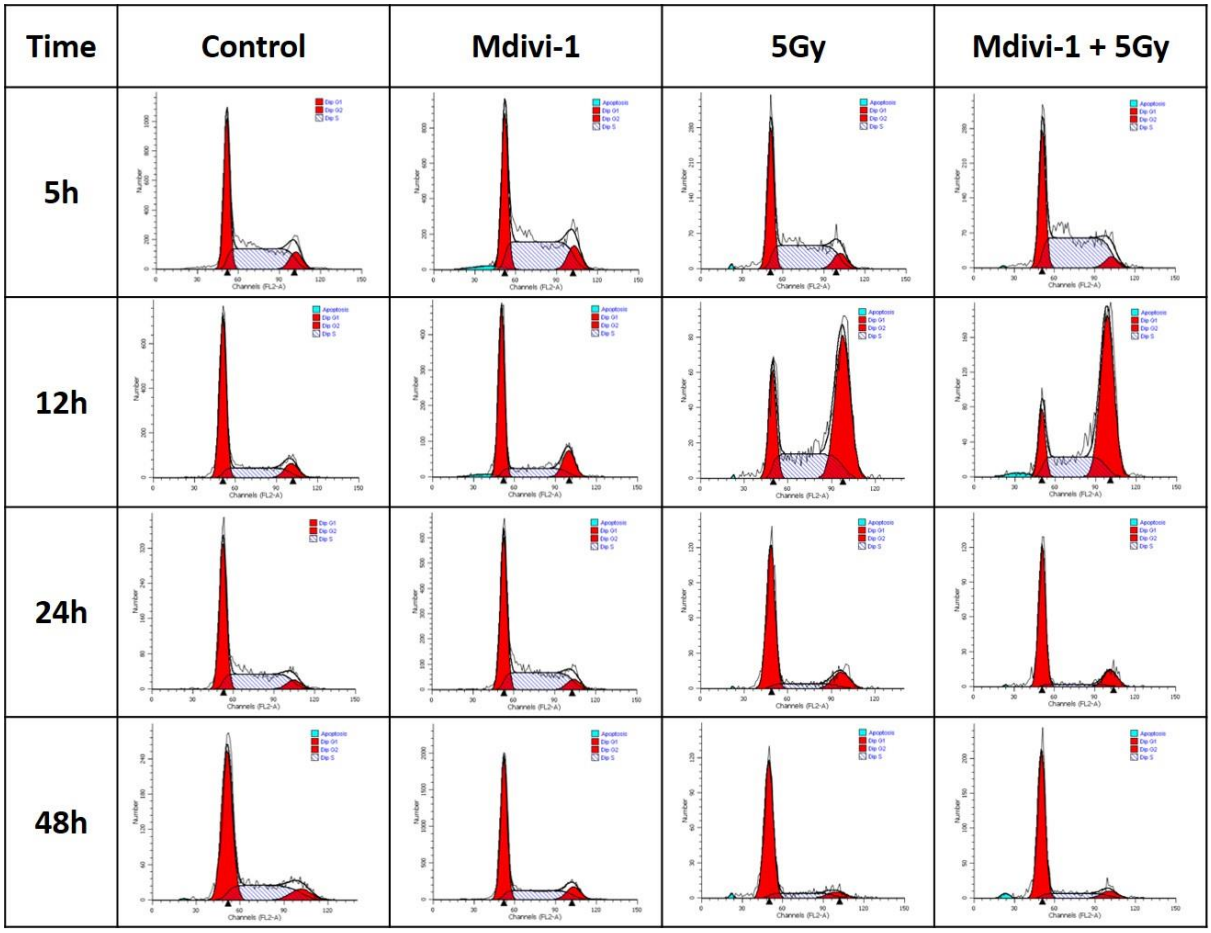

Figure 5.14. Representative cell cycle profiles for cells treated with Mdivi-1, 5 Gy or Mdivi-1 and 5 Gy. Indicated times represent time after irradiation. Cells were treated with Mdivi-1 for 6 h (1 h prior to irradiation followed by 5 h post-irradiation). Replicate data is presented in Figure 5.15.

At 5 h after irradiation with 5 Gy, a similar increase in S-phase cells ($p = 0.02$) and decrease in G1 cells ($p = 0.04$) to that observed with Mdivi-1 treatment was noted. A radiation-induced G2/M arrest was observed at 12 h post-irradiation ($p < 0.001$) relative to control samples, as shown by an approximately 6-fold increase in the proportion of cells in G2/M with a concomitant 70 % decrease in the proportion of cells in G1-phase ($p < 0.001$). At 24 h post-irradiation, the G2/M proportion was still increased 3-fold relative to the control samples. The proportion of cells in S-phase was, however, reduced by 70 %. An increase in the proportion of cells in G1-phase was evident at both 24 and 48 h. At 48 h, a decreased proportion of cells in S-phase was observed.

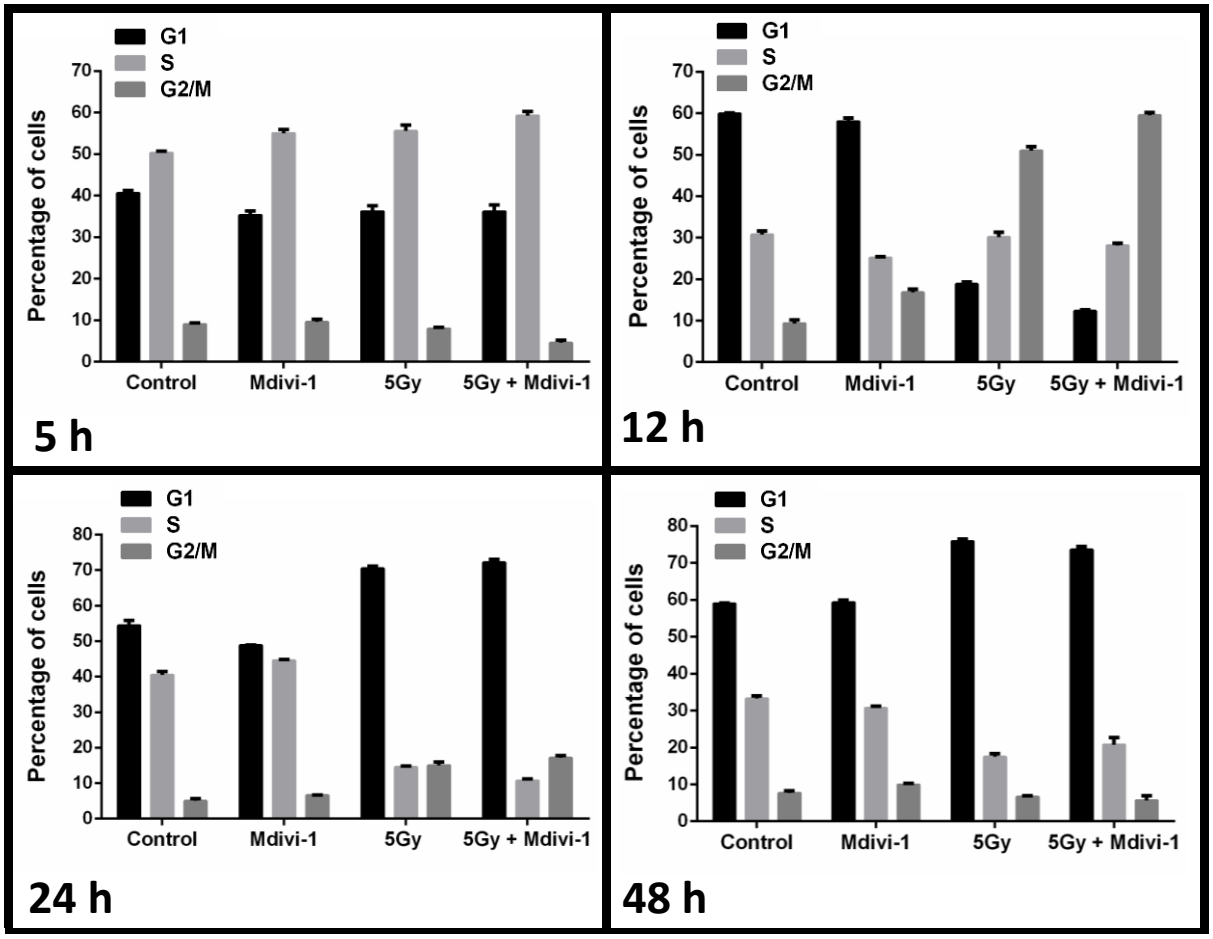

Figure 5.15. Alterations in A549 cell cycle dynamics were demonstrated following Mdivi-1 treatment alone and in combination with irradiation. Cells were treated with Mdivi-1 for 6 h (1 h prior to irradiation followed by 5 h post-irradiation). Time after irradiation is indicated. Data are shown as mean ± SEM and represent 3 replicate samples.

For the combined treatment, the cell cycle distributions at 6 and 12 h were comparatively similar to that observed with both the Mdivi-1 and 5 Gy individual treatments. At 6 h, a more pronounced increase in S-phase cells and a 50 % decrease in G2/M cells ($p < 0.01$) compared to control samples was observed.

The combined treatment of cells with Mdivi-1 and 5 Gy enhanced the radiation-induced G2/M cell cycle arrest at 12 h, as seen by a decrease in the proportion of cells in G1-phase ($p < 0.001$) and a slightly increased proportion of cells in S- and G2-phases relative to irradiation alone (Figure 5.15). At 24 h, the S-phase population was decreased relative to 5 Gy alone while the other phases showed similar proportions of cells relative to that of 5 Gy. The cell cycle distributions at 48 h were similar to that after 5 Gy alone. Cell cycle distributions were normalised to account for slight variations over time in background controls analysed at equivalent times.

5.4. Discussion

Mitochondrial fusion may occur as a consequence of cellular stress[690, 691] and has been shown to guard against radiation-induced mitotic catastrophe[466] and cell death including UV-induced apoptosis[501]. Chapter 4 described the correlations between measures of mitochondrial morphology and function, and cellular radiosensitivity. Although inherent radiosensitivity did not specifically correlate with any single measure of mitochondrial activity in the cell lines analysed, it is possible that modulation of mitochondrial fission and fusion processes may influence the response of cells to radiation.

The mitochondrial division inhibitor, Mdivi-1, has previously been shown to have protective effects against several toxic conditions including exposure to cytotoxic drugs. Thus, we initially hypothesised that inhibition of mitochondrial fission using Mdivi-1 would reduce cellular response to radiation. However, since mitochondrial dynamics have a crucial physiological role, it was thought that Mdivi-1 may also induce cytotoxic effects. Evidence that modulation of mitochondrial dynamics can influence the response of tumour cells to radiation would demonstrate a proof of principle that may hold clinical utility.

In the present study, treatments leading to mitochondrial changes that could be easily controlled or were rapidly reversible were preferred. Mdivi-1 treatment forms such an approach as it induces transient mitochondrial protein inhibition. Embryonic lethality[389, 390] is frequently observed when fusion or fission is abolished with the use of gene knock-out models suggesting that complete loss of these processes is incompatible with life.

Other protein modification tools, such as dominant negative mutants and RNA knockdown, e.g. siRNA, of relevant proteins are commonly used in similar experiments. However, such approaches typically have longer-lasting and more extreme effects on the cells than are expected with Mdivi-1 and may confound investigations into modulation of radiation response. For example, DRP1 knockdown was shown to alter OPA1 expression and induce apoptosis, possibly by affecting cristae structure [24, 692]. In addition, prolonged DRP1 depletion may inhibit cell proliferation possibly through mitochondrial dysfunction[435]. The use of Mdivi-1 has the advantage that investigations can be carried out in an otherwise physiological setting thereby avoiding indirect effects associated with protein depletion. In addition, Mdivi-1 effects are rapid and can be assessed immediately allowing it to be used as a fine regulator of DRP1 activity[693].

5.4.1. Effect of Mdivi-1 on mitochondrial dynamics in A549 cells

The A549 cell line displayed diverse mitochondrial morphological characteristics that could be readily quantified to assess induced alterations in mitochondrial fission and fusion. In addition, this cell line had a relatively high spare respiratory capacity that may suggest that it would be amenable to modulation of mitochondrial function.

Mdivi-1-induced fusion

Cassidy-Stone et al. (2008)[559] first described Mdivi-1-induced fusion. Mdivi-1 has been shown to increase mitochondrial length and connectivity[599, 609, 694-696] as a result of inhibition of fission processes. In addition, alterations in mitochondrial electrical continuity, sometimes referred to as functional fusion, has also been used to demonstrate Mdivi-1-induced effects on mitochondria[21, 507].

Morphological assessment of fusion

In the current work, A549 cells were shown to be responsive to Mdivi-1 treatment using Categorical morphology assessment. A significant increase in the proportion of cells displaying fused mitochondria was demonstrated for Mdivi-1 concentrations of 10 to 100 µM, although the increase was only statistically significant up to 50 µM. This shift in mitochondrial dynamics was detectable despite the modest level of inherent fragmentation of approximately 40 % (Figure 5.5).

Mdivi-1-induced changes in ΔΨm

In addition to the morphological demonstration of fusion, Mdivi-1 was also shown to induce an increase in ΔΨm. The higher ΔΨm was consistent with the shift towards fusion as DRP1-induced fragmentation has frequently been shown to result in loss of ΔΨm[437, 441, 449, 697].

High Mdivi-1 doses may affect the net detectable fusion

Compared to lower Mdivi-1 concentrations, the 100 µM concentration may have been expected to induce even higher levels of fusion. However, the level of fragmentation was found to be reduced compared to lower concentrations. A dose-dependent increase in fusion has been reported previously in COS cells *in vitro*, which expressed increased net-like or perinuclear mitochondria after exposure to concentrations of Mdivi-1 as high as 200 µM[559]. However, owing to a high background fragmentation index (90 %) in COS cells, higher Mdivi-1 doses may have been required to induce comparable levels of fusion to that observed in our experiments.

While this may be an explanation for observing increased fusion with higher doses of Mdivi-1, because of differences in the criteria for categorisation of cells, the experiments cannot be compared directly.

As indicated previously, mitochondrial fusion may result from modulation of proteins involved in mitochondrial dynamics, such as DRP1, or as a direct consequence of cellular stress. While there was no direct morphological evidence of cellular stress in the present experiments, e.g. swollen mitochondria, stress-induced fusion may be relevant at higher concentrations of Mdivi-1 that induce cytotoxicity. Any mitochondrial fragmentation associated with cytotoxicity or cell death processes may oppose Mdivi-1-induced fusion, and possibly account for the smaller change observed with the 100 µM concentration.

DRP1-independent mitochondrial fragmentation may occur in cells that are primed for death[585, 698]. It is possible that the fission associated with cell death and that associated with maintenance of mitochondrial dynamics are distinct processes likely to be governed by their own respective pathways[468].

A study involving the rescue of induced fission in neuronal cells determined 10 µM Mdivi-1 to be the optimum concentration for preventing fragmentation in these cells. However, a concentration of 30 µM resulted in the formation of 'donuts', which may be interpreted as fragmentation and be related to toxicity in these cells[699]. In addition, they reported fragmentation induced by both a fusion and a fission protein, which showed distinct morphological and qualitative differences. Thus at high concentrations, it is possible that alternative fragmentation processes may counteract Mdivi-1-induced fusion.

Small-fragment analysis of fusion

The Mdivi-1-induced increase in fusion was demonstrated using both Categorical and Small-fragment analysis of mitochondrial morphology. A statistically significant change in fragmentation, given by the number of cells containing ≤ 10 small mitochondrial fragments, was observed in cells treated with 30 µM Mdivi-1. Small-fragment analysis was found to provide a more objective and simpler measure of fragmentation than the Categorical method. These two methods quantify unique aspects of mitochondrial fragmentation which may be expressed differently after modulation of fission.

Small-fragment analysis using 10 µM Mdivi-1 did not induce a detectable change in fragmentation, as had been shown using the Categorical method. Variations in the Mdivi-1 exposure times prior to fragmentation analysis using the two methods may account for the differences in results for the lower concentration. It is possible that an early decrease in fragmentation demonstrated at 3 h for the Categorical method was transient and may not have been detectable at 6 h, when Small-fragment analysis was performed. In addition, the Small-fragment analysis may be dependent on the small-fragment threshold value selected. Lower concentrations of Mdivi-1 may be less effective in preventing fission resulting in fewer cells with mitochondrial fragment number corresponding to the 10-fragment threshold.

Although induced fusion following Mdivi-1 treatment has been frequently reported, some studies have failed to show a net change in mitochondrial dynamics[468, 700]. As observed in this study, the lack of a consistent detectable change with 10 µM Mdivi-1 may have been related to the concentration, exposure time or the choice of quantification method. It is possible that although fusion may be occurring it may not be evident as altered fragmentation status.

Notably, Mdivi-1 has been shown to affect TRAIL-induced apoptosis despite a lack of change in net fusion[468]. Thus, modulation of survival may still be possible in the absence of demonstrable Mdivi-1-induced fusion. Alternatively, such modulation, if fusion is not being induced, may partly be due to potential off-target effects. Certain DRP1-independent effects have been observed using Mdivi-1[701] and may play a role independently of mitochondrial dynamics. Overall, a large number of studies report Mdivi-1-induced changes in mitochondrial dynamics as a significant mechanism of action.

Evaluation of fragmentation assessment methods

The Small-fragment analysis method is based on the identification of the proportion of cells expressing a defined number of small (< 3 µm) mitochondrial fragments that may allow distinction between treated and untreated groups. This is a simple and relatively fast method that relies on the determination of cells expressing a small number of mitochondrial fragments improving the precision of the count. Ease of assessment and improved objectivity may render the Small-fragment method more precise than the Categorical method.

The threshold fragment number for the investigation of Mdivi-1 effects was determined by selecting multiple ranges of fragment numbers (Figure 5.6). The ≤ 10 small-fragment sub-group was determined to be the most suitable sub-group for distinguishing between the treated and untreated cells on the basis of statistical significance and proportion of relevant cells.

Both the ≤ 10 and the ≤ 5 small-fragment sub-groups showed statistical significance, however the latter category represented only a small proportion of cells and therefore would be expected to be less accurate.

While the induction of fusion was apparent for Mdivi-1 treatment, a limitation of Small-fragment analysis may be that certain treatments may not necessarily induce an increased number of fragments of the size evaluated. Therefore, it is important that the fragment size be defined when applying this method for specific treatment modalities.

In contrast to other observational approaches, a shift in mitochondrial dynamics indicated with Small-fragment analysis, does not necessarily describe the predominant mitochondrial morphology of the cells. For example, a cell that typically displays predominantly fused mitochondria may, in addition, have a large number of small fragments. Using Small-fragment analysis, this cell would be classified as fragmented, which intuitively may seem incorrect. The inconsistency with a descriptive classification of cells would suggest that the method may not be suited for assessing the inherent mitochondrial morphology of cells. However, it can be argued that assessing the change in the number of small mitochondrial fragments may be of particular value when determining a response to treatment, as it allows quantification of the *process* instead of relying on the predominant morphological phenotype.

It has been observed that smaller mitochondrial fragments are more likely to fuse while long, complex filaments are more likely to fragment[702]. Changes in these processes may therefore be noted by quantification of a change in the number of small mitochondrial fragments, as applied in Small-fragment analysis. Taking into account the dynamic nature of fusion and fission, this classification of cells, although not intuitively descriptive, has the potential to reveal shifts in the dynamic process, as demonstrated in this study. In addition, the Small-fragment analysis should be applicable regardless of the inherent fusion status of the cell population because it depends on a constantly evaluable sub-population of cells.

It is uncertain which of the two methods of analysis is more sensitive to detect a change in fragmentation status. However, it is suggested that the Categorical method is more suited to estimation of the inherent mitochondrial morphology of a population of cells while the Small-fragment analysis is more suited to detecting a change in mitochondrial dynamics in the context of cytotoxicity. Hence, the two methods may complement one another.

Other techniques for assessment of fusion processes

In addition to the morphological assessment of mitochondria, techniques to demonstrate effects on fusion and fission proteins such as DRP1 have been developed. These include Western blotting[588, 590, 613, 696] and immunocytochemistry[611, 699, 700, 703] for total or phosphorylated DRP1 and often include assessment of DRP1 translocation by determination of the mitochondrial and cytosolic DRP1 content separately. There is generally a good correlation between the changes observed at the protein level and the effects on mitochondrial dynamics; however very few studies have used both approaches and the evidence for correlation is therefore limited.

5.4.2. Mdivi-1-induced cytotoxicity

As eluded to above, manipulation of mitochondrial dynamics may have negative consequences for the cell. The effect of Mdivi-1 on cell survival was therefore determined in addition to the investigation of a potential role for modulation of mitochondrial dynamics in radiation response. A range of Mdivi-1 concentrations and exposure times were selected based on a demonstrated decrease in mitochondrial fragmentation.

Effects of Mdivi-1 on survival were dose- and time-dependent. A549 cells exposed to Mdivi-1 for 6 h displayed minimal cytotoxicity however, 16 h exposures and concentrations of 20 µM and above were cytotoxic (Figure 5.8). Several studies have determined that Mdivi-1 has cytotoxic effects in normal[441, 469, 573, 585] and cancer cell lines[21, 23, 144, 573, 582, 583]. The level of toxicity displayed in our experiments was similar to that demonstrated by others. Typically, concentrations of 20-50 µM were able to induce toxicity with exposures of 16 h and longer. Toxicity from Mdivi-1 exposures longer than 5 h has been reported[144], however, other studies showed only modest decreases in cell viability with exposures up to 24 h, even with concentrations up to 50 µM[23, 468]. Such treatment, that also showed no net change in mitochondrial dynamics, induced only minimal effects on apoptosis and survival in lung cancer, melanoma and osteosarcoma cells[468].

Similar to our results concerning cell death, Rehman et al. (2012)[21] showed increased apoptosis after 30 µM Mdivi-1 exposure for 16 h. Moreover, similar toxicity to that observed in our A549 cell line, approximately 30 %, was demonstrated in ovarian cancer cells following a 16 h treatment with 50 µM Mdivi-1[583]. Concentrations above 25 and 75 µM were found to be toxic to normal neurons and immortalised hippocampal cells, respectively[441]. In general, Mdivi-1 concentrations of less than 20 µM or short exposure times have not resulted in toxicity[569, 584, 586, 588, 589], which is consistent with our findings.

5.4.3. Effect of Mdivi-1 on cellular response to radiation

Mdivi-1-induced fusion has previously been shown to modulate response to cytotoxic agents other than radiation. Overall, the literature suggests that low Mdivi-1 concentrations and short exposure times either do not influence cell survival or have a protective effect when used in combination with cytotoxic agents. In contrast, higher Mdivi-1 concentrations and longer exposure times result in toxicity, particularly in cancer cells and sensitise cells to cytotoxic therapy. It was hypothesised that Mdivi-1 may modulate radiation response. Two different doses of Mdivi-1 that induced similar levels of fusion but displayed disparate toxicities were combined with radiation.

Significant radiation enhancement by Mdivi-1

Mdivi-1 (30 µM) significantly enhanced radiation sensitivity after 16 h exposure augmenting radiation-induced cell death up to 40 % after 5 Gy (Figure 5.12). Overall, the dose modification factor at 0.1 survival was estimated to be 1.17. Such Mdivi-1 exposures induced notable cytotoxicity alone, representing a 60 % reduction in survival.

Potential mechanisms for sensitisation include effects on repair, differences in initial cellular damage induction, cell cycle distribution changes and altered cell death processes among others. Investigations into the possible mechanisms involved are outlined in Chapter 6.

In contrast to the Mdivi-1-induced radiosensitising effect demonstrated, one of the few studies reporting the effects of Mdivi-1 on radiation response showed that Mdivi-1 prevented radiation-induced fission and reduced the mitotic catastrophe in normal mouse embryonic fibroblasts, suggesting a protective effect. Similarly, use of DRP1 knock-out models resulted in an increase in radiation survival relative to wildtype cells[466]. Other studies combining Mdivi-1 and radiation investigated an effect on mitochondrial status. Mitochondrial fission caused by localised cytoplasmic microbeam irradiation using alpha particles was reduced by Mdivi-1 treatment although respiratory dysfunction could not be prevented[43].

A similar decrease in fission was observed in DRP1 knockdown lymphoma models after UV-irradiation. In these cells, Bax translocation was reduced and cell viability was increased[221] suggesting a role for DRP1 in UV-induced cell death.

The 10 µM Mdivi-1 dose, although shown to induce fusion, did not influence radiation survival. Consistent with our findings, the 10 µM Mdivi-1 concentration was previously shown to be the lowest concentration able to induce a change in mammalian cell mitochondrial morphology[559].

A requirement for the initial investigations was to select the lowest dose (time- and concentration-dependent) that induced a change in mitochondrial morphology without significant toxicity. In this way, any potential effect on radiation response by Mdivi-1 activity could be related to its effect on mitochondrial dynamics specifically rather than as a consequence of cytotoxic effects. Notably, the 10 μM Mdivi-1 concentration did not show a change in fragmentation based on Small-fragment analysis. Therefore, it is possible that the lack of a change in radiosensitivity may be associated with a lack of change in fragmentation status. As fragmentation in this assay is defined by the proportion of cells displaying more than a threshold number of small mitochondrial fragments as opposed to those appearing to be predominantly fragmented, the number of small mitochondrial fragments available for modulation may be important with respect to radiosensitivity.

However, no change in radiation survival was observed for a 6 h exposure to 30 μM Mdivi-1 either pre- or post-irradiation. This suggests that increased fusion, either at the time of irradiation or for a critical time afterwards, does not influence cellular radiation response. Despite the immediate post-irradiation period being an important time for damage repair, exposures to Mdivi-1 during this period failed to modulate radiation survival.

No apparent effect of Mdivi-1 on PLD or SLD repair

Studies investigating the effect of Mdivi-1 on repair of radiation-induced damage are lacking. As expected, as a result of PLD repair, the radiation survival in the post-irradiation treatment schedule was considerably greater than that of the pre-irradiation schedule. Mdivi-1 did not affect PLD repair as evidenced by no difference in radiation survival with delayed plating.

To our knowledge, the influence of Mdivi-1 on PLD repair has not been reported previously. However, PLD repair has been found to be influenced by other modulators of mitochondrial function. For example, reduced mitochondrial ROS from the application of a mitochondrially-targeted antioxidant showed enhanced PLD repair following irradiation[704].

The influence of Mdivi-1 on the repair of radiation-induced sub-lethal damage was investigated using a split dose repair experiment. A549 repair capability has been suggested to be partly responsible for the resistance of these cells to radiation in addition to overexpression of MDM2, which results in reduced p53 expression[648]. Split dose repair appeared to saturate within an hour after irradiation in our cells and was unaffected by the presence of Mdivi-1. Consistent with our results, it has been shown that DRP1 inhibition does not appear to influence repair of radiation-induced DNA damage as no difference in residual γ-H2AX levels after 10 Gy was observed when comparing wildtype and DRP1 knock-out cells[466].

Since repair inhibition has been shown at 22°C in A549 cells[705], split-dose repair experiments were performed at 37°C. Potentially confounding factors, including repopulation and re-assortment of cells in the cell cycle that may occur when cells are incubated at 37°C, can be considered negligible given that repair was largely complete within 1 h.

Inefficient repair of radiation-induced damage may have potentially contributed to the radiosensitising effect of Mdivi-1 described above. Although not specifically investigated, the 16 h Mdivi-1 pre-treatment, which resulted in radiosensitisation, may have had a residual effect on cellular repair capability.

Effect of Mdivi-1 on radiation-induced cell cycle arrest

Mdivi-1 has been shown to induce changes in cell cycle distribution[507, 569-572, 582] and DRP1 knock-down caused a G2/M arrest[88]. Mdivi-1 may partly exert its effects through induced alterations in cell cycle dynamics. This is relevant to radiation since radiosensitivity varies in the cell cycle.

As expected, radiation induced a significant G2/M arrest in the A549 cells. Mdivi-1 also induced a similar, but less pronounced increase in G2/M cells at this time-point. This may represent an Mdivi-1 -induced cell cycle arrest at G2/M or could be a result of the passage of a cohort of S-phase cells into G2/M. Since Mdivi-1 initially induced a slight increase in the proportion of cells in S-phase, a later increase in G2/M may simply be the result of recruitment of cells into S-phase from G0/G1 and partial synchronisation. The slight S-phase increase observed at 24 h is also consistent with such a cohort.

Mdivi-1 appeared to increase the radiation-induced G2/M arrest, however, partial synchronisation of S-phase cells may also have increased the proportion of G2/M cells. The reduced proportion of G1 cells at 12 h for the irradiated Mdivi-1 treated samples compared with radiation alone may indicate an extended G2/M arrest. Such an augmented G2/M arrest may potentially be a result of increased damage incurred with the addition of Mdivi-1.

DNA damage is the primary stimulus for radiation-induced cell cycle arrest and there is some evidence that Mdivi-1-induced arrest may be initiated by similar lesions. Longer exposure times and lower concentrations than used here induced an increase in micronuclei[573] however, Mdivi-1 treatment did not lead to increased γ-H2AX[582], suggesting that direct double-strand breaks may not be induced.

An alternative mechanism, namely DNA replication stress, manifested as an activation of Chk1 has been proposed[572]. In addition, DRP1 knock-down caused aberrant centrosome amplification leading to abnormal spindle attachment[573]. The resultant misalignment of chromosomes, which was also observed with Mdivi-1 treatment by other investigators independently[144, 466], initiated cell cycle arrest as a consequence of activation of checkpoint proteins or changes in cyclin levels.

It is relevant to mention here that Mdivi-1 caused a small increase in the number of mitotic cells after 6 h exposure and these results will be presented in Chapter 6. If this arrest is sustained or amplified after removal of Mdivi-1 (6 h treatment), it may account for the increased G2/M proportion observed at 12 h. This suggests that residual effects persist after Mdivi-1 removal. An increase in the S-phase proportion without a significant increase in G2/M cells, however, was demonstrated in our experiments following 6 h Mdivi-1 treatment. As a result of potential partial synchronisation, an increase in G2/M may be attributed to the passage of this S-phase cohort.

Previous reports, which are consistent with the above findings, link Mdivi-1 effects with cyclin activity. A report indicated that exposure of cells to Mdivi-1 upregulates cyclin E levels resulting in an increase in the number of cells in S-phase[144]. In our study, a similar increase in the S-phase population was noted 5 h after irradiation and this could represent a transient S-phase block. This type of arrest is thought to be initiated to prevent replication of damaged DNA[113, 118, 122].

Overall, we showed that Mdivi-1 alone is capable of causing a G2/M arrest after only a few hours exposure. In addition, we found strengthening of the radiation-induced G2/M arrest when Mdivi-1 was combined with radiation and suggest that this may be a result of additional damage stimulus.

5.5. Conclusions

- Mdivi-1 treatment caused a decrease in mitochondrial fragmentation at a range of concentrations, as determined using the Categorical method. Small-fragment analysis supported the finding of increased fusion at higher concentrations.
- Mdivi-1 reduced cell survival. However, toxicity was dependent on concentration and exposure time. A 16 h Mdivi-1 (30 μM) treatment was significantly toxic.
- Mdivi-1 enhanced cell kill when combined with radiation.
- Mdivi-1 significantly radiosensitised A549 lung cancer cells.
- Mdivi-1 did not alter the cellular radiation response after short treatments.
- Despite the observed change in mitochondrial dynamics, 10 μM Mdivi-1 did not influence radiosensitivity with 6 h Mdivi-1 treatment pre- or post-irradiation.
- Mdivi-1 did not influence sub-lethal damage repair or potentially-lethal damage repair.
- Mdivi-1 induced a significant G2/M cell cycle arrest several hours after exposure and extended the radiation-induced G2/M arrest.

Overall, Mdivi-1 caused mitochondrial fusion and cellular toxicity, and was demonstrated to be an effective modulator of cell cycle dynamics and radiation sensitivity. However, Mdivi-1 did not influence the repair of radiation-induced damage. From these results, it would appear that fission-inhibitors such as Mdivi-1 represent a novel class of agents that may have potential use as radiosensitisers in the clinic.

CHAPTER 6

MDIVI-1-INDUCED EFFECTS ON CELL PROLIFERATION AND SURVIVAL

In Chapter 5, it was demonstrated that the mitochondrial division inhibitor Mdivi-1, could, in addition to influencing radiation response, induce mitochondrial fusion, cytotoxicity and alter cell cycle dynamics. While certain mechanistic aspects were considered previously, it is the intention in this chapter to provide further analysis of the effects of Mdivi-1 on certain cellular processes that may contribute to a mechanistic understanding of how Mdivi-1 modulates radiation response. Processes examined included cell death using clonogenic survival and apoptosis assays, cytogenetic damage induction and cell cycle progression.

When assessing the effect of an agent on radiation response, a number of modulatory processes can be considered. Factors related to mitochondrial function may be important. The activation and efficiency of cell death mechanisms, including apoptosis, affects radiation response. Also, cellular ability to initiate a damage response leading to recognition of damage and repair determines the amount of residual cytogenetic damage. Cell cycle arrest facilitates repair of damage and may be influenced by mitochondrial dynamics.

In addition to the reported effects of Mdivi-1, it was noted in previous experiments that Mdivi-1 caused detachment of cells. Hence, detached and residual cells were investigated independently as this may have had mechanistic implications. The effect of Mdivi-1 on the cell cycle was established using flow cytometry to document cell cycle phase and morphological criteria to quantify mitoses and metaphases. Histone immunocytochemistry was used to confirm G2/M status. In addition, the ability of Mdivi-1 to induce cytogenetic damage was investigated using the cytokinesis block micronucleus assay.

Investigations of Mdivi-1 effects were conducted in two cell models, which have different substrate-adherence dependence and susceptibility to apoptosis. Although similar end-points were assessed for both cell lines, methods for each are described separately.

6.1. Aims

To investigate Mdivi-1-induced cellular effects that may be related to the observed modulation of radiation response, specifically:

a) To determine the fate of cells that remain adherent or become detached after Mdivi-1-treatment and the contribution of these populations to radiation survival
b) To elucidate the effect of Mdivi-1 treatment on the cell cycle
c) To determine whether Mdivi-1 induces cytogenetic damage and/or modulates radiation-induced cytogenetic damage
d) To determine the level of Mdivi-1-induced apoptosis and the influence of Mdivi-1 on radiation-induced apoptosis

6.2. Methods

6.2.1. Effects of Mdivi-1 on A549 lung cancer cells

6.2.1.1. Viability of detached Mdivi-1-treated cells

Clonogenic survival of cells detached during Mdivi-1 treatment was assessed independently of the adherent cell population. In addition, the contribution of this population of cells to the radiosensitising effect of Mdivi-1, described in Chapter 5, was examined.

Survival of adherent and detached A549 cells after treatment with Mdivi-1 and radiation

The adherent and detached cells from the same sample were assayed separately to determine the contribution of each to the decreased cell survival following Mdivi-1 treatment.

Experimental groups included the untreated control, Mdivi-1 (30 μM), 5 Gy and 5 Gy with Mdivi-1. For each of these groups, an unseparated sample was assessed. In addition, a replicate sample for each of the Mdivi-1-containing groups was included for assessment of the adherent and detached cells separately. Clonogenic survival for each group was assessed using a post-plated experiment, similar to that described previously (Appendix B1.4).

Briefly, cells were seeded and treated the following day with Mdivi-1 or the vehicle for 16 h followed by irradiation as required. Control samples were mock-treated. Detached cells were separated from adherent cells by collecting the culture- and rinse-medium containing loose cells.

The adherent cells were collected by trypsinisation. For the samples where the adherent and detached cells were to be separated, the dishes were examined after washing to ensure that all detached cells had been collected. Clonogenicity was assessed as described previously. In addition, the total number of cells in each sample was calculated to determine the proportion of adherent to detached cells.

6.2.1.2. Effects of Mdivi-1 on the cell cycle

The proportion of cells in mitosis after Mdivi-1 treatment

The mitotic index, i.e. the proportion of cells in mitosis, of Mdivi-1-treated cells and control samples, was determined using two different methods. Firstly, the mitotic index was estimated by microscopic quantification of cells displaying the typical condensed chromatin morphology using Hoechst 33342 staining (Figure 6.1). Secondly, DAPI staining of metaphase spreads and associated morphological criteria were used to identify cells arrested in metaphase, specifically.

Mitotic cells, which displayed typical condensed chromatin and finger-like extensions[706] were quantified manually using fluorescence microscopy (Appendix D). A 400x magnification and the blue (WB) fluorescence filter was used for visualisation of the Hoechst 33342 (1 µg/ml in PBS) stained chromatin. At least 500 cells were assessed per slide. Interphase cells were distinguished from mitotic cells by their more uniformly, less-intensely stained chromatin (Figure 6.1).

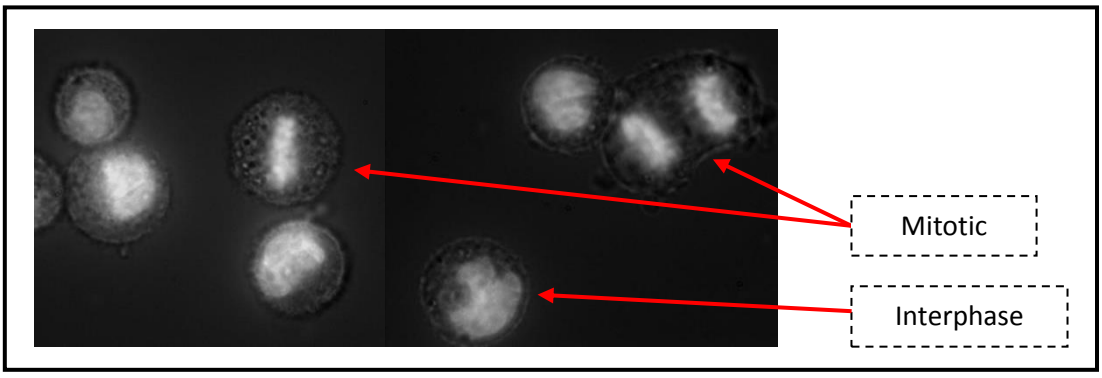

Figure 6.1. A549 cells stained with Hoechst 33342. 400x magnification. Typical mitotic and interphase cells are labelled.

The A549 mitotic index was investigated at 6, 16, 24 and 48 h after Mdivi-1 treatment. Cells were plated at the required density in 35 x 10 mm CELLSTAR® cell culture dishes (Greiner Bio-One) to obtain approximately 500 000 cells at collection. Samples were incubated overnight for the cells to adhere. The medium was replaced with 2 ml RPMI (FCS and AB) containing Mdivi-1 or the vehicle and samples were incubated at 37°C for the required time.

Cells were trypsinised and the medium and PBS washes were collected in 12 ml CELLSTAR® cell culture tubes (Greiner Bio-One) together with the trypsinised cells. After centrifugation at 100 RCF for 10 minutes, cells were stained with 500 µl Hoechst 33342 (1 µg/ml in PBS). Samples were incubated for 15 minutes at 37°C and the Hoechst-containing PBS was replaced with 500 µl paraformaldehyde fixative (Appendix D2.3). After a 20 minute incubation at room temperature, cells were stored in PBS at 4°C protected from light.

Metaphase analysis of Mdivi-1-treated cells

The experimental groups and Mdivi-1 treatment schedules described in the previous section were used for metaphase analysis. After the required treatment time, cells were trypsinised and collected as described previously. Each sample was washed once with 5 ml RPMI (FCS and AB). After centrifugation at 100 RCF for 10 minutes the supernatant was replaced with 4 ml mildly hypotonic, pre-warmed 75 mM KCl (Sigma-Aldrich) and cells were incubated at 37°C for 10 minutes to induce swelling. The KCl was removed following centrifugation and 4 ml of ice-cold fixative solution A (methanol:acetic acid:Ringer's solution as described in Appendix D2.3) was added dropwise to the cell pellet while vortexing. The samples were incubated on ice at 4°C for 24 h and then thoroughly mixed by vortexing. After a 15 minute centrifugation at 200 RCF, cells were resuspended in 4 ml of ice-cold fixative solution B (methanol:acetic acid as described in Appendix D2.3). This step was repeated twice and samples stored at -20°C.

Samples were evaluated using fluorescence microscopy and were prepared by drying 40 µl of the cell sample on a 76 x 26 mm glass slide (Lasec) for 30 minutes. Cells were stained with VECTASHIELD Antifade Mounting Medium with DAPI (Vector Laboratories Inc., Burlingame, CA, USA) and mounted with a 22 x 22 mm glass coverslips (Lasec). Metaphase chromosomes were manually assessed using fluorescence microscopy (WB filter; Appendix D) at 400x magnification and images were captured at 1000x magnification by means of the Moticam Pro Monochrome Scientific CCD camera (Motic) as described previously.

Immunocytochemical assessment of mitotic cells after Mdivi-1 treatment

The increased mitotic index observed in A549 cells treated with Mdivi-1 was confirmed using immunohistochemical detection of Histone-3, which is phosphorylated in mitosis[707]. Cells were seeded at a density of 20 000 cells/ml into 35 x 10 mm CELLSTAR® cell culture dishes (Greiner Bio-One) containing 22 x 22 mm glass coverslips. The treatment groups included an untreated control, Mdivi-1 and 5 Gy. A sample treated with Nocodazole (0.5 µg/ml, Sigma-Aldrich) was included as a positive control.

In addition, two experimental control samples, namely, an autofluorescence control (no antibody) and a secondary antibody control (no primary antibody), were included to control for non-specific fluorescence. The cells were incubated at 37°C overnight to allow adherence to the coverslips. The incubation medium was replaced with RPMI (FCS and AB) containing Mdivi-1, Nocodazole or the vehicle. Samples were incubated for 16 h at 37°C. The medium was collected from each plate and processed separately as Mdivi-1 treatment was shown to cause cells to detach.

The detached cells were collected by centrifugation at 200 RCF for 10 minutes and fixed with 500 µl paraformaldehyde in PBS (4 %). After a wash with 500 µl PBS, the cells were incubated in 200 µl permeabilisation buffer (0.2 % Triton X-100 in PBS) for 10 minutes. The permeabilisation buffer was replaced with 200 µl blocking buffer (2 % BSA, 0.1 % Triton X-100 in PBS, Sigma-Aldrich) and the cells were incubated at room temperature for 45 minutes. After centrifugation to remove the excess blocking buffer, cells were incubated in 200 µl of the primary anti-phospho-Histone-H3 [pSer^{10}] antibody (1/500 dilution, Sigma-Aldrich) for 12 h at 4°C. Samples were washed with 500 µl PBS, then incubated with 50 µl of secondary antibody (anti-rabbit IgG FITC conjugate, Sigma-Aldrich) at room temperature for 1 h and stored at 4°C in PBS.

A similar protocol was used for cells attached to coverslips except that the volume of most solutions was increased to 1 ml to facilitate adequate flooding of coverslips. Antibody solutions were applied in 500 µl volumes. No centrifugation steps were required and an additional wash was included between each step. Adherent cells on coverslips and cell suspensions were mounted on glass slides and samples were visualised using fluorescence microscopy as described previously (Appendix D).

Cell cycle analysis by flow cytometry

Samples were collected after 6, 16, 24 and 48 h exposure to 50 µM Mdivi-1 or the vehicle. In addition, samples were collected 6, 12, 18, 24, 48 and 72 h after 5 Gy. The protocol for preparation of cells for flow cytometric analysis is detailed in Appendix G. Briefly, samples were collected by trypsinisation after the appropriate exposure, washed and fixed with 70 % ethanol (Sigma-Aldrich). The samples were stored at -20^{o}C. Twenty four hours prior to analysis, cells were treated with RNAse A solution (1 mg/ml) and stained with propidium iodide (500 µg/ml). Sample acquisition and analysis of cell cycle profiles were carried out at the UCT Flow Cytometry Core Facility (IDM) using a BD FACSCalibur™ flow cytometer (BD Biosciences) and the ModFit LT™ v3.3.11 data analysis program (Verity Software House).

6.2.1.3. Assessment of Mdivi-1-induced cell death

Mdivi-1-induced apoptosis

Development of apoptosis was quantified after treatment with 30 and 50 μM Mdivi-1 concentrations. The apoptotic index (proportion of apoptotic cells relative to the total cell population) was evaluated after 6, 16, 24, 48 and 72 h of Mdivi-1 treatment.

Cells were seeded into 48-well CELLSTAR® multi-well culture plates (Greiner Bio-One) at a density of 50 000 cells/ml. Cells were incubated at 37°C overnight to adhere to the plastic. The RPMI incubation medium was replaced with medium containing either Mdivi-1 or the vehicle and cells were incubated for the required time. Cells were then collected by trypsinisation, stained with Hoechst 33342 (1 μg/ml in PBS) and assessed as described previously.

Apoptosis was quantified manually by fluorescence microscopy (Appendix D1) using morphological criteria. Cells containing densely-stained, rounded nuclear fragments as a result of condensation and fragmentation of the nucleus [260, 261] were considered apoptotic (Figure 2.6). Cellular blebbing observed under light microscopy was used for additional confirmation of apoptosis. A 400x magnification and the blue (WB) filter were used for visualisation of apoptotic nuclei. A minimum of 500 cells were scored per slide. At least 3 replicate samples were included for each group.

Mdivi-1 and radiation-induced apoptosis

Cells were irradiated with 5 Gy after 16 h Mdivi-1 treatment, washed and incubated for 30 h post-irradiation to allow sufficient time for apoptotic development. The experimental groups included a control, Mdivi-1, 5 Gy and Mdivi-1 with 5 Gy. Cells were plated at a density of 100 000 cells per cm^2 in 35 x 10 mm CELLSTAR® cell culture dishes (Greiner Bio-One) and incubated overnight at 37°C in RPMI medium (FCS and AB) prior to treatment. Cells were treated with Mdivi-1 or the vehicle for 16 h. The treatment medium and two 2 ml RPMI washes were collected in 12 ml CELLSTAR® cell culture tubes (Greiner Bio-One). The samples were centrifuged at 100 RCF for 10 minutes, washed and returned to their respective dishes. Cells were irradiated or mock-treated and incubated for a further 30 h. Samples were trypsinised and processed for assessment of the apoptotic index as described previously. In a separate experiment, apoptosis induced by a combination of radiation and a lower Mdivi-1 exposure (10 μM for 5 h) was also evaluated.

6.2.1.4. Effects of Mdivi-1 on radiation-induced cytogenetic damage

Micronucleus assay

The effect of Mdivi-1 on radiation-induced cytogenetic damage was determined using the micronucleus assay. The experimental groups included a control, Mdivi-1, 5 Gy irradiated and Mdivi-1 with 5 Gy. Cells were seeded at a density of 50 000 cells/ml in 35 x 10 mm CELLSTAR® cell culture dishes (Greiner Bio-One) and incubated at 37°C overnight to allow cells to adhere. The RPMI incubation medium (FCS and AB) was replaced with medium containing either Mdivi-1 or the vehicle and cells were incubated at 37°C for 16 h. Relevant samples were irradiated and the control samples were mock-treated. The incubation medium was collected into 12 ml CELLSTAR® cell culture tubes (Greiner Bio-One), centrifuged at 100 RCF for 15 minutes and washed twice with 3 ml RPMI medium. Each plate containing adherent cells was washed 3 times with 2 ml RPMI and the washes were collected. After centrifugation, detached cells were resuspended in 2 ml RPMI and transferred back to their original dishes. A volume of 40 µl of cytochalasin B solution was added to each sample, yielding a final concentration of 2 µg/ml. Cells were incubated at 37°C for a further 24 h to allow nuclear division and then trypsinised and collected as described previously. Cells were fixed using the methanol-acetic acid fixation technique described in section 6.2.1.2. Samples were stored at -20°C until required.

For microscopic evaluation 30 µl of sample was applied to a 76 x 26 mm glass slide (Lasec) and allowed to dry. The cells were then stained with acridine orange solution (BDH Laboratory supplies). Slides were dipped into 10 µg/ml acridine orange solution for 1 minute, rinsed in ddH_2O and dipped in 0.004 M Gurr phosphate buffer, pH: 6.8 (BDH Laboratory supplies) for 1 minute. Coverslips were mounted with 50 µl of Gurr phosphate buffer.

Micronuclei were assessed in binucleate cells (Figure 2.5). The criteria for identification of micronuclei included: a rounded and smooth appearance; similar shape, colour and texture as the other nuclei; less than 1/3 the diameter of the other nuclei with no overlap[249, 708].

Binucleates containing distinct nuclear membranes and complete division of cell nuclei were included, while cells with nuclei displaying cytoplasmic bridges were excluded[709]. Micronuclei were distinguished from extruded nuclear material or nuclear blebbing. At least 500 cells were evaluated per slide (n = 3).

6.2.1.5. Effects of radiation on Mdivi-1 inhibition of mitochondrial fission

Small-fragment analysis, as described in Chapter 5, section 5.2.1.1 was used to determine a fragmentation index based on the number of small mitochondrial fragments observed in each cell after treatment with radiation and Mdivi-1. Groups included a control, Mdivi-1 (30 μM), 5 Gy and Mdivi-1 with 5 Gy. Cells were plated as described previously and incubated in Mdivi-1 or the vehicle for 1 h. The relevant samples were irradiated as described and incubated for 5 h in Mdivi-1 or the vehicle. Unirradiated control samples were mock treated. Samples were stained with MitoTracker® Red, fixed and assessed microscopically as described. Cells were classified using a threshold value of 10 small mitochondrial fragments.

6.2.2. Mdivi-1 effects in U937 monocytic leukaemia cells

6.2.2.1. The effects of Mdivi-1 on the cell cycle

The proportion of cells in mitosis after Mdivi-1 treatment

Initially, the mitotic index for U937 cells was determined following 5, 24, 48 and 72 h of Mdivi-1 treatment. In addition, this end-point was determined in irradiated samples with or without Mdivi-1 for the corresponding exposure times. Experimental procedures were as described for A549 cells above. However, there was no requirement for cells to adhere overnight or be trypsinised as U937 cells were grown in suspension. To assess the effect of Mdivi-1 removal on the mitotic index, similar experiments were conducted in which a single Mdivi-1 exposure time of 24 h was used. Mitoses were assessed at times up to 72 h after Mdivi-1 removal.

Metaphase analysis of Mdivi-1-treated cells

The experimental procedure for metaphase analysis for U937 cells was as described for the A549 cells above. However, a shorter KCl incubation time of 5 minutes was required. Longer incubation times were found to induce rupturing of U937 cells.

Microscope slides were prepared as described previously for metaphase analysis and cells were stained with VECTASHIELD Antifade Mounting Medium with DAPI (Vector Laboratories). Metaphases were quantified using the MSearch module (Metafer-based metaphase finder-pattern recognition algorithm) v4.0 on the Metasystems Metafer high performance slide-scanning platform (Metasystems Group Inc., Watertown, MA) equipped with a Zeiss Axioskop 2 fluorescence microscope (Carl Zeiss, Göttingen, Germany).

Two replicate slides were included for control and Mdivi-1 samples and a minimum of 5000 cells were analysed per slide. Prior to acquisition of experimental data, a user-trained classifier on the Metafer was applied and the capacity of the module to identify metaphases was verified manually.

6.2.2.2. Assessment of Mdivi-1 induced cell death

Mdivi-1-induced apoptosis

The experimental procedure for apoptosis analysis was similar to that described previously. The method was adapted by resuspending the U937 cells in Mdivi-1 or the vehicle prior to seeding into 48-well CELLSTAR® multi-well culture plates (Greiner Bio-One). After the required treatment times, cells were collected and the wells were rinsed once with 500 µl of RPMI to ensure that all cells were collected. Mdivi-1 exposure times ranged from 5 to 48 h. Hoechst 33342 (1 µg/ml in PBS) staining and evaluation of samples was as described previously. At least three replicate samples were included for analysis.

In addition to the assessment of apoptosis after selected incubation times in Mdivi-1, cells were analysed using a 24 h Mdivi-1 exposure followed by an additional incubation period in Mdivi-1-free medium of up to 96 h to allow time for development of apoptosis.

Mdivi-1-induced modulation of radiation-induced apoptosis

Radiation-induced apoptosis in U937 cells at high doses (20 Gy) generally occurs within a few hours while lower doses (5 Gy) result in delayed apoptosis that is expressed following release of the G2/M arrest and is frequently associated with mitosis[204]. We initially investigated the modulation of radiation-induced apoptosis in U937 cells at high doses of 20 and 30 Gy. The 20 Gy samples were analysed at 5 and 24 h while 30 Gy samples were analysed from 5 to 48 h. At least three replicates were included for analysis. The experimental groups included, controls, irradiated, Mdivi-1 and irradiated with Mdivi-1. Relevant samples were irradiated in a 4 ml volume in 12 ml CELLSTAR® cell culture tubes (Greiner Bio-One) placed horizontally with full build-up. Mdivi-1 or the vehicle was added immediately following irradiation and cells were then seeded into 35 x 10 mm CELLSTAR® cell culture dishes (Greiner Bio-One) and incubated at 37°C for the selected treatment times.

The modulation of radiation-induced apoptosis was subsequently investigated with a lower radiation dose of 3 Gy for comparison with doses closer to the therapeutic range. Sample groups included an untreated control, Mdivi-1, 3 Gy and 3 Gy with Mdivi-1. The Mdivi-1 exposure times were from 5 up to 72 h. Experimental procedures were as described in previous sections.

Modulation of radiation-induced apoptosis following delayed addition of Mdivi-1

The following experiment investigated the effect of Mdivi-1 on radiation-induced apoptosis when an interval between irradiation and the application of Mdivi-1 was incorporated. The previously described apoptosis assay was modified by delaying addition of Mdivi-1 by 6, 24 or 48 h after irradiation. Cells were exposed to Mdivi-1 for 24 and 48 h according to the schedules shown in Figure 6.2.

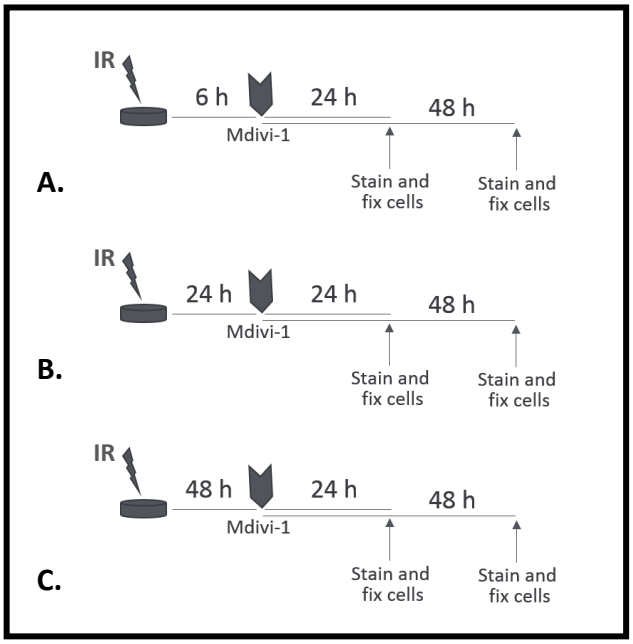

Figure 6.2. Irradiation schedules for investigation of the effect of Mdivi-1 on radiation-induced apoptosis with an interval between 3 Gy and the application of Mdivi-1 in U937 cells. Cells were incubated in Mdivi-1 for either 24 or 48 h, following intervals of 6, 24 or 48 h, respectively.

6.2.2.3. Effect of Mdivi-1 treatment on radiation-induced cytogenetic damage

Micronucleus assay

The U937 cells were seeded at a density of 60 000 cells/ml in 60 x 15 mm CELLSTAR® cell culture dishes (Greiner Bio-One) and were incubated at 37°C in RPMI (with FCS and AB) containing either Mdivi-1 (10 µM) or the vehicle for 24 h. Samples were collected after the required incubation time, centrifuged at 100 RCF and washed once with 5 ml RPMI. Cells were resuspended in 4 ml RPMI (FCS and AB) and irradiated or mock-treated. A volume of 80 µl cytochalasin B solution was added to each sample yielding a final concentration of 2 µg/ml. Cells were transferred to cell culture dishes (Greiner Bio-One) and incubated at 37°C for a further 24 h to allow nuclear division. Cells were fixed, mounted on slides and stained as described previously for the A549 cells.

6.2.3. Statistical analyses

GraphPad PRISM v6.05 (GraphPad software) was used for statistical analyses and construction of graphs for the experiments detailed above. Groups were considered to be statistically significantly different if a p-value smaller than 0.05 was achieved and error bars represent SEM.

In evaluations of survival, the mitotic and apoptotic indices, and micronuclei frequency, the two-tailed Student's T-test was used for pairwise comparisons to evaluate differences between treated and untreated groups. ANOVA and the Fisher's LSD test was used for multiple comparisons. Differences between cell cycle distributions were compared using the two-tailed Student's T-test.

6.3. Results

6.3.1. Effects of Mdivi-1 in A549 cells

6.3.1.1. Viability of detached Mdivi-1-treated cells

Differential survival of adherent and detached cells after Mdivi-1 treatment

Mdivi-1 treatment for 16 or 24 h resulted in the accumulation of rounded and detached cells (Figure 6.3). The absolute survival of cells after 30 μM Mdivi-1 treatment for 16 h was confirmed to be approximately 30 % (Figure 6.4), demonstrating reproducibility of the results reported in Chapter 5 (Figure 5.11). The proportion of cells that detached with Mdivi-1 treatment represented, on average, 28 % of the total cell number. Survival of adherent cells was approximately 25 % higher than that of the unseparated population (the total cell complement), while that of the detached cells was approximately 60 % lower ($p < 0.001$). In addition, the detached cells had a 73 % lower survival than that of the adherent cells after Mdivi-1 exposure.

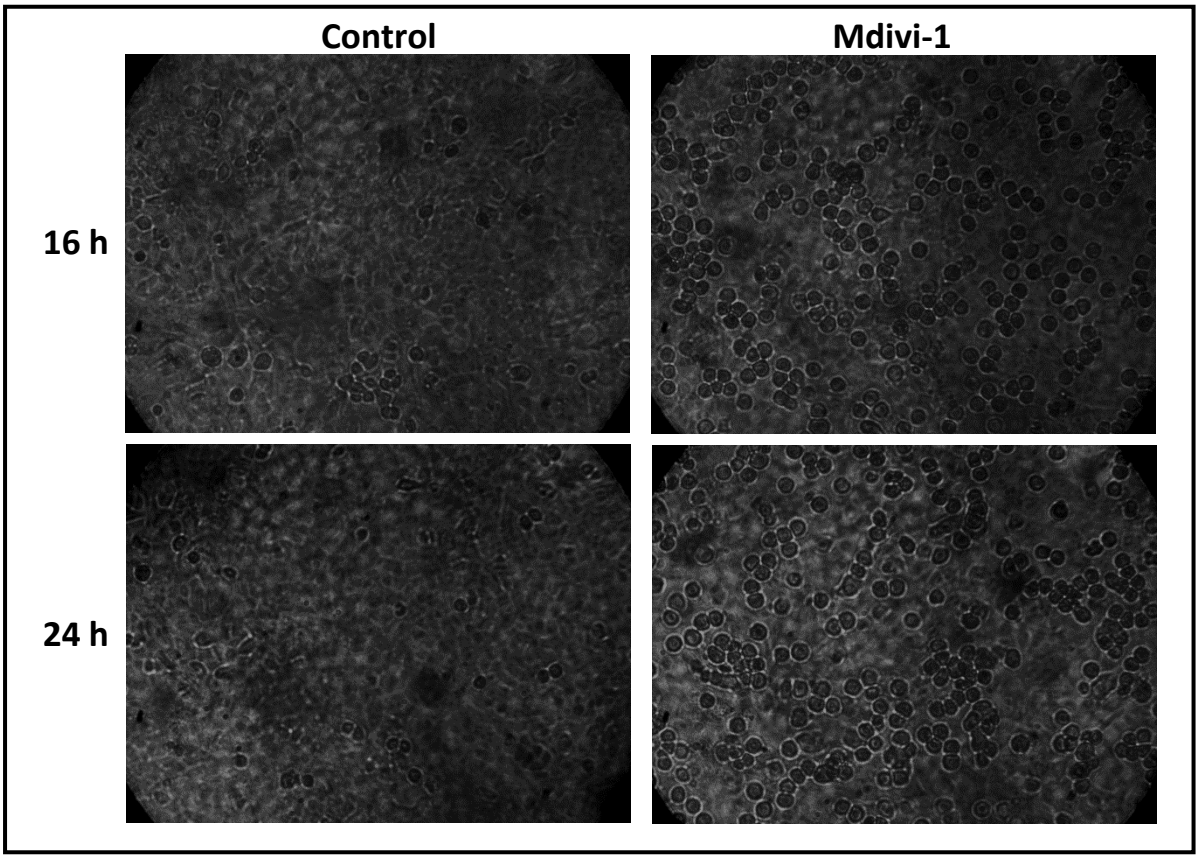

Figure 6.3. Accumulation of rounded and detached A549 cells following Mdivi-1 exposure. 100x magnification.

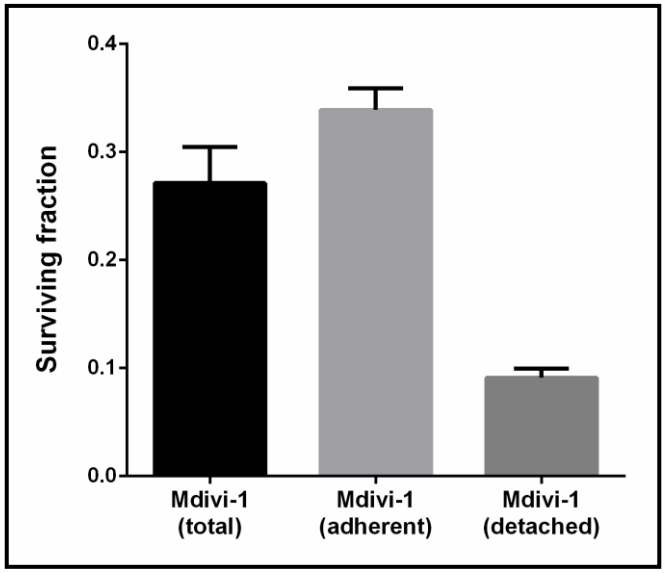

Figure 6.4. Differential clonogenic survival after Mdivi-1 treatment for 16 h in the adherent and detached A549 cell populations compared to the total cell complement. Data are shown as mean ± SEM and represent 4 replicate samples from 2 independent experiments.

Differential modulation of radiation response by Mdivi-1 in adherent and detached cells

The effects of Mdivi-1 and radiation for the unseparated, the detached and the adherent cell populations were compared (Figure 6.5A-C). The radiosensitising effect of Mdivi-1, as reported in Chapter 5, was confirmed and is shown in Figure 6.5A. Survival after irradiation alone or combined with Mdivi-1 was 10 and 1 %, respectively. When the surviving fraction was corrected for Mdivi-1 toxicity, radiation survival was 3 %, indicating significant radiosensitisation ($p < 0.001$).

In addition, the adherent and detached cell populations of equivalent groups were assessed separately for Mdivi-1-induced radiosensitisation. When Mdivi-1 was combined with 5 Gy, similar qualitative differences in survival between the total, adherent and detached cell populations were found (Figures 6.5B and C), as was observed for Mdivi-1 treatment alone (Figure 6.3). When the effects of 5 Gy in addition to Mdivi-1 were assessed, 65 % higher survival was observed in the adherent cell population than in the total population while the detached cells showed a 79 % lower survival (Figure 6.5B).

Figure 6.5C presents the surviving fractions after 5 Gy for the same groups corrected for Mdivi-1 toxicity. The radiosensitivity of the detached cells was significantly greater than that of the adherent cells ($p < 0.01$). The adherent and detached cell populations each showed an approximately 40 % change in radiation survival relative to that of the total population irradiated in the presence of Mdivi-1. The reductions in radiation survival, relative to that of 5 Gy alone, were 81 and 55 %, for detached and adherent cells, respectively.

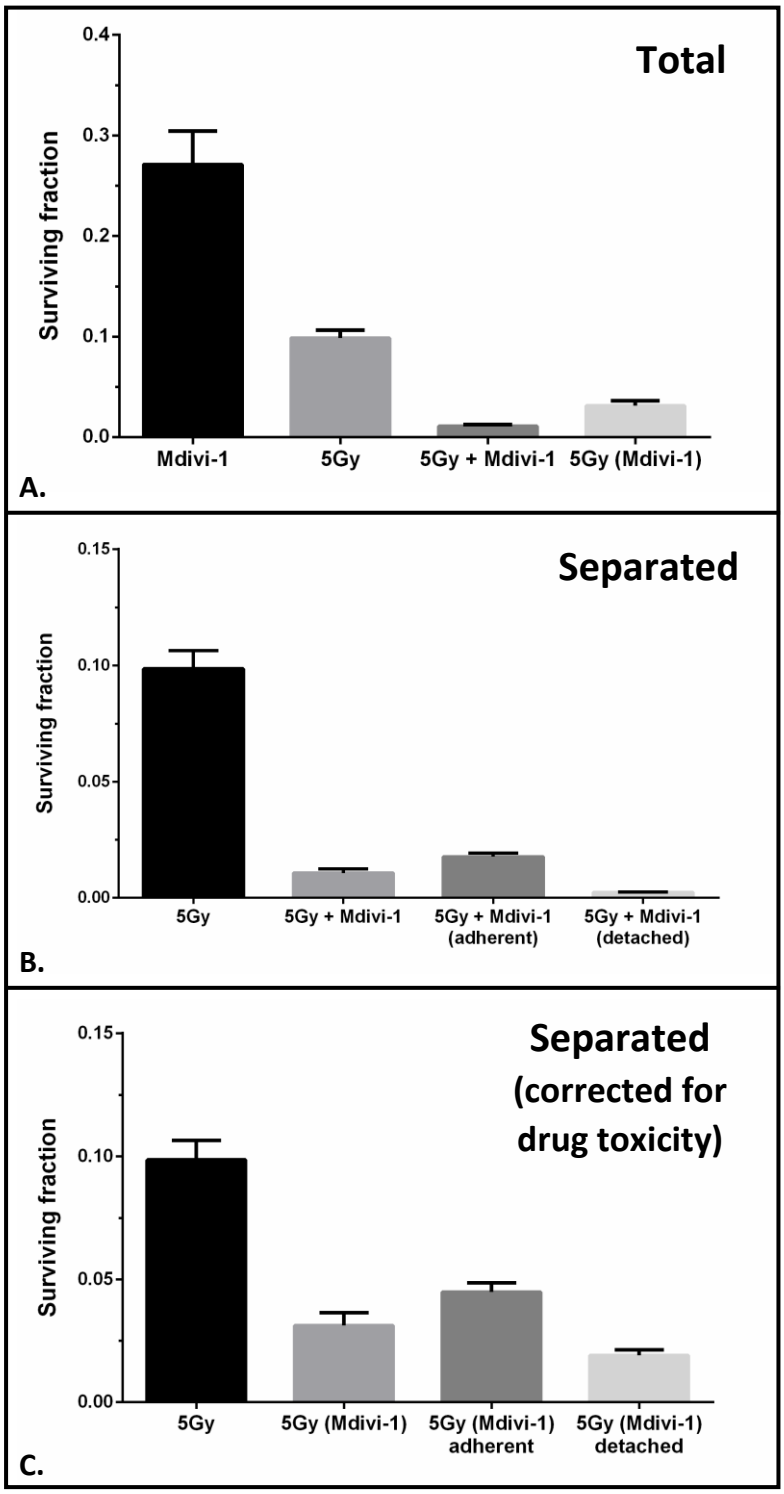

Figure 6.5. Mdivi-1-induced radiosensitisation in A549 cells. **A)** Clonogenic survival following Mdivi-1 and radiation treatments for the total cell complement. The surviving fractions for Mdivi-1 (30 µM for 16 h), 5 Gy, 5 Gy combined with Mdivi-1 [5 Gy + Mdivi-1] and 5 Gy corrected for Mdivi-1 toxicity [5 Gy (Mdivi-1)] are shown. **B)** Reduced clonogenic survival following Mdivi-1 treatment combined with 5 Gy for the separated cell populations. This graph presents the combined toxicity of 5 Gy and Mdivi-1. **C)** Clonogenic survival as shown in (B) but corrected for Mdivi-1 toxicity reflecting radiosensitisation. Data are shown as mean ± SEM and represent 4 replicate samples from 2 independent experiments.

6.3.1.2. Proportion of cells in mitosis after Mdivi-1 treatment

Mdivi-1 (30 µM) treatment induced an increase in the mitotic index of cells relative to control samples for exposure times up to 24 h (Figure 6.6A). The greatest increase, which was 11-fold that of the control, was observed following 16 h continuous Mdivi-1 treatment ($p < 0.001$). Mitoses were subsequently reduced to 5-fold that of the control sample when treatment was extended to 24 h ($p < 0.001$), representing an approximately 30 % decrease relative to the 16 h treatment. Mdivi-1 treatment for 48 and 72 h did not show a significant difference in the mitotic index relative to control samples. Similar results to those obtained for 30 µM Mdivi-1 were obtained for 20 and 50 µM Mdivi-1 concentrations (Figure 6.6B). However, 20 µM induced approximately 50 % less of an increase in mitoses than either the 30 or the 50 µM treatments. The mitotic index for the 20 and 50 µM treatments were significantly greater than that of the control samples for both the 16 and 24 h treatments ($p < 0.001$).

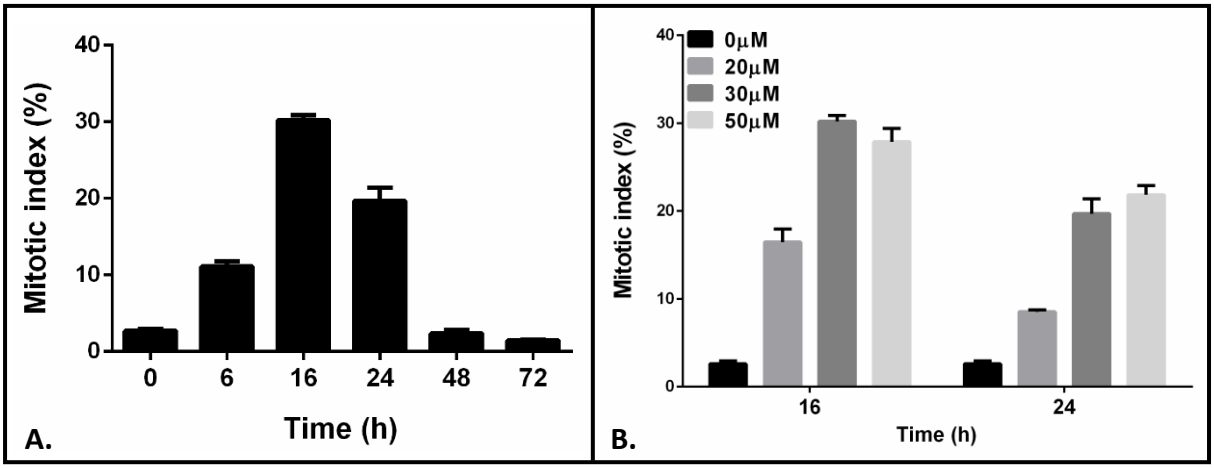

Figure 6.6. Changes in the mitotic index of A549 cells following Mdivi-1 treatment. **A)** Time course showing an increase in mitotic cells up to 16 h. **B)** The mitotic index following 20, 30 and 50 µM Mdivi-1 treatments for 16 and 24 h. Data are shown as mean ± SEM and represent 4 replicate samples.

6.3.1.3. Metaphase analysis after Mdivi-1 treatment

A 16 h Mdivi-1 treatment induced an increase in the proportion of metaphase cells (Figure 6.7).

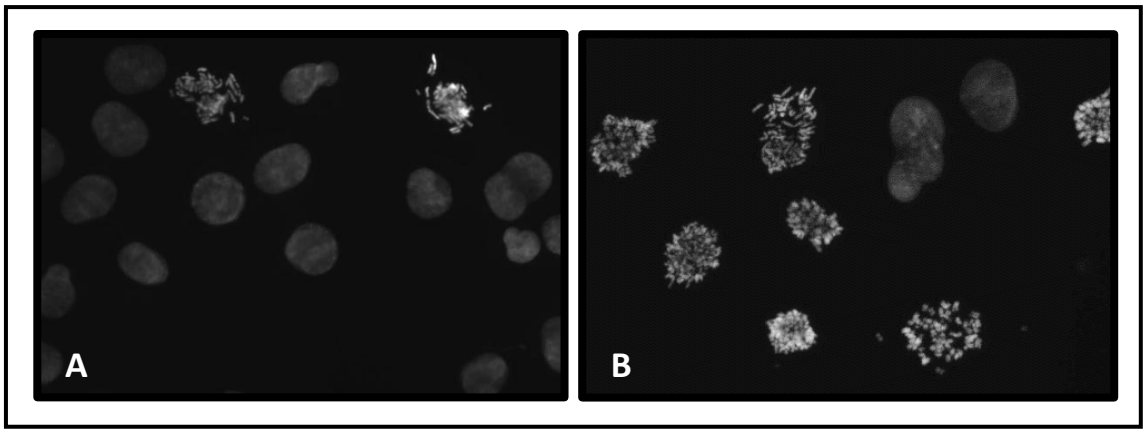

Figure 6.7. Mdivi-1 induced a significant increase in A549 metaphase cells after a 16 h treatment. Representative images from metaphase spreads for **A)** a control sample and **B)** an Mdivi-1-treated sample showing the higher proportion of cells in metaphase compared to those in interphase. 400x magnification.

6.3.1.4. Immunohistochemical assessment of mitotic cells

The increase in mitotic cells observed following Mdivi-1 treatment, as indicated above, was also visualised using phospho-histone 3 staining (p-H3). Cells were labelled with both DAPI and p-H3, which is specific for G2/M phase cells. DAPI stained both mitotic and interphase cells (Figure 6.8A). The brightly stained (condensed) chromatin of the mitotic cell in Figure 6.8B is contrasted with the absence of staining of the interphase nucleus.

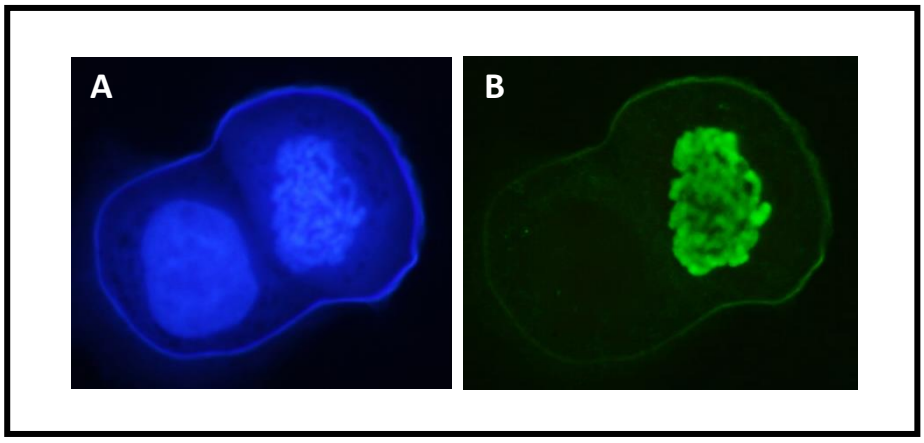

Figure 6.8. High magnification (1000x) example of differential p-H3 staining in mitotic and interphase cells. **A)** Mitotic and interphase nuclei stained with DAPI. **B)** FITC-labelled p-H3 staining of the same cells.

An example illustrating the higher mitotic index induced by Mdivi-1, as indicated by an increased number of p-H3 stained cells, is shown in Figure 6.9. The proportion of p-H3 stained cells for each of the fields is 5, 60 and 25 % for the untreated control, Nocodazole positive control and Mdivi-1-treated cells, respectively.

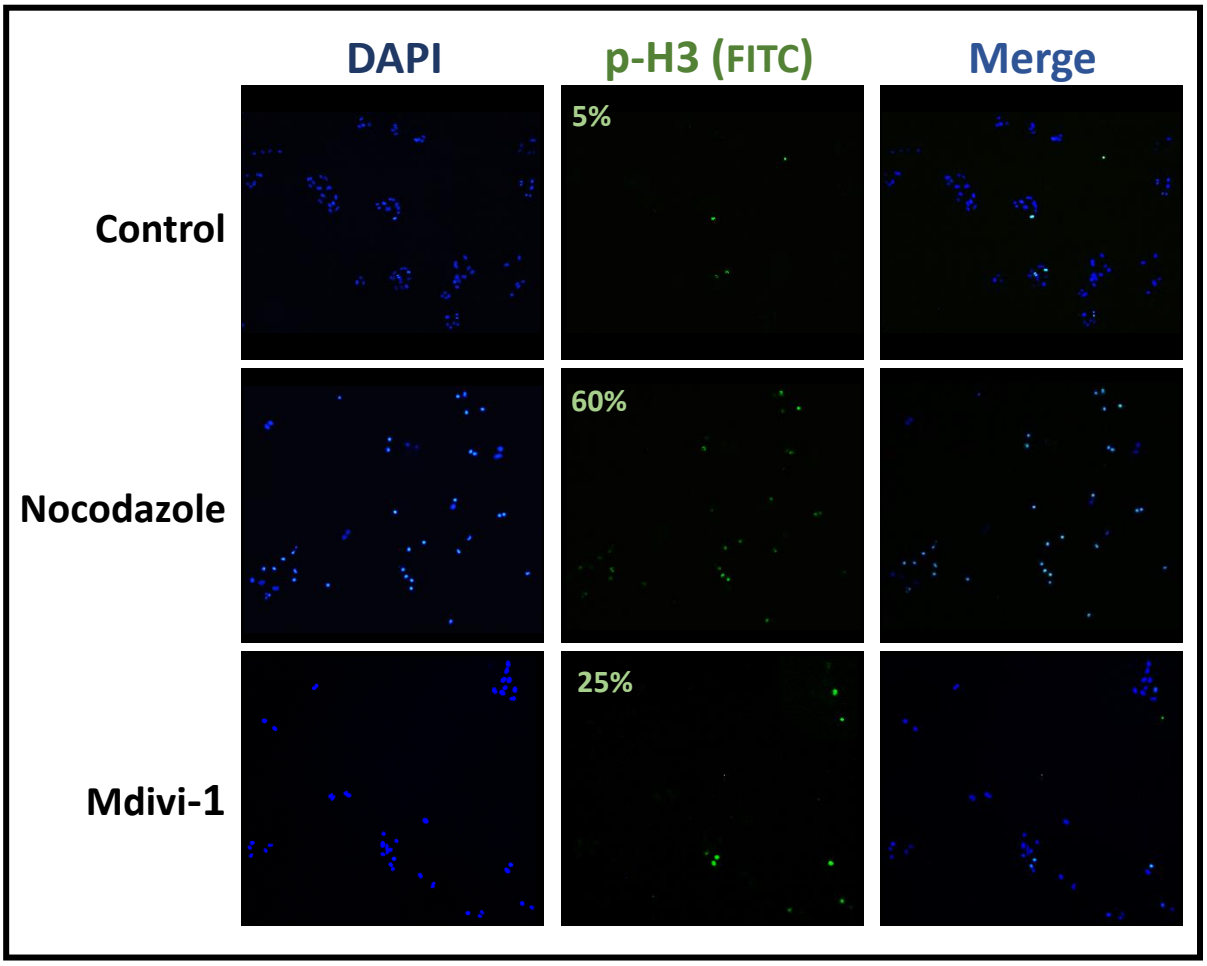

Figure 6.9. Mitotic cells identified by phospho-Histone 3 immunofluorescence. Representative images for an untreated control, nocodazole positive control and Mdivi-1-treated sample are shown (100x magnification). Phospho-Histone 3 staining of mitotic nuclei (centre). Bright staining typically identifies cells in metaphase while G2- and early M-phase cells are more faintly labelled. Cells were counterstained with DAPI. The percentage of cells that showed Phospho-Histone 3 positivity is given for each sample.

6.3.1.5. Cell cycle analysis

Representative cell cycle analysis profiles for the Mdivi-1 and 5 Gy treatments are shown in Figure 6.10. Graphical representations of the cell cycle analysis results incorporating multiple replicates are given in Figures 6.11 and 6.12 for Mdivi-1 and 5 Gy, respectively.

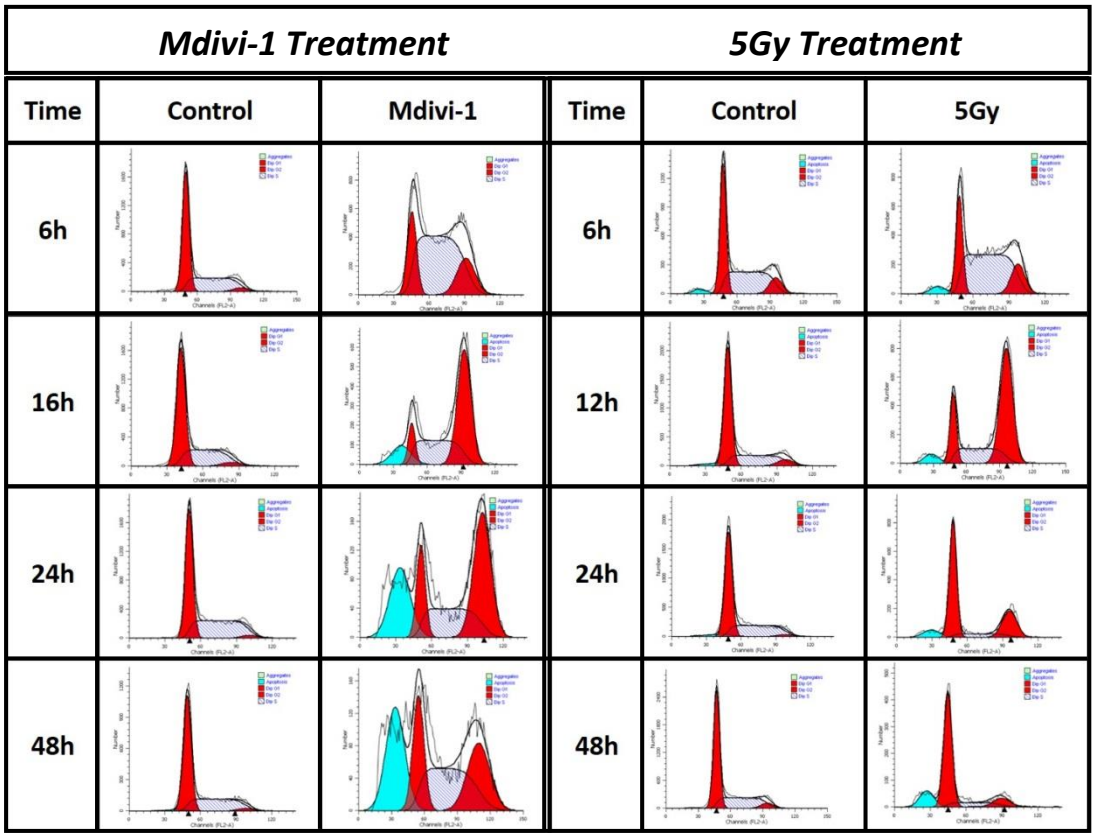

Figure 6.10. Representative A549 cell cycle analysis profiles for Mdivi-1 treatments and 5 Gy irradiated samples. A comparison of the G2/M arrest induced by each treatment is shown. The maximum G2/M arrest was observed at 16 h for the Mdivi-1 treatment and at 12 h for the 5 Gy treatment. The blue pre-G1 peak represents the level of cellular fragmentation (apoptosis) in the samples and is shown graphically in Figure 6.15.

Cell cycle analysis after Mdivi-1 treatment

For the Mdivi-1 treatment, the proportion of cells in G2/M phase was increased for all exposure times analysed relative to that of the control samples ($p < 0.01$). A G2/M cell cycle arrest was observed at 6 h, reflected as a 4-fold increase in G2/M to 16 % (Figure 6.11). At 16 and 24 h the G2/M proportion was increased further to 56 and 51 %, respectively. At 48 h, the proportion of G2/M cells was reduced, relative to the 24 h treatment, to 32 %.

A significant reduction of cells in G1 (68 %), relative to control samples, was observed after 6 h Mdivi-1 treatment ($p < 0.01$) with an 85 % reduction in G1 ($p < 0.01$) at 16 h. For the 24 and 48 h Mdivi-1 exposures, the proportion of G1 cells was reduced by 70 and 55 %, respectively.
In addition, a 70 % increase in the proportion of cells in S-phase, relative to the control samples, was observed at 6 h ($p < 0.01$).

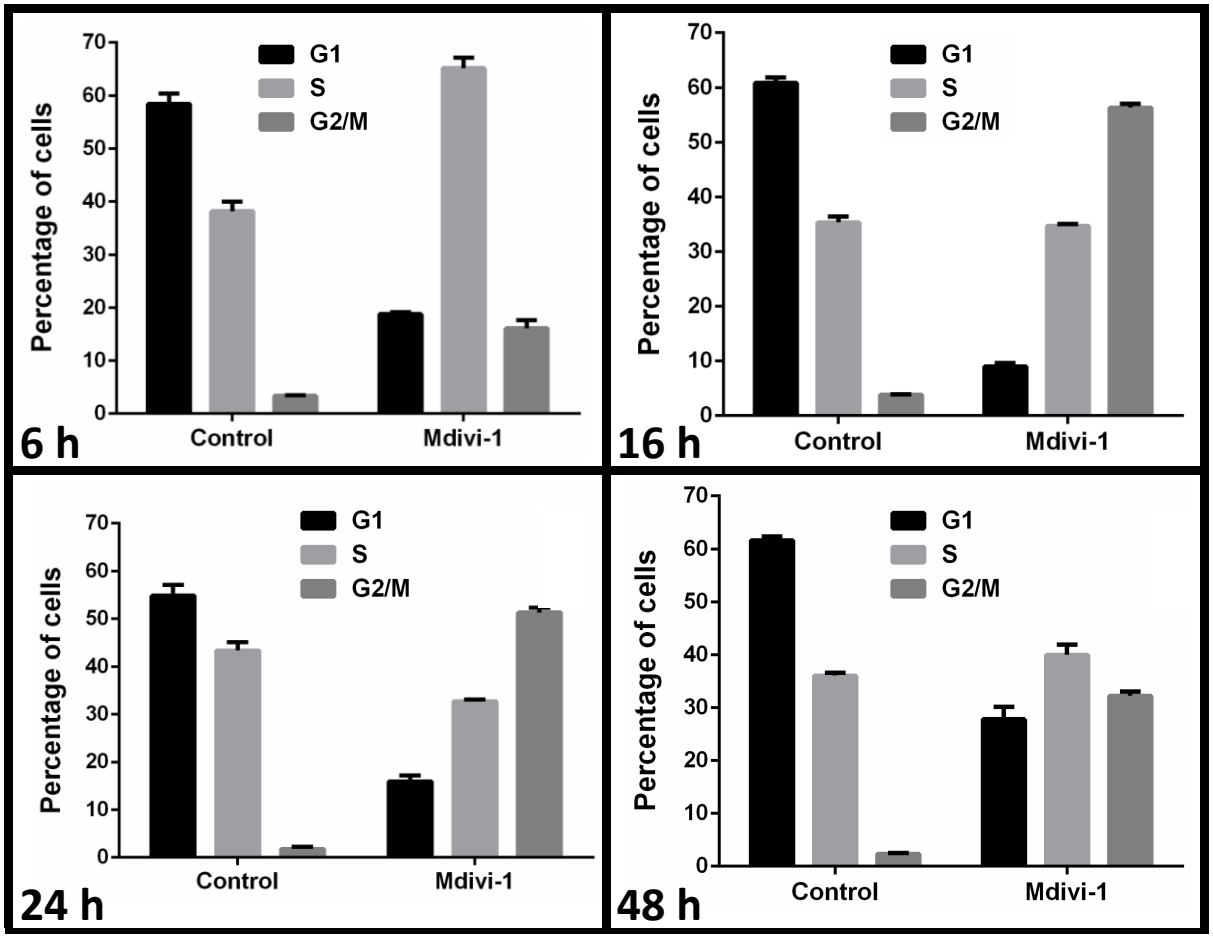

Figure 6.11. A549 cell cycle dynamics following Mdivi-1 treatment. Notably, an increase in the proportion of cells in G2/M was observed at 16 h. Data are shown as mean ± SEM and represent 4 replicate samples.

Cell cycle analysis after 5 Gy

While representative cell cycle profiles for irradiated samples were included in Figure 6.10, a summary of the results is given in Figure 6.12. A radiation-induced cell cycle arrest, as shown previously in Chapter 5, was demonstrated at 12 h. Consistent with previous results, the proportion of cells in G2/M at 12 h post-irradiation was 57 %. The 18 and 24 h treatments displayed a similar increase in the proportion of cells in G2/M, namely 32 and 27 %, respectively. The arrest was still apparent at 18 and 24 h.

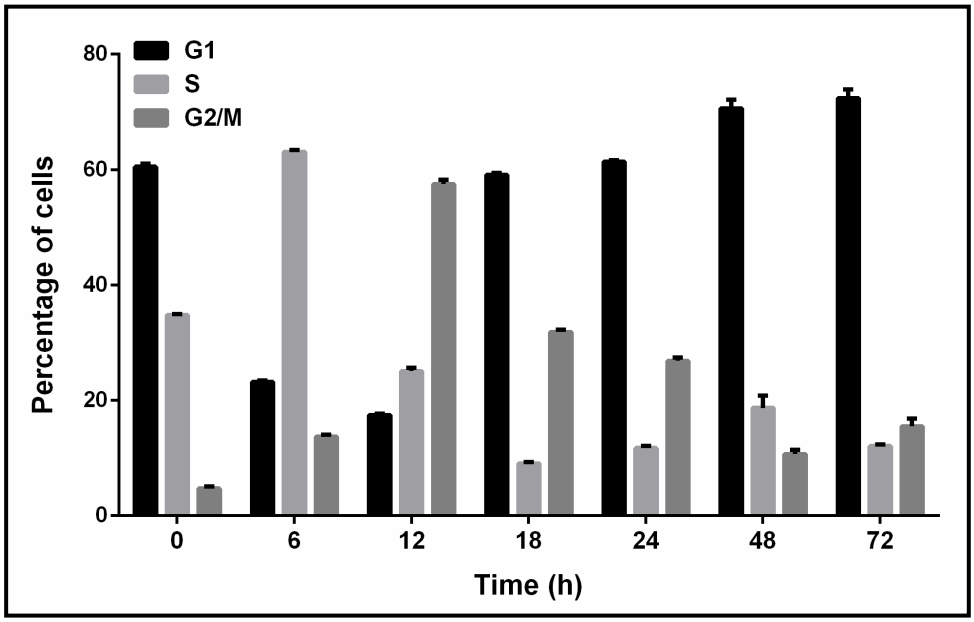

Figure 6.12. A549 cell cycle dynamics following 5 Gy irradiation. The radiation-induced G2/M cell cycle arrest was demonstrated at 12 h. A representative control profile at 0 h is included for comparison. Data are shown as mean ± SEM and represent 4 replicate samples.

6.3.1.6. The effect of Mdivi-1 treatment on radiation-induced cytogenetic damage

Micronuclei were assessed after irradiation, 16 h Mdivi-1 exposure or Mdivi-1 for 16 h followed by 5 Gy (Figure 6.13). Irradiation induced the highest level of cytogenetic damage, which was 8-fold higher than that of the control samples ($p < 0.001$). In addition, Mdivi-1 significantly induced a level of micronuclei that was 4-fold higher than the control samples ($p < 0.01$). Mdivi-1 in combination with 5 Gy, however, induced similar levels of cytogenetic damage as that observed after 5 Gy alone. This combined treatment yielded an approximately 30 % increase in micronucleus-containing cells relative to Mdivi-1 alone ($p < 0.001$ relative to control samples).

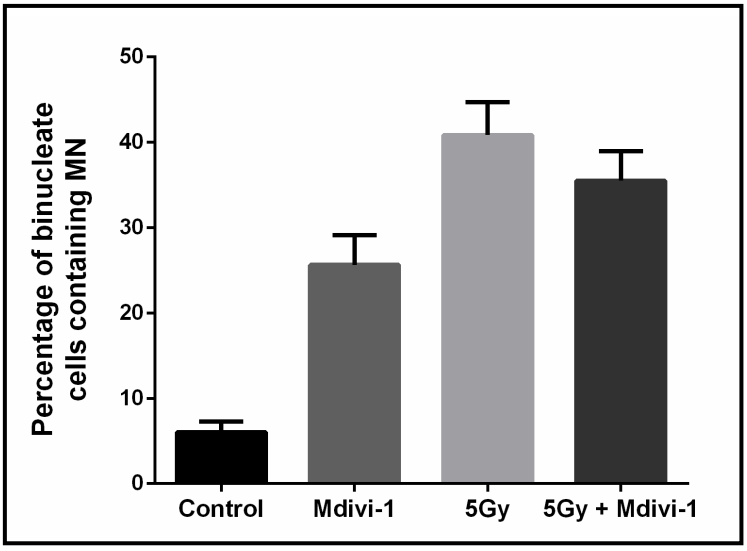

Figure 6.13. Radiation- and Mdivi-1-induced micronuclei (MN) in A549 cells. Data are shown as mean ± SEM and represent 3 replicate samples.

6.3.1.7. Mdivi-1-induced apoptosis

Mdivi-1 induced an increase in the apoptotic index for treatments of 16 h and longer (Figure 6.14). However, the apoptotic index at 6 h was not significantly different from the control samples. Specifically, at 24 h a 3-fold increase was observed for 30 µM Mdivi-1 ($p < 0.001$) while 50 µM Mdivi-1 induced a 4-fold increase in apoptosis ($p = 0.001$). The greatest increase in apoptotic index was observed at 48 and 72 h for 30 and 50 µM Mdivi-1, respectively. Both treatments, however, induced less than 10 % apoptosis.

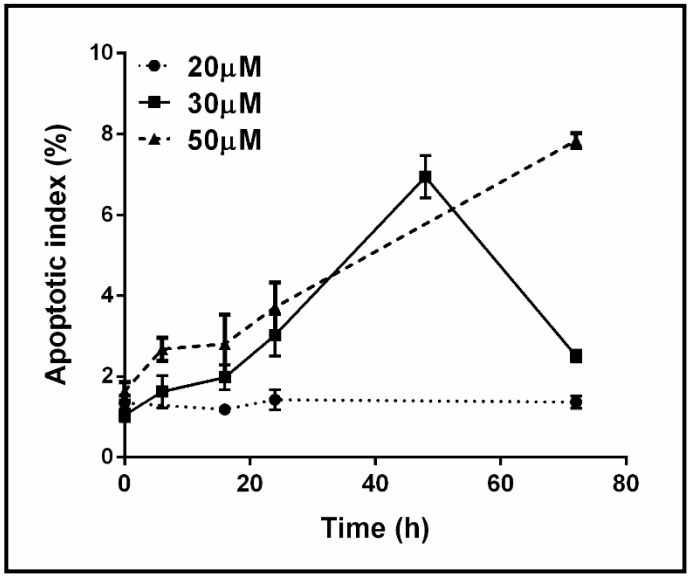

Figure 6.14. Mdivi-1 induced a time- and dose-dependent increase in apoptosis in A549 cells with 30 and 50 µM treatments. Data are shown as mean ± SEM and represent at least 3 replicate samples.

The apoptotic index at 72 h for 30 µM Mdivi-1 was significantly lower than that observed with the 50 µM treatment ($p < 0.001$) and was not significantly different from that of the control samples. Using 20 µM Mdivi-1, no significant difference in apoptosis could be demonstrated.

Cell cycle analysis profiles shown in Figure 6.10 include the sub-G1 peaks, which indicate the proportion of fragmented cells in each sample and include apoptotic cells. A summary for each treatment is shown in Figure 6.15. In general, a lower proportion of apoptotic cells was observed using the Hoechst assay for the same Mdivi-1 treatment. After 16 h Mdivi-1 exposure, 8 % of the cells showed fragmented nuclei, a 20-fold increase relative to control samples. Longer exposure times of 24 and 48 h induced 23 and 27 % apoptosis, respectively.

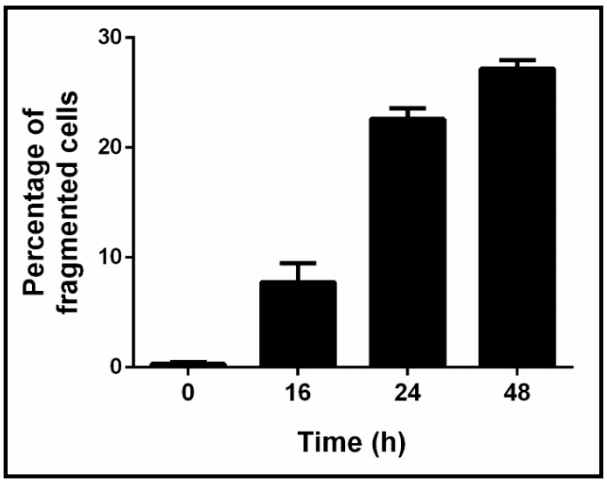

Figure 6.15. Cell cycle analysis showed an increasing proportion of fragmented cells induced by 50 µM Mdivi-1 treatment. Data are shown as mean ± SEM and represent 4 replicate samples.

6.3.1.8. Mdivi-1-induced apoptosis post Mdivi-1 removal

The potential for Mdivi-1 to induce apoptosis after removal of the drug was also investigated. A 6 h Mdivi-1 (50 µM) did not result in an increase in apoptosis when measured directly after exposure (Figure 6.16). Incubation in Mdivi-1-free medium for up to four days after treatment resulted in a slightly higher apoptotic index (1.5-fold increase) relative to the control samples, however, the absolute percentage was negligible.

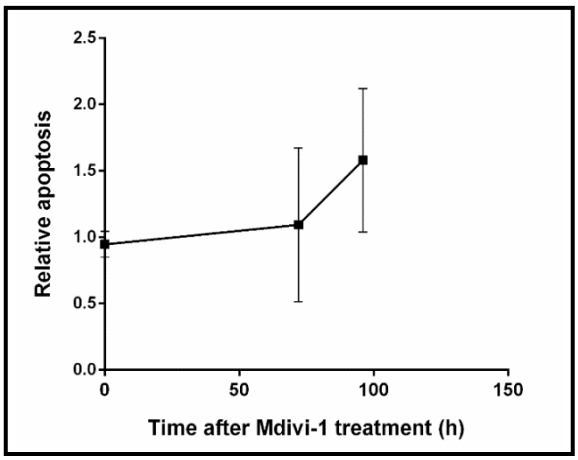

Figure 6.16. A549 relative apoptosis with time after removal of Mdivi-1 following a 6 h treatment. Data are shown as mean ± SEM and represent 3 replicate samples.

6.3.1.9. Mdivi-1-induced modulation of radiation-induced apoptosis

Radiation-induced apoptosis was investigated for the 16 h Mdivi-1 (30 μM) pre-treatment, which previously showed radiosensitisation using the clonogenic assay (Chapter 5). Apoptosis was assessed at 30 h after treatment to allow opportunity for apoptosis development (Figure 6.17). At 30 h post-irradiation, 5 Gy increased the apoptotic index to approximately 8-fold that of the control samples ($p < 0.001$). Mdivi-1 induced an approximately 5-fold increase in apoptosis relative to control samples ($p = 0.01$) at 30 h post-treatment. The absolute percentages were only 1.4 and 2 % for Mdivi-1 and 5 Gy, respectively. The combined effect of Mdivi-1 and radiation resulted in a slightly higher apoptotic index relative to Mdivi-1 alone ($p < 0.01$) however, it was not significantly different from that seen for radiation alone.

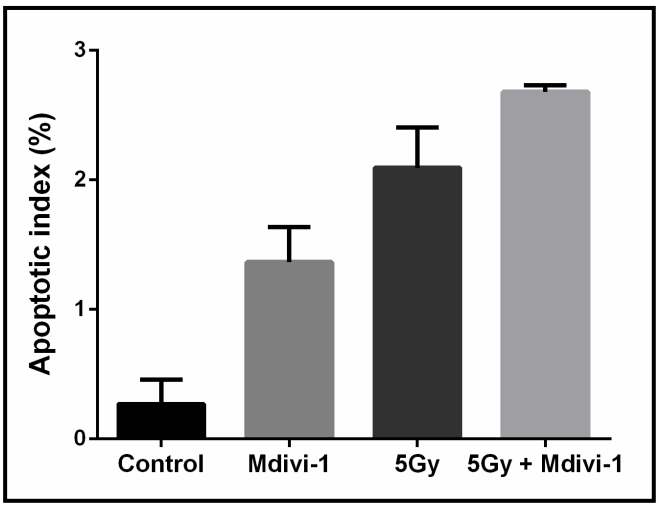

Figure 6.17. Modulation of radiation-induced apoptosis and development of apoptosis after Mdivi-1 removal. Apoptosis was quantified at 30 h post-treatment in A549 cells. Data are shown as mean ± SEM and represent 3 replicate samples.

For comparison, an alternative Mdivi-1 and radiation treatment schedule was assessed. A 24 h continuous Mdivi-1 (10 μM) exposure did not induce significant apoptosis relative to the control samples (Figure 6.18). However, when combined with radiation, the apoptotic index was 40 % lower than that induced by radiation alone ($p = 0.01$).

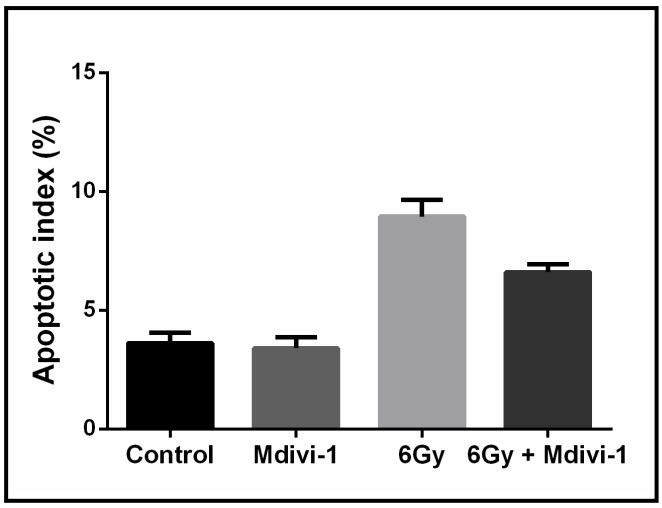

Figure 6.18. Mdivi-1 treatment at a concentration unable to induce apoptosis inhibited radiation-induced apoptosis in A549 cells. Data are shown as mean ± SEM and represent at least 3 replicate samples.

6.3.1.10. Effect of radiation on Mdivi-1-induced increase in mitochondrial fusion

Small-fragment analysis to demonstrate the effect of radiation on Mdivi-1-induced changes in fragmentation index is shown in Figure 6.19. Radiation was not shown to influence mitochondrial fragmentation. An increase in the proportion of cells containing ≤ 10 small fragments, i.e. increased fusion, was observed for the 6 h Mdivi-1 treatment ($p < 0.01$). However, the effect of the combined treatment was approximately 10 % less than that observed with the Mdivi-1 treatment alone.

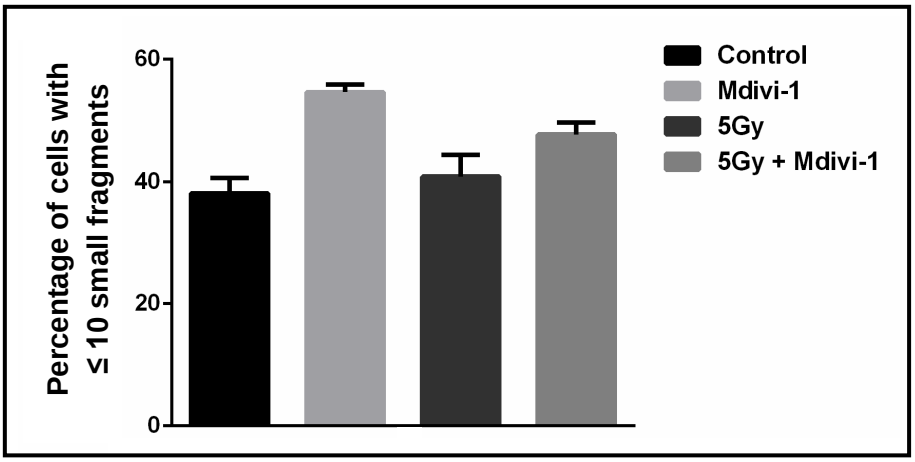

Figure 6.19. Inhibition of Mdivi-1-induced mitochondrial fusion by radiation. Data are shown as mean ± SEM and represent 3 replicate samples.

6.3.2. Mdivi-1 effects in U937 cells

6.3.2.1. Mdivi-1-induced apoptosis

A time-dependent increase in apoptosis was observed after Mdivi-1 exposure (Figure 6.20), with an approximately 10-fold increase in apoptosis relative to control samples for 10 µM Mdivi-1 exposures longer than 20 h. All exposure times assessed, with the exception of the 5 h treatment, showed significant increases in apoptosis ($p < 0.001$). The absolute amount of apoptosis at 24 h was 40±8 %.

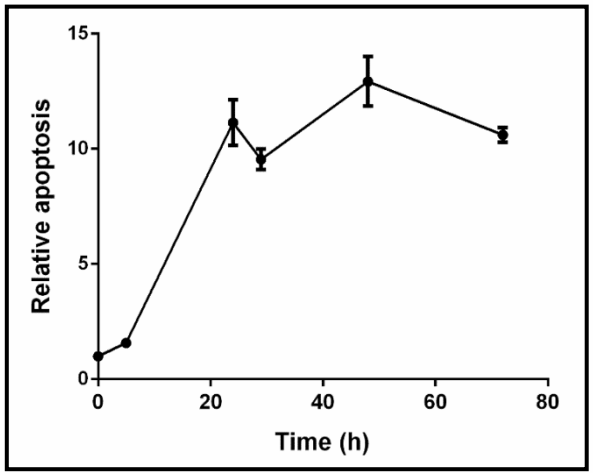

Figure 6.20. Mdivi-1-induced apoptosis in U937 cells with time. The relative apoptosis is presented normalised to the respective control samples. Data are shown as mean ± SEM and represent 4 replicate samples.

6.3.2.2. Mdivi-1-induced apoptosis post Mdivi-1 removal

A decrease in the apoptotic index over time was observed after Mdivi-1 removal. At 24 h after removal a 25 % reduction in apoptosis, relative to that of the 24 h time-point ($p = 0.02$), was determined (Figure 6.21). The apoptotic index was similar to the control samples at four days after Mdivi-1 removal.

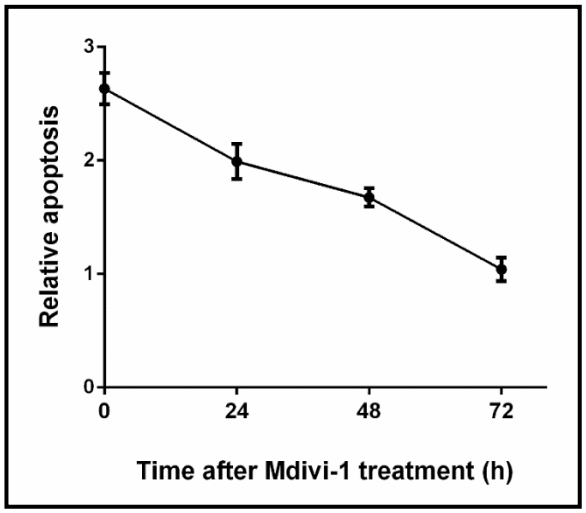

Figure 6.21. Mdivi-1-induced apoptosis with increasing incubation times in Mdivi-1-free medium following a 24 h exposure in U937 cells. The relative apoptosis is presented normalised to the respective control samples. Data are shown as mean ± SEM and represent 3 replicate samples.

6.3.2.3. Mdivi-1-induced modulation of radiation-induced apoptosis

For the U937 cell line, the apoptotic index was quantified for radiation and Mdivi-1 treatments applied concurrently. Radiation doses of 3, 30 and 30 Gy were investigated (Figures 6.22 and 6.23).

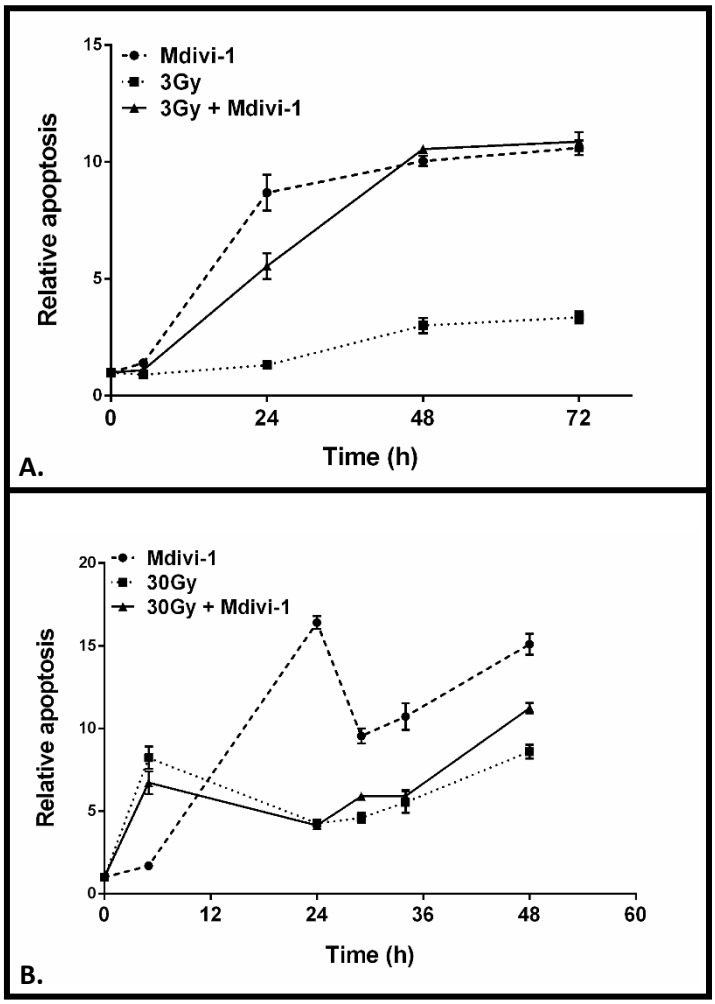

Figure 6.22. Mdivi-1-induced modulation of radiation-induced apoptosis in U937 cells. **A)** After 3 Gy. **B)** After 30 Gy. Apoptosis is expressed relative to a control value determined at each time-point. Data are shown as mean ± SEM and represent 3 replicate samples.

Temporal changes in apoptosis

The effect of Mdivi-1 on apoptosis induced by 3 Gy is shown in Figure 6.22A. In general, the apoptotic index increased over time with all treatments up to 72 h. Mdivi-1 and radiation applied independently induced approximately 10- and 3-fold increases in the apoptotic index, respectively, at 72 h relative to control samples ($p = < 0.001$). The combined effect of Mdivi-1 and radiation at 72 h also yielded an approximate 10-fold increase in the apoptotic index relative to control samples ($p < 0.001$).

The effect of Mdivi-1 on apoptosis induced by 30 Gy is shown in Figure 6.22B. All groups displayed an increase in apoptosis after treatment relative to control samples. Apoptosis was substantially enhanced for Mdivi-1 treatments of 24 h or longer and 48 h induced an approximately 15-fold increase relative to control samples ($p < 0.001$). The combination of radiation and Mdivi-1 induced an approximately 11-fold increase in apoptosis after 48 h relative to control samples ($p < 0.001$). However, the combination did not induce a higher apoptotic index than Mdivi-1 alone. The absolute apoptosis induced by each treatment was approximately 50, 30 and 40 % for Mdivi-1, 30 Gy, and Mdivi-1 with 30 Gy, respectively.

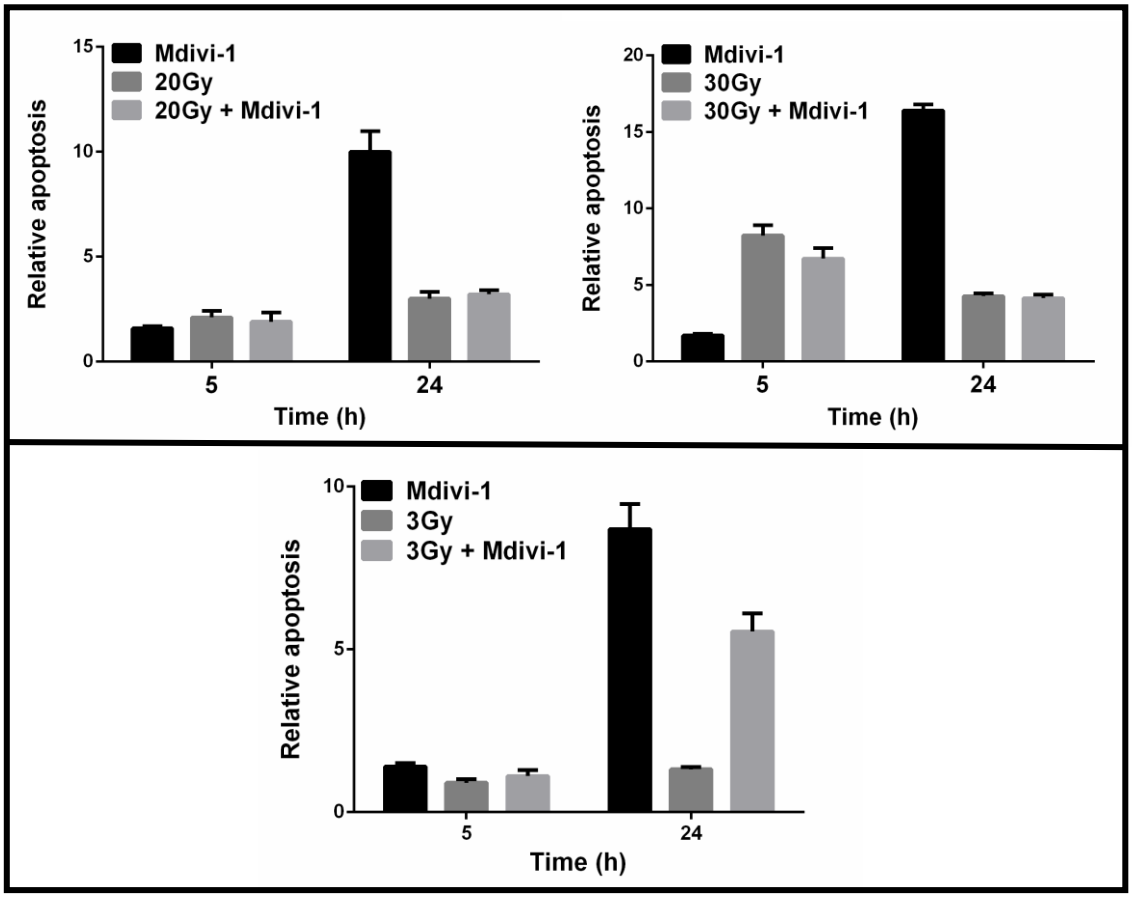

Figure 6.23. Mdivi-1-induced modulation of radiation-induced apoptosis in U937 cells. Comparison of the apoptosis induced by 3, 20 and 30 Gy at 5 and 24 h when combined with Mdivi-1. The relative apoptosis is presented normalised to the respective control samples. Data are shown as mean ± SEM and represent 3 replicate samples.

Two Mdivi-1 exposure times for all radiation doses used are compared in Figure 6.23. As noted previously, 5 h Mdivi-1 exposure induced minimal apoptosis. Significant increases, relative to the control samples, were observed at 5 h for 20 and 30 Gy alone (approximately 4- and 8-fold, respectively) and in combination with Mdivi-1. However, no significant increase in apoptosis at 5 h was observed for 3 Gy treatments.

At 24 h, Mdivi-1 induced an 8- to 15-fold increase in apoptosis relative to the control samples. For 30 Gy, the apoptotic index was approximately 4-fold that of the control samples at 24 h ($p < 0.001$), notably less than observed at 5 h. In contrast, the lower doses of radiation examined induced a higher apoptotic index at 24 h than at 5 h, yielding values of 1.7- and 3-fold higher than control samples for 3 and 20 Gy, respectively. The combination of Mdivi-1 and radiation for both 20 and 30 Gy did not induce higher levels of apoptosis than radiation alone. However, 3 Gy combined with Mdivi-1 induced an approximate 5-fold increase in apoptosis at 24 h ($p < 0.001$). The combined effect at 24 h was 1.5-fold less than that induced by Mdivi-1 alone.

6.3.2.4. Effect of post-irradiation Mdivi-1 scheduling on apoptosis-induction

As established above, the combined effect of Mdivi-1 and radiation was reduced relative to that of Mdivi-1 alone when combined with radiation. Changes to the scheduling of Mdivi-1 treatment following irradiation may provide insight into the interaction between Mdivi-1 and radiation. Therefore, experiments were performed in which Mdivi-1 was applied at various times after irradiation to determine whether any enhancement of apoptosis over that induced by Mdivi-1 alone could be induced when Mdivi-1 was scheduled differently to the concurrent application used previously. The results are presented in Figure 6.24.

No change in the apoptotic index was observed relative to Mdivi-1 treatment alone for the addition of Mdivi-1 at 6 h after irradiation. The combined treatment, although scheduled differently, induced similar levels of apoptosis to those shown in previous investigations where Mdivi-1 was applied concurrently with radiation (data not shown).

For an interval of 24 h between irradiation and Mdivi-1, the 48 h Mdivi-1 exposure induced a slight but significantly different apoptotic index relative to Mdivi-1 alone ($p = 0.0124$) (Figure 6.24A). A similar level of radiation-induced apoptosis, of approximately 4-fold that of the control samples, was observed at 48 and 72 h post-irradiation.

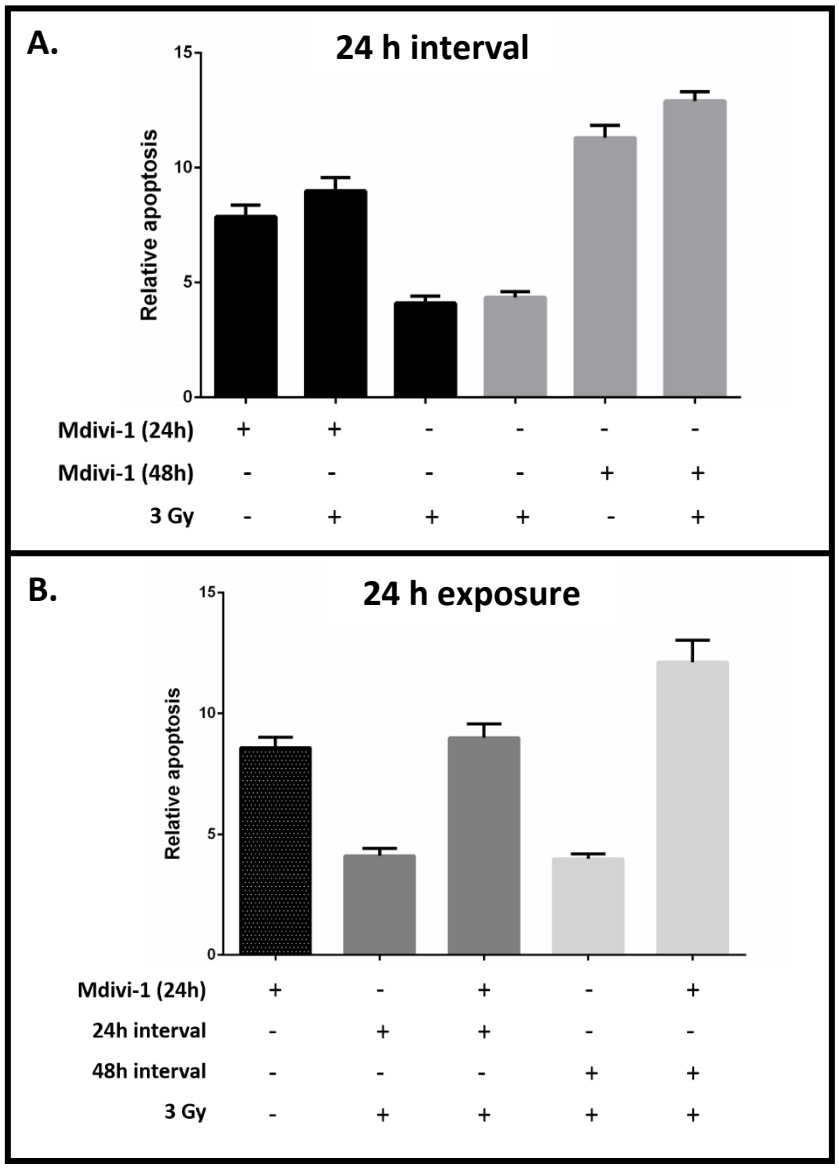

Figure 6.24. Differences in the scheduling of radiation and Mdivi-1 treatments alters the apoptotic index in U937 cells. **A)** Comparison of the combined effect of radiation and either 24 or 48 h Mdivi-1 exposure following a 24 h interval after 3 Gy. **B)** Comparison of the combined effect of radiation and a 24 h Mdivi-1 exposure following either a 24 or 48 h interval after 3 Gy. Data are shown as mean ± SEM and represent 3 replicate samples.

Figure 6.24B depicts the results for a constant 24 h Mdivi-1 exposure and either a 24 or 48 h gap after irradiation. The combined treatment with a 48 h interval showed an increase in apoptosis relative to Mdivi-1 alone. At 72 h, corresponding to an interval of 48 h, a 43 % increase in the apoptotic index relative to Mdivi-1 alone was observed ($p < 0.01$). A similar increase in apoptosis to that observed with Mdivi-1 alone was observed when cells were treated 48 h after irradiation relative to those that received treatment 24 h after irradiation. Importantly, the apoptotic index induced by radiation alone at 48 and 72 h was similar, approximately 4-fold relative to the control samples.

6.3.2.5. Proportion of mitotic cells after Mdivi-1 treatment

U937 mitoses were increased after incubation in Mdivi-1 for up to 72 h and in combination with radiation (Figure 6.25A and B). The highest mitotic index, a 5-fold increase relative to control samples, was observed at 48 h, however this increase was not significantly different from those observed at 5 and 24 h, which were approximately 3- and 2-fold, respectively. At 72 h, the Mdivi-1 -induced increase in mitotic index was 1.5-fold that observed for control samples.

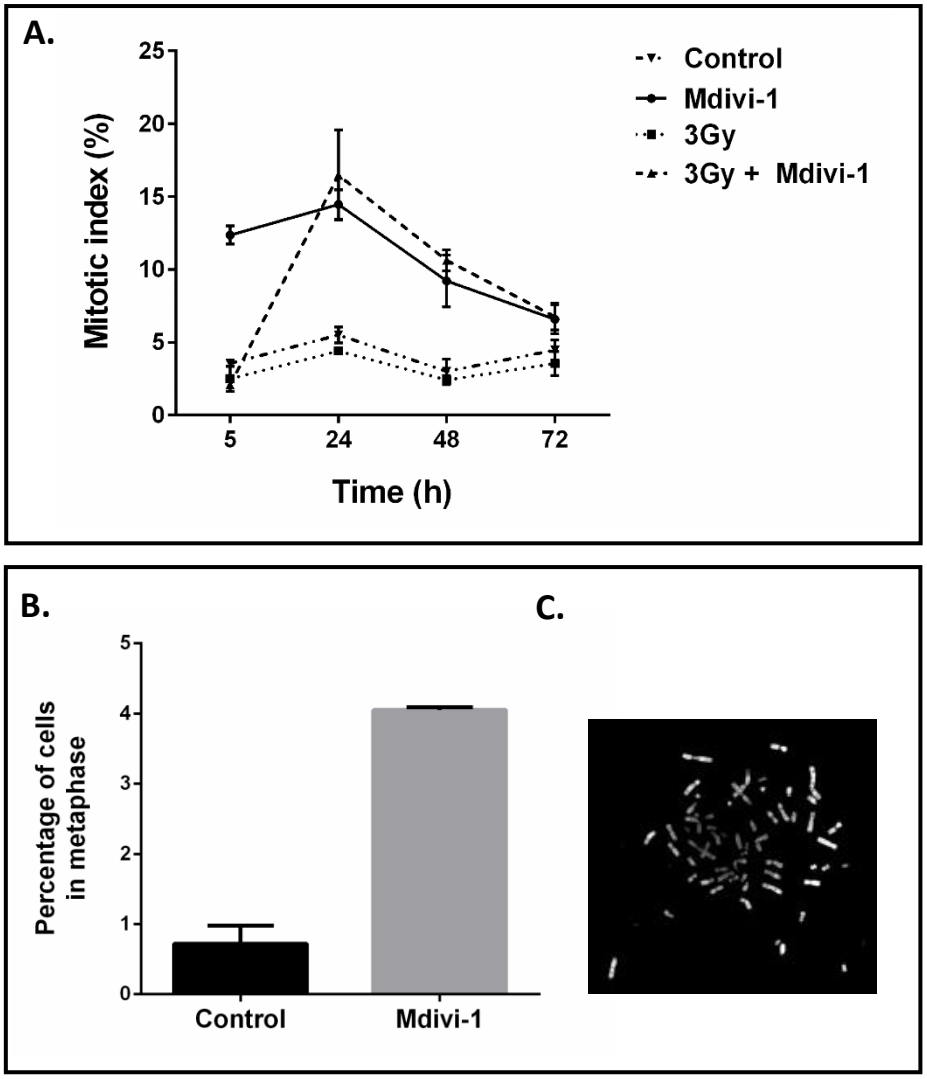

Figure 6.25. Mitosis-associated alterations induced by 3 Gy and Mdivi-1 in U937 cells. **A)** Time dependent alterations in the mitotic index. Data are shown as mean ± SEM and represent at least 3 replicate samples. **B)** Metaphases induced by a 48 h Mdivi-1 exposure. Data are shown as mean ± SEM and represent at least 20000 cells from 2 replicate samples. **C)** A representative metaphase spread.

A decrease in mitotic index of 30 and 20 % at 5 and 24 h, respectively was observed following 3 Gy. There was no difference between the irradiated and control samples at 48 h. At 5 h, the combined Mdivi-1 and 3 Gy treatment showed a reduced (6-fold) mitotic index relative to Mdivi-1 alone. However, by 48 h, the combination of Mdivi-1 and 3 Gy gave a 5-fold increase in mitotic index, which was similar to the Mdivi-1 treatment ($p < 0.001$). At 72 h, the combined treatment increased the mitotic index approximately 2-fold relative to that of the control samples.

Assessment of the proportion of cells in metaphase (Figure 6.25B) for a 48 h treatment with Mdivi-1 (10 µM), using the Metafer Msearch automated metaphase finder showed an approximately 5-fold increase in the number of metaphases (4 %) which is consistent with an increase in mitotic cells at 48 h (Figure 6.25A).

6.3.2.6. Reversibility of Mdivi-1-induced cell cycle effects

The Mdivi-1 induced increase in mitoses was reduced to background levels within 24 h after Mdivi-1 removal (Figure 6.26).

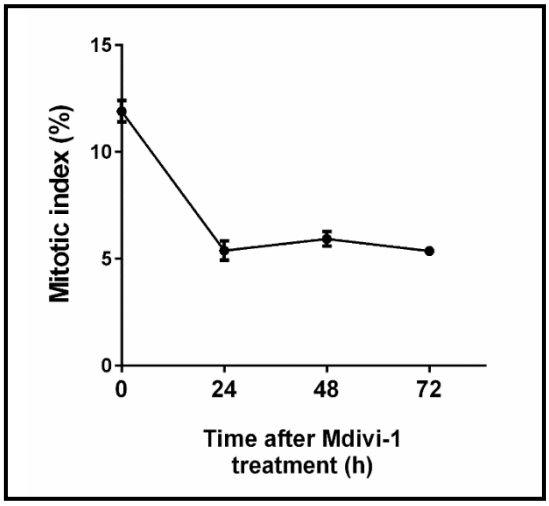

Figure 6.26. Reduction in U937 mitotic index after Mdivi-1 removal. Mdivi-1 induced an increase in mitotic cells during the initial 24 h incubation period however the increase was not maintained after removal of Mdivi-1. Data are shown as mean ± SEM and represent 3 replicate samples.

6.3.2.7. Mdivi-1 induction of cytogenetic damage

Mdivi-1 induced cytogenetic damage in the U937 cells indicated by an increase in the frequency of micronucleus-containing cells ($p < 0.01$). The absolute percentage of micronucleus positive cells induced by a 24 h Mdivi-1 treatment was less than 10 % (Figure 6.27). Radiation induced a 13-fold increase in micronucleus-containing cells relative to control samples ($p < 0.001$). Notably, the proportion of cells containing micronuclei for the combined treatment was 20 % lower than radiation alone ($p < 0.01$).

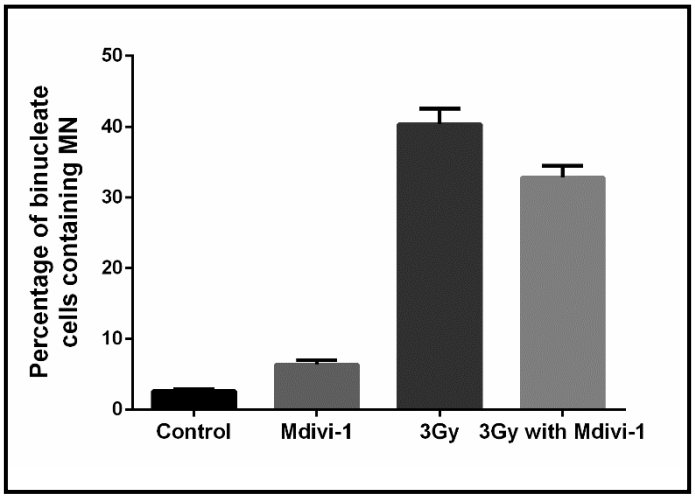

Figure 6.27. Induction of micronuclei (MN) by Mdivi-1 and irradiation in U937 cells. The combined additive effects of Mdivi-1 and radiation are illustrated in the right-hand bar. Data are shown as mean ± SEM and represent 3 replicate samples.

6.4. Discussion

We described novel findings in Chapter 5 in which Mdivi-1 was shown to significantly enhance radiosensitivity. While such findings may have therapeutic potential, further studies are required to contribute to an understanding of the mechanisms involved. In this chapter we present our investigations into the effects of Mdivi-1 that have the potential to influence radiation response.

Current understanding of the actions of Mdivi-1 suggests that this agent is able to induce cytogenetic damage, cell cycle arrest and cell death in a variety of model systems, as well as to modulate the cytotoxicity of other agents. In this chapter, we investigated similar end-points after Mdivi-1 treatment for their potential role in the radiosensitising effect of Mdivi-1.

In addition to effects on survival, we found that Mdivi-1 caused rounding and detachment of adherent cells, which suggests that other drug-induced changes, may occur. Adherent cells can detach from culture plates as a result of cell death but may also detach during division as mitotic cells round up and become loosely attached. The initial experiments described in this chapter were conducted to interrogate the viability of the detached cells in order to determine the contribution of this population of cells to the decrease in survival observed following Mdivi-1 treatment. Further investigations aimed to determine the contribution of apoptosis and cytogenetic damage to Mdivi-1-induced cell death. In addition, the ability of Mdivi-1 to affect cellular response to radiation-induced damage by influencing the passage of cells through the cell cycle was investigated.

6.4.1. Viability of detached Mdivi-1-treated cells

Mdivi-1 may induce complex changes in cultured cells including growth arrest and cell death. It was observed that treated cells were differentially affected by Mdivi-1 with a proportion of the cells becoming detached while the majority remained adherent. The appearance of floating cells in culture may indicate cell death. However, rounding up of cultured cells is also characteristic of mitotic cells which generally remain loosely adherent to the surface of the culture plate[710, 711]. Typically, after such de-adhesion, cells progress through mitosis and re-attach[712-714]. Complete detachment may occur when mechanically agitated. Thus, both cytotoxic treatment and potentially prolonged mitotic arrest may result in the accumulation of floating cells. However, it is common to find a high level of apoptosis in such a detached population[715-717].

It has been reported that cells becoming detached following cytotoxic treatment may later re-adhere[718], suggesting that survival after drug-induced detachment is possible. In this study, clonogenic assays were modified to assess the survival of the adherent and detached populations of cells separately.

Effect of Mdivi-1 in adherent and detached cells

Cell survival following the Mdivi-1 treatment alone was initially investigated. Overall, Mdivi-1 was confirmed to reduce A549 cell survival significantly. A large proportion of the detached cells died, however, approximately 10 % were observed to survive, demonstrating that detachment of cells was not only as a result of cell death. In addition, more than half of the adherent cells did not survive Mdivi-1 treatment. The differential influence of Mdivi-1 treatment on the two cell fractions provides insight into the mechanism of Mdivi-1-induced cell death in that cell detachment, although a consequence of Mdivi-1 exposure, is not entirely related to cell death. This finding prompted the assessment of mitoses in Mdivi-1-treated cells which will be discussed below.

Importantly, in an experiment of this nature, where treatment results in detachment of cells, collection of these non-adherent cells is essential so as not to underestimate the effect of the treatment. Visual inspection of cells during potentially cytotoxic treatments, as well as the collection of detached cells, is critical as discarding these cells may lead to spurious results.

To confirm that cells had not been lost during separation of the adherent and detached populations, the surviving fractions for each group were also calculated as a proportion of the total cell complement. It was confirmed that the effect of Mdivi-1 on survival of the separated populations, when summed, yielded a surviving fraction similar to that obtained for the unseparated population.

Combined effect of Mdivi-1 and radiation in adherent and detached cells

Initial experiments indicated that Mdivi-1 could induce radiosensitisation. Subsequently, in experiments using separated populations of adherent and detached cells, it was shown that both sub-populations were radiosensitised by Mdivi-1. In addition, the detached cells exposed to Mdivi-1 appeared to be more radiosensitive than the adherent cells. Through necessity, certain assumptions were made in evaluating the effect of radiation in the presence of Mdivi-1. Given that cells do not detach early after irradiation, as they do with Mdivi-1, it was assumed, that after 5 Gy, the surviving fractions of the separated populations would be the same as that of the unseparated population. The radiosensitivity of the sub-populations would ideally have been determined relative to controls that had received only radiation, but that could be separated into equivalent adherent and detached sub-populations.

Similar to our previous results with unseparated cells, Mdivi-1 also added to the cytotoxicity caused by radiation in the separated populations. The detached cells were shown to be more susceptible to the combined Mdivi-1 and radiation treatment than the adherent cells. Overall, the observations that Mdivi-1 treatment adds to the radiation efficacy suggests therapeutic potential.

6.4.2. Effects of Mdivi-1 on the cell cycle

Mdivi-1-induced effects on G2 and mitosis

Mdivi-1 treatment induced an increase in mitotic cells in both the A549 and U937 cell lines. Phospho-H3 immunohistochemical analyses that detect cells in late G2 and mitosis provided additional evidence for an increase in mitotic index during Mdivi-1 treatment and verified the criteria used for manual morphological scoring.

In A549 cells, an Mdivi-1 exposure of a few hours was shown to result in a small but significant increase in the mitotic index relative to control samples. This increase was consistent with the cell cycle analysis results reported in Chapter 5. Longer Mdivi-1 exposures (16 hours), however, induced a more pronounced cell cycle arrest, with approximately 30 % of the cells in mitosis. It can be speculated that the rounded, detached or loosely adherent cells observed in culture after Mdivi-1 treatment to some extent represented mitoses. While there appeared to be a gradual release of the cell cycle arrest from 24 hours, the reduced mitotic index observed at longer time-points may in part be as a result of the proliferation of surviving cells.

The Mdivi-1-induced increase in mitotic index in the A549 cells was confirmed using flow cytometry. Mdivi-1-treated cells displayed an initial brief S-phase arrest prior to a G2/M arrest that reached maximal levels by approximately 16 hours. Mdivi-1 treatment induced a large proportion, at least 50 %, of the cells to be arrested in G2/M phase, which was comparable to the cell cycle arrest induced by 5 Gy. The increased G2/M proportion after 16 h Mdivi-1 may explain the significant radiosensitisation observed as cells in this phase are particularly radiosensitive.

As shown in Chapter 5, even brief exposure to Mdivi-1 could result in a subsequent increase in G2/M, however, this was not sustained. In contrast, the G2/M arrest during more extended treatments was maintained while cells were exposed to Mdivi-1 suggesting continued accumulation of Mdivi-1 arrested cells.

However, some dissipation of the G2/M arrest was observed with continuous Mdivi-1 treatment. These results are consistent with the decrease in mitoses reported above for longer exposures. The increases in both the G1- and the sub-G1 peaks as G2/M decreased suggest that a proportion of cells exiting the Mdivi-1-induced arrest undergo cell death while the rest continue to cycle.

In U937 cells, the mitoses were similarly increased after Mdivi-1 treatment although the increase was earlier and less pronounced than that observed for the A549 cells. The proportion of mitotic cells also remained constant for an extended period up to 48 hours. This sustained level of mitoses, despite continued Mdivi-1 exposure, may suggest stabilisation of the mitotic fraction. Alternatively, mitotic cells may undergo apoptosis, thus eliminating them from the evaluable mitotic proportion. As mentioned previously, another factor expected to influence the quantitation of mitoses is the proliferation of cells surviving Mdivi-1 treatment. Therefore, the mitotic index determined will be the net effect of all competing processes. Taken together, the kinetics of response to Mdivi-1 appears to differ in the U937 apoptosis-responsive cells compared to that of the A549 cells.

Previously reported Mdivi-1-induced cell cycle effects

Mitochondrial dynamics are carefully regulated during the cell cycle[503] and modulation, using inhibitors of fission such as Mdivi-1, has the potential to control cell cycle progression. Extensive fission occurs prior to mitosis in order to allow equal distribution of mitochondria between daughter cells[443, 504]. Mdivi-1-induced cell cycle arrest in our cell models was proposed to result from reduced mitochondrial fragmentation prior to mitosis.

The results presented are supported by a number of researchers, who have similarly reported an Mdivi-1-induced G2/M cell cycle arrest[88, 571, 573, 696]. Further evidence of Mdivi-1 effects on the cell cycle came from synchronisation experiments in which cells specifically arrested in mitosis, were prevented from progressing through the cell cycle[21, 572]. Although, specific interactions of Mdivi-1 with the cell cycle are not well described, Marsboom et al. (2012)[571] determined that the Mdivi-1-induced arrest occurred at prometaphase. They showed that Mdivi-1 prevented a decrease in cyclin B1 levels that would normally be associated with later stages of mitosis. Degradation of cyclin B1 occurs via Cdh1 and leads to inactivation of the mitosis promoting factor and mitotic exit[719] suggesting that Mdivi-1 may interact at this level.

Mechanistic aspects of the Mdivi-1-induced mitotic arrest

A few studies have investigated further potential mechanisms related to the Mdivi-1-induced cell cycle arrest. Given the role of Mdivi-1 as a fission inhibitor, the Mdivi-1-induced mitotic or G2/M-phase arrest has been ascribed to mitochondrial hyperfusion[88, 696]. Such hyperfusion was associated with decreased phosphorylation and inactivation of DRP1[571, 696]. In addition, siRNA knockdown of DRP1-induced hyperfusion and caused an arrest similar to that observed using Mdivi-1[88, 572]. Such alterations in DRP1 expression have been reported to influence cell cycle progression by regulating cyclin levels. For example, DRP1 deficient breast cancer cells that were synchronised at mitosis did not show an expected cyclin B1 increase or cdc2 dephosphorylation initially[572], both of which have been associated with entry into mitosis in normal cells[720]. Release from the arrest in these DRP1-deficient cells, however, was shown to slowly initiate dephosphorylation of cdc2 resulting in gradual progression through the cell cycle[572]. Thus, alterations in DRP1 expression may modulate G2 to M transition directly or indirectly.

There is some controversy concerning whether the Mdivi-1-induced cell cycle arrest is exclusively related to its role as an inhibitor of DRP1. In two studies, downregulation of DRP1 in breast cancer cells[593] and DRP1 knock-out in mouse embryonic fibroblast cells[466] did not have an effect on the cell cycle. However, one investigator indicated that DRP1 knockdown was only 85 % and residual protein may have been sufficient to prevent cell cycle changes[593]. In addition, Qian et al. (2012)[572], who showed a G2/M arrest in breast cancer cells treated with Mdivi-1, suggested that, although hyperfusion was deemed necessary for cell cycle arrest, the effect may partly be non-mitochondrial. Restoration of an induced fragmented mitochondrial status by double knockdown of DRP1 and OPA1, a fusion protein, did not completely prevent the cell cycle arrest. Additional evidence suggesting that the arrest is partly non-mitochondrial came from the use of Rho0 cells, which lack mitochondrial DNA. These cells still arrested at G2/M and underwent hyperfusion upon knockdown of DRP1[572].

Mdivi-1-induced effects on G1 and S-phase

In the current work, when cell cycle profiles for Mdivi-1 treatment and 5 Gy were compared, it was apparent that, although a similar G2/M arrest was induced by each agent, the G1 populations were differentially affected. The proportion of G1 cells accumulated to a greater extent after irradiation than after Mdivi-1 treatment. This may be consistent with reports of time-dependent increases in the movement of cells into S-phase[144] and into G1[507], respectively, after Mdivi-1 exposure. However, it may also suggest that, in contrast to radiation, Mdivi-1 does not induce G1-checkpoint activation.

The Mdivi-1-induced S-phase arrest was previously demonstrated and discussed in Chapter 5. Mdivi-1-induced hyperfusion in serum-starved G0 cells has been shown to increase cyclin E levels which initiate the movement of cells into S-phase[144]. The investigators suggested that mitochondrial hyperfusion is sufficient to induce entry into S-phase in the absence of growth factor stimulation.

The S-phase arrest demonstrated after a few hours of Mdivi-1 exposure in our study, may be a similar response, possibly related to increased cyclin E. Overexpression of cyclin E has been associated with DNA damage and increased initiation or stalling of DNA replication[721, 722]. Qian et al. (2014)[582] identified similar replication stress induced by Mdivi-1, although the S-phase proportion was reduced. Although our analysis showed that S-phase was increased after a short Mdivi-1 treatment, our results were consistent with those of Qian et al. (2014)[582] in that S-phase was reduced with a 24 h treatment, which was a similar exposure time.

In addition, an intra- S-phase arrest, in response to DNA damage, has been reported previously[115, 117]. Mdivi-1-induced DNA damage during S-phase is plausible, as aberrant mitochondrial fusion may lead to increased ROS production[435] that can cause DNA breaks[723, 724]. DNA damage induced during replication or as a result of increased ROS may immediately interfere with cell cycle progression or enhance a later arrest. Alternatively, a short G1 arrest followed by a semi-synchronised movement of cells may account for the increase in S-phase. An Mdivi-1-associated early S-phase arrest, which was attributed to a transient G1 arrest, was similarly observed for the irradiated cells. Mdivi-1 may, thus, likewise have the potential to initiate a transient G1-arrest prior to the G2/M arrest.

Differential Mdivi-1 effects in cancer and normal cells

Importantly, it has been demonstrated that Mdivi-1 induced a cell cycle arrest in a number of cancer cell lines but not in normal fibroblasts or epithelial cells[573]. In contrast, cell cycle arrest was observed in vascular and pulmonary artery smooth muscle cells treated with Mdivi-1[569-571]. The latter experiments, however, were conducted under conditions of serum starvation, high glucose and hyperproliferation that represent aberrant or stressful environments. The observation that Mdivi-1 may affect normal tissue less holds promise for this drug as a cancer therapeutic. Further experimental work is required to elucidate Mdivi-1 effects in normal tissue.

In general, in the current work, the observed Mdivi-1-induced increase in mitotic index was consistent with the hypothesis that an Mdivi-1-induced cell cycle arrest is associated with aberrant mitotic transition. Mechanistically, Mdivi-1 may induce an arrest either by acting directly as a mitotic inhibitor or as a DNA damaging agent that indirectly activates the G2 checkpoint.

Overall, results suggest that there is significant variation in the kinetics of cell cycle arrest after Mdivi-1 treatment in the models examined. Differential responses may be related to their individual sensitivities to apoptosis or checkpoint activation.

6.4.3. Mdivi-1 effects on the radiation-induced cell cycle arrest

As mentioned above, Mdivi-1 treatments in U937 cells induced a mitotic arrest earlier than in the A549 cells. However, when Mdivi-1 was combined with radiation, this early increase in mitotic index was not observed. A radiation-induced G2/M arrest has been shown to occur and may preclude Mdivi-1 effects related to mitosis as cycling cells may be susceptible to interaction with Mdivi-1. An increased mitotic index was subsequently observed and was comparable to that induced by Mdivi-1 alone. The mitotic index of the irradiated samples was increased at 24 h (Figure 6.25) suggesting release from the radiation-induced G2/M arrest. The delayed Mdivi-1 effects may thus have been influenced by the arrest.

In addition, Mdivi-1 was reported to augment the radiation-induced G2/M arrest (Chapter 5, Figure 5.15). Cell cycle analysis based on DNA content alone does not distinguish between G2- and M- phase cells, therefore, any G2/M arrest observed may represent both cells arrested in mitosis and/or activation of the G2/M checkpoint. In this work, Mdivi-1 was found to induce an increase in mitotic index, however, this does not rule out accumulation of cells in G2, which would be expected to occur in response to DNA damage. Cytogenetic damage, as discussed below, was previously shown to be a consequence of Mdivi-1 treatment. Therefore, additional Mdivi-1-induced DNA damage may arrest cells prior to mitosis. Mdivi-1, like radiation, may induce activation of the G2/M checkpoint, with the result that a lower level of mitoses is observed with the combined treatment. Taken together, the delayed increase in mitoses induced by Mdivi-1 in the context of radiation treatment is likely a result of the inability of G2/M arrested cells to move into mitosis which is proposed to be a requirement for Mdivi-1-induced cell cycle arrest. Overall, the results suggest that Mdivi-1 effects interact with radiation effects to influence the radiation-induced arrest.

While not specifically examined in this study, oxidative stress associated with mitochondrial dysfunction may have a potential role in the Mdivi-1 effect on the radiation-induced cell cycle arrest. Cell cycle arrest occurs in response to DNA damage[725], nutrient deprivation[726] or cellular stress[126, 140]. Specifically, ROS- and stress-activated protein kinases that signal cell death or growth arrest, are often increased in response to stress[727, 728].

Mdivi-1 inhibition of mitochondrial division may result in the aberrant release of ROS due to its effects on mitochondrial function. A G2/M arrest induced by increased oxidative stress as a consequence of Mdivi-1 treatment may alternatively be a result of secondary nuclear damage[38, 154].

Potential therapeutic application of Mdivi-1 as a mitotic inhibitor and radiosensitiser

The observation that Mdivi-1 induced a cell cycle arrest in cancer cells may be important therapeutically both for the potential use of Mdivi-1 alone and in combination with radiation as anti-cancer therapy. Mitotic inhibitors such as taxanes[729] or vinca alkaloids[730] interfere with microtubule formation and induce both mitotic arrest and cell death that restrict tumour growth[731]. Mdivi-1 may similarly have potential as a mitotic inhibitor that may be exploited to enhance radiation effects. Mitotic inhibitors that inhibit tubulin and prevent the formation of spindle fibres are not tumour-specific and these agents are therefore also toxic to normal dividing tissue. As mentioned previously, Mdivi-1 was shown to have no effect on mitosis in fibroblasts and untransformed cell lines[573] suggesting that Mdivi-1 toxicity may be largely tumour-specific and may therefore, have future clinical utility. As cells in mitosis are particularly sensitive to radiation, Mdivi-1 may be a promising agent for modulation of radiation therapy of tumours due to the accumulation of cells in mitosis.

6.4.4. Assessment of Mdivi-1-induced cell death

Mdivi-1 reduced survival of A549 cells as assessed by clonogenic assays (Chapter 5). Here, we reported that Mdivi-1 induced a significant but limited amount of apoptosis (less than 10 %) in A549 cells. In contrast, significant apoptosis was observed when Mdivi-1 treatments were investigated in the U937 cell line. Approximately 40 % apoptosis was induced by 24 h Mdivi-1 exposure and a similar level was maintained with treatments up to 72 h. The U937 cells are generally considered to be more sensitive to apoptosis induction than the A549 cells suggesting that Mdivi-1 can induce apoptosis in cells that are susceptible to this mechanism of cell death.

In Chapter 5, we established that A549 clonogenic survival after 16 h Mdivi-1 treatment was reduced to 30 % (Figure 5.8). The minimal apoptosis observed suggests that alternative modes of cell death e.g. necrosis may be important in Mdivi-1 related cytotoxicity. Similar phenomena have been observed in ischaemia-reperfusion cardiac models.

For example, a study involving the administration of Mdivi-1 at the time of re-oxygenation found that, although Mdivi-1 inhibited apoptosis, overall cell death was exacerbated. In this case, necroptosis (programmed necrosis) was postulated to be the mode of cell death, as the necrosis inhibitor Necrostatin was demonstrated to reduce overall cell death[732].

In spite of U937 cells being functionally p53-deficient as a consequence of a large deletion in the p53 gene[733] they are relatively apoptosis-sensitive. A549 cells have a wildtype p53 expression but express high levels of MDM2 and, as a result, are more resistant to apoptosis[734].

In our study, lower Mdivi-1 concentrations, namely, 10 and 20 µM and short, 6 h exposures did not result in a significant increase in apoptosis or reduced survival in A549 cells. However, apoptosis was significantly increased using longer exposure times up to 72 h and higher concentrations of Mdivi-1, which is consistent with the general trend reported in previous studies[23, 441, 582, 585]. In general, apoptosis has been observed when the dose is increased above a certain threshold, usually concentrations greater than 20 µM and exposures of more than 6 h[22, 469, 585]. In particular, a study by Rehman et al. (2012)[21], showed that a minimum of 16 h Mdivi-1 treatment yielded apoptosis.

Despite initial increases in apoptosis for both 30 and 50 µM Mdivi-1 treatments in A549 cells, the level of apoptosis was greatest at 72 h using 50 µM Mdivi-1 while apoptosis was significantly reduced at 72 h using 30 µM Mdivi-1. It was speculated that the higher concentration prevented proliferation of cells, perhaps by inducing a more efficient cell cycle arrest resulting in an apparently higher level of apoptosis with longer treatments. Uninhibited proliferation of surviving cells in the sample exposed to the lower concentration may have led to an apparently lower level of apoptosis. It is acknowledged that the amount of apoptosis observed is dependent on the assessment time. Continued development of drug-induced cell death and the proliferation of unaffected cells will influence the value determined at a given time.

Cell cycle analysis showed that, as the number of mitotic cells induced by Mdivi-1 treatment decreased, the proportion of fragmented cells, represented by the sub-G1 peak, increased suggesting apoptosis may be a consequence of prolonged arrest in these cells. The sub-G1 peaks, an additional estimation of the level of apoptosis induced by Mdivi-1 treatments, suggested significantly more apoptosis than that obtained by microscopic evaluation. Although the sub-G1 peak in flow cytometry, representing dead or fragmented cells, primarily detects apoptosis as a result of DNA fragmentation, necrosis may also increase the sub-G1 peak[735]. This may explain the higher apparent apoptotic index observed with cell cycle analysis compared to morphological assessment of apoptosis.

Reported effects of Mdivi-1 on apoptosis

Mdivi-1, which inhibits mitochondrial fragmentation, might be expected to prevent apoptosis, a process associated with fragmentation. Mdivi-1 has been shown to protect against STS-induced apoptosis and the associated mitochondrial fission[559].

The limited induction of apoptosis we observed after Mdivi-1 treatment, in spite of a significant reduction in survival, is consistent with a protective role for Mdivi-1 but suggests stimulation of other forms of cell death. In a similar study, Qian et al. (2014)[582] reported minimal apoptosis but significantly decreased survival of breast cancer cells following Mdivi-1 treatment. Despite this evidence, the extensive apoptosis observed in U937 cells suggests that the balance of apoptosis induction exceeds any apoptosis inhibition.

The above experiments assessed apoptosis immediately following exposure to the drug. It was thought that continuous exposure to a cytotoxic agent such as Mdivi-1 may prevent expression of cell death. Hence, apoptosis was also assessed by incubating cells in drug-free medium for a period after exposure. Both cell lines, however, showed a progressively reduced level of apoptosis with increasing time after exposure indicating no further increase in apoptosis. The presence of Mdivi-1 may therefore be required for the accumulation of apoptotic cells. However, the gradual reduction in apoptosis may also partly be a result of the proliferation of unaffected cells over time.

From the results it is clear that there is considerable variation in the response of different models to Mdivi-1.

6.4.5. Modulation of radiation-induced apoptosis by Mdivi-1

Mdivi-1-induced modulation of radiation-induced apoptosis was initially investigated using the Mdivi-1 treatment shown by us to induce radiosensitisation in the A549 cell line. Apoptosis was quantified at 30 h after irradiation to allow for the release of the G2/M arrest which is required for cells to enter mitosis and which usually occurs by 48 h. Although apoptosis was low, samples treated with Mdivi-1 showed significantly increased apoptosis relative to that of the control samples. The combined effect of Mdivi-1 and radiation did not increase the level of apoptosis significantly above that induced by irradiation alone. This sub-additive response when Mdivi-1 was combined with radiation may be attributed to an extended cell cycle arrest induced by Mdivi-1. In Chapter 5, it was reported that the combination of radiation and Mdivi-1 significantly increased the G2/M arrest within a few hours. Mdivi-1 treatment alone yielded a G2/M arrest of more than 50 % of the cells, with 30 % of the cells being mitotic at the time of irradiation.

A greater proportion of the cells may be affected by radiation, as they are in the radiosensitive M-phase, and may more effectively undergo mitotic catastrophe. The sub-additive apoptotic response could therefore manifest as a result of cells undergoing mitotic catastrophe instead of apoptosis when Mdivi-1 is combined with radiation. In addition, many of the cells affected by radiation may have already been lethally targeted by Mdivi-1, i.e. overlapping intracellular targets.

In general, minimal apoptosis could be demonstrated in the A549 cells, which is consistent with the notion that many solid tumours are resistant to apoptosis. In addition, early apoptosis after radiation does not occur readily in epithelial cells, as cell death generally occurs later once mitosis has occurred[736]. Consequently, we examined radiation-induced apoptosis in U937 leukaemia cells, which undergo both early and post-mitotic apoptosis.

In U937 cells, Mdivi-1 was shown to significantly increase apoptosis when applied on its own. However, results suggest that high doses of 20 or 30 Gy interfered with the expression of Mdivi-1 -induced apoptosis, as evidenced by a reduced apoptotic index for the combined treatment relative to Mdivi-1 alone. Such high doses given in a single fraction may induce strong, often permanent G2/M arrest as a result of increased damage[737, 738]. The demonstration of the effects of Mdivi-1 on the passage of cells through mitosis suggests that Mdivi-1-induced damage may, in part, be related to aberrant mitosis. Radiation-induced G2/M arrest prevents cells from entering mitosis possibly preventing the Mdivi-1-induced damage necessary for apoptosis. The Mdivi-1-induced apoptosis appeared to be suppressed in irradiated samples up to approximately 40 h post-irradiation. By 48 h, the apoptotic index from the combined Mdivi-1 and radiation treatment had started to rise, however, the level failed to reach that of Mdivi-1 alone. This may suggest partial release of the radiation arrest.

In contrast, the combination of a lower (3 Gy) radiation dose with Mdivi-1 induced a similar apoptotic index compared to Mdivi-1 alone from 48 h. As cycling of cells was able to occur from 24 h after 3 Gy, the comparable level of apoptosis suggests that a higher proportion of cells may have been available for interaction with Mdivi-1 following release from the arrest.

Although the apoptosis increased with time for the combined treatment, no increase above the level induced by Mdivi-1 alone was observed. As discussed for the A549 cells, such a sub-additive response may be attributed to overlapping of intracellular targets. Alternatively, Mdivi-1 itself can enhance the radiation-induced G2/M arrest of cells, further preventing expression of radiation or Mdivi-1-induced damage. Cell cycling therefore appears to be required for expression of Mdivi-1-induced apoptosis.

A recent experiment that combined the use of radiation and Mdivi-1, reported that Mdivi-1 protected against radiation-induced damage in normal mouse embryonic fibroblasts[466]. Mdivi-1 reduced mitotic catastrophe and suppressed the increase in centrosome number induced by radiation. The protection against radiation-induced mitotic catastrophe was replicated using DRP1-knock-out and mutant models[466]. While not specifically implicated, it is possible that cell cycle arrest may have played a role in the reduced cellular effects.

Overall, as expected, less apoptosis was induced by 3 Gy compared to 30 Gy. High and low dose responses also differed with respective to the latent period before significant apoptosis occurred. Negligible apoptosis was observed a few hours after a low dose compared to a significant increase relative to control samples for a high dose. This is consistent with higher radiation doses being able to induce early, interphase cell death while lower doses induce primarily mitosis-related cell death in this cell line[204]. While the relevance of using high or single doses of 20 or 30 Gy may be questioned in the context of therapeutic utility, it may nevertheless be mechanistically informative. It is however possible that stimulation of cell death after such high doses may be mechanistically different from that induced by lower doses.

6.4.6. Effects of delaying Mdivi-1 application after irradiation

To allow for maximal expression of apoptosis induced by the combined Mdivi-1 and radiation treatments, we altered the scheduling of the two agents by delaying the addition of Mdivi-1 for an interval sufficient for at least partial release of the G2/M arrest. Despite a constant exposure to Mdivi-1, by leaving a longer interval the apoptosis was significantly increased. In addition, the combined effect was greater than that observed for Mdivi-1 alone. While an interval up to 24 h did not change the previous outcome, a 48 h interval was effective in increasing the proportion above the level induced by Mdivi-1 alone. The additional apoptosis achieved by delayed application of Mdivi-1, is consistent with a requirement of mitosis for expression of both Mdivi-1- and radiation-induced apoptosis in these cells. As radiation-induced apoptosis remained constant, the increased apoptosis observed with the longer interval was not ascribed to increased radiation-induced effects but was attributed to an enhanced Mdivi-1-related effect.

6.4.7. Effect of Mdivi-1 on radiation-induced cytogenetic damage

Mdivi-1, an inhibitor of mitochondrial fission, induced a significant increase in the amount of cytogenetic damage, as assessed by micronuclei, in both cell lines tested (Figures 6.13 and 6.27).

Cytogenetic damage induced following Mdivi-1 treatment was less in the U937 than in the A549 cell line. This may be due to a reduced inherent susceptibility of U937 cells or competing processes such as apoptosis, which may result in lower detection. In this cell line, chromosomal damage, which has been associated with Mdivi-1 exposure, may efficiently induce apoptosis and thus may render damage undetectable. For micronuclei assessment cells are required to undergo karyokinesis without cytokinesis for the formation of bi-nucleate cells. As Mdivi-1 effects are related to mitotic arrest, differences in the response of cells to aberrant mitosis may affect detection of micronuclei.

In contrast, similar responses in the two cell lines were observed when Mdivi-1 was combined with radiation. Mdivi-1 pre-treatment, prior to irradiation, inhibited the induction of cytogenetic damage. For reasons described above, this may also be related to mitotic arrest, which may prevent expression of Mdivi-1-induced damage in the absence of karyokinesis. In addition, mitotic cells are known to be more sensitive to radiation and therefore, an Mdivi-1-induced mitotic arrest may result in increased radiation-induced cell death thereby reducing the proportion of evaluable cells.

Similar to our results, DRP1-deficiency[572] and Mdivi-1 treatment[573] was previously associated with micronuclei, however, Mdivi-1 has also been shown to protect against radiation-induced micronuclei formation [466].

6.4.8. Mechanisms of Mdivi-1-induced micronuclei formation

The mechanisms of Mdivi-1 induction of micronuclei are not well-established. In general, micronuclei may occur as a result of improper attachment of chromosomes to the spindle or direct damage leading to broken chromosomal fragments[247, 248]. Mdivi-1 or reduced DRP1 expression has been associated with DNA replication errors[582] and aberrant centrosome duplication with improper spindle attachment to kinetochores of chromatids[573]. Cytogenetic aberrations are commonly associated with mitotic arrest and slippage[739, 740]. Arrested cells may divide, potentially displaying cytogenetic damage or aneuploidy. Mitotic slippage, whereby cells exit mitosis without dividing, leading to polyploidy[126], occurs following prolonged mitotic arrest as a result of degradation of cyclin B[132] and securin [741]. An increase in the number of polyploid cells after Mdivi-1 treatment has been described previously[572, 573]. In addition, early progression to anaphase without prolonged mitotic arrest has been shown to cause micronuclei formation[742].

Since Mdivi-1 is cytotoxic, it may be expected to induce DNA damage, either directly or indirectly. Mdivi-1 was able to enhance a cisplatin -induced γ-H2AX signal, indicative of an increased number of DNA double-strand breaks although it did not induce double-strand breaks itself[582]. Whether this is a general phenomenon needs to be evaluated further, particularly at increased Mdivi-1 doses and in combination with radiation.

DRP1-deficient cancer cells have been shown to display abnormal nuclear morphology and micronuclei, indicating chromosomal instability[572]. Micronuclei were observed within regions of aggregated mitochondria which may represent areas of increased fusion[572]. Misalignment of mitotic chromosomes has been reported following Mdivi-1 treatment[144, 573]. Wang et al. (2015)[573] specifically demonstrated the presence of acentrosomal multipolar spindles in Mdivi-1-treated cells with consequent mis-segregation of chromosomes and mitotic catastrophe. Defective spindle attachment to chromosomes was associated with dysregulation of centrosome replication and abnormal karyokinesis[573]. It can be speculated that abnormal mitochondrial dynamics including localisation may provide a physical barrier to spindle development.

Of interest, chromosome misalignment could be demonstrated in HCT-116 colorectal cancer cells expressing mutant DRP1 and hyperfusion but was not observed in equivalent p53-null cells. The damage response pathway whereby cells either undergo apoptosis or arrest has been shown to be influenced partly by p53 status[743]. p53 has been associated with both G1 and G2-checkpoint arrest[744] that prevent cells containing chromosomal aberrations from continuing to cycle. p53-deficient cells, however, may bypass such checkpoints and maintain misaligned chromosomes.

Oxidative stress may lead to double-strand breaks and the occurrence of micronuclei. Mitochondrial fission is associated with mitochondrial quality control mechanisms including mitophagy[511], which is necessary for the elimination of dysfunctional mitochondria[745, 746]. The inability to remove dysfunctional mitochondria leads to increased oxidative stress[435] and consequently DNA damage[723]. It is possible that inhibition of fission by Mdivi-1 may thus result in oxidative stress and provide an additional pathway for cytogenetic damage.

6.4.9. Potential kinetics of Mdivi-1 interaction with radiation

A paradox exists in that Mdivi-1 enhances radiation-induced cell kill, yet apparently inhibits expression of certain radiation-induced cellular consequences, such as micronuclei. Further, as a recurring theme, the combined effects of Mdivi-1 and radiation were frequently reduced compared to those of the individual agents. In each case, the previously observed Mdivi-1-enhanced radiation arrest may have been a contributory factor.

With respect to the reduced induction of micronuclei with the combined treatment, delayed cycling of cells may result in lower micronuclei expression as chromosomal fragments become excluded during anaphase. In addition, the longer arrest may increase the opportunity for repair prior to division. The apparent reduction in cytogenetic damage may in fact reflect the increase in cell death from combined treatment due to M-phase radiosensitivity of Mdivi-1 arrested cells. Hence mitotic catastrophe and subsequent cell death may outweigh demonstrable cytogenetic damage.

The previously identified Mdivi-1-induced increase in fusion was reduced when Mdivi-1 was combined with radiation. However, no change in mitochondrial morphology after irradiation was found using Small-fragment analysis. Mitochondrial fragmentation has previously been demonstrated after irradiation[57, 466] which may counteract the increased fusion observed with Mdivi-1. Alternatively, it is possible that the level of fragmentation induced by irradiation in our cell line was below the detectable threshold for Small-fragment analysis in the absence of Mdivi-1.

6.5. Conclusions

- Mdivi-1 reduced survival in both detached and adherent A549 cell populations.
- Both populations were radiosensitised by Mdivi-1, however, the detached cells were significantly more affected.
- Mdivi-1 induced a G2/M arrest.
- Survival of a proportion of the detached cells suggested that detachment was not solely related to cell death. Since cells in G2/M round up and detach, it is likely that some of the detached cells represent an arrested population.
- Mdivi-1 modulated the radiation-induced cell cycle arrest but differential kinetics were apparent for the cell lines examined. Since radiation-induced cell cycle arrest influenced the Mdivi-1 response, cell division may be necessary for expression of Mdivi-1 effects including apoptosis and cytogenetic damage.
- Mdivi-1 induced apoptosis in both cell lines examined. U937 cells, which are considered to be apoptosis-responsive, were particularly sensitive to Mdivi-1. Radiosensitisation, reported previously, was not due to apoptosis.
- Mdivi-1 induced cytogenetic damage expressed as micronuclei. In addition, Mdivi-1 interfered with the development of cytogenetic damage after irradiation.
- A sub-additive response for the drug-radiation combination was consistently found for all end-points examined except where an interval between treatments was allowed, which yielded an approximately additive response.

Overall, Mdivi-1 modulated several processes which have the potential to influence radiation response.

CHAPTER 7

FINAL DISCUSSION AND CONCLUSIONS

This study initially characterised a group of cancer cell lines in terms of radiosensitivity, cellular respiration, mitochondrial morphology and ΔΨm and investigated potential correlations between inherent radiation-responsiveness and mitochondrial status. In addition, modulation of mitochondrial dynamics was shown to influence radiation response in two of the characterised cancer cell lines. Further, the effects of Mdivi-1 on cell cycle dynamics, apoptosis and cytogenetic damage were examined.

The current chapter presents a brief summary of the findings as they relate to the original research questions that prompted these investigations.

7.1. Is the radiation responsiveness of cancer cells associated with mitochondrial morphology or function?

Investigations into the relationship between radiation response and mitochondrial status, including morphological and functional characteristics, demonstrated some correlation. Increased mitochondrial fusion was strongly correlated with decreased radiation response, however, statistical significance was not reached. In addition, ΔΨm was correlated with measures of the intrinsic radiosensitivity of the cell lines, but also did not reach significance. In general, indicators of mitochondrial function, namely respiratory indices and ΔΨm correlated strongly and significantly. Strong correlations were also observed between mitochondrial morphology and measures of mitochondrial function.

7.2. Does modulation of mitochondrial dynamics influence cellular integrity or response to radiation?

We initially postulated that Mdivi-1, a mitochondrial fission inhibitor, would protect against radiation-induced cell death. However, no protective effect was observed. In contrast, Mdivi-1 significantly increased the sensitivity of cancer cells to radiation treatment.

7.2.1. Does Mdivi-1 induce mitochondrial fusion?

Mdivi-1 was shown to alter mitochondrial morphology resulting in a shift towards increased fusion. A wide range of Mdivi-1 concentrations induced a rapid increase in the number of cells displaying predominantly fused mitochondria. However, a dose dependence was observed, with lower Mdivi-1 concentrations failing to induce a shift towards fusion.

7.2.2. Does inhibition of mitochondrial fission alter survival of cancer cells?

Mdivi-1 was demonstrated to significantly reduce survival in the cell lines tested. In general, Mdivi-1 treatments in excess of 6 h were required to influence the survival and the toxicity was cell line dependent. A higher Mdivi-1 concentration was required to induce toxicity in the A549 lung cancer cell line compared to the U937 monocytic leukaemia cell line. Differential effects may potentially be related to the inherent capacity of the cell lines for programmed cell death.

7.2.3. Does inhibition of mitochondrial fission influence radiation survival of cancer cells?

Mdivi-1 was demonstrated to significantly sensitise A549 lung cancer cells to radiation. Overall, Mdivi-1 was found to augment radiation sensitivity by approximately 20 %. In general, for such modulation, doses at which a degree of Mdivi-1-induced toxicity was evident were required.

7.2.4. Does inhibition of mitochondrial fission influence repair of radiation-induced damage?

Mdivi-1 was not shown to modulate sub-lethal- or potentially-lethal damage repair as measured using clonogenic cell survival.

7.2.5. Does inhibition of mitochondrial fission influence cell cycle dynamics and/or radiation-induced cell cycle arrest?

While both Mdivi-1 and radiation were found to induce a cell cycle arrest independently, Mdivi-1 also enhanced the radiation-induced G2/M cell cycle arrest in A549 cells.

7.3. How does Mdivi-1 alter radiation response?

The effects of Mdivi-1 treatment on two cancer cell lines were shown to influence processes known to be involved in radiation response. Mdivi-1 was shown to induce apoptosis, cell cycle arrest and cytogenetic damage in both cell lines investigated. Mdivi-1 was shown to modulate the radiation-induced effects on these processes, however, in general, responses were sub-additive.

7.3.1. Does Mdivi-1 delay cells in mitosis?

In both cell lines investigated, Mdivi-1 induced a significant G2/M cell cycle arrest, and an increase in both mitotic index and metaphase cells specifically, which may indicate a mitotic delay. The accumulation of cells in mitosis and subsequent apoptosis suggests that the mitotic arrest may be required for Mdivi-1-induced cytotoxicity.

7.3.2. Does Mdivi-1 influence the level of mitosis after irradiation?

In the U937 cell line, Mdivi-1 caused a notable increase in mitoses with exposure. However, when combined with radiation, which also increased the mitotic index, a sub-additive response was obtained. It is likely that a radiation-induced cell cycle arrest prevented entry of cells into mitosis and thus, the Mdivi-1 induced accumulation of mitotic cells.

7.3.3. Does Mdivi-1 cause apoptosis in cancer cells?

Mdivi-1 induced significant apoptosis. The U937 cells were more sensitive to Mdivi-1-induced apoptosis than the A549 cells with up to 40 % of the cells undergoing apoptosis after 24 h of treatment. As the apoptotic index decreased after the removal of Mdivi-1, it can be speculated that expression of Mdivi-1-induced damage requires continuous exposure.

Mdivi-1 would appear to be capable of inducing apoptosis in apoptosis-responsive cells, such as the U937 cells. However, the lack of correlation between clonogenic survival and apoptosis in the A549 cell line suggests that Mdivi-1 may induce other modes of cell death in more resistant cells.

7.3.4. Does Mdivi-1 modulate radiation-induced apoptosis in cancer cells?

It was consistently observed that Mdivi-1 combined with radiation did not increase the apoptotic index above that observed for Mdivi-1 alone. However, in U937 cells, once irradiation and Mdivi-1 treatment were separated by a time interval, equivalent to the time required for release of the radiation-induced G2/M arrest, the apoptotic index was increased relative to Mdivi-1 treatment alone. Our results thus suggest that the passage through mitosis may be required for the expression of Mdivi-1-induced effects.

7.3.5. Does Mdivi-1 induce cytogenetic damage?

Mdivi-1 was shown to induce cytogenetic damage in both cell lines but to a lesser extent in the U937 cell line. It can be speculated that cells that are resistant to apoptosis, such as the A549 cells, are more likely to survive and express cytogenetic damage. Apoptosis-sensitive cells, however, are likely to be eliminated early, thus reducing the number of evaluable cells displaying cytogenetic damage.

7.3.6. Does Mdivi-1 modulate the induction of radiation-induced cytogenetic damage?

Radiation induced high levels of cytogenetic damage in both cell lines. The combined treatment of Mdivi-1 and radiation resulted in fewer cells displaying cytogenetic damage than induced by radiation alone. This may suggest that Mdivi-1 protects against radiation-induced cytogenetic damage. However, the reduced effect may be attributed to an Mdivi-1-induced accumulation of cells in mitosis prior to irradiation. Increased radiosensitivity of these cells may increase the probability of mitotic cell death and selective reduction of the population evaluable for assessment of cytogenetic damage.

Study limitations

Studies were conducted in an *in vitro* system and would need to be replicated *in vivo* for further pre-clinical testing. In addition, a limited number of cell lines were included for analysis, particularly the radiomodulation experiments, thus restricting generalisability. Cancer type-specific effects could also not be fully elucidated, however distinct differences in the responses of cells from malignancies of solid- and haematological origin were suggested. The lack of inclusion of normal cells prevented the evaluation of potential differential effects. Further, evidence of changes at a protein level, e.g. DRP1 expression, after mitochondrial modulation would strengthen conclusions regarding Mdivi-1 effects. Finally, single radiation doses were used for most investigations and the effect of combination with fractionation remains unclear.

Clinical prospects and future work

Having demonstrated a proof of principle, it is envisaged that drugs like Mdivi-1 may be developed further for clinical use. Provision of mitochondrial modulating agents to patients prior to radiotherapy treatments could possibly enhance tumour response. However, extensive clinical development would be required before this goal could be realised. Investment in the design of specific drugs that can regulate mitochondrial dynamics precisely and with minimal toxicity may also be worthwhile. As a therapeutic strategy, manipulating mitochondrial dynamics may offer a favourable therapeutic ratio as Mdivi-1 has been shown to be relatively well-tolerated in normal tissue models.

Screening for tumour mitochondrial function may be useful in predicting sensitivity to treatment. Currently, techniques exist for the diagnosis of mitochondrial diseases through clinical, histopathological, biochemical and molecular examinations. The development of markers that can act as a proxy for tumour mitochondrial status is an important future consideration. Such a tool may be useful to inform treatment and may also have prognostic application.

Further avenues for investigation may include mechanistic studies, and the inclusion of additional models and fractionation schemes. It would be important to replicate the radiation experiments with Mdivi-1 in additional models to determine if the radiosensitisation demonstrated is generalisable. In addition, the assessment of DRP1 and other associated proteins in response to modulation of mitochondrial dynamics would yield a more holistic interpretation. Other approaches to modulate mitochondrial dynamics, including siRNA knock-down of relevant proteins would provide additional evidence for construction of a universal theory. The investigation of such effects in additional cell lines, including normal cells, other types of cancer and in *in vivo* models, will contribute to this understanding.

OVERALL CONCLUSIONS

Radiation response is influenced by changes in mitochondrial dynamics. Although measures of cellular radiosensitivity did not correlate significantly with inherent mitochondrial membrane potential, respiration or morphology, Mdivi-1 treatment, which resulted in increased mitochondrial fusion, significantly radiosensitised lung cancer cells. In addition, Mdivi-1 reduced clonogenic survival, increased apoptotic cell death and induced cytogenetic damage in two cancer models. Mdivi-1, induced an increase in mitotic cells and a G2/M arrest, and enhanced the radiation-induced cell cycle arrest. However, combined Mdivi-1 and radiation treatments frequently yielded sub-additive responses for measures other than clonogenic survival, and did not influence radiation-induced damage repair.

Overall, the evidence presented demonstrates the potential for the modulation of mitochondrial dynamics to induce cytotoxic effects in tumours and to enhance the effectiveness of radiation therapy. Such approaches represent a novel paradigm for cancer treatment.

Appendices

APPENDIX A

CELL LINES AND CULTURE TECHNIQUES

1. Cell lines

The cell lines obtained for this study are listed in Table 4.1, p. 58). A549 (cat. 86012804), T47D (cat. 85102201) and U937 cells (cat. 85011440) were obtained from the European Collection of Authenticated Cell Cultures (ECACC) (Porton Down, Salisbury, UK). DU145 cells were obtained from the International Centre for Genetic Engineering and Biotechnology (ICGEB), University of Cape Town (UCT) and the MDA-MB-231 and HeLa cells were received from the Department of Medicine, UCT. Cells within 5 passages were used in experiments. Mycoplasma testing was performed bi-monthly.

2. Cell culture

Cell lines were incubated at 37°C with 100 % humidity and 5% CO_2 /95% O_2. A549, T47D, U937, MDA-MB-231 and HeLa cells were grown in RPMI (Roswell Park Memorial Institute) 1640 culture medium (Sigma-Aldrich, St. Louis, MO, USA) while DU145 cells were grown in Dulbecco's Modified Eagle's medium (DMEM) cell culture medium (Sigma-Aldrich) (Appendix A2.1). Cell culture medium was supplemented with 10 % heat inactivated fetal calf serum (FCS) (Highveld Biological, Johannesburg, SA) and 1 % antibiotics (AB) (penicillin and streptomycin) (Highveld Biological) unless otherwise indicated.

2.1. Cell culture media

RPMI/DMEM	10.4/13.4 g
$NaHCO_3$ (Sigma-Aldrich)	2/3.7 g

Made up to 1L with ddH_2O

Filtered using a sterile 0.22 µm Corning® bottle-top vacuum filter system (Sigma-Aldrich) and stored at 4°C.

2.2. Sub-culture of cells

Cells were passaged every 2-3 days as required. Adherent cell lines were sub-cultured by trypsinisation as follows; the cell culture medium was removed and cells were washed with 1 ml phosphate buffered saline (PBS) (Appendix A 2.2.1).

A volume of 1 ml trypsin (Highveld Biological) (Appendix A2.2.2) was added and cells were incubated for 10 minutes at 37°C. The trypsin was inactivated with culture medium and then removed by centrifugation for 5 minutes at 100 RCF. The cells were resuspended in fresh medium and the cell number determined using a haemocytometer. An appropriate number of cells was then seeded into a 25 cm^2 CELLSTAR® sterile cell culture flask (Greiner Bio-One GmbH, Frickenhausen, Germany) and incubated as described previously.

The U937 suspension culture does not require enzymatic treatment for sub-culturing. Cells were cultured in 75 cm^2 CELLSTAR® sterile suspension culture flasks (Greiner Bio-One). For sub-culture, a sample of cells was diluted to the appropriate seeding density in fresh medium.

2.2.1. 1x PBS (0.01 M)

100 mM NaCl (Sigma-Aldrich)	5.84 g
20 mM NaH_2PO_4 (Sigma-Aldrich)	2.4 g
80 mM Na_2HPO_4 (Sigma-Aldrich)	11.36 g
Made up to 1L with ddH_2O (pH = 7.4)	

2.2.2. Trypsin (0.05 %)

Trypsin powder (Difco Laboratories, MI, USA)	0.5 g
NaCl	11.24 g
KCl	0.4 g
$NaHCO_3$	0.58 g
Di sodium EDTA (BDH Laboratory supplies, Poole, UK)	0.2 g
Made up to 1L with ddH_2O	

Filtered using a sterile 0.22 µm Corning® bottle-top vacuum filter system and stored at 4°C.

2.3. Trypan blue cell viability assay

The viability of cells was assessed using trypan blue solution (0.4 %) (Gibco, Massachusetts, USA). This dye stains cells only if the cell membrane has been compromised. A small volume (100 µl) of cells in suspension was transferred to a 0.5 ml Eppendorf tube (Greiner Bio-One) containing an equal volume of trypan blue solution (1:1). Cells were visualised on a WILD M12 phase contrast microscope (Wild, Heerbrugg, Switzerland) at 100x magnification and quantified using a haemocytometer. Cells were scored and designated as viable or non-viable depending on trypan blue uptake.

APPENDIX B

CELL SURVIVAL ASSAYS AND RADIATION SETUP

1. Clonogenic cell survival assays

1.1. Pre-plated clonogenic survival assay: Adherent cells

A suitable number of exponentially growing cells were plated into 60 mm CELLSTAR® cell culture dishes (Greiner Bio-One) for a yield of at least 100 colonies after treatment. Culture dishes were incubated overnight at 37°C for cells to adhere before irradiation.

Cells were γ-irradiated in quadruplicate using a ^{60}Co source with a dose rate of approximately 1 Gy/min at a source to surface distance (SSD) of 80 cm. Please refer to Appendix B2 for the irradiation setup. Unirradiated control samples were mock treated. Culture dishes were incubated at 37°C for up to three weeks depending on the cellular doubling time and period to form colonies for each cell line. When colonies of at least 50 cells were observed, the culture medium was removed and the cells were rinsed with 1 ml PBS. Colonies were then stained with 2 ml crystal violet solution [0.2 %] (Appendix B1.1.1) for five minutes. Following a rinse with water to remove excess dye, culture dishes were air dried and colony number was determined manually. Colonies of at least 50 cells were counted and cell number was confirmed microscopically using a WILD M40 inverted microscope (Wild) fitted with a Fluotar 10x Ph0.4 objective lens.

1.1.1. Crystal violet solution (0.2 %)

Crystal violet (Sigma-Aldrich)	200 mg
Methanol (Merck, NJ, USA)	10 ml
ddH_2O	90 ml

Clarified using No 1. Whatman filter paper (Sigma-Aldrich).

1.2. Pre-plated clonogenic survival assay: Suspension cells

The clonogenic assay was adapted for the U937 non-adherent cell line to facilitate formation of colonies within an agarose-based culture medium that prevented the cells from separating after division. The modified medium (Appendix B1.2.3.) consisted of 0.6 % low melting point agarose (Appendix B1.2.1), 2x RPMI culture medium (Appendix B1.2.2) and FCS in the ratio 5:4:1.

U937 cell number was determined in 1x RPMI culture medium and calculated volumes of cells were added to give a final volume of 2 ml. After careful mixing, cells were transferred to 35 x 10 mm CELLSTAR® cell culture dishes (Greiner Bio-One) and incubated at room temperature for 1 h. A short incubation of 10 minutes at 4°C facilitated setting of the agarose prior to irradiation. Cells were irradiated as described above and incubated at 37°C for 1 week until visible colonies had formed.

1.2.1. Agarose (0.6 %)

Low melting point agarose (Sigma-Aldrich)	0.6 g
ddH_2O	100 ml

Heated to dissolve and autoclaved to sterilise.

1.2.2. 2x RPMI culture medium

RPMI 1640	1.04 g
$NaHCO_3$	0.2 g

Made up to 50 ml with ddH_2O

Filter sterilised with a 0.2 µm Supelco minisart syringe filter (Sigma-Aldrich) and heated to 45°C in a water bath (FMH Instruments, Labotec, Midrand, SA).

1.2.3. Semi-solid culture medium

0.6 % Agarose (cooled to 45°C)	50 ml
2x RPMI medium (Appendix B1.2.2.)	40 ml
FCS	10 ml

1.3. Post-plated clonogenic survival assay

Mdivi-1 (Sigma-Aldrich) was found to cause mitotic arrest of > 10 % of cells after 6 h treatment.
As cells in mitosis become round and easily detached, pre-plated experiments may result in loss of cells during wash steps. Post-plated experiments however circumvent this problem by plating cells for colony formation after treatment.

For post-plated clonogenic assays, an equal number of cells were plated into 25 cm^2 CELLSTAR® sterile cell culture flasks (Greiner Bio-One) at a low density (100 000 cells/ml) and incubated overnight at 37°C. Up to 4 flasks per treatment group, as detailed in the relevant methodology sections were included for analysis. Replicates were processed in separate experiments. After treatment the medium containing any detached cells, and PBS washes were collected in 12 ml CELLSTAR® cell culture tubes (Greiner Bio-One).

The remaining cells were trypsinised for 10 minutes and added to the respective tube. Samples were washed 3x with 3 ml of medium and cells were collected by centrifugation at 100 RCF. A cell count was performed for each test group using a haemocytometer. From this, dilutions were made and cells were plated into 60 mm CELLSTAR® cell culture dishes (Greiner Bio-One) for a yield of at least 100 colonies. Culture dishes, in triplicate, were incubated for up to 10 days at 37°C for colony formation. Colonies were stained with crystal violet as was described previously.

1.4. Clonogenic assay for separated adherent and detached cell populations

Cells at a density of 150 000 cells/ml were plated into 35 x 10 mm CELLSTAR® cell culture dishes (Greiner Bio-One) and incubated in 2 ml RPMI (with FCS and AB) at 37°C overnight to adhere. Two plates per sample were used where adherent and detached cells were to be separated. The cells from both dishes were pooled to ensure an adequate number could be collected for plating. The incubation medium was replaced with 1 ml RPMI containing 30 µM Mdivi-1 (Chapter 6, section 6.2.1) or the vehicle and cells were irradiated, if required, and incubated at 37°C for 16 h.

For the unseparated samples, collection of cells was as described previously for post-plated experiments. For samples to be separated, cells were collected by transferring the incubation medium from the dishes to a 12 ml CELLSTAR® cell culture tube (Greiner Bio-One). Each plate was washed multiple times with 1 ml PBS to ensure all detached cells had been collected. The remaining adherent cells were trypsinised and cells were collected in a separate 12 ml CELLSTAR® cell culture tube (Greiner Bio-One). All samples were centrifuged at 100 RCF for 15 minutes to pellet cells and washed twice with 4 ml RPMI (with FCS and AB) to remove Mdivi-1.

Cell pellets were resuspended in an appropriate volume of RPMI (with FCS and AB) for a cell count and the required numbers of cells were plated out for each sample to give at least 100 colonies for analysis. Five replicate plates were incubated at 37°C for 7-10 days to allow colony formation and then stained with crystal violet as described previously. In addition, the total number of cells in each sample was calculated in order to determine the relative proportion of adherent to detached cells.

2. Radiation setup

An Eldorado 8 Cobalt teletherapy unit (Atomic Energy of Canada Ltd, Ottawa, Canada) with a fixed head was used for γ-irradiation of cells. Photographs of the irradiation setup are shown in Figure B1. The ^{60}Co source produces a beam of γ-rays of 1.17 and 1.33 MeV energies. This unit provides an irradiation field size of 10 x 10 cm^2 (within 95 % isodose) at an SSD of 80 cm. Samples were irradiated with 5 mm Perspex build-up and full back scatter.

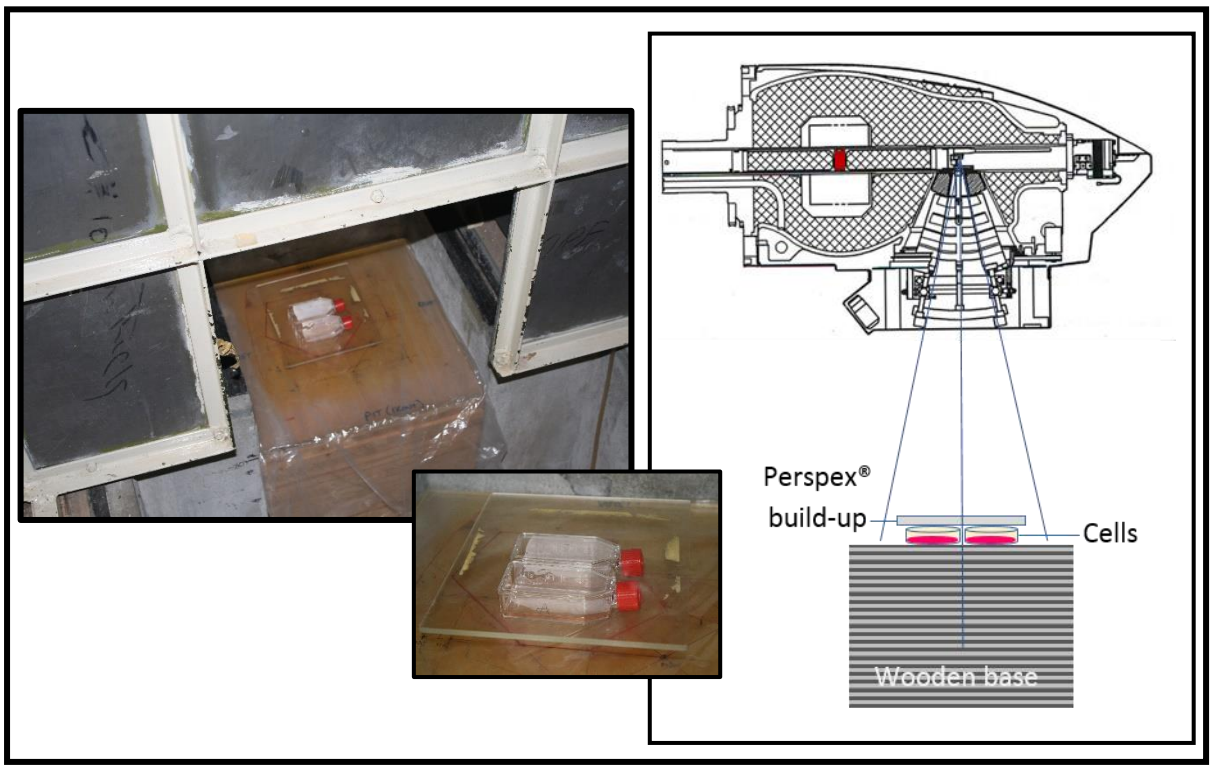

Figure B1: Radiation setup. **A.** The ^{60}Co teletherapy unit used for γ-irradiation of cells. Insert: Two flasks demonstrating placement of build-up for irradiation. **B.** Schematic representation of the ^{60}Co radiation setup.

APPENDIX C

STAINING OF MITOCHONDRIA

1. MitoTracker® Red staining protocol

Adherent A549, T47D and DU145 cells were plated at a density of 100 000 cells per 10 cm^2 onto 22 x 22 mm glass coverslips (Lasec, Cape Town, South Africa) in 35 x 10 mm CELLSTAR® cell culture dishes (Greiner Bio-One). Cells were incubated in the appropriate culture medium (with FCS and AB) at 37°C for 24 h prior to staining.

MitoTracker® Red (Molecular Probes® Inc) stock solution (100 µM in DMSO) was diluted to give an optimised final working solution (Appendix C, Table C1) in the appropriate pre-warmed culture medium (with FCS and AB) for each cell line. Solutions maintained a DMSO concentration of < 0.1 %. A volume of 1 ml MitoTracker® Red solution was added and cells were incubated at 37°C for up to 25 minutes depending on the cell type (Appendix C, Table C1). The cells on the coverslips were washed twice with 2 ml of medium. Cells were fixed for 20 minutes at room temperature using 4 % paraformaldehyde prepared in medium (Appendix D2.2). The fixative was replaced with PBS and samples were stored at 4°C.

For microscopic visualisation, coverslips were mounted onto 76 x 26 mm glass slides (Lasec) as described in Chapter 4. Fluorescence microscopy is detailed in Appendix D. During processing, cells were protected from light as MitoTracker® Red is fluorescent and light sensitive.

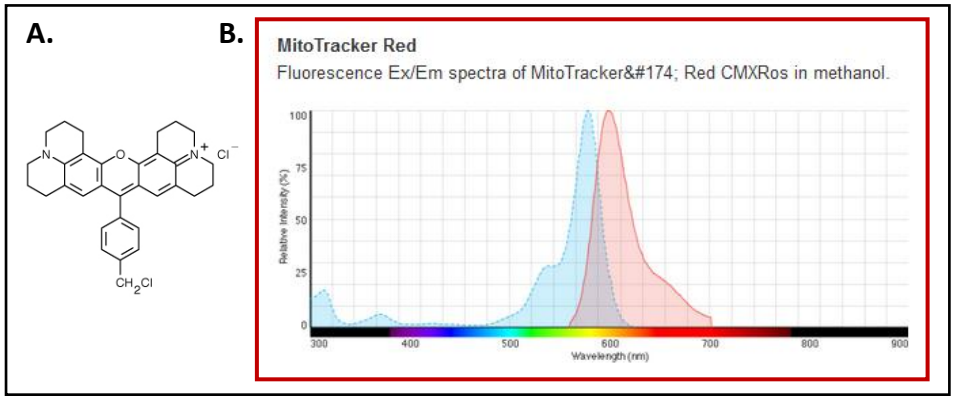

Figure C1: MitoTracker® Red CMXRos ($C_{32}H_{32}Cl_2N_2O$). **A)** Chemical structure. **B)** Excitation and emission spectra (from: http://www.lifetechnologies.com/order/catalog/product/M7512).

Table C1: MitoTracker® Red concentrations and incubation times

Cell line	[MitoRed]	Incubation time
A549	100 nM	15 minutes
DU145	100 nM	25 minutes
T47D	80 nM	15 minutes

2. Comparison of mitochondrial staining techniques

2.1. Live cell imaging

Samples from each cell line were stained with MitoTracker® Red (Molecular Probes® Inc.) and assessed using live cell imaging as described in Chapter 4 to confirm that the mitochondrial morphology of fixed cells was comparable to that observed in live cells. Images of mitochondria from live cells are shown in Figure C3 for comparison with the mito-RFP-transfected cells (Figure C4), confocal microscopy images (Figure C5) and the morphological subtypes shown in Appendix E.

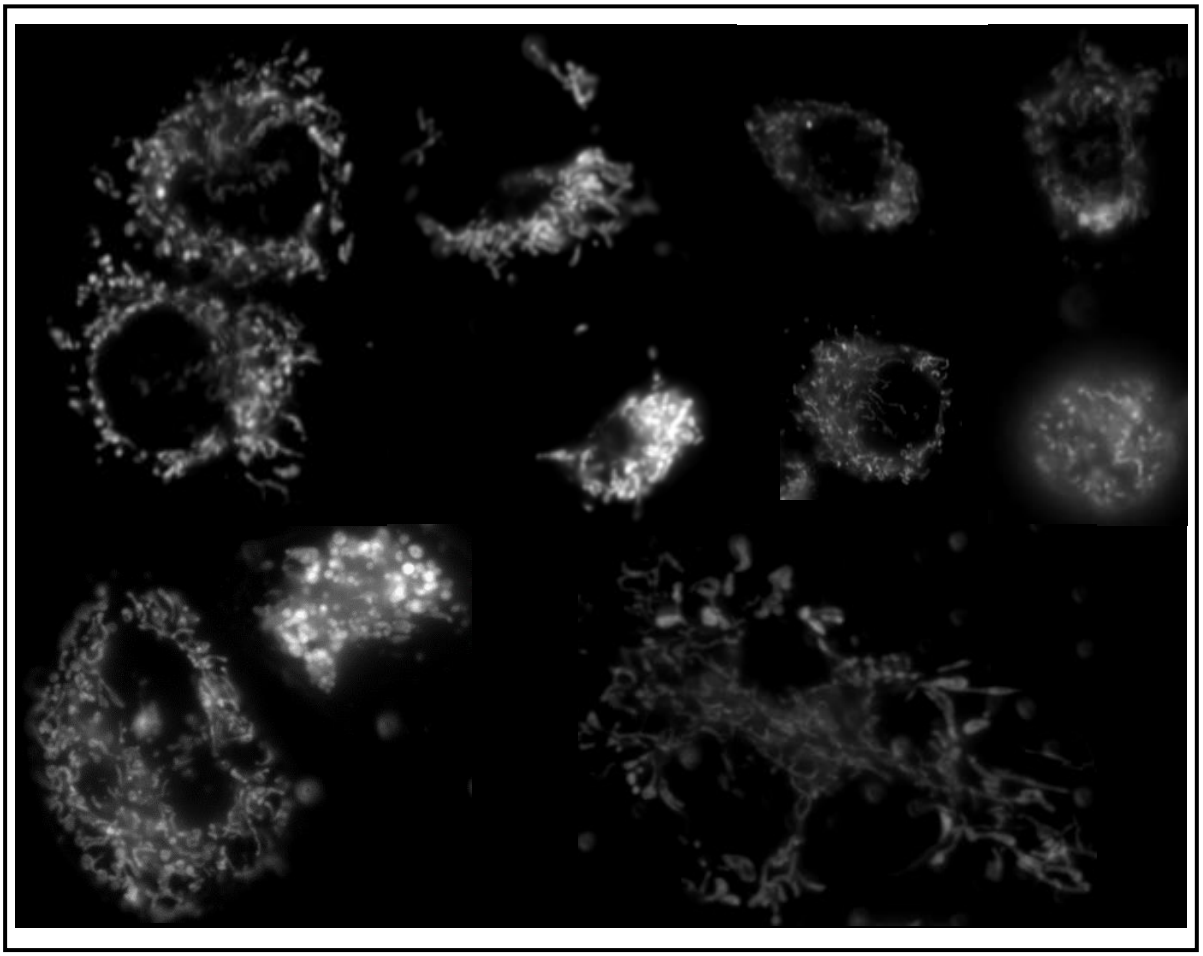

Figure C2: Live cell imaging of A549 mitochondria using MitoTracker® Red. 1000x magnification.

2.2. Mito-RFP transfection

The A549 cell line was transfected with a red fluorescent protein construct (mito-RFP) to label mitochondria (CellLight® Mitochondria-RFP, BacMam 2.0; Molecular Probes Inc). Briefly, 2 µl of the BacMan reagent was added per 10 000 cells in the appropriate culture medium. Cells were incubated at 37°C for 16 h. Figure C4 shows a collection of transfected cells that represent a spectrum of the mitochondrial morphologies observed using this technique.

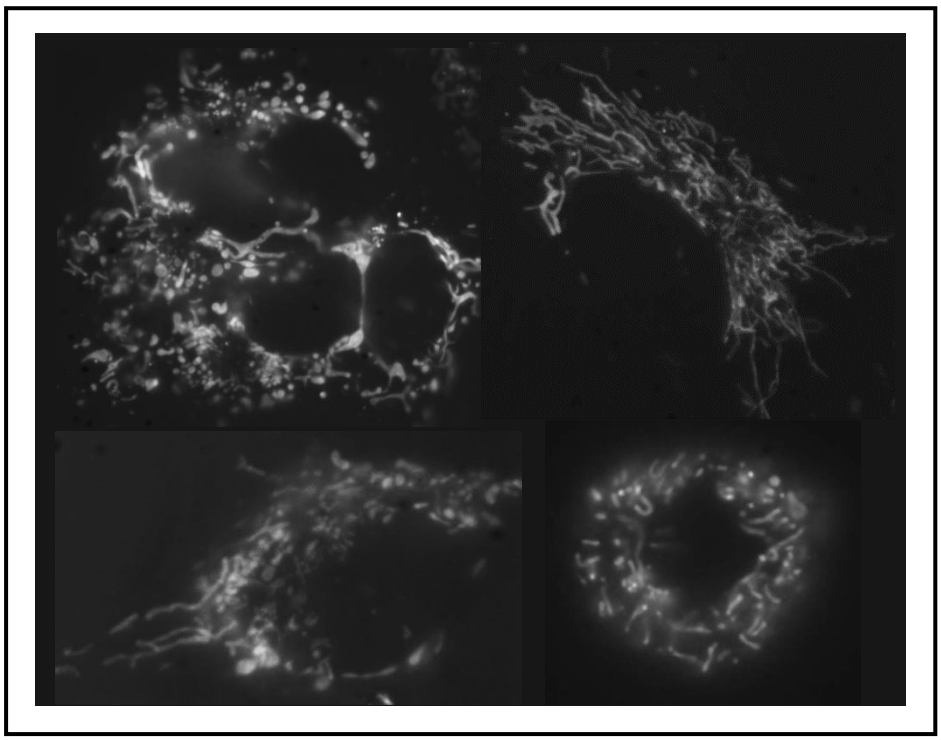

Figure C3: Mitochondria in mito-RFP-transfected A549 cells. 1000x magnification.

2.3. Confocal microscopy

In order to further evaluate the quality of the images obtained using conventional fluorescence microscopy, mitochondria were imaged using confocal microscopy (Figure C5). Cells were stained with MitoTracker® Red and the mitochondria were visualised using a Zeiss Axiovert 200M LSM 510 Meta Confocal Microscope with pulsed infrared laser for 2-photon excitation (UCT Confocal and Light Imaging Facility). Images were collected using a Zeiss AxioCam and analysed using LSM software for post-acquisition image processing, AxioVision 4.7 (Carl Zeiss).

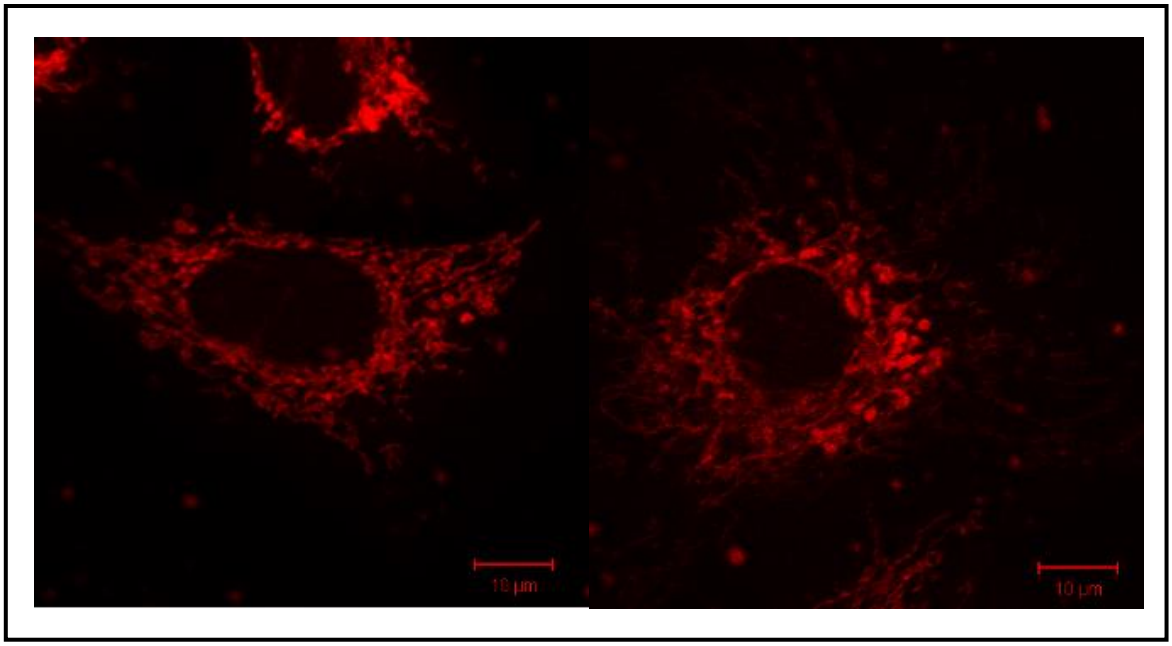

Figure C4: Confocal microscopy images of A549 cells stained with MitoTracker® Red. 1000x magnification.

3. JC-1 staining protocol for mitochondrial membrane potential assessment

3.1. Staining of cells

All cell lines were stained in suspension to determine the relative ΔΨm. U937 cells were seeded into 60 mm CELLSTAR® cell culture dishes (Greiner Bio-One) at a density of 250 000 cells/ml. Adherent A549, T47D, and DU145 cells were cultured in 35 x 10 mm CELLSTAR® cell culture dishes (Greiner Bio-One) to a density of 500 000 cells/ml. The cell culture medium was replaced 3 h prior to assessment. After trypsinisation as required, cells were collected in 12 ml CELLSTAR® cell culture tubes (Greiner Bio-One) and centrifuged at 100 RCF for 10 minutes. The supernatant was carefully removed and the pellet was resuspended directly in JC-1 stain (Appendix C3.1.1). Samples were incubated at 37°C for 20 minutes and collected by centrifugation at 100 RCF for 5 minutes giving a total JC-1 staining time of 25 minutes. Cells were washed once with 2 ml of cell culture medium and were resuspended in a final volume of 100 µl of medium. Samples were mounted onto 76 x 26 mm glass slides (Lasec), covered with 22 x 22 mm glass coverslips (Lasec). Slides were maintained at 37°C and imaged 30 minutes after staining to allow for JC-1 aggregation.

3.1.1. JC-1 stain preparation

JC-1 (Sigma-Aldrich) was reconstituted in DMSO at a concentration of 3 mM. Solutions were diluted to 5 µM in the appropriate culture medium (with FCS and AB) giving a final DMSO concentration of 0.17 %. For dilutions, the JC-1 stock solution and the appropriate cell culture medium were pre-warmed and JC-1 was added while vortexing. Solutions were maintained at 37°C until use to ensure continued dissolution of JC-1.

3.2. Quantification of fluorescence images using Image J

RAW image files (.CR2) were converted to "Tagged Image File Format" (.tiff) using Digital Photo Professional v3.4. Images collected using blue light excitation, showing both ‘green’ and ‘orange’ fluorescence were used to demarcate specific regions for intensity measurements. Images were opened in Image J v1.48 (NIH)[634] and were separated into red, green and blue channels. The green channel image was converted to 8-bit and a threshold was applied to include all cells in the field but exclude background fluorescence. Selected areas were identified as regions of interest (ROI) and saved in the ROI manager.

The original combined image was then re-opened and the saved ROI set was applied to the image. Quality control of the ROI set was done manually to ensure the entire cell was included in the analysis and artifacts were excluded.

The average grey value per cell was measured using the green channel from this image only. In addition, the saved ROI mask was applied to the corresponding image captured using green light excitation. This image was also divided into blue, green and red channels and the red channel was used to quantify the red fluorescence in each of the corresponding cells. Included in the ROI mask were five regions chosen from areas of the image that did not contain cells. The average value from these five measurements, namely the average background reading, was subtracted from the 'red' or 'green' mean grey values respectively to give a corrected mean grey value. Once red and green values were collected for all cells in a field the Red:Green ratio was calculated by dividing the 'red' mean grey value by the 'green' mean grey value.

3.3. High magnification images of mitochondria stained with JC-1

3.3.1. JC-1 staining of adherent cells cultured on coverslips

Adherent A549, T47D, and DU145 cells were plated into 35 x 10 mm CELLSTAR® cell culture dishes (Greiner Bio-One) at a density of 100 000 cells per 10 cm^2 onto 22 x 22m m glass coverslips. Cells were incubated overnight to adhere in the appropriate culture medium (with FCS and AB) at 37°C prior to staining. The culture medium was replaced with JC-1 stain (Appendix C3.1.1) and incubated at 37°C for 15 minutes. Coverslips were washed once with culture medium and mounted onto 76 x 26 mm glass slides (Lasec). Slides were incubated at 37°C for 25 minutes before viewing. A subset of high magnification images were collected for each of the cell lines to document differences in JC-1 aggregate distribution within the mitochondria of individual cells and between cell types. Samples were imaged with the UPlanFl 100x/0.75 objective (Olympus) using the WB fluorescence filter block (Appendix D, Table D1). Images were captured using a Moticam Pro 285D monochrome scientific CCD camera (Peltier cooled) for Olympus fluorescent microscope (Motic).

APPENDIX D

FLUORESCENCE MICROSCOPY

1. Fluorescence microscopy and image capture

Cell culture and staining has been described previously. For adherent cell lines, stained cells on glass coverslips (Lasec) were rinsed with PBS and mounted on a 76 x 26 mm glass slide (Lasec) with 15 µl mounting solution (Appendix D1.1). Coverslips were sealed with nail varnish where aqueous mounting solutions were used and high magnification (1000x) was required. Samples mounted with Mowiol and ProLong® Gold did not need to be sealed once mountant had hardened. For cells in suspension, 10 µl of sample was mixed with 10 µl mounting solution (Appendix D1.1) on a 76 x 26 mm glass slide. The sample was covered with a 22 x 22 mm glass coverslip and sealed as required. For live cell viewing, cells were mounted immediately with 15 µl of the appropriate cell culture medium. Cells were visualised using light or fluorescence microscopy, as required. All preparations for fluorescence microscopy were performed under low-light conditions.

Slides were visualised using a BX41 Olympus fluorescence microscope (Olympus). The UPlanFl 100x/1.30 oil immersion objective (Olympus) was used for high magnification microscopy and the UPlanFl 10x or 40x/0.75 objective for lower magnifications (Olympus).

The appropriate filter block was selected based on the fluorescent label used in each experiment (Appendix D, Table D1). Images were captured using a Moticam Pro 285D monochrome scientific CCD camera (Peltier cooled) for Olympus fluorescent microscope (Motic).

Table D1: Characteristics of fluorescent labels

Fluorescent label/ stain	Filter block	Excitation/Emission (max) nm	Light (Ex/Em) nm
MitoTracker Red	WG	579/599	Green/Red
JC-1	WB & WG	490/520 & 590	Blue/Green & Green/Red
FITC	WB	495/519	Blue/Green
Acridine Orange	WB	502/525 & 460/650	Blue/Green (and orange)
DAPI/Hoechst	WUV	368/461	UV/Blue

2. General mounting, fixing and staining solutions for microscopy

2.1. Mounting solutions

a) Mowiol:

Glycerol (Sigma-Aldrich)	6 g
Mowiol (Sigma-Aldrich)	2.4 g
ddH_2O	6 ml

The mixture was incubated at room temperature for 2 h followed by the addition of 12 ml 0.2 M Tris, pH 8.5 (Sigma-Aldrich). After incubation for a further 10 minutes at 60°C, the Mowiol was centrifuged at 5000 RCF for 15 minutes to remove undissolved solids. Long-term and short-term storage of aliquots was at -20°C at 4°C, respectively.

b) Glycerol:PBS (8:2) solution combined in a 2 ml cryogenic vial (Greiner Bio-One).

c) VECTASHIELD Antifade Mounting Medium: DAPI (Vector Laboratories Inc.).

d) ProLong® Gold Antifade Mountant (Fairland, Johannesburg, SA).

2.2. Staining solutions

2.2.1. Hoechst 33342 (1 µg/ml)

1 mg/ml Hoechst 33342 (Sigma-Aldrich)	10 µl
PBS	10 ml

2.2.2. Acridine orange solution (10 µg/ml)

1 mg/ml Acridine orange stock solution	400 µl
Gurr's phosphate buffer	40 ml

2.2.2.1. Acridine orange stock (1 mg/ml)

Acridine orange (BDH Laboratory supplies)	0.1 g
ddH_2O	100 ml

2.2.2.2. Gurr's phosphate buffer (0.004 M, pH 6.8)

0.54 M KH_2PO_4	100 ml
0.57 M Na_2HPO_4	50 ml

Made up to 1L with ddH_2O

2.3. Fixing solutions and buffers

2.3.1. Paraformaldehyde (4 %)

Paraformaldehyde (Sigma-Aldrich)	0.4 g
PBS or medium as required	10 ml

The solution was heated to 60°C and the pH was adjusted with 25 µl 1N NaOH to obtain a clear solution and ooled to room temperature before application.

2.3.2. Metaphase fixative solutions A and B

A = Methanol:acetic acid:Ringers solution (4:1:5)

B = Methanol:acetic acid (4:1)

2.3.3. KCl (75 mM)

KCl	5.6 g

Made up to 1L with ddH_2O and pre-warmed to 37°C before use.

2.3.4. Ringers solution (75 mM)

NaCl	6.5 g
KCl	0.42 g
$CaCl_2$	0.25 g
$NaHCO_3$	0.2 g

Made up to 1L with ddH_2O

APPENDIX E

MITOCHONDRIAL MORPHOLOGICAL SUBTYPES

1. Morphological classification

1.1. Image processing

Mitochondrial images were analysed using Image J software (NIH)[634] and were processed using a convolution filter as described in Chapter 4. The process is summarised in Figure E1.

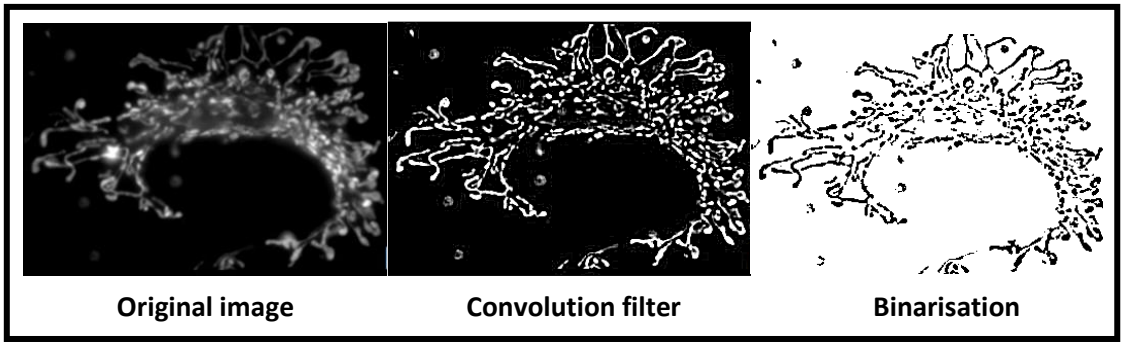

Figure E1: Processing of images for morphological assessment of mitochondria in MitoTracker® Red stained cells.

1.2. Quality control

Slides containing a large proportion of cells that appeared to be rounded and swollen were excluded as this morphology has been reported to represent deterioration of cells and/or dysfunctional mitochondria[474, 567].

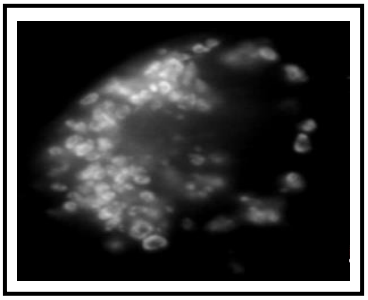

Figure E2: Representative example of a cell containing swollen mitochondria indicating potential sample deterioration. 1000x magnification.

1.3. Morphological assessment by categorisation

1.3.1. Acquisition and documentation of representative images

Morphological data was acquired manually from direct observation and not from images. However, certain images were captured to document morphology. Representative images were captured with a Moticam Pro 285D monochrome scientific CCD camera (Motic). Exposure settings were adjusted to optimise capture of both brightly-stained perinuclear mitochondria and faint peripheral fragments. Image J v1.48 (NIH)[634] was used for image processing to enhance the brightness and contrast mainly to highlight fine detail. Adjustments were made solely for clarity and did not significantly alter image content.

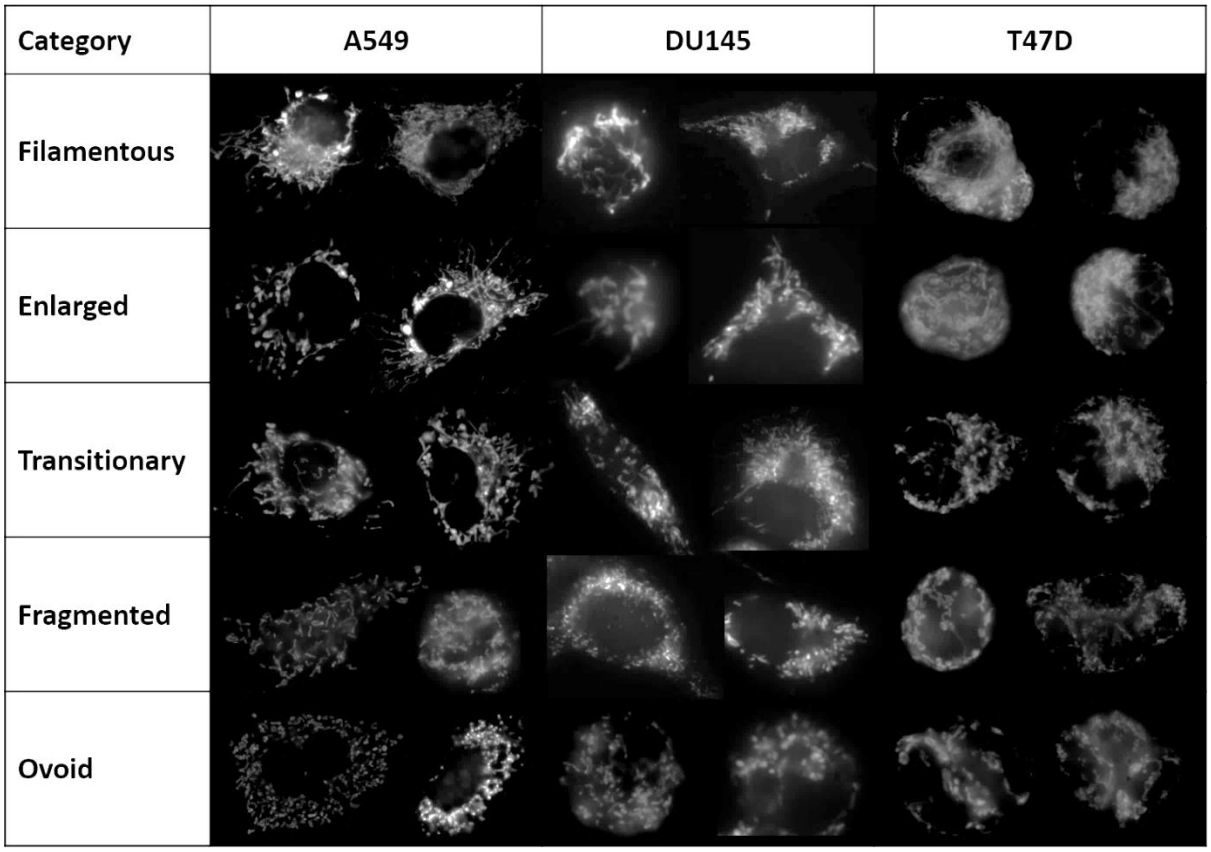

Figure E3: Mitochondrial morphological categories and examples of each for the cell types analysed. 1000x magnification.

1.4. Morphological assessment by Small-fragment analysis

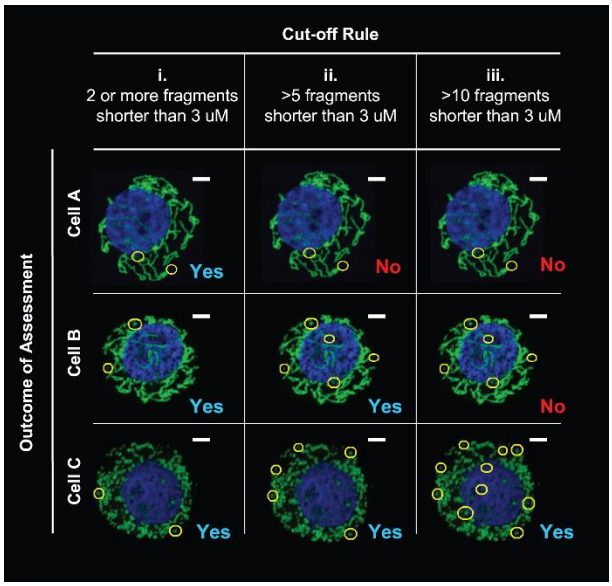

Figure E4: Diagram illustrating the cut-off rule for morphological categorisation of cells based on mitochondrial fragmentation. Copyright: ©2013 Farrand et al. [688]

APPENDIX F

HIGH-RESOLUTION RESPIROMETRY

1. Preparation of cells

Cells for analysis of oxygen consumption were plated at 200 000 cells/ml in 75 cm^2 CELLSTAR® sterile cell culture flasks (Greiner Bio-One). Exponentially growing adherent A549, T47D and DU145 cells were harvested by trypsinisation and, with the U937 non-adherent cells, were centrifuged at 100 RCF and resuspended in the appropriate culture medium containing FCS and AB. Cells were diluted to 800 000 cells/ml and were maintained in 75 cm^2 CELLSTAR® sterile cell culture flasks (Greiner Bio-One) at 37°C and with gentle agitation until analysis.

2. Respirometry apparatus

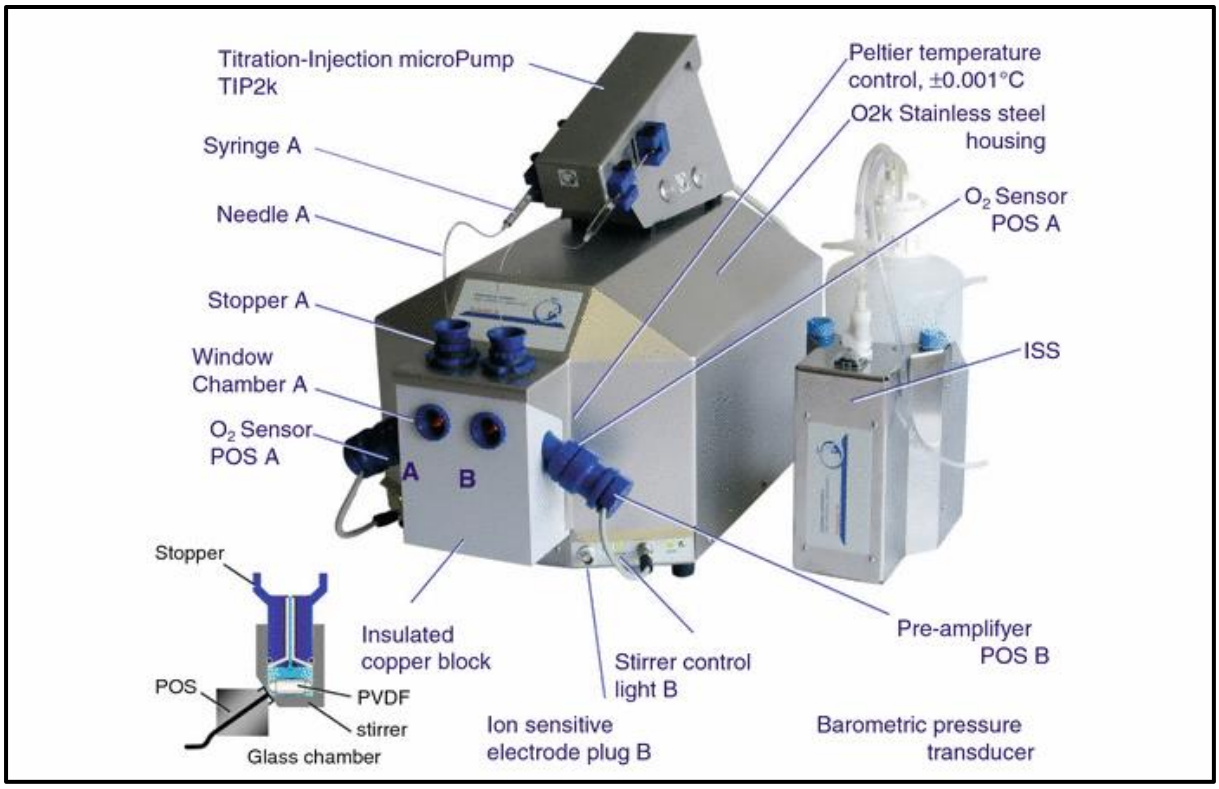

Figure G1: The OROBOROS Oxygraph-2k (O2k series C) for high resolution respirometry. Reproduced with permission from OROBOROS Instruments Inc. (http://www.oroboros.at)[327].

APPENDIX G

FLOW CYTOMETRY

1. Experimental protocol and sample preparation

A549 cells were seeded into 25 cm^2 CELLSTAR® sterile cell culture flasks (Greiner Bio-One) at the required density to obtain approximately 500 000 cells/ml for analysis. Specific protocol details are provided in the experimental chapters. Following the required treatment time, the medium containing any detached cells was collected into a 12 ml CELLSTAR® cell culture tube (Greiner Bio-One). Adherent cells were washed with 1 ml PBS, trypsinised for 10 minutes at 37°C and added to the medium. After centrifugation at 100 RCF for 10 minutes, cells were washed twice with 2 ml PBS. Note: Throughout this protocol the PBS was supplemented with 2 % FCS. Cells were resuspended in 1 ml PBS and 3 ml ice cold absolute ethanol (Sigma-Aldrich) ([Final] = 75 %) was added dropwise to each sample while vortexing. After incubation at 4°C for 1 h, samples were stored at -20°C in preparation for staining 24 h prior to analysis.

1.1. Staining of cells for cell cycle analysis

Samples were vortexed and centrifuged for 20 minutes at 200 RCF to pellet cells. The supernatant was discarded and cells were resuspended in 2 ml PBS. Following an additional wash step, the cells were resuspended in 500 µl of 1 mg/ml RNAse A solution [0.025 g RNAse A (Sigma-Aldrich) in 25 ml PBS] and were mixed thoroughly. Samples were incubated at 37°C for 30 minutes and 50 µl of 500 µg/ml propidium iodide [0.001 g propidium iodide (Sigma-Aldrich) in 2 ml PBS] was added directly to the RNAse A solution ([Final] = 50 µg/ml). Samples were stored in the dark at 4°C until analysis.

2. Flow cytometric analysis

Flow cytometry and cell cycle profile analysis were carried out with the assistance of the UCT Flow Cytometry Core Facility (Institute of Infectious Disease and Molecular Medicine). At the time of sample acquisition, each sample was filtered using a 5 mL Falcon round bottom polystyrene test tube with cell strainer cap (Fisher Scientific) and analysed using a BD FACSCalibur™ flow cytometer (BD Biosciences).

APPENDIX H

DRP1 IMMUNO-DETECTION

The presence of DRP1 was demonstrated in A549 cells by means of immunocytochemistry and Western blotting (Figure H1A and B). Antibodies for detection included the primary anti-DRP1 antibody (1/200 dilution, Santa-Cruz Biotechnology, Dallas, Texas, US) and secondary antibodies, anti-mouse IgG FITC conjugate (Sigma-Aldrich) and anti-mouse IgG peroxidase (Sigma-Aldrich) for immunocytochemistry and Western blotting, respectively.

For immunocytochemistry A549 cells were seeded onto glass coverslips, stained with MitoTracker® Red and fixed with paraformaldehyde as described previously. After antibody probing cells were counter-stained with Hoechst 33342.

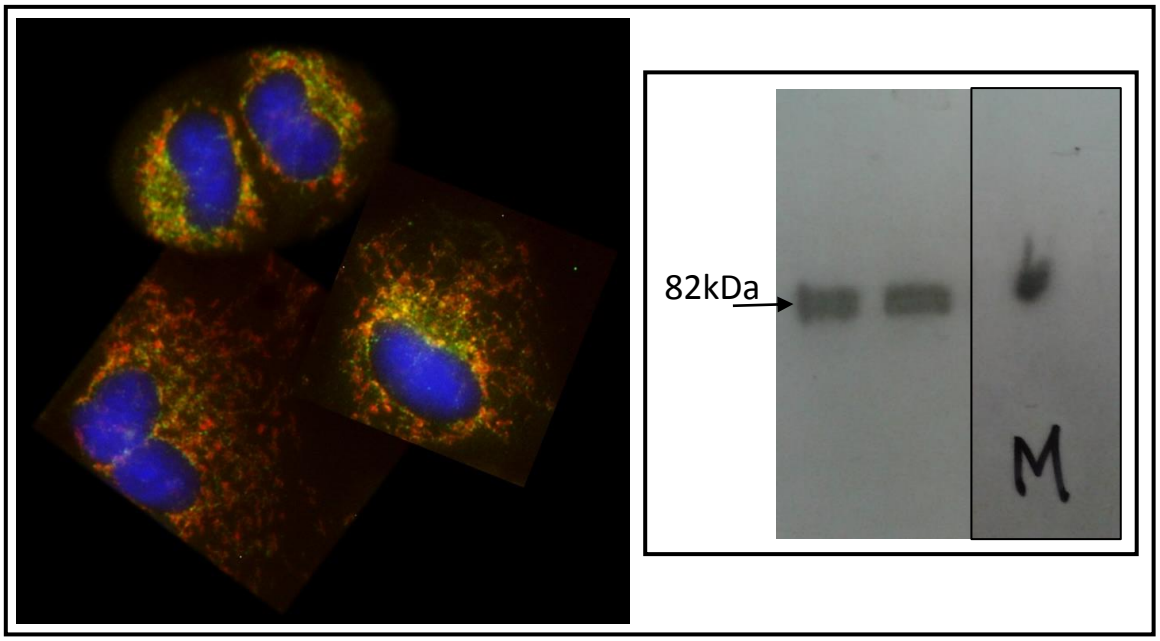

Figure H1: A) Visualisation of DRP1 (green) in A549 cells counter-stained with MitoTracker® Red (mitochondria) and Hoechst 33342 (nuclei). Yellow regions suggest areas of co-localisation of DRP1 with the mitochondrion. 1000x magnification. **B)** Western blot for the detection of DRP1 in A549 whole cell lysates.

REFERENCES

1. Srinivasan S, Guha M, Kashina A, Avadhani NG. Mitochondrial dysfunction and mitochondrial dynamics-The cancer connection. Biochim Biophys Acta. 2017;1858(8):602-14.
2. van Gisbergen MW, Voets AM, Starmans MH, de Coo IF, Yadak R, Hoffmann RF, et al. How do changes in the mtDNA and mitochondrial dysfunction influence cancer and cancer therapy? Challenges, opportunities and models. Mutat Res Rev Mutat Res. 2015;764:16-30.
3. Boland ML, Chourasia AH, Macleod KF. Mitochondrial dysfunction in cancer. Front Oncol. 2013;3:292.
4. Liang BC, Grootveld M. The importance of mitochondria in the tumourigenic phenotype: gliomas as the paradigm (review). Int J Mol Med. 2011;27(2):159-71.
5. Ralph SJ, Neuzil J. Mitochondria as targets for cancer therapy. Mol Nutr Food Res. 2009;53(1):9-28.
6. Ralph SJ, Rodriguez-Enriquez S, Neuzil J, Saavedra E, Moreno-Sanchez R. The causes of cancer revisited: "mitochondrial malignancy" and ROS-induced oncogenic transformation - why mitochondria are targets for cancer therapy. Mol Aspects Med. 2010;31(2):145-70.
7. Biasutto L, Dong LF, Zoratti M, Neuzil J. Mitochondrially targeted anti-cancer agents. Mitochondrion. 2010;10(6):670-81.
8. Neuzil J, Dong LF, Rohlena J, Truksa J, Ralph SJ. Classification of mitocans, anti-cancer drugs acting on mitochondria. Mitochondrion. 2013;13(3):199-208.
9. Oliver CL, Miranda MB, Shangary S, Land S, Wang S, Johnson DE. (-)-Gossypol acts directly on the mitochondria to overcome Bcl-2- and Bcl-X(L)-mediated apoptosis resistance. Mol Cancer Ther. 2005; 4(1):23-31.
10. Simons AL, Ahmad IM, Mattson DM, Dornfeld KJ, Spitz DR. 2-Deoxy-D-glucose combined with cisplatin enhances cytotoxicity via metabolic oxidative stress in human head and neck cancer cells. Cancer Res. 2007;67(7):3364-70.
11. Trachootham D, Zhou Y, Zhang H, Demizu Y, Chen Z, Pelicano H, et al. Selective killing of oncogenically transformed cells through a ROS-mediated mechanism by beta-phenylethyl isothiocyanate. Cancer Cell. 2006;10(3):241-52.
12. Belzacq AS, Jacotot E, Vieira HL, Mistro D, Granville DJ, Xie Z, et al. Apoptosis induction by the photosensitizer verteporfin: identification of mitochondrial adenine nucleotide translocator as a critical target. Cancer Res. 2001;61(4):1260-4.
13. Sasaki R, Suzuki Y, Yonezawa Y, Ota Y, Okamoto Y, Demizu Y, et al. DNA polymerase gamma inhibition by vitamin K3 induces mitochondria-mediated cytotoxicity in human cancer cells. Cancer Sci. 2008;99(5): 1040-8.
14. Thomas KJ, Jacobson MR. Defects in mitochondrial fission protein dynamin-related protein 1 are linked to apoptotic resistance and autophagy in a lung cancer model. PLoS One. 2012;7(9):e45319.
15. Frank S, Gaume B, Bergmann-Leitner ES, Leitner WW, Robert EG, Catez F, et al. The role of dynamin-related protein 1, a mediator of mitochondrial fission, in apoptosis. Dev Cell. 2001;1(4):515-25.
16. Fang L, Hemion C, Goldblum D, Meyer P, Orgul S, Frank S, et al. Inactivation of MARCH5 prevents mitochondrial fragmentation and interferes with cell death in a neuronal cell model. PLoS One. 2012; 7(12):e52637.
17. Karbowski M, Youle RJ. Dynamics of mitochondrial morphology in healthy cells and during apoptosis. Cell Death Differ. 2003;10(8):870-80.
18. Suen DF, Norris KL, Youle RJ. Mitochondrial dynamics and apoptosis. Genes Dev. 2008;22(12):1577-90.
19. Sugioka R, Shimizu S, Tsujimoto Y. Fzo1, a protein involved in mitochondrial fusion, inhibits apoptosis. J Biol Chem. 2004;279(50):52726-34.
20. Neuspiel M, Zunino R, Gangaraju S, Rippstein P, McBride H. Activated mitofusin 2 signals mitochondrial fusion, interferes with Bax activation, and reduces susceptibility to radical induced depolarization. J Biol Chem. 2005;280(26):25060-70.
21. Rehman J, Zhang HJ, Toth PT, Zhang Y, Marsboom G, Hong Z, et al. Inhibition of mitochondrial fission prevents cell cycle progression in lung cancer. FASEB J. 2012;26(5):2175-86.
22. Kim B, Kim JS, Yoon Y, Santiago MC, Brown MD, Park JY. Inhibition of Drp1-dependent mitochondrial division impairs myogenic differentiation. Am J Physiol Regul Integr Comp Physiol. 2013;305(8):R927-38.

23. Akita M, Suzuki-Karasaki M, Fujiwara K, Nakagawa C, Soma M, Yoshida Y, et al. Mitochondrial division inhibitor-1 induces mitochondrial hyperfusion and sensitizes human cancer cells to TRAIL-induced apoptosis. Int J Oncol. 2014;45(5):1901-12.
24. Inoue-Yamauchi A, Oda H. Depletion of mitochondrial fission factor DRP1 causes increased apoptosis in human colon cancer cells. Biochem Biophys Res Commun. 2012;421(1):81-5.
25. Qian W, Salamoun J, Wang J, Roginskaya V, Van Houten B, Wipf P. The combination of thioxodihydro-quinazolinones and platinum drugs reverses platinum resistance in tumor cells by inducing mitochondrial apoptosis independent of Bax and Bak. Bioorg Med Chem Lett. 2015;25(4):856-63.
26. Whelan RS, Konstantinidis K, Wei A-C, Chen Y, Reyna DE, Jha S, et al. Bax regulates primary necrosis through mitochondrial dynamics. Proc Natl Acad Sci. 2012;109(17):6566-71.
27. Gogvadze V, Orrenius S, Zhivotovsky B. Mitochondria in cancer cells: what is so special about them? Trends Cell Biol. 2008;18(4):165-73.
28. Quennet V, Yaromina A, Zips D, Rosner A, Walenta S, Baumann M, et al. Tumor lactate content predicts for response to fractionated irradiation of human squamous cell carcinomas in nude mice. Radiother Oncol. 2006;81(2):130-5.
29. Sattler UG, Meyer SS, Quennet V, Hoerner C, Knoerzer H, Fabian C, et al. Glycolytic metabolism and tumour response to fractionated irradiation. Radiother Oncol. 2010;94(1):102-9.
30. Meijer TW, Kaanders JH, Span PN, Bussink J. Targeting hypoxia, HIF-1, and tumor glucose metabolism to improve radiotherapy efficacy. Clin Cancer Res. 2012;18(20):5585-94.
31. Baskar R, Lee KA, Yeo R, Yeoh KW. Cancer and radiation therapy: current advances and future directions. Int J Med Sci. 2012;9(3):193-9.
32. Moding EJ, Kastan MB, Kirsch DG. Strategies for optimizing the response of cancer and normal tissues to radiation. Nat Rev Drug Discov. 2013;12(7):526-42.
33. Delaney G, Jacob S, Featherstone C, Barton M. The role of radiotherapy in cancer treatment. Cancer. 2005;104(6):1129-37.
34. Cancer Research UK. Achieving a world-class radiotherapy service across the UK [Report]. London: 2009. Available from: http://www.cancerresearchuk.org/about-us/we-develop-policy/
35. Haimovitz-Friedman A, Kan C-C, Ehleiter D, Persaud RS, McLoughlin M, Fuks Z, et al. Ionizing radiation acts on cellular membranes to generate ceramide and initiate apoptosis. J Exp Med. 1994;180(2):525-35.
36. Valerie K, Yacoub A, Hagan MP, Curiel DT, Fisher PB, Grant S, et al. Radiation-induced cell signaling: inside-out and outside-in. Mol Cancer Ther. 2007;6(3):789-801.
37. Gatenby JB, Mukerji R, Wigoder SB. The effect of x-radiation on the spermatogenesis of *Abraxas grossulariata*. Proc R Soc Lond B Biol Sci. 1929;105(739):446-69.
38. Richter C, Park J-W, Ames BN. Normal oxidative damage to mitochondrial and nuclear DNA is extensive. Proc Natl Acad Sci. 1988;85(17):6465-7.
39. May A, Bohr VA. Gene-specific repair of γ-ray-induced DNA strand breaks in colon cancer cells: no coupling to transcription and no removal from the mitochondrial genome. Biochem Biophys Res Commun. 2000;269(2):433-7.
40. Gong B, Chen Q, Almasan A. Ionizing radiation stimulates mitochondrial gene expression and activity. Radiat Res. 1998;150(5):505-12.
41. Kulkarni R, Marples B, Balasubramaniam M, Thomas RA, Tucker JD. Mitochondrial gene expression changes in normal and mitochondrial mutant cells after exposure to ionizing radiation. Radiat Res. 2010;173(5):635-44.
42. Yamamori T, Yasui H, Yamazumi M, Wada Y, Nakamura Y, Nakamura H, et al. Ionizing radiation induces mitochondrial reactive oxygen species production accompanied by upregulation of mitochondrial electron transport chain function and mitochondrial content under control of the cell cycle checkpoint. Free Radic Biol Med. 2012;53(2):260-70.
43. Zhang B, Davidson MM, Zhou H, Wang C, Walker WF, Hei TK. Cytoplasmic irradiation results in mitochondrial dysfunction and DRP1-dependent mitochondrial fission. Cancer Res. 2013;73(22):6700-10.
44. Wu J, Zhang B, Wuu Y-R, Davidson MM, Hei TK. Targeted cytoplasmic irradiation and autophagy. Mutat Res. 2017;pii: S0027-5107(16)30147-6. doi: 10.1016/j.mrfmmm.2017.02.004.
45. MacCardle RC, Congdon CC. Mitochondrial changes in hepatic cells of X-irradiated mice. Am J Pathol. 1955;31(4):725.

46. Okada S, Peachy LD. Effect of gamma irradiation on the desoxyribonuclease II activity of isolated mitochondria. J Biophys Biochem Cytol. 1957;3(2):239-48.
47. Schjeide OA, Ragan N, McCandless RG, Bishop F. Effect of X-irradiation on cellular inclusions in chicken embryo livers. Radiat Res. 1960;13(2):205-13.
48. Parsons DF. An electron microscope study of radiation damage in the mouse oocyte. J Cell Biol. 1962;14:31-48.
49. Montgomery PB, Karney D, Reynolds RC, McClendon D. Cellular and subcellular effects of ionizing radiations. Am J Pathol. 1964;44(5):727.
50. Goldfeder A, Selig JN. Radiosensitivity and biological properties of tumors: XIV. Correlation between mitochondrial structure, oxidative metabolism, and radiosensitivity. Radiat Res. 1969;37(3):499-524.
51. Liu H, Waterhouse J, Meyer J. An ultrastructural study of the effects of x irradiation on the oral epithelium of the rat: quantitative aspects. Radiat Res. 1977;69(3):459-74.
52. Bereiter-Hahn J, Voth M. Dynamics of mitochondria in living cells: shape changes, dislocations, fusion, and fission of mitochondria. Microsc Res Tech. 1994;27(3):198-219.
53. Somosy Z. Radiation response of cell organelles. Micron. 2000;31(2):165-81.
54. Malakhova L, Bezlepkin VG, Antipova V, Ushakova Ty, Fomenko L, Sirota N, et al. The increase in mitochondrial DNA copy number in the tissues of γ-irradiated mice. Cell Mol Biol Lett. 2005;10(4):721.
55. Murphy JE, Nugent S, Seymour C, Mothersill C. Mitochondrial DNA point mutations and a novel deletion induced by direct low-LET radiation and by medium from irradiated cells. Mutat Res Genet Toxicol Environ Mutagen. 2005;585(1):127-36.
56. Nugent S, Mothersill CE, Seymour C, McClean B, Lyng FM, Murphy JE. Altered mitochondrial function and genome frequency post exposure to γ-radiation and bystander factors. Int J Radiat Biol. 2010;86(10): 829-41.
57. Kobashigawa S, Suzuki K, Yamashita S. Ionizing radiation accelerates Drp1-dependent mitochondrial fission, which involves delayed mitochondrial reactive oxygen species production in normal human fibroblast-like cells. Biochem Biophys Res Commun. 2011;414(4):795-800.
58. Kobashigawa S, Kashino G, Suzuki K, Yamashita S, Mori H. Ionizing radiation-induced cell death is partly caused by increase of mitochondrial reactive oxygen species in normal human fibroblast cells. Radiat Res. 2015;183(4):455-64.
59. Bartoletti-Stella A, Mariani E, Kurelac I, Maresca A, Caratozzolo MF, Iommarini L, et al. Gamma rays induce a p53-independent mitochondrial biogenesis that is counter-regulated by HIF1alpha. Cell Death Dis. 2013;4:e663.
60. Noguchi M, Kanari Y, Yokoya A, Narita A, Fujii K. Live-cell imaging study of mitochondrial morphology in mammalian cells exposed to x-rays. Radiat Prot Dosimetry. 2015;166(1-4):101-3.
61. Barjaktarovic Z, Schmaltz D, Shyla A, Azimzadeh O, Schulz S, Haagen J, et al. Radiation-induced signaling results in mitochondrial impairment in mouse heart at 4 weeks after exposure to X-rays. PLoS One. 2011; 6(12):e27811.
62. Zanchetta LM, Garcia A, Lyng F, Walsh J, Murphy JE. Mitophagy and mitochondrial morphology in human melanoma-derived cells post exposure to simulated sunlight. Int J Radiat Biol. 2011;87(5):506-17.
63. Sridharan V, Aykin-Burns N, Tripathi P, Krager KJ, Sharma SK, Moros EG, et al. Radiation-induced alterations in mitochondria of the rat heart. Radiat Res. 2014;181(3):324-34.
64. Goldfeder A. An overview of fifty years in cancer research: autobiographical essay. Cancer Res. 1976;36(1):1-9.
65. Warren S. Effects of radiation on normal tissues. CA Cancer J Clin. 1980;30(6):350-5.
66. Zhou X, Liu X, Zhang X, Zhou R, He Y, Li Q, et al. Non-randomized mtDNA damage after ionizing radiation via charge transport. Sci Rep. 2012;2:780.
67. Wen Q, Hu Y, Ji F, Qian G. Mitochondrial DNA alterations of peripheral lymphocytes in acute lymphoblastic leukemia patients undergoing total body irradiation therapy. Radiat Oncol. 2011;6:133.
68. Schilling-Toth B, Sandor N, Kis E, Kadhim M, Safrany G, Hegyesi H. Analysis of the common deletions in the mitochondrial DNA is a sensitive biomarker detecting direct and non-targeted cellular effects of low dose ionizing radiation. Mutat Res. 2011;716(1-2):33-9.
69. Prithivirajsingh S, Story MD, Bergh SA, Geara FB, Ang KK, Ismail SM, et al. Accumulation of the common mitochondrial DNA deletion induced by ionizing radiation. FEBS Lett. 2004;571(1-3):227-32.

70. Zhou X, Li N, Wang Y, Wang Y, Zhang X, Zhang H. Effects of X-irradiation on mitochondrial DNA damage and its supercoiling formation change. Mitochondrion. 2011;11(6):886-92.
71. Hall E, Giaccia A. Radiobiology for the Radiologist. 7th ed. Philadelphia, USA: Wolters Kluwer Health, Lippincott Williams & Wilkins; 2012. p. 9, 26, 39 and 41.
72. Desouky O, Ding N, Zhou G. Targeted and non-targeted effects of ionizing radiation. J Radiat Res Appl Sci. 2015;8(2):247-54.
73. Sutherland BM, Bennett PV, Sidorkina O, Laval J. Clustered damages and total lesions induced in dna by ionizing radiation: oxidized bases and strand breaks. Biochemistry. 2000;39(27):8026-31.
74. Goodhead DT. initial events in the cellular effects of ionizing radiations: clustered damage in DNA. Int J Radiat Biol. 1994;65(1):7-17.
75. Ward JF. Radiation Mutagenesis: The initial DNA lesions responsible. Radiat Res. 1995;142(3):362-8.
76. Cerutti PA. Effects of ionizing radiation on mammalian cells. Sci Nat. 1974;61(2):51-9.
77. Frankenberg-Schwager M. Induction, repair and biological relevance of radiation-induced DNA lesions in eukaryotic cells. Radiat Environ Biophys. 1990;29(4):273-92.
78. Ward JF. DNA damage as the cause of ionizing radiation-induced gene activation. Radiat Res. 1994; 138(1s):S85-S8.
79. Ramakrishnan N, Chiu S-m, Oleinick NL. Yield of DNA-protein cross-links in γ-irradiated Chinese hamster cells. Cancer Res. 1987;47(8):2032-5.
80. Savage JRK. A brief survey of aberration origin theories. Mutat Res. 1998;404(1–2):139-47.
81. Obe G, Pfeiffer P, Savage JRK, Johannes C, Goedecke W, Jeppesen P, et al. Chromosomal aberrations: formation, identification and distribution. Mutat Res. 2002;504(1–2):17-36.
82. Kano Y, Little JB. Persistence of X-ray-induced chromosomal rearrangements in long-term cultures of human diploid fibroblasts. Cancer Res. 1984;44(9):3706-11.
83. Giglia-Mari G, Zotter A, Vermeulen W. DNA damage response. Cold Spring Harb Perspect Biol. 2011; 3(1):a000745.
84. Harper JW, Elledge SJ. The DNA damage response: ten years after. Mol Cell. 2007;28(5):739-45.
85. Ciccia A, Elledge SJ. The DNA damage response: making it safe to play with knives. Mol Cell. 2010; 40(2):179-204.
86. Kroemer G, Zamzami N, Susin SA. Mitochondrial control of apoptosis. Immunol Today. 1997;18(1):44-51.
87. Yang J, Liu X, Bhalla K, Kim CN, Ibrado AM, Cai J, et al. Prevention of apoptosis by Bcl-2: release of cytochrome c from mitochondria blocked. Science. 1997;275(5303):1129-32.
88. Westrate LM, Sayfie AD, Burgenske DM, MacKeigan JP. Persistent mitochondrial hyperfusion promotes G2/M accumulation and caspase-dependent cell death. PLoS One. 2014;9(3):e91911.
89. Xiong W, Jiao Y, Huang W, Ma M, Yu M, Cui Q, et al. Regulation of the cell cycle via mitochondrial gene expression and energy metabolism in HeLa cells. Acta Biochim Biophys Sin (Shanghai). 2012;44(4):347-58.
90. Hamanaka RB, Chandel NS. Mitochondrial reactive oxygen species regulate cellular signaling and dictate biological outcomes. Trends Biochem Sci. 2010;35(9):505-13.
91. Benard G, Bellance N, Jose C, Melser S, Nouette-Gaulain K, Rossignol R. Multi-site control and regulation of mitochondrial energy production. Biochim Biophys Acta. 2010;1797(6-7):698-709.
92. Singh KK. Mitochondria damage checkpoint in apoptosis and genome stability. FEMS Yeast Res. 2004; 5(2):127-32.
93. Richardson RB, Harper ME. Mitochondrial stress controls the radiosensitivity of the oxygen effect: Implications for radiotherapy. Oncotarget. 2016;7(16):21469-83.
94. Branzei D, Foiani M. Regulation of DNA repair throughout the cell cycle. Nat Rev Mol Cell Biol. 2008; 9(4):297-308.
95. Delacote F, Lopez BS. Importance of the cell cycle phase for the choice of the appropriate DSB repair pathway, for genome stability maintenance: the trans-S double-strand break repair model. Cell Cycle. 2008;7(1):33-8.
96. Wouters B. Cell death after irradiation: how, when and why cells die. In: Michael C. Joiner, Albert van de Kogel, editors. Basic Clinical Radiobiology. 4th ed. Great Britain: Edward Arnold; 2009. p. 33.
97. Maity A, McKenna WG, Muschel RJ. The molecular basis for cell cycle delays following ionizing radiation: a review. Radiother Oncol. 1994;31(1):1-13.

98. Di Leonardo A, Linke SP, Clarkin K, Wahl GM. DNA damage triggers a prolonged p53-dependent G1 arrest and long-term induction of Cip1 in normal human fibroblasts. Genes Dev. 1994;8(21):2540-51.
99. Linke SP, Clarkin KC, Wahl GM. p53 Mediates permanent arrest over multiple cell cycles in response to γ-irradiation. Cancer Res. 1997;57(6):1171-9.
100. Suzuki K, Mori I, Nakayama Y, Miyakoda M, Kodama S, Watanabe M. Radiation-induced senescence-like growth arrest requires TP53 function but not telomere shortening. Radiat Res. 2001;155(1):248-53.
101. Chaturvedi P, Eng WK, Zhu Y, Mattern MR, Mishra R, Hurle MR, et al. Mammalian Chk2 is a downstream effector of the ATM-dependent DNA damage checkpoint pathway. Oncogene. 1999;18(28):4047.
102. Westphal CH. Cell-cycle signaling: ATM displays its many talents. Curr Biol. 1997;7(12):R789-R92.
103. Tibbetts RS, Brumbaugh KM, Williams JM, Sarkaria JN, Cliby WA, Shieh S-Y, et al. A role for ATR in the DNA damage-induced phosphorylation of p53. Genes Dev. 1999;13(2):152-7.
104. Chehab NH, Malikzay A, Stavridi ES, Halazonetis TD. Phosphorylation of Ser-20 mediates stabilization of human p53 in response to DNA damage. Proc Natl Acad Sci. 1999;96(24):13777-82.
105. Waldman T, Kinzler KW, Vogelstein B. p21 Is necessary for the p53-mediated G1 arrest in human cancer cells. Cancer Res. 1995;55(22):5187-90.
106. El-Deiry WS, Harper JW, O'Connor PM, Velculescu VE, Canman CE, Jackman J, et al. WAF1/CIP1 is induced in p53-mediated G1 arrest and apoptosis. Cancer Res. 1994;54(5):1169-74.
107. Kastan MB, Onyekwere O, Sidransky D, Vogelstein B, Craig RW. Participation of p53 protein in the cellular response to DNA damage. Cancer Res. 1991;51(23 Part 1):6304-11.
108. Kastan MB, Zhan Q, El-Deiry WS, Carrier F, Jacks T, Walsh WV, et al. A mammalian cell cycle checkpoint pathway utilizing p53 and GADD45 is defective in ataxia-telangiectasia. Cell. 1992;71(4):587-97.
109. Kuerbitz SJ, Plunkett BS, Walsh WV, Kastan MB. Wild-type p53 is a cell-cycle checkpoint determinant following irradiation. Proc Natl Acad Sci U S A. 1992;89(16):7491-5.
110. Bunz F, Dutriaux A, Lengauer C, Waldman T, Zhou S, Brown J, et al. Requirement for p53 and p21 to sustain G2 arrest after DNA damage. Science. 1998;282(5393):1497-501.
111. Donzelli M, Draetta GF. Regulating mammalian checkpoints through Cdc25 inactivation. EMBO Rep. 2003;4(7):671-7.
112. Sorensen CS, Syljuasen RG, Falck J, Schroeder T, Ronnstrand L, Khanna KK, et al. Chk1 regulates the S-phase checkpoint by coupling the physiological turnover and ionizing radiation-induced accelerated proteolysis of Cdc25A. Cancer Cell. 2003;3(3):247-58.
113. Bartek J, Lukas J. Chk1 and Chk2 kinases in checkpoint control and cancer. Cancer Cell. 2003;3(5):421-9.
114. Mailand N, Podtelejnikov AV, Groth A, Mann M, Bartek J, Lukas J. Regulation of G2/M events by Cdc25A through phosphorylation-dependent modulation of its stability. EMBO J. 2002;21(21):5911-20.
115. Bartek J, Lukas J. Mammalian G1- and S-phase checkpoints in response to DNA damage. Curr Opin Cell Biol. 2001;13(6):738-47.
116. Willis N, Rhind N. Regulation of DNA replication by the S-phase DNA damage checkpoint. Cell Div. 2009;4(1):13.
117. Larner J, Lee H, Dijkwel P, Little R, Schildkraut C, Hamlin J. Radiation down-regulates replication origin activity throughout the S phase in mammalian cells. Nucleic Acids Res. 1999;27(3):803-9.
118. Rhind N, Russell P. Checkpoints: it takes more than time to heal some wounds. Curr Biol. 2000;10.
119. Falck J, Mailand N, Syljuasen RG, Bartek J, Lukas J. The ATM-Chk2-Cdc25A checkpoint pathway guards against radioresistant DNA synthesis. Nature. 2001;410(6830):842-7.
120. Falck J, Petrini JH, Williams BR, Lukas J, Bartek J. The DNA damage-dependent intra-S phase checkpoint is regulated by parallel pathways. Nat Genet. 2002;30(3):290-4.
121. Bartek J, Lukas C, Lukas J. Checking on DNA damage in S phase. Nat Rev Mol Cell Biol. 2004;5(10): 792-804.
122. Feijoo C, Hall-Jackson C, Wu R, Jenkins D, Leitch J, Gilbert DM, et al. Activation of mammalian Chk1 during DNA replication arrest a role for Chk1 in the intra-S phase checkpoint monitoring replication origin firing. J Cell Biol. 2001;154(5):913-24.
123. Cimprich KA, Cortez D. ATR: an essential regulator of genome integrity. Nat Rev Mol Cell Biol. 2008;9(8): 616-27.
124. Zirkle RE. Ultraviolet-microbeam irradiation of newt-cell cytoplasm: spindle destruction, false anaphase, and delay of true anaphase. Radiat Res. 1970;41(3):516-37.

125. Mikhailov A, Cole RW, Rieder CL. DNA damage during mitosis in human cells delays the metaphase/ anaphase transition via the spindle-assembly checkpoint. Curr Biol. 2002;12(21):1797-806.
126. Burgess A, Rasouli M, Rogers S. Stressing mitosis to death. Front Oncol. 2014;4:140.
127. Musacchio A, Salmon ED. The spindle-assembly checkpoint in space and time. Nat Rev Mol Cell Biol. 2007;8(5):379-93.
128. Lara-Gonzalez P, Westhorpe FG, Taylor SS. The spindle assembly checkpoint. Curr Biol. 2012;22(22): R966-R80.
129. Peters J-M. The anaphase promoting complex/cyclosome: a machine designed to destroy. Nat Rev Mol Cell Biol. 2006;7(9):644-56.
130. Herzog F, Primorac I, Dube P, Lenart P, Sander B, Mechtler K, et al. Structure of the anaphase-promoting complex/cyclosome interacting with a mitotic checkpoint complex. Science. 2009;323(5920):1477-81.
131. Chao WC, Kulkarni K, Zhang Z, Kong EH, Barford D. Structure of the mitotic checkpoint complex. Nature. 2012;484(7393):208-13.
132. Brito DA, Rieder CL. Mitotic checkpoint slippage in humans occurs via cyclin B destruction in the presence of an active checkpoint. Curr Biol. 2006;16(12):1194-200.
133. McCloy RA, Rogers S, Caldon CE, Lorca T, Castro A, Burgess A. Partial inhibition of Cdk1 in G2 phase overrides the SAC and decouples mitotic events. Cell Cycle. 2014;13(9):1400-12.
134. Alexandrou AT, Li JJ. Cell cycle regulators guide mitochondrial activity in radiation-induced adaptive response. Antioxid Redox Signal. 2014;20(9):1463-80.
135. Buchakjian MR, Kornbluth S. The engine driving the ship: metabolic steering of cell proliferation and death. Nat Rev Mol Cell Biol. 2010;11(10):715-27.
136. Vanamala J, Radhakrishnan S, Reddivari L, Bhat VB, Ptitsyn A. Resveratrol suppresses human colon cancer cell proliferation and induces apoptosis via targeting the pentose phosphate and the talin-FAK signaling pathways-A proteomic approach. Proteome Sci. 2011;9(1):49.
137. Finkel T, Hwang PM. The Krebs cycle meets the cell cycle: mitochondria and the G1-S transition. Proc Natl Acad Sci U S A. 2009;106(29):11825-6.
138. Koczor CA, Shokolenko IN, Boyd AK, Balk SP, Wilson GL, Ledoux SP. Mitochondrial DNA damage initiates a cell cycle arrest by a Chk2-associated mechanism in mammalian cells. J Biol Chem. 2009;284(52): 36191-201.
139. MacFarlane M, Robinson GL, Cain K. Glucose—a sweet way to die: Metabolic switching modulates tumor cell death. Cell Cycle. 2012;11(21):3919-25.
140. Mandal S, Guptan P, Owusu-Ansah E, Banerjee U. Mitochondrial regulation of cell cycle progression during development as revealed by the tenured mutation in Drosophila. Dev Cell. 2005;9(6):843-54.
141. Owusu-Ansah E, Yavari A, Mandal S, Banerjee U. Distinct mitochondrial retrograde signals control the G1-S cell cycle checkpoint. Nat Genet. 2008;40(3):356-61.
142. Sweet S, Singh G. Accumulation of human promyelocytic leukemia (HL-60) cells at two energetic cell cycle checkpoints. Cancer Res. 1995;55(22):5164-7.
143. Wang Z, Fan M, Candas D, Zhang T-Q, Qin L, Eldridge A, et al. Cyclin B1/Cdk1 coordinates mitochondrial respiration for cell-cycle G2/M progression. Dev Cell. 2014;29(2):217-32.
144. Mitra K, Wunder C, Roysam B, Lin G, Lippincott-Schwartz J. A hyperfused mitochondrial state achieved at G1-S regulates cyclin E buildup and entry into S phase. Proc Natl Acad Sci U S A. 2009;106(29):11960-5.
145. Sakamaki T, Casimiro MC, Ju X, Quong AA, Katiyar S, Liu M, et al. Cyclin D1 determines mitochondrial function in vivo. Mol Cell Biol. 2006;26(14):5449-69.
146. Wang C, Li Z, Lu Y, Du R, Katiyar S, Yang J, et al. Cyclin D1 repression of nuclear respiratory factor 1 integrates nuclear DNA synthesis and mitochondrial function. Proc Natl Acad Sci U S A. 2006;103(31): 11567-72.
147. Chen Z, Odstrcil EA, Tu BP, McKnight SL. Restriction of DNA replication to the reductive phase of the metabolic cycle protects genome integrity. Science. 2007;316(5833):1916-9.
148. Formentini L, Martínez-Reyes I, Cuezva JM. The mitochondrial bioenergetic capacity of carcinomas. IUBMB life. 2010;62(7).
149. Pandey BN, Gordon DM, De Toledo SM, Pain D, Azzam EI. Normal human fibroblasts exposed to high-or low-dose ionizing radiation: differential effects on mitochondrial protein import and membrane potential. Antioxid Redox Signal. 2006;8(7-8):1253-61.

150. Martinez-Diez M, Santamaria G, Ortega AD, Cuezva JM. Biogenesis and dynamics of mitochondria during the cell cycle: significance of 3'UTRs. PLoS One. 2006;1:e107.
151. Liu L, Trimarchi JR, Smith PJ, Keefe DL. Mitochondrial dysfunction leads to telomere attrition and genomic instability. Aging Cell. 2002;1(1):40-6.
152. Kim GJ, Fiskum GM, Morgan WF. A role for mitochondrial dysfunction in perpetuating radiation-induced genomic instability. Cancer Res. 2006;66(21):10377-83.
153. Dayal D, Martin SM, Owens KM, Aykin-Burns N, Zhu Y, Boominathan A, et al. Mitochondrial complex II dysfunction can contribute significantly to genomic instability after exposure to ionizing radiation. Radiat Res. 2009;172(6):737-45.
154. Yakes FM, Van Houten B. Mitochondrial DNA damage is more extensive and persists longer than nuclear DNA damage in human cells following oxidative stress. Proc Natl Acad Sci. 1997;94(2):514-9.
155. Li BY, Sun J, Wei H, Cheng YZ, Xue L, Cheng ZH, et al. Radon-induced reduced apoptosis in human bronchial epithelial cells with knockdown of mitochondria DNA. J Toxicol Environ Health A. 2012;75(18): 1111-9.
156. Cloos CR, Daniels DH, Kalen A, Matthews K, Du J, Goswami PC, et al. Mitochondrial DNA depletion induces radioresistance by suppressing G2 checkpoint activation in human pancreatic cancer cells. Radiat Res. 2009;171(5):581-7.
157. Singh KK, Russell J, Sigala B, Zhang Y, Williams J, Keshav KF. Mitochondrial DNA determines the cellular response to cancer therapeutic agents. Oncogene. 1999;18(48):6641-6.
158. Tang JT, Yamazaki H, Inoue T, Koizumi M, Yoshida K, Ozeki S, et al. Mitochondrial DNA influences radiation sensitivity and induction of apoptosis in human fibroblasts. Anticancer Res. 1999;19(6b): 4959-64.
159. Boutros R, Lobjois V, Ducommun B. CDC25 phosphatases in cancer cells: key players? Good targets? Nat Rev Cancer. 2007;7(7):495-507.
160. Hein AL, Ouellette MM, Yan Y. Radiation-induced signaling pathways that promote cancer cell survival (review). Int J Oncol. 2014;45(5):1813-9.
161. Lee J, Paull T. Activation and regulation of ATM kinase activity in response to DNA double-strand breaks. Oncogene. 2007;26(56):7741-8.
162. Shiloh Y. ATM and related protein kinases: safeguarding genome integrity. Nat Rev Cancer. 2003;3(3):155-68.
163. Zhou BB, Elledge SJ. The DNA damage response: putting checkpoints in perspective. Nature. 2000; 408 (6811):433-9.
164. Shieh S-Y, Ikeda M, Taya Y, Prives C. DNA damage-induced phosphorylation of p53 alleviates inhibition by MDM2. Cell. 1997;91(3):325-34.
165. Haupt Y, Maya R, Kazaz A, Oren M. Mdm2 promotes the rapid degradation of p53. Nature. 1997;387 (6630):296-9.
166. Schreiber V, Dantzer F, Ame J-C, De Murcia G. Poly (ADP-ribose): novel functions for an old molecule. Nat Rev Mol Cell Biol. 2006;7(7):517-28.
167. Bakkenist CJ, Kastan MB. DNA damage activates ATM through intermolecular autophosphorylation and dimer dissociation. Nature. 2003;421(6922):499.
168. Burma S, Chen BP, Murphy M, Kurimasa A, Chen DJ. ATM phosphorylates histone H2AX in response to DNA double-strand breaks. J Biol Chem. 2001;276(45):42462-7.
169. Bekker-Jensen S, Lukas C, Kitagawa R, Melander F, Kastan MB, Bartek J, et al. Spatial organization of the mammalian genome surveillance machinery in response to DNA strand breaks. J Cell Biol. 2006;173(2): 195-206.
170. Kanaar R, Hoeijmakers JH, van Gent DC. Molecular mechanisms of DNA double-strand break repair. Trends Cell Biol. 1998;8(12):483-9.
171. Saleh-Gohari N, Helleday T. Conservative homologous recombination preferentially repairs DNA double-strand breaks in the S phase of the cell cycle in human cells. Nucleic Acids Res. 2004;32(12):3683-8.
172. Walker JR, Corpina RA, Goldberg J. Structure of the Ku heterodimer bound to DNA and its implications for double-strand break repair. Nature. 2001;412(6847):607-14.
173. Mahaney BL, Meek K, Lees-Miller SP. Repair of ionizing radiation-induced DNA double-strand breaks by non-homologous end-joining. Biochem J. 2009;417(3):639-50.

174. Meek K, Dang V, Lees-Miller SP. DNA-PK: the means to justify the ends? Adv Immunol. 2008;99:33-58.
175. Wang M, Wu W, Wu W, Rosidi B, Zhang L, Wang H, et al. PARP-1 and Ku compete for repair of DNA double strand breaks by distinct NHEJ pathways. Nucleic Acids Res. 2006;34(21):6170-82.
176. Haince J-F, McDonald D, Rodrigue A, Déry U, Masson J-Y, Hendzel MJ, et al. PARP1-dependent kinetics of recruitment of MRE11 and NBS1 proteins to multiple DNA damage sites. J Biol Chem. 2008;283(2): 1197-208.
177. Zhu Z, Chung W-H, Shim EY, Lee SE, Ira G. Sgs1 helicase and two nucleases Dna2 and Exo1 resect DNA double-strand break ends. Cell. 2008;134(6):981-94.
178. Huen MS, Sy SM, Chen J. BRCA1 and its toolbox for the maintenance of genome integrity. Nat Rev Mol Cell Biol. 2010;11(2):138-48.
179. Li X, Heyer W-D. Homologous recombination in DNA repair and DNA damage tolerance. Cell Res. 2008;18(1):99-113.
180. Kelley MR, Logsdon D, Fishel ML. Targeting DNA repair pathways for cancer treatment: what's new? Future Oncol (London, England). 2014;10(7):1215-37.
181. Dietlein F, Thelen L, Reinhardt HC. Cancer-specific defects in DNA repair pathways as targets for personalized therapeutic approaches. Trends Genet. 2014;30(8):326-39.
182. Furda AM, Marrangoni AM, Lokshin A, Van Houten B. Oxidants and not alkylating agents induce rapid mtDNA loss and mitochondrial dysfunction. DNA repair. 2012;11(8):684-92.
183. Kazak L, Reyes A, Holt IJ. Minimizing the damage: repair pathways keep mitochondrial DNA intact. Nat Rev Mol Cell Biol. 2012;13(10):659-71.
184. Szczesny B, Tann AW, Longley MJ, Copeland WC, Mitra S. Long patch base excision repair in mammalian mitochondrial genomes. J Biol Chem. 2008;283(39):26349-56.
185. de Souza-Pinto NC, Mason PA, Hashiguchi K, Weissman L, Tian J, Guay D, et al. Novel DNA mismatch-repair activity involving YB-1 in human mitochondria. DNA repair. 2009;8(6):704-19.
186. Chen XJ. Mechanism of homologous recombination and implications for aging-related deletions in mitochondrial DNA. Microbiol Mol Biol Rev. 2013;77(3):476-96.
187. Achanta G, Sasaki R, Feng L, Carew JS, Lu W, Pelicano H, et al. Novel role of p53 in maintaining mitochondrial genetic stability through interaction with DNA Pol γ. EMBO J. 2005;24(19):3482-92.
188. Mummenbrauer T, Janus F, Müller B, Wiesmüller L, Deppert W, Grosse F. p53 protein exhibits 3′-to-5′ exonuclease activity. Cell. 1996;85(7):1089-99.
189. Bacman SR, Williams SL, Moraes CT. Intra-and inter-molecular recombination of mitochondrial DNA after in vivo induction of multiple double-strand breaks. Nucleic Acids Res. 2009;37(13):4218-26.
190. Gilkerson RW, Schon EA, Hernandez E, Davidson MM. Mitochondrial nucleoids maintain genetic autonomy but allow for functional complementation. J Cell Biol. 2008;181(7):1117-28.
191. Qin L, Fan M, Candas D, Jiang G, Papadopoulos S, Tian L, et al. CDK1 enhances mitochondrial bioenergetics for radiation-induced dna repair. Cell Rep. 2015;13(10):2056-63.
192. Yazlovitskaya EM, Uzhachenko R, Voziyan PA, Yarbrough WG, Ivanova AV. A novel radioprotective function for the mitochondrial tumor suppressor protein Fus1. Cell Death Dis. 2013;4:e687.
193. Nahas SA, Davies R, Fike F, Nakamura K, Du L, Kayali R, et al. Comprehensive profiling of radiosensitive human cell lines with DNA damage response assays identifies the neutral comet assay as a potential surrogate for clonogenic survival. Radiat Res. 2012;177(2):176-86.
194. Arbini AA, Guerra F, Greco M, Marra E, Gandee L, Xiao G, et al. Mitochondrial DNA depletion sensitizes cancer cells to PARP inhibitors by translational and post-translational repression of BRCA2. Oncogenesis. 2013;2:e82.
195. Ambrose M, Goldstine JV, Gatti RA. Intrinsic mitochondrial dysfunction in ATM-deficient lymphoblastoid cells. Hum Mol Genet. 2007;16(18):2154-64.
196. Kulkarni R, Thomas RA, Tucker JD. Expression of DNA repair and apoptosis genes in mitochondrial mutant and normal cells following exposure to ionizing radiation. Environ Mol Mutagen. 2011;52(3):229-37.
197. Das A, McDonald DG, Dixon-Mah YN, Jacqmin DJ, Samant VN, Vandergrift III WA, et al. RIP1 and RIP3 complex regulates radiation-induced programmed necrosis in glioblastoma. Tumor Biol. 2015:1-10.
198. Robert T, Vanoli F, Chiolo I, Shubassi G, Bernstein KA, Rothstein R, et al. HDACs link the DNA damage response, processing of double-strand breaks and autophagy. Nature. 2011;471(7336):74-9.

199. Roos WP, Kaina B. DNA damage-induced cell death: from specific DNA lesions to the DNA damage response and apoptosis. Cancer lett. 2013;332(2):237-48.
200. Meyn RE, Milas L, Ang KK. The role of apoptosis in radiation oncology. Int J Radiat Biol. 2009;85(2): 107-15.
201. Meyn RE. Apoptosis and response to radiation: implications for radiation therapy. Oncology (Williston Park, NY). 1997;11(3):349-56,61,65.
202. Dewey WC, Ling CC, Meyn RE. Radiation-induced apoptosis: relevance to radiotherapy. Int J Radiat Oncol Biol Phys. 1995;33(4):781-96.
203. Marekova M, Vavrova J, Vokurkova D. Monitoring of premitotic and postmitotic apoptosis in gamma-irradiated HL-60 cells by the mitochondrial membrane protein-specific monoclonal antibody APO2.7. Gen Physiol Biophys. 2003;22(2):191-200.
204. Shinomiya N, Kuno Y, Yamamoto F, Fukasawa M, Okumura A, Uefuji M, et al. Different mechanisms between premitotic apoptosis and postmitotic apoptosis in X-irradiated U937 cells. Int J Radiat Oncol Biol Phys. 2000;47(3):767-77.
205. Shinomiya N. New concepts in radiation-induced apoptosis: 'premitotic apoptosis' and 'postmitotic apoptosis'. J Cell Mol Med. 2001;5(3):240-53.
206. Algan Ö, Stobbe CC, Helt AM, Hanks GE, Chapman JD. Radiation inactivation of human prostate cancer cells: the role of apoptosis. Radiat Res. 1996;146(3):267-75.
207. Danial NN. BCL-2 family proteins: critical checkpoints of apoptotic cell death. Clin Cancer Res. 2007; 13(24):7254-63.
208. Jürgensmeier JM, Xie Z, Deveraux Q, Ellerby L, Bredesen D, Reed JC. Bax directly induces release of cytochrome c from isolated mitochondria. Proc Natl Acad Sci. 1998;95(9):4997-5002.
209. Saelens X, Festjens N, Walle LV, Van Gurp M, van Loo G, Vandenabeele P. Toxic proteins released from mitochondria in cell death. Oncogene. 2004;23(16):2861-74.
210. Hengartner MO. The biochemistry of apoptosis. Nature. 2000;407(6805):770-6.
211. Zou H, McGarry TJ, Bernal T, Kirschner MW. Identification of a vertebrate sister-chromatid separation inhibitor involved in transformation and tumorigenesis. Science (New York, NY). 1999;285.
212. Aslan JE, Thomas G. Death by committee: organellar trafficking and communication in apoptosis. Traffic. 2009;10(10):1390-404.
213. Lorenzo HK, Susin SA, Penninger J, Kroemer G. Apoptosis inducing factor (AIF): a phylogenetically old, caspase-independent effector of cell death. Cell Death Differ. 1999;6(6):516-24.
214. Park SY, Chang I, Kim J-Y, Kang SW, Park S-H, Singh K, et al. Resistance of mitochondrial DNA-depleted cells against cell death role of mitochondrial superoxide dismutase. J Biol Chem. 2004;279(9):7512-20.
215. Sheridan C, Delivani P, Cullen SP, Martin SJ. Bax-or Bak-induced mitochondrial fission can be uncoupled from cytochrome C release. Mol Cell. 2008;31(4):570-85.
216. Arnoult D. Mitochondrial fragmentation in apoptosis. Trends Cell Biol. 2007;17(1):6-12.
217. Estaquier J, Arnoult D. Inhibiting Drp1-mediated mitochondrial fission selectively prevents the release of cytochrome c during apoptosis. Cell Death Differ. 2007;14(6):1086-94.
218. Karbowski M, Lee YJ, Gaume B, Jeong SY, Frank S, Nechushtan A, et al. Spatial and temporal association of Bax with mitochondrial fission sites, Drp1, and Mfn2 during apoptosis. J Cell Biol. 2002;159(6):931-8.
219. Parone PA, James DI, Da Cruz S, Mattenberger Y, Donze O, Barja F, et al. Inhibiting the mitochondrial fission machinery does not prevent Bax/Bak-dependent apoptosis. Mol Cell Biol. 2006;26(20):7397-408.
220. Frezza C, Cipolat S, de Brito OM, Micaroni M, Beznoussenko GV, Rudka T, et al. OPA1 controls apoptotic cristae remodeling independently from mitochondrial fusion. Cell. 2006;126(1):177-89.
221. Wang P, Wang P, Liu B, Zhao J, Pang Q, Agrawal SG, et al. Dynamin-related protein Drp1 is required for Bax translocation to mitochondria in response to irradiation-induced apoptosis. Oncotarget. 2015;6(26): 22598-612.
222. Ryu SW, Choi K, Park JH, Park YM, Kim S, Choi C. Mitofusin 1 inhibits an apoptosis-associated amino-terminal conformational change in Bax, but not its mitochondrial translocation, in a GTPase-dependent manner. Cancer Lett. 2012;323(1):62-8.
223. Olichon A, Baricault L, Gas N, Guillou E, Valette A, Belenguer P, et al. Loss of OPA1 perturbates the mitochondrial inner membrane structure and integrity, leading to cytochrome c release and apoptosis. J Biol Chem. 2003;278(10):7743-6.

224. Arnoult D, Grodet A, Lee YJ, Estaquier J, Blackstone C. Release of OPA1 during apoptosis participates in the rapid and complete release of cytochrome c and subsequent mitochondrial fragmentation. J Biol Chem. 2005;280(42):35742-50.
225. Hanahan D, Weinberg RA. Hallmarks of cancer: the next generation. Cell. 2011;144(5):646-74.
226. Szumiel I. Intrinsic radiation sensitivity: cellular signaling is the key. Radiat Res. 2008;169(3):249-58.
227. West CM, Davidson SE, Elyan SA, Swindell R, Roberts SA, Orton CJ, et al. The intrinsic radiosensitivity of normal and tumour cells. Int J Radiat Biol. 1998;73(4):409-13.
228. Biade S, Stobbe C, Chapman J. The intrinsic radiosensitivity of some human tumor cells throughout their cell cycles. Radiat Res. 1997;147(4):416-21.
229. Seong KM, Kim CS, Jeon HY, Oh S-H, Nam SY, Yang KH, et al. Intrinsic radiosensitivity correlated with radiation-induced ROS and cell cycle regulation. Mol Cell Toxicol. 2010;6(1):1-7.
230. Ruiz de Almodovar JM, Nunez MI, McMillan TJ, Olea N, Mort C, Villalobos M, et al. Initial radiation-induced DNA damage in human tumour cell lines: a correlation with intrinsic cellular radiosensitivity. Br J Cancer. 1994;69(3):457-62.
231. El-Awady RA, Dikomey E, Dahm-Daphi J. Radiosensitivity of human tumour cells is correlated with the induction but not with the repair of DNA double-strand breaks. Br J Cancer. 2003;89(3):593-601.
232. Loeffler JS, Harris JR, Dahlberg WK, Little JB. In vitro radiosensitivity of human diploid fibroblasts derived from women with unusually sensitive clinical responses to definitive radiation therapy for breast cancer. Radiat Res. 1990;121(2):227-31.
233. Weichselbaum RR, Dahlberg W, Little JB. Inherently radioresistant cells exist in some human tumors. Proc Natl Acad Sci U S A. 1985;82(14):4732-5
234. Malaise EP, Fertil B, Deschavanne PJ, Chavaudra N, Brock WA. Initial slope of radiation survival curves is characteristic of the origin of primary and established cultures of human tumor cells and fibroblasts. Radiat Res. 1987;111(2):319-33.
235. Puck TT, Marcus PI. Action of X-rays on mammalian cells. J Exp Med. 1956;103(5):653-66.
236. Jeggo P, Lavin MF. Cellular radiosensitivity: how much better do we understand it? Int J Radiat Biol. 2009;85(12):1061-81.
237. Chadwick KH, Leenhouts HP. A molecular theory of cell survival. Phys Med Biol. 1973;18(1):78.
238. Chadwick K, Leenhouts H. The molecular model for cell survival following radiation. The molecular theory of radiation biology. Berlin: Springer-verlag; 1981. p. 25-50.
239. Kellerer AM, Rossi HH. A generalized formulation of dual radiation action. Radiat Res. 1978;75(3):471-88.
240. Fertil B, Dertinger H, Courdi A, Malaise EP. Mean inactivation dose: a useful concept for intercomparison of human cell survival curves. Radiat Res. 1984;99(1):73-84.
241. Malaise EP, Fertil B. The mean inactivation dose: Experimental versus theoretical. Radiat Res. 1986;108 (2):222-5.
242. Vijayakumar S, Ng T, Raudkivi U, Meaney T. Mean Inactivation Dose (D). A critical analysis of a neglected parameter in radiotherapy. Acta Oncol. 1990;29(1):65-72.
243. Belli M, Simula S. The calculation of the mean inactivation dose by approximated methods. Radiat Res. 1991;128(1):112-4.
244. Fenech M, Morley AA. Measurement of micronuclei in lymphocytes. Mutat Res. 1985;147(1):29-36.
245. Fenech M. Cytokinesis-block micronucleus cytome assay. Nat Protoc. 2007;2(5):1084-104.
246. Schmid W. Chemical mutagen testing on in vivo somatic mammalian cells. Agents Actions. 1973;3(2): 77-85.
247. Fenech M, Kirsch-Volders M, Natarajan AT, Surralles J, Crott JW, Parry J, et al. Molecular mechanisms of micronucleus, nucleoplasmic bridge and nuclear bud formation in mammalian and human cells. Mutagenesis. 2011;26(1):125-32.
248. Bhattathiri VN, Bindu L, Remani P, Chandralekha B, Davis CA, Nair MK. Serial cytological assay of micronucleus induction: a new tool to predict human cancer radiosensitivity. Radiother Oncol. 1996;41(2):139-42.
249. Guzman P, Sotelo-Regil RC, Mohar A, Gonsebatt ME. Positive correlation between the frequency of micronucleated cells and dysplasia in Papanicolaou smears. Environ Mol Mutagen. 2003;41(5):339-43.
250. Yadav AS, Sharma MK. Increased frequency of micronucleated exfoliated cells among humans exposed in vivo to mobile telephone radiations. Mutat Res Genet Toxicol Environ Mutagen. 2008;650(2):175-80.

251. Carbonari K, Gonçalves L, Roth D, Moreira P, Fernández R, Martino-Roth MdG. Increased micronucleated cell frequency related to exposure to radiation emitted by computer cathode ray tube video display monitors. Genet Mol Biol. 2005;28(3):469-74.
252. Okada T, Kashino G, Nishiura H, Tano K, Watanabe M. Micronuclei formation induced by X-ray irradiation does not always result from DNA double-strand breaks. J Radiat Res. 2012;53(1):93-100.
253. Organisation for Economic Co-operation and Development. OECD guidelines: *in vitro* mammalian cell micronucleus test. Paris: OECD Publishing; 2016. Available from: http://dx.doi.org/10.1787/9789264264861-en.
254. Shibamoto Y, Streffer C, Fuhrmann C, Budach V. Tumor radiosensitivity prediction by the cytokinesis-block micronucleus assay. Radiat Res. 1991;128(3):293-300.
255. Mariya Y, Streffer C, Fuhrmann C, Wojcik A. Correlation of radiation-induced micronucleus frequency with clonogenic survival in cells of one diploid and two tetraploid murine tumor cell lines of the same origin. Radiat Res. 1997;147(1):29-34.
256. Kerr JF, Wyllie AH, Currie AR. Apoptosis: a basic biological phenomenon with wideranging implications in tissue kinetics. Br J Cancer. 1972;26(4):239-57.
257. Hanahan D, Weinberg RA. The hallmarks of cancer. Cell. 2000;100(1):57-70.
258. Liu JR, Opipari AW, Tan L, Jiang Y, Zhang Y, Tang H, et al. Dysfunctional apoptosome activation in ovarian cancer implications for chemoresistance. Cancer Res. 2002;62(3):924-31.
259. Soengas MS, Capodieci P, Polsky D, Mora J, Esteller M, Opitz-Araya X, et al. Inactivation of the apoptosis effector Apaf-1 in malignant melanoma. Nature. 2001;409(6817):207-11.
260. Allen RT, Hunter WJ, Agrawal DK. Morphological and biochemical characterization and analysis of apoptosis. J Pharmacol Toxicol Methods. 1997;37(4):215-28.
261. Saraste A, Pulkki K. Morphologic and biochemical hallmarks of apoptosis. Cardiovasc Res. 2000;45(3): 528-37.
262. Belloc F, Dumain P, Boisseau MR, Jalloustre C, Reiffers J, Bernard P, et al. A flow cytometric method using Hoechst 33342 and propidium iodide for simultaneous cell cycle analysis and apoptosis determination in unfixed cells. Cytometry. 1994;17(1):59-65.
263. Vermes I, Haanen C, Steffens-Nakken H, Reutellingsperger C. A novel assay for apoptosis flow cytometric detection of phosphatidylserine expression on early apoptotic cells using fluorescein labelled annexin V. J Immunol Methods. 1995;184(1):39-51.
264. Zhang G, Gurtu V, Kain SR, Yan G. Early detection of apoptosis using a fluorescent conjugate of annexin V. Biotechniques. 1997;23(3):525-31.
265. Darzynkiewicz Z, Bruno S, Del Bino G, Gorczyca W, Hotz M, Lassota P, et al. Features of apoptotic cells measured by flow cytometry. Cytometry. 1992;13(8):795-808.
266. Bertho ÁL, Santiago MA, Coutinho SG. Flow cytometry in the study of cell death. Mem Inst Oswaldo Cruz. 2000;95(3):429-33.
267. Fairbairn DW, Walburger DK, Fairbairn JJ, O'Neill KL. Key morphologic changes and DNA strand breaks in human lymphoid cells: discriminating apoptosis from necrosis. Scanning. 1996;18(6):407-16.
268. Gavrieli Y, Sherman Y, Ben-Sasson SA. Identification of programmed cell death in situ via specific labeling of nuclear DNA fragmentation. J Cell Biol. 1992;119(3):493-501.
269. Negoescu A, Lorimier P, Labat-Moleur F, Drouet C, Robert C, Guillermet C, et al. In situ apoptotic cell labeling by the TUNEL method: improvement and evaluation on cell preparations. J Histochem Cytochem. 1996;44(9):959-68.
270. Huerta S, Goulet EJ, Huerta-Yepez S, Livingston EH. Screening and Detection of Apoptosis. J Surg Res. 2007;139(1):143-56.
271. Green DR, Reed JC. Mitochondria and apoptosis. Science. 1998;281(5381):1309.
272. Endlich B, Radford IR, Forrester HB, Dewey WC. Computerized video time-lapse microscopy studies of ionizing radiation-induced rapid-interphase and mitosis-related apoptosis in lymphoid cells. Radiat Res. 2000;153(1):36-48.
273. Claude A. Fractionation of mammalian liver cells by differential centrifugation II. Experimental procedures and results. J Exp Med. 1946;84(1):61-89.
274. Ernster L, Schatz G. Mitochondria: a historical review. J Cell Biol. 1981;91(3):227s-55s.
275. Siekevitz P. Powerhouse of the cell. Sci Am. 1957;197:131-44.

276. Warburg O. The prime cause and prevention of cancer. Lindau, Germany: Dean Burk; 1966.
277. Warburg O. On the origin of cancer cells. Science. 1956;123(3191):309-14.
278. Warburg O, Wind F, Negelein E. The metabolism of tumors in the body. J Gen Physiol. 1927;8(6):519.
279. Crabtree HG. Observations on the carbohydrate metabolism of tumours. Biochem J. 1929;23(3):536.
280. Som P, Atkins HL, Bandoypadhyay D, Fowler JS, MacGregor RR, Matsui K, et al. A fluorinated glucose analog, 2-fluoro-2-deoxy-D-glucose (F-18): nontoxic tracer for rapid tumor detection. J Nucl Med. 1980;21(7):670-5
281. Kelloff GJ, Hoffman JM, Johnson B, Scher HI, Siegel BA, Cheng EY, et al. Progress and promise of FDG-PET imaging for cancer patient management and oncologic drug development. Clin Cancer Res. 2005;11(8): 2785-808.
282. Kroemer G, Pouyssegur J. Tumor cell metabolism: cancer's Achilles' heel. Cancer Cell. 2008;13(6):472-82.
283. Ward PS, Thompson CB. Metabolic reprogramming: a cancer hallmark even warburg did not anticipate. Cancer Cell. 2012;21(3):297-308.
284. Tong X, Zhao F, Thompson CB. The molecular determinants of de novo nucleotide biosynthesis in cancer cells. Curr Opin Genet Dev. 2009;19(1):32-7.
285. DeBerardinis RJ, Lum JJ, Hatzivassiliou G, Thompson CB. The biology of cancer: metabolic reprogramming fuels cell growth and proliferation. Cell Metab. 2008;7(1):11-20.
286. Lunt SY, Vander Heiden MG. Aerobic glycolysis: meeting the metabolic requirements of cell proliferation. Annu Rev Cell Dev Biol. 2011;27:441-64.
287. Berg JM, Tymoczko JL, Stryer L. Biochemistry, 6th Ed. New York: W.H. Freeman; 2006.
288. DeBerardinis RJ, Cheng T. Q's next: the diverse functions of glutamine in metabolism, cell biology and cancer. Oncogene. 2010;29(3):313-24.
289. Berg JM TJ, Tymoczko JL, Stryer L.ymoczko JL, Stryer L. The glycolytic pathway is tightly controlled. 2002. In: Biochemistry, 5th ed [Internet]. New York: WH Freeman.
Available from: https://www.ncbi.nlm.nih.gov/ books/NBK22395.
290. Gatenby RA, Gillies RJ. Why do cancers have high aerobic glycolysis? Nat Rev Cancer. 2004;4(11):891-9.
291. Zheng J. Energy metabolism of cancer: Glycolysis versus oxidative phosphorylation (Review). Oncol Lett. 2012;4(6):1151-7.
292. Radde BN, Ivanova MM, Mai HX, Salabei JK, Hill BG, Klinge CM. Bioenergetic differences between MCF-7 and T47D breast cancer cells and their regulation by oestradiol and tamoxifen. Biochem J. 2015;465(1): 49-61.
293. Viale A, Corti D, Draetta GF. Tumors and mitochondrial respiration: a neglected connection. Cancer Res. 2015;75(18):3687-91.
294. Rich P. The molecular machinery of Keilin's respiratory chain. Biochem Soc Trans. 2003;31(6):1095-105.
295. Wallace DC. Mitochondria and cancer. Nat Rev Cancer. 2012;12(10):685-98.
296. Mailloux RJ, Harper M-E. Uncoupling proteins and the control of mitochondrial reactive oxygen species production. Free Radic Biol Med. 2011;51(6):1106-15.
297. Brookes PS. Mitochondrial H(+) leak and ROS generation: an odd couple. Free Radic Biol Med. 2005; 38(1):12-23.
298. Echtay KS, Roussel D, St-Pierre J, Jekabsons MB, Cadenas S, Stuart JA, et al. Superoxide activates mitochondrial uncoupling proteins. Nature. 2002;415(6867):96-9.
299. Hileman EO, Liu J, Albitar M, Keating MJ, Huang P. Intrinsic oxidative stress in cancer cells: a biochemical basis for therapeutic selectivity. Cancer Chemother Pharmacol. 2004;53(3):209-19.
300. Guo G, Yan-Sanders Y, Lyn-Cook BD, Wang T, Tamae D, Ogi J, et al. Manganese superoxide dismutase-mediated gene expression in radiation-induced adaptive responses. Mol Cell Biol. 2003;23(7):2362-78.
301. Epperly MW, Gretton JE, Sikora CA, Jefferson M, Bernarding M, Nie S, et al. Mitochondrial localization of superoxide dismutase is required for decreasing radiation-induced cellular damage. Radiat Res. 2003; 160(5):568-78.
302. Sun J, Chen Y, Li M, Ge Z. Role of Antioxidant Enzymes on Ionizing Radiation Resistance. Free Radic Biol Med. 1998;24(4):586-93.
303. Hosoki A, Yonekura S-I, Zhao Q-L, Wei Z-L, Takasaki I, Tabuchi Y, et al. Mitochondria-targeted superoxide dismutase (SOD2) regulates radiation resistance and radiation stress response in hela cells. J Radiat Res. 2012;53(1):58-71.

304. Greenberger JS, Berhane H, Shinde A, Rhieu BH, Bernard M, Wipf P, et al. Can radiosensitivity associated with defects in dna repair be overcome by mitochondrial-targeted antioxidant radioprotectors. Front Oncol. 2014;4:24.
305. Cai X, Hao J, Zhang X, Yu B, Ren J, Luo C, et al. The polyhydroxylated fullerene derivative C60(OH)24 protects mice from ionizing-radiation-induced immune and mitochondrial dysfunction. Toxicol Appl Pharmacol. 2010;243(1):27-34.
306. Derdak Z, Mark NM, Beldi G, Robson SC, Wands JR, Baffy G. The mitochondrial uncoupling protein-2 promotes chemoresistance in cancer cells. Cancer Res. 2008;68(8):2813-9.
307. Kuninaka S, Ichinose Y, Koja K, Toh Y. Suppression of manganese superoxide dismutase augments sensitivity to radiation, hyperthermia and doxorubicin in colon cancer cell lines by inducing apoptosis. Br J Cancer. 2000;83(7):928-34.
308. Ide T, Tsutsui H, Hayashidani S, Kang D, Suematsu N, Nakamura K-i, et al. Mitochondrial DNA damage and dysfunction associated with oxidative stress in failing hearts after myocardial infarction. Circ Res. 2001;88(5):529-35.
309. Sasaki MS, Ejima Y, Tachibana A, Yamada T, Ishizaki K, Shimizu T, et al. DNA damage response pathway in radioadaptive response. Mutat Res. 2002;504(1):101-18.
310. Diehn M, Cho RW, Lobo NA, Kalisky T, Dorie MJ, Kulp AN, et al. Association of reactive oxygen species levels and radioresistance in cancer stem cells. Nature. 2009;458(7239):780-3.
311. Sullivan LB, Chandel NS. Mitochondrial reactive oxygen species and cancer. Cancer Metab. 2014;2(1):17.
312. Shchepina LA, Pletjushkina OY, Avetisyan AV, Bakeeva LE, Fetisova EK, Izyumov DS, et al. Oligomycin, inhibitor of the F 0 part of H+-ATP-synthase, suppresses the TNF-induced apoptosis. Oncogene. 2002; 21(53):8149-57.
313. Alberts B BD, Lewis J, Raff M, Roberts K and Watson J. The Mitochondrion. In: Molecular biology of the cell [Internet]. New York, London: Garland Publishing, Inc. 2002. Available from: https://www.ncbi.nlm.nih.gov/books/NBK26894/
314. Nicholls DG, Budd SL. Mitochondria and neuronal survival. Physiol Rev. 2000;80(1):315-60.
315. Kim J-w, Tchernyshyov I, Semenza GL, Dang CV. HIF-1-mediated expression of pyruvate dehydrogenase kinase: a metabolic switch required for cellular adaptation to hypoxia. Cell Metab. 2006;3(3):177-85.
316. Semenza GL. HIF-1 mediates the Warburg effect in clear cell renal carcinoma. J Bioenerg Biomembr. 2007;39(3):231-4.
317. Desler C, Hansen TL, Frederiksen JB, Marcker ML, Singh KK, Juel Rasmussen L. Is there a link between mitochondrial reserve respiratory capacity and aging? J Aging Res. 2012;2012:192503.
318. Hill B, Dranka B, Zou L, Chatham J, Darley-Usmar V. Importance of the bioenergetic reserve capacity in response to cardiomyocyte stress induced by 4-hydroxynonenal. Biochem J. 2009;424:99-107.
319. Gong G, Liu J, Liang P, Guo T, Hu Q, Ochiai K, et al. Oxidative capacity in failing hearts. Am J Physiol Heart Circ Physiol. 2003;285(2):H541-H8.
320. Yadava N, Nicholls DG. Spare respiratory capacity rather than oxidative stress regulates glutamate excitotoxicity after partial respiratory inhibition of mitochondrial complex I with rotenone. J Neurosci. 2007;27(27):7310-7.
321. Choi SW, Gerencser AA, Nicholls DG. Bioenergetic analysis of isolated cerebrocortical nerve terminals on a microgram scale: spare respiratory capacity and stochastic mitochondrial failure. J Neurochem. 2009; 109(4):1179-91.
322. Dranka BP, Hill BG, Darley-Usmar VM. Mitochondrial reserve capacity in endothelial cells: The impact of nitric oxide and reactive oxygen species. Free Radic Biol Med. 2010;48(7):905-14.
323. van der Windt GJ, Everts B, Chang C-H, Curtis JD, Freitas TC, Amiel E, et al. Mitochondrial respiratory capacity is a critical regulator of CD8+ T cell memory development. Immunity. 2012;36(1):68-78.
324. Brandon M, Baldi P, Wallace DC. Mitochondrial mutations in cancer. Oncogene. 2006;25(34):4647-62.
325. Yu M. Generation, function and diagnostic value of mitochondrial DNA copy number alterations in human cancers. Life Sci. 2011;89(3):65-71.
326. Jerby L, Wolf L, Denkert C, Stein GY, Hilvo M, Oresic M, et al. Metabolic associations of reduced proliferation and oxidative stress in advanced breast cancer. Cancer Res. 2012;72(22):5712-20.

327. Pesta D, Gnaiger E. High-resolution respirometry: OXPHOS protocols for human cells and permeabilized fibers from small biopsies of human muscle. In: Palmeira CM, Moreno, editors. Mitochondrial bioenergetics: methods and protocols, methods in molecular biology. Vol 810. New York: Springer Science and Business Media; 2012. p. 27, 28, 31 and 34.
328. Severinghaus JW, Astrup PB. History of blood gas analysis. IV. Leland Clark's oxygen electrode. J Clin Monit. 1986;2(2):125-39.
329. Zhang J, Nuebel E, Wisidagama DR, Setoguchi K, Hong JS, Van Horn CM, et al. Measuring energy metabolism in cultured cells, including human pluripotent stem cells and differentiated cells. Nat Protoc. 2012;7(6):1068-85.
330. Chance B, Williams G. Respiratory enzymes in oxidative phosphorylation III. The steady state. J Biol Chem. 1955;217(1):409-28.
331. Korzeniewski B. 'Idealized' State 4 and state 3 in mitochondria vs. rest and work in skeletal muscle. PLoS One. 2015;10(2):e0117145.
332. Brand MD, Nicholls DG. Assessing mitochondrial dysfunction in cells. Biochem J. 2011;435(2):297-312.
333. Maldonado EN, Patnaik J, Mullins MR, Lemasters JJ. Free tubulin modulates mitochondrial membrane potential in cancer cells. Cancer Res. 2010;70(24):10192-201
334. Modica-Napolitano JS, Aprille JR. Delocalized lipophilic cations selectively target the mitochondria of carcinoma cells. Adv Drug Deliv Rev. 2001;49(1):63-70.
335. Davis S, Weiss M, Wong J, Lampidis TJ, Chen LB. Mitochondrial and plasma membrane potentials cause unusual accumulation and retention of rhodamine 123 by human breast adenocarcinoma-derived MCF-7 cells. J Biol Chem. 1985;260(25):13844-50.
336. Nadakavukaren KK, Nadakavukaren JJ, Chen LB. Increased rhodamine 123 uptake by carcinoma cells. Cancer Res. 1985;45(12 Part 1):6093-9.
337. Sánchez-Cenizo L, Formentini L, Aldea M, Ortega AD, García-Huerta P, Sánchez-Aragó M, et al. Up-regulation of the ATPase inhibitory factor 1 (IF1) of the mitochondrial H+-ATP synthase in human tumors mediates the metabolic shift of cancer cells to a Warburg phenotype. J Biol Chem. 2010;285 (33):25308-13.
338. Sánchez-Aragó M, Formentini L, Cuezva JM. Mitochondria-mediated energy adaption in cancer: The H+-ATP synthase-geared switch of metabolism in human tumors. Antioxid Redox Signal. 2013;19(3):285-98.
339. Heerdt BG, Houston MA, Augenlicht LH. The intrinsic mitochondrial membrane potential of colonic carcinoma cells is linked to the probability of tumor progression. Cancer Res. 2005;65(21):9861-7.
340. Moreno-Sanchez R, Rodriguez-Enriquez S, Marin-Hernandez A, Saavedra E. Energy metabolism in tumor cells. FEBS J. 2007;274(6):1393-418.
341. Heerdt BG, Houston MA, Wilson AJ, Augenlicht LH. The intrinsic mitochondrial membrane potential (ΔΨm) is associated with steady-state mitochondrial activity and the extent to which colonic epithelial cells undergo butyrate-mediated growth arrest and apoptosis. Cancer Res. 2003;63(19):6311-9.
342. Ward MW, Huber HJ, Weisova P, Dussmann H, Nicholls DG, Prehn JH. Mitochondrial and plasma membrane potential of cultured cerebellar neurons during glutamate-induced necrosis, apoptosis, and tolerance. J Neurosci. 2007;27(31):8238-49.
343. Hennet T, Bertoni G, Richter C, Peterhans E. Expression of BCL-2 protein enhances the survival of mouse fibrosarcoid cells in tumor necrosis factor-mediated cytotoxicity. Cancer Res. 1993;53(6):1456-60.
344. Liang XJ, Finkel T, Shen DW, Yin JJ, Aszalos A, Gottesman MM. SIRT1 contributes in part to cisplatin resistance in cancer cells by altering mitochondrial metabolism. Mol Cancer Res. 2008;6(9):1499-506.
345. Galluzzi L, Larochette N, Zamzami N, Kroemer G. Mitochondria as therapeutic targets for cancer chemotherapy. Oncogene. 2006;25(34):4812-30.
346. Smiley ST, Reers M, Mottola-Hartshorn C, Lin M, Chen A, Smith TW, et al. Intracellular heterogeneity in mitochondrial membrane potentials revealed by a J-aggregate-forming lipophilic cation JC-1. Proc Natl Acad Sci U S A. 1991;88(9):3671-5.
347. Cossarizza A, Baccaranicontri M, Kalashnikova G, Franceschi C. A new method for the cytofluorometric analysis of mitochondrial membrane potential using the j-aggregate forming lipophilic cation 5,5',6,6'-tetrachloro-1,1',3,3'-tetraethylbenzimidazolcarbocyanine iodide (JC-1). Biochem Biophys Res Commun. 1993;197(1):40-5.

348. Salvioli S, Ardizzoni A, Franceschi C, Cossarizza A. JC-1, but not DiOC6(3) or rhodamine 123, is a reliable fluorescent probe to assess ΔΨ changes in intact cells: implications for studies on mitochondrial functionality during apoptosis. FEBS Lett. 1997;411(1):77-82.
349. Reers M, Smith TW, Chen LB. J-aggregate formation of a carbocyanine as a quantitative fluorescent indicator of membrane potential. Biochemistry. 1991;30(18):4480-6.
350. Rego AC, Vesce S, Nicholls DG. The mechanism of mitochondrial membrane potential retention following release of cytochrome c in apoptotic GT1-7 neural cells. Cell Death Differ. 2001;8(10):995-1003.
351. Gudz TI, Pandelova IG, Novgorodov SA. Stimulation of respiration in rat thymocytes induced by ionizing radiation. Radiat Res. 1994;138(1):114-20.
352. Nugent SM, Mothersill CE, Seymour C, McClean B, Lyng FM, Murphy JE. Increased mitochondrial mass in cells with functionally compromised mitochondria after exposure to both direct γ radiation and bystander factors. Radiat Res. 2007;168(1):134-42.
353. Zhang S, Wen G, Huang SX, Wang J, Tong J, Hei TK. Mitochondrial alteration in malignantly transformed human small airway epithelial cells induced by alpha-particles. Int J Cancer. 2013;132(1):19-28.
354. Leach JK, Van Tuyle G, Lin P-S, Schmidt-Ullrich R, Mikkelsen RB. Ionizing radiation-induced, mitochondria-dependent generation of reactive oxygen/nitrogen. Cancer Res. 2001;61(10):3894-901.
355. Zhang H, Maguire D, Swarts S, Sun W, Yang S, Wang W, et al. Replication of murine mitochondrial DNA following irradiation. Adv Exp Med Biol. 2009;645:43-8.
356. Zhang SB, Maguire D, Zhang M, Tian Y, Yang S, Zhang A, et al. Mitochondrial DNA and functional investigations into the radiosensitivity of four mouse strains. Int J Cell Biol. 2014;2014:850460.
357. Azimzadeh O, Scherthan H, Sarioglu H, Barjaktarovic Z, Conrad M, Vogt A, et al. Rapid proteomic remodeling of cardiac tissue caused by total body ionizing radiation. Proteomics. 2011;11(16):3299-311.
358. Yoshida K, Yamazaki H, Ozeki S, Inoue T, Yoshioka Y, Yoneda M, et al. Mitochondrial genotypes and radiation-induced micronucleus formation in human osteosarcoma cells in vitro. Oncology Rep. 2001; 8(3):615-9.
359. Yoshioka Y, Yamazaki H, Yoshida K, Ozeki S, Inoue T, Yoneda M, et al. Impact of mitochondrial DNA on radiation sensitivity of transformed human fibroblast cells: clonogenic survival, micronucleus formation and cellular ATP level. Radiat Res. 2004;162(2):143-7.
360. Yamazaki H, Yoshida K, Yoshioka Y, Isohashi F, Ozeki S, Koizumi M, et al. Impact of mitochondrial DNA on hypoxic radiation sensitivity in human fibroblast cells and osteosarcoma cell lines. Oncology Rep. 2008;19 (6):1545-9.
361. Paglin S, Lee N-Y, Nakar C, Fitzgerald M, Plotkin J, Deuel B, et al. Rapamycin-sensitive pathway regulates mitochondrial membrane potential, autophagy, and survival in irradiated MCF-7 cells. Cancer Res. 2005; 65(23):11061-70.
362. Belka C, Rudner J, Wesselborg S, Strepczynska A, Marini P, Lepple-Wienhues A, et al. Differential role of caspase-8 and BID activation during radiation-and CD95-induced apoptosis. Oncogene. 2000;19(9): 1181-90.
363. Viktorsson K, Ekedahl J, Lindebro MC, Lewensohn R, Zhivotovsky B, Linder S, et al. Defective stress kinase and Bak activation in response to ionizing radiation but not cisplatin in a non-small cell lung carcinoma cell line. Exp Cell Res. 2003;289(2):256-64.
364. Kulkarni R, Reither A, Thomas RA, Tucker JD. Mitochondrial mutant cells are hypersensitive to ionizing radiation, phleomycin and mitomycin C. Mutat Res. 2009;663(1-2):46-51.
365. Chen H, Chan DC. Emerging functions of mammalian mitochondrial fusion and fission. Hum Mol Genet. 2005;14 Spec No. 2:R283-9.
366. Benard G, Rossignol R. Ultrastructure of the mitochondrion and its bearing on function and bioenergetics. Antioxid Redox Signal. 2008;10(8):1313-42.
367. Westermann B. Bioenergetic role of mitochondrial fusion and fission. Biochim Biophys Acta. 2012;1817 (10):1833-8.
368. Skulachev VP. Mitochondrial filaments and clusters as intracellular power-transmitting cables. Trends Biochem Sci. 2001;26(1):23-9.
369. Arismendi-Morillo G. Electron microscopy morphology of the mitochondrial network in gliomas and their vascular microenvironment. Biochim Biophys Acta. 2011;1807(6):602-8.

370. Chung S, Dzeja PP, Faustino RS, Perez-Terzic C, Behfar A, Terzic A. Mitochondrial oxidative metabolism is required for the cardiac differentiation of stem cells. Nat Clin Pract Cardiovasc Med. 2007;4(Suppl 1): S60-S7.
371. Hyde BB, Twig G, Shirihai OS. Organellar vs cellular control of mitochondrial dynamics. Semin Cell Dev Biol. 2010;21(6):575-81.
372. Lewis M, Lewis W. Mitochondria in tissue culture. Science. 1914:330-3.
373. Chambers R. Microdissection Studies on the Germ Cell. Science. 1915;41(1051):290-3.
374. Gatenby JB. Memoirs: The cytoplasmic inclusions of the germ-cells. part iv. notes on the dimorphic spermatozoa of paludina and the giant germ-nurse cells of testacella and helix. J Cell Sci. 1919; 2(252):401-43.
375. Lewis WH. Giant centrospheres in degenerating mesenchyme cells of tissue cultures. J Exp Med. 1920;31(3):275.
376. Landecker H. Seeing things: from microcinematography to live cell imaging. Nat Methods. 2009; 6(10):707-9.
377. Bereiter-Hahn J. Behavior of mitochondria in the living cell. Int Rev Cytol. 1990;122:1-63.
378. Hoffmann H-P, Avers CJ. Mitochondrion of yeast: ultrastructural evidence for one giant, branched organelle per cell. Science. 1973;181(4101):749-51.
379. Poot M, Zhang YZ, Kramer JA, Wells KS, Jones LJ, Hanzel DK, et al. Analysis of mitochondrial morphology and function with novel fixable fluorescent stains. J Histochem Cytochem. 1996;44(12):1363-72.
380. Nunnari J, Marshall W, Straight A, Murray A, Sedat JW, Walter P. Mitochondrial transmission during mating in Saccharomyces cerevisiae is determined by mitochondrial fusion and fission and the intramitochondrial segregation of mitochondrial DNA. Mol Biol Cell. 1997;8(7):1233-42.
381. Jakobs S. High resolution imaging of live mitochondria. Biochim Biophys Acta. 2006;1763(5):561-75.
382. Sesaki H, Jensen RE. Division versus fusion: Dnm1p and Fzo1p antagonistically regulate mitochondrial shape. J Cell Biol. 1999;147(4):699-706.
383. Bleazard W, McCaffery JM, King EJ, Bale S, Mozdy A, Tieu Q, et al. The dynamin-related GTPase Dnm1 regulates mitochondrial fission in yeast. Nat Cell Biol. 1999;1(5):298-304.
384. Santel A, Fuller MT. Control of mitochondrial morphology by a human mitofusin. J Cell Sci. 2001;114 (Pt 5):867-74.
385. Rojo M, Legros F, Chateau D, Lombès A. Membrane topology and mitochondrial targeting of mitofusins, ubiquitous mammalian homologs of the transmembrane GTPase Fzo. J Cell Sci. 2002;115(8):1663-74.
386. Mozdy AD, Shaw JM. A fuzzy mitochondrial fusion apparatus comes into focus. Nat Rev Mol Cell Biol. 2003;4(6):468-78.
387. Hales KG, Fuller MT. Developmentally regulated mitochondrial fusion mediated by a conserved, novel, predicted GTPase. Cell. 1997;90(1):121-9.
388. Hermann GJ, Thatcher JW, Mills JP, Hales KG, Fuller MT, Nunnari J, et al. Mitochondrial fusion in yeast requires the transmembrane GTPase Fzo1p. J Cell Biol. 1998;143(2):359-73.
389. Chen H, Detmer SA, Ewald AJ, Griffin EE, Fraser SE, Chan DC. Mitofusins Mfn1 and Mfn2 coordinately regulate mitochondrial fusion and are essential for embryonic development. J Cell Biol. 2003;160(2): 189-200.
390. Ishihara N, Nomura M, Jofuku A, Kato H, Suzuki SO, Masuda K, et al. Mitochondrial fission factor Drp1 is essential for embryonic development and synapse formation in mice. Nat Cell Biol. 2009;11(8):958-66.
391. Koshiba T, Detmer SA, Kaiser JT, Chen H, McCaffery JM, Chan DC. Structural basis of mitochondrial tethering by mitofusin complexes. Science. 2004;305(5685):858-62.
392. Ishihara N, Eura Y, Mihara K. Mitofusin 1 and 2 play distinct roles in mitochondrial fusion reactions via GTPase activity. J Cell Sci. 2004;117(26):6535-46.
393. de Brito OM, Scorrano L. Mitofusin 2: a mitochondria-shaping protein with signaling roles beyond fusion. Antioxid Redox Signal. 2008;10(3):621-33.
394. de Brito OM, Scorrano L. Mitofusin 2 tethers endoplasmic reticulum to mitochondria. Nature. 2008;456 (7222):605-10.
395. Merkwirth C, Langer T. Mitofusin 2 builds a bridge between ER and mitochondria. Cell. 2008;135(7): 1165-7.

396. Liu X, Weaver D, Shirihai O, Hajnoczky G. Mitochondrial 'kiss-and-run': interplay between mitochondrial motility and fusion-fission dynamics. EMBO J. 2009;28(20):3074-89.
397. Yi M, Weaver D, Hajnóczky G. Control of mitochondrial motility and distribution by the calcium signal: a homeostatic circuit. J Cell Biol. 2004;167(4):661-72.
398. Fritz S, Weinbach N, Westermann B. Mdm30 is an F-box protein required for maintenance of fusion-competent mitochondria in yeast. Mol Biol Cell. 2003;14(6):2303-13.
399. Mishra P, Carelli V, Manfredi G, Chan DC. Proteolytic cleavage of Opa1 stimulates mitochondrial inner membrane fusion and couples fusion to oxidative phosphorylation. Cell Metab. 2014;19(4):630-41.
400. Karavaeva IE, Shekhireva KV, Severin FF, Knorre DA. Does mitochondrial fusion require transmembrane potential? Biochemistry (Mosc). 2015;80(5):549-58.
401. Twig G, Graf SA, Wikstrom JD, Mohamed H, Haigh SE, Elorza A, et al. Tagging and tracking individual networks within a complex mitochondrial web with photoactivatable GFP. Am J Physiol Cell Physiol. 2006;291(1):C176-84.
402. Legros F, Lombes A, Frachon P, Rojo M. Mitochondrial fusion in human cells is efficient, requires the inner membrane potential, and is mediated by mitofusins. Mol Biol Cell. 2002;13(12):4343-54.
403. Ishihara N, Jofuku A, Eura Y, Mihara K. Regulation of mitochondrial morphology by membrane potential, and DRP1-dependent division and FZO1-dependent fusion reaction in mammalian cells. Biochem Biophys Res Commun. 2003;301(4):891-8.
404. Heath-Engel HM, Shore GC. Mitochondrial membrane dynamics, cristae remodelling and apoptosis. Biochim Biophys Acta. 2006;1763(5):549-60.
405. Malka F, Guillery O, Cifuentes-Diaz C, Guillou E, Belenguer P, Lombès A, et al. Separate fusion of outer and inner mitochondrial membranes. EMBO Rep. 2005;6(9):853-9.
406. Olichon A, Emorine LJ, Descoins E, Pelloquin L, Brichese L, Gas N, et al. The human dynamin-related protein OPA1 is anchored to the mitochondrial inner membrane facing the inter-membrane space. FEBS lett. 2002;523(1):171-6.
407. Wong ED, Wagner JA, Gorsich SW, McCaffery JM, Shaw JM, Nunnari J. The dynamin-related GTPase, Mgm1p, is an intermembrane space protein required for maintenance of fusion competent mitochondria. J Cell Biol. 2000;151(2):341-52.
408. Delettre C, Griffoin J-M, Kaplan J, Dollfus H, Lorenz B, Faivre L, et al. Mutation spectrum and splicing variants in the OPA1 gene. Hum Genet. 2001;109(6):584-91.
409. Satoh M, Hamamoto T, Seo N, Kagawa Y, Endo H. Differential sublocalization of the dynamin-related protein OPA1 isoforms in mitochondria. Biochem Biophys Res Commun. 2003;300(2):482-93.
410. Song Z, Chen H, Fiket M, Alexander C, Chan DC. OPA1 processing controls mitochondrial fusion and is regulated by mRNA splicing, membrane potential, and Yme1L. J Cell Biol. 2007;178(5):749-55.
411. Duvezin-Caubet S, Jagasia R, Wagener J, Hofmann S, Trifunovic A, Hansson A, et al. Proteolytic processing of OPA1 links mitochondrial dysfunction to alterations in mitochondrial morphology. J Biol Chem. 2006; 281(49):37972-9.
412. Griparic L, Kanazawa T, van der Bliek AM. Regulation of the mitochondrial dynamin-like protein Opa1 by proteolytic cleavage. J Cell Biol. 2007;178(5):757-64.
413. Delettre C, Lenaers G, Griffoin J-M, Gigarel N, Lorenzo C, Belenguer P, et al. Nuclear gene OPA1, encoding a mitochondrial dynamin-related protein, is mutated in dominant optic atrophy. Nat Genet. 2000;26 (2):207-10.
414. Alexander C, Votruba M, Pesch UE, Thiselton DL, Mayer S, Moore A, et al. OPA1, encoding a dynamin-related GTPase, is mutated in autosomal dominant optic atrophy linked to chromosome 3q28. Nat Genet. 2000;26(2):211-5.
415. Scorrano L, Ashiya M, Buttle K, Weiler S, Oakes SA, Mannella CA, et al. A distinct pathway remodels mitochondrial cristae and mobilizes cytochrome c during apoptosis. Dev Cell. 2002;2(1):55-67.
416. Jahani-Asl A, Cheung EC, Neuspiel M, MacLaurin JG, Fortin A, Park DS, et al. Mitofusin 2 protects cerebellar granule neurons against injury-induced cell death. J Biol Chem. 2007;282(33):23788-98.
417. Chen H, McCaffery JM, Chan DC. Mitochondrial fusion protects against neurodegeneration in the cerebellum. Cell. 2007;130(3):548-62.
418. Chen Y, Lv L, Jiang Z, Yang H, Li S, Jiang Y. Mitofusin 2 protects hepatocyte mitochondrial function from damage induced by GCDCA. PLoS One. 2013;8(6):e65455.

419. Chiche J, Rouleau M, Gounon P, Brahimi-Horn MC, Pouyssegur J, Mazure NM. Hypoxic enlarged mitochondria protect cancer cells from apoptotic stimuli. J Cell Physiol. 2010;222(3):648-57.
420. Paumard P, Vaillier J, Coulary B, Schaeffer J, Soubannier V, Mueller DM, et al. The ATP synthase is involved in generating mitochondrial cristae morphology. EMBO J. 2002;21(3):221-30.
421. Amutha B, Gordon DM, Gu Y, Pain D. A novel role of Mgm1p, a dynamin-related GTPase, in ATP synthase assembly and cristae formation/maintenance. Biochem J. 2004;381(1):19-23.
422. Imoto M, Tachibana I, Urrutia R. Identification and functional characterization of a novel human protein highly related to the yeast dynamin-like GTPase Vps1p. J Cell Sci. 1998;111(10):1341-9.
423. Smirnova E, Shurland D-L, Ryazantsev SN, van der Bliek AM. A human dynamin-related protein controls the distribution of mitochondria. J Cell Biol. 1998;143(2):351-8.
424. Otsuga D, Keegan BR, Brisch E, Thatcher JW, Hermann GJ, Bleazard W, et al. The dynamin-related GTPase, Dnm1p, controls mitochondrial morphology in yeast. J Cell Biol. 1998;143(2):333-49.
425. Shin H-W, Shinotsuka C, Torii S, Murakami K, Nakayama K. Identification and subcellular localization of a novel mammalian dynamin-related protein homologous to yeast Vps1p and Dnm1p. J Biochem. 1997; 122(3):525-30.
426. Yoon Y, Pitts KR, Dahan S, McNiven MA. A novel dynamin-like protein associates with cytoplasmic vesicles and tubules of the endoplasmic reticulum in mammalian cells. J Cell Biol. 1998;140(4):779-93.
427. Kamimoto T, Nagai Y, Onogi H, Muro Y, Wakabayashi T, Hagiwara M. Dymple, a novel dynamin-like high molecular weight GTPase lacking a proline-rich carboxyl-terminal domain in mammalian cells. J Biol Chem. 1998;273(2):1044-51.
428. Hinshaw J. Dynamin and its role in membrane fission 1. Annu Rev Cell Dev Biol. 2000;16(1):483-519.
429. Koch A, Thiemann M, Grabenbauer M, Yoon Y, McNiven MA, Schrader M. Dynamin-like protein 1 is involved in peroxisomal fission. J Biol Chem. 2003;278(10):8597-605.
430. Chang CR, Blackstone C. Dynamic regulation of mitochondrial fission through modification of the dynamin-related protein Drp1. Ann N Y Acad Sci. 2010;1201:34-9.
431. Labrousse AM, Zappaterra MD, Rube DA, van der Bliek AM. C. elegans dynamin-related protein DRP-1 controls severing of the mitochondrial outer membrane. Mol Cell. 1999;4(5):815-26.
432. Yoon Y, Pitts KR, McNiven MA. Mammalian dynamin-like protein DLP1 tubulates membranes. Mol Biol Cell. 2001;12(9):2894-905.
433. Smirnova E, Griparic L, Shurland D-L, Van Der Bliek AM. Dynamin-related protein Drp1 is required for mitochondrial division in mammalian cells. Mol Biol Cell. 2001;12(8):2245-56.
434. Yoon YS, Yoon DS, Lim IK, Yoon SH, Chung HY, Rojo M, et al. Formation of elongated giant mitochondria in DFO-induced cellular senescence: involvement of enhanced fusion process through modulation of Fis1. J Cell Physiol. 2006;209(2):468-80.
435. Parone PA, Da Cruz S, Tondera D, Mattenberger Y, James DI, Maechler P, et al. Preventing mitochondrial fission impairs mitochondrial function and leads to loss of mitochondrial DNA. PLoS One. 2008;3(9): e3257.
436. Malena A, Loro E, Di Re M, Holt IJ, Vergani L. Inhibition of mitochondrial fission favours mutant over wild-type mitochondrial DNA. Hum Mol Genet. 2009;18(18):3407-16.
437. Qi X, Qvit N, Su Y-C, Mochly-Rosen D. A novel Drp1 inhibitor diminishes aberrant mitochondrial fission and neurotoxicity. J Cell Sci. 2013;126(3):789-802.
438. Oettinghaus B, D'Alonzo D, Barbieri E, Restelli LM, Savoia C, Licci M, et al. DRP1-dependent apoptotic mitochondrial fission occurs independently of BAX, BAK and APAF1 to amplify cell death by BID and oxidative stress. Biochim Biophys Acta. 2016;1857(8):1267-76.
439. Germain M, Mathai JP, McBride HM, Shore GC. Endoplasmic reticulum BIK initiates DRP1-regulated remodelling of mitochondrial cristae during apoptosis. EMBO J. 2005;24(8):1546-56.
440. Wei MC, Zong W-X, Cheng EH-Y, Lindsten T, Panoutsakopoulou V, Ross AJ, et al. Proapoptotic BAX and BAK: A Requisite Gateway to Mitochondrial Dysfunction and Death. Science. 2001;292(5517):727-30.
441. Grohm J, Kim SW, Mamrak U, Tobaben S, Cassidy-Stone A, Nunnari J, et al. Inhibition of Drp1 provides neuroprotection in vitro and in vivo. Cell Death Differ. 2012;19(9):1446-58.
442. Friedman JR, Lackner LL, West M, DiBenedetto JR, Nunnari J, Voeltz GK. ER tubules mark sites of mitochondrial division. Science. 2011;334(6054):358-62.

443. Archer SL. Mitochondrial dynamics-mitochondrial fission and fusion in human diseases. N Engl J Med. 2013;369(23):2236-51.
444. Rowland AA, Voeltz GK. Endoplasmic reticulum-mitochondria contacts: function of the junction. Nat Rev Mol Cell Biol. 2012;13(10):607-25.
445. Breckenridge DG, Germain M, Mathai JP, Nguyen M, Shore GC. Regulation of apoptosis by endoplasmic reticulum pathways. Oncogene. 2003;22(53):8608-18.
446. Tieu Q, Nunnari J. Mdv1p is a WD repeat protein that interacts with the dynamin-related GTPase, Dnm1p, to trigger mitochondrial division. J Cell Biol. 2000;151(2):353-66.
447. Mozdy A, McCaffery J, Shaw J. Dnm1p GTPase-mediated mitochondrial fission is a multi-step process requiring the novel integral membrane component Fis1p. J Cell Biol. 2000;151(2):367-80.
448. Suzuki M, Jeong S-Y, Karbowski M, Youle RJ, Tjandra N. The solution structure of human mitochondria fission protein Fis1 reveals a novel TPR-like helix bundle. J Mol Biol. 2003;334(3):445-58.
449. Mai S, Klinkenberg M, Auburger G, Bereiter-Hahn J, Jendrach M. Decreased expression of Drp1 and Fis1 mediates mitochondrial elongation in senescent cells and enhances resistance to oxidative stress through PINK1. J Cell Sci. 2010;123(Pt 6):917-26.
450. Correia-Melo C, Passos JF. Mitochondria: Are they causal players in cellular senescence? Biochim Biophys Acta. 2015;1847(11):1373-9.
451. Lee S, Jeong SY, Lim WC, Kim S, Park YY, Sun X, et al. Mitochondrial fission and fusion mediators, hFis1 and OPA1, modulate cellular senescence. J Biol Chem. 2007;282(31):22977-83.
452. Yoon Y, Krueger EW, Oswald BJ, McNiven MA. The mitochondrial protein hFis1 regulates mitochondrial fission in mammalian cells through an interaction with the dynamin-like protein DLP1. Mol Cell Biol. 2003;23(15):5409-20.
453. James DI, Parone PA, Mattenberger Y, Martinou J-C. hFis1, a novel component of the mammalian mitochondrial fission machinery. J Biol Chem. 2003;278(38):36373-9.
454. Lee YJ, Jeong SY, Karbowski M, Smith CL, Youle RJ. Roles of the mammalian mitochondrial fission and fusion mediators Fis1, Drp1, and Opa1 in apoptosis. Mol Biol Cell. 2004;15(11):5001-11.
455. Karbowski M, Jeong S-Y, Youle RJ. Endophilin B1 is required for the maintenance of mitochondrial morphology. J Cell Biol. 2004;166(7):1027-39.
456. Gandre-Babbe S, van der Bliek AM. The novel tail-anchored membrane protein Mff controls mitochondrial and peroxisomal fission in mammalian cells. Mol Biol Cell. 2008;19(6):2402-12.
457. Otera H, Wang C, Cleland MM, Setoguchi K, Yokota S, Youle RJ, et al. Mff is an essential factor for mitochondrial recruitment of Drp1 during mitochondrial fission in mammalian cells. J Cell Biol. 2010;191(6):1141-58.
458. Palmer CS, Elgass KD, Parton RG, Osellame LD, Stojanovski D, Ryan MT. Adaptor proteins MiD49 and MiD51 can act independently of Mff and Fis1 in Drp1 recruitment and are specific for mitochondrial fission. J Biol Chem. 2013;288(38):27584-93.
459. Loson OC, Song Z, Chen H, Chan DC. Fis1, Mff, MiD49, and MiD51 mediate Drp1 recruitment in mitochondrial fission. Mol Biol Cell. 2013;24(5):659-67.
460. Johnson LV, Walsh ML, Bockus BJ, Chen LB. Monitoring of relative mitochondrial membrane potential in living cells by fluorescence microscopy. J Cell Biol. 1981;88(3):526-35.
461. Baracca A, Sgarbi G, Solaini G, Lenaz G. Rhodamine 123 as a probe of mitochondrial membrane potential: evaluation of proton flux through F 0 during ATP synthesis. Biochim Biophys Acta. 2003;1606(1):137-46.
462. Floryk D, Houstek J. Tetramethyl rhodamine methyl ester (TMRM) is suitable for cytofluorometric measurements of mitochondrial membrane potential in cells treated with digitonin. Biosci Rep. 1999;19 (1):27-34.
463. Petit PX, O'Connor JE, Grunwald D, Brown SC. Analysis of the membrane potential of rat-and mouse-liver mitochondria by flow cytometry and possible applications. Eur J Biochem. 1990;194(2):389-97.
464. Pendergrass W, Wolf N, Poot M. Efficacy of MitoTracker Green™ and CMXrosamine to measure changes in mitochondrial membrane potentials in living cells and tissues. Cytometry Part A. 2004;61(2):162-9.
465. Zhang J, Xu P, Wang Y, Wang M, Li H, Lin S, et al. Astaxanthin prevents pulmonary fibrosis by promoting myofibroblast apoptosis dependent on Drp1-mediated mitochondrial fission. J Cell Mol Med. 2015;19(9): 2215-31.

466. Yamamori T, Ike S, Bo T, Sasagawa T, Sakai Y, Suzuki M, et al. Inhibition of the mitochondrial fission protein dynamin-related protein 1 (Drp1) impairs mitochondrial fission and mitotic catastrophe after x-irradiation. Mol Biol Cell. 2015;26(25):4607-17.
467. Karbowski M, Norris KL, Cleland MM, Jeong SY, Youle RJ. Role of Bax and Bak in mitochondrial morphogenesis. Nature. 2006;443(7112):658-62.
468. Suzuki-Karasaki Y, Fujiwara K, Saito K, Suzuki-Karasaki M, Ochiai T, Soma M. Distinct effects of TRAIL on the mitochondrial network in human cancer cells and normal cells: role of plasma membrane depolarization. Oncotarget. 2015;6(25):21572-88.
469. Serasinghe Madhavika N, Wieder Shira Y, Renault Thibaud T, Elkholi R, Asciolla James J, Yao Jonathon L, et al. Mitochondrial division is requisite to ras-induced transformation and targeted by oncogenic mapk pathway inhibitors. Mol Cell. 2015;57(3):521-36.
470. Whelan DR, Bell TD. Image artifacts in single molecule localization microscopy: why optimization of sample preparation protocols matters. Sci Rep. 2015;5:7924.
471. Rizzuto R, Brini M, De Giorgi F, Rossi R, Heim R, Tsien RY, et al. Double labelling of subcellular structures with organelle-targeted GFP mutants in vivo. Curr Biol. 1996;6(2):183-8.
472. Collins TJ, Berridge MJ, Lipp P, Bootman MD. Mitochondria are morphologically and functionally heterogeneous within cells. EMBO J. 2002;21(7):1616-27.
473. Cottet-Rousselle C, Ronot X, Leverve X, Mayol JF. Cytometric assessment of mitochondria using fluorescent probes. Cytometry A. 2011;79(6):405-25.
474. Benard G, Bellance N, James D, Parrone P, Fernandez H, Letellier T, et al. Mitochondrial bioenergetics and structural network organization. J Cell Sci. 2007;120(5):838-48.
475. Chen H, Chomyn A, Chan DC. Disruption of fusion results in mitochondrial heterogeneity and dysfunction. J Biol Chem. 2005;280(28):26185-92.
476. Plecita-Hlavata L, Lessard M, Santorova J, Bewersdorf J, Jezek P. Mitochondrial oxidative phosphorylation and energetic status are reflected by morphology of mitochondrial network in INS-1E and HEP-G2 cells viewed by 4Pi microscopy. Biochim Biophys Acta. 2008;1777(7-8):834-46.
477. Gerweck LE, Seetharaman K. Cellular pH gradient in tumor versus normal tissue: potential exploitation for the treatment of cancer. Cancer Res. 1996;56(6):1194-8.
478. Vaupel P. Tumor microenvironmental physiology and its implications for radiation oncology. Semin Radiat Oncol. 2004;14(3):198-206.
479. Vaupel P, Thews O, Hoeckel M. Treatment resistance of solid tumors: role of hypoxia and anemia. Med Oncol. 2001;18(4):243-59.
480. Shah MA, Schwartz GK. Cell Cycle-mediated Drug Resistance: An emerging concept in cancer therapy. clin cancer res. 2001;7(8):2168-81.
481. Gerweck LE. Tumor pH: Implications for treatment and novel drug design. Semin Radiat Oncol. 1998; 8(3):176-82.
482. Pelicano H, Xu R-h, Du M, Feng L, Sasaki R, Carew JS, et al. Mitochondrial respiration defects in cancer cells cause activation of Akt survival pathway through a redox-mediated mechanism. J Cell Biol. 2006; 175(6):913-23.
483. Thews O, Koenig R, Kelleher D, Kutzner J, Vaupel P. Enhanced radiosensitivity in experimental tumours following erythropoietin treatment of chemotherapy-induced anaemia. Br J Cancer. 1998;78(6):752.
484. Pham N-A, Richardson T, Cameron J, Chue B, Robinson BH. Altered mitochondrial structure and motion dynamics in living cells with energy metabolism defects revealed by real time microscope imaging. Microsc Microanal. 2004;10(02):247-60.
485. Rossignol R, Gilkerson R, Aggeler R, Yamagata K, Remington SJ, Capaldi RA. Energy substrate modulates mitochondrial structure and oxidative capacity in cancer cells. Cancer Res. 2004;64(3):985-93.
486. Liot G, Bossy B, Lubitz S, Kushnareva Y, Sejbuk N, Bossy-Wetzel E. Complex II inhibition by 3-NP causes mitochondrial fragmentation and neuronal cell death via an NMDA-and ROS-dependent pathway. Cell Death Differ. 2009;16(6):899-909.
487. Koopman WJ, Visch H-J, Verkaart S, van den Heuvel LW, Smeitink JA, Willems PH. Mitochondrial network complexity and pathological decrease in complex I activity are tightly correlated in isolated human complex I deficiency. Am J Physiol Cell Physiol. 2005;289(4):C881-C90.

488. Schauss AC, Huang H, Choi S-Y, Xu L, Soubeyrand S, Bilodeau P, et al. A novel cell-free mitochondrial fusion assay amenable for high-throughput screenings of fusion modulators. BMC Biol. 2010;8(1):100.
489. Guillery O, Malka F, Frachon P, Milea D, Rojo M, Lombes A. Modulation of mitochondrial morphology by bioenergetics defects in primary human fibroblasts. Neuromuscul Disord. 2008;18(4):319-30.
490. Lyamzaev KG, Izyumov DS, Avetisyan AV, Yang F, Pletjushkina OY, Chernyak BV. Inhibition of mitochondrial bioenergetics: the effects on structure of mitochondria in the cell and on apoptosis. Acta biochim Pol. 2004;51(2):553-62.
491. De Vos KJ, Allan VJ, Grierson AJ, Sheetz MP. Mitochondrial function and actin regulate dynamin-related protein 1-dependent mitochondrial fission. Curr Biol. 2005;15(7):678-83.
492. Pletjushkina OY, Lyamzaev K, Popova E, Nepryakhina O, Ivanova OY, Domnina L, et al. Effect of oxidative stress on dynamics of mitochondrial reticulum. Biochim Biophys Acta. 2006;1757(5):518-24.
493. Baricault L, Ségui B, Guégand L, Olichon A, Valette A, Larminat F, et al. OPA1 cleavage depends on decreased mitochondrial ATP level and bivalent metals. Exp Cell Res. 2007;313(17):3800-8.
494. Karbowski M, Arnoult D, Chen H, Chan DC, Smith CL, Youle RJ. Quantitation of mitochondrial dynamics by photolabeling of individual organelles shows that mitochondrial fusion is blocked during the Bax activation phase of apoptosis. J Cell Biol. 2004;164(4):493-9.
495. Valdez LB, Zaobornyj T, Boveris A. Mitochondrial metabolic states and membrane potential modulate mtNOS activity. Biochim Biophys Acta. 2006;1757(3):166-72.
496. Vayssier-Taussat M, Kreps SE, Adrie C, Dall'Ava J, Christiani D, Polla BS. Mitochondrial membrane potential: a novel biomarker of oxidative environmental stress. Environ Health Perspect. 2002;110 (3):301.
497. Perry SW, Norman JP, Barbieri J, Brown EB, Gelbard HA. Mitochondrial membrane potential probes and the proton gradient: a practical usage guide. Biotechniques. 2011;50(2):98-115.
498. Ly JD, Grubb DR, Lawen A. The mitochondrial membrane potential (Delta psi m) in apoptosis; an update. Apoptosis. 2003;8(2):115-28.
499. Wang Y, Blandino G, Givol D. Induced p21waf expression in H1299 cell line promotes cell senescence and protects against cytotoxic effect of radiation and doxorubicin. Oncogene. 1999;18(16):2643-9.
500. Hutter E, Renner K, Pfister G, Stöckl P, Jansen-Dürr P, Gnaiger E. Senescence-associated changes in respiration and oxidative phosphorylation in primary human fibroblasts. Biochem J. 2004;380(Pt 3): 919-28.
501. Tondera D, Grandemange S, Jourdain A, Karbowski M, Mattenberger Y, Herzig S, et al. SLP-2 is required for stress-induced mitochondrial hyperfusion. EMBO J. 2009;28(11):1589-600.
502. Lee S, Kim S, Sun X, Lee J-H, Cho H. Cell cycle-dependent mitochondrial biogenesis and dynamics in mammalian cells. Biochem Biophys Res Commun. 2007;357(1):111-7.
503. Salazar-Roa M, Malumbres M. Fueling the Cell Division Cycle. Trends Cell Biol. 2017;27(1):69-81.
504. Taguchi N, Ishihara N, Jofuku A, Oka T, Mihara K. Mitotic phosphorylation of dynamin-related GTPase Drp1 participates in mitochondrial fission. J Biol Chem. 2007;282(15):11521-9.
505. Arakaki N, Nishihama T, Owaki H, Kuramoto Y, Suenaga M, Miyoshi E, et al. Dynamics of mitochondria during the cell cycle. Biol Pharm Bull. 2006;29(9):1962-5.
506. Kanfer G, Courthéoux T, Peterka M, Meier S, Soste M, Melnik A, et al. Mitotic redistribution of the mitochondrial network by Miro and Cenp-F. Nat Commun. 2015;6:8015.
507. Chalmers S, Saunter C, Wilson C, Coats P, Girkin JM, McCarron JG. Mitochondrial motility and vascular smooth muscle proliferation. Arteriosclerosis, thrombosis, and vascular biology. 2012;32(12):3000-11.
508. Li D, Li X, Guan Y, Guo X. Mitofusin-2-mediated tethering of mitochondria and endoplasmic reticulum promotes cell cycle arrest of vascular smooth muscle cells in G0/G1 phase. Acta Biochim Biophys Sin. 2015;47(6):441-50.
509. Schieke SM, McCoy JP, Jr., Finkel T. Coordination of mitochondrial bioenergetics with G1 phase cell cycle progression. Cell Cycle. 2008;7(12):1782-7.
510. Mussman JG, Horn HF, Carroll PE, Okuda M, Tarapore P, Donehower LA, et al. Synergistic induction of centrosome hyperamplification by loss of p53 and cyclin E overexpression. Oncogene. 2000;19(13):1635.
511. Lemasters JJ. Selective mitochondrial autophagy, or mitophagy, as a targeted defense against oxidative stress, mitochondrial dysfunction, and aging. Rejuvenation Res. 2005;8(1):3-5.

512. Mishra P, Chan DC. Mitochondrial dynamics and inheritance during cell division, development and disease. Nat Rev Mol Cell Biol. 2014;15(10):634-46.
513. Shidara Y, Yamagata K, Kanamori T, Nakano K, Kwong JQ, Manfredi G, et al. Positive contribution of pathogenic mutations in the mitochondrial genome to the promotion of cancer by prevention from apoptosis. Cancer Res. 2005;65(5):1655-63.
514. Park JS, Sharma LK, Li H, Xiang R, Holstein D, Wu J, et al. A heteroplasmic, not homoplasmic, mitochondrial DNA mutation promotes tumorigenesis via alteration in reactive oxygen species generation and apoptosis. Hum Mol Genet. 2009;18(9):1578-89.
515. Butow RA, Avadhani NG. Mitochondrial signaling: the retrograde response. Mol Cell. 2004;14(1):1-15.
516. Goodpasture EW. Observations on mitochondria of tumors. J Med Res. 1918;38(2):213.
517. Singh L, Nag TC, Kashyap S. Ultrastructural changes of mitochondria in human retinoblastoma: correlation with tumor differentiation and invasiveness. Tumor Biol. 2016;37(5):5797-803.
518. Satoh M, Yagawa K. Electron microscopic study on mitochondria in Hürthle cell adenoma of thyroid. Pathol Int. 1981;31(6):1079-87.
519. González-cámpora R, Herrero-Zapatero A, Lerma E, Sanchez F, Galera H. Hürthle cell and mitochondrion-rich cell tumors. A clinicopathologic study. Cancer. 1986;57(6):1154-63.
520. Arismendi-Morillo G. Electron microscopy morphology of the mitochondrial network in human cancer. Int J Biochem Cell Biol. 2009;41(10):2062-8.
521. Gasparre G, Porcelli AM, Bonora E, Pennisi LF, Toller M, Iommarini L, et al. Disruptive mitochondrial DNA mutations in complex I subunits are markers of oncocytic phenotype in thyroid tumors. Proc Natl Acad Sci. 2007;104(21):9001-6.
522. Ordóñez NG. Mesothelioma with clear cell features: an ultrastructural and immunohistochemical study of 20 cases. Hum Pathol. 2005;36(5):465-73.
523. Xu R-h, Pelicano H, Zhou Y, Carew JS, Feng L, Bhalla KN, et al. Inhibition of glycolysis in cancer cells: a novel strategy to overcome drug resistance associated with mitochondrial respiratory defect and hypoxia. Cancer Res. 2005;65(2):613-21.
524. Nakashima N, Goto K, Takeuchi J. Malignant papillary cystadenoma lymphomatosum. Virchows Archiv. 1983;399(2):207-19.
525. Arismendi-Morillo GJ, Castellano-Ramirez AV. Ultrastructural mitochondrial pathology in human astrocytic tumors: potentials implications pro-therapeutics strategies. J Elec Microsc. 2008;57(1):33-9.
526. Zhang H, Gao P, Fukuda R, Kumar G, Krishnamachary B, Zeller KI, et al. HIF-1 inhibits mitochondrial biogenesis and cellular respiration in VHL-deficient renal cell carcinoma by repression of C-MYC activity. Cancer Cell. 2007;11(5):407-20.
527. Cuezva JM, Krajewska M, de Heredia ML, Krajewski S, Santamaría G, Kim H, et al. The bioenergetic signature of cancer a marker of tumor progression. Cancer Res. 2002;62(22):6674-81.
528. Corn PG, Ricci MS, Scata KA, Arsham AM, Simon MC, Dicker DT, et al. Mxi1 is induced by hypoxia in a HIF-1–dependent manner and protects cells from c-Myc-induced apoptosis. Cancer Biol Ther. 2005;4(11): 1285-94.
529. Kashatus JA, Nascimento A, Myers LJ, Sher A, Byrne FL, Hoehn KL, et al. Erk2 phosphorylation of Drp1 promotes mitochondrial fission and MAPK-driven tumor growth. Mol Cell. 2015;57(3):537-51.
530. Gallardo ME, Moreno-Loshuertos R, López C, Casqueiro M, Silva J, Bonilla F, et al. m. 6267G> A: a recurrent mutation in the human mitochondrial DNA that reduces cytochrome c oxidase activity and is associated with tumors. Hum Mutat. 2006;27(6):575-82.
531. Dakubo G, Parr R, Costello L, Franklin R, Thayer R. Altered metabolism and mitochondrial genome in prostate cancer. J Clin Pathol. 2006;59(1):10-6.
532. Chatterjee A, Mambo E, Sidransky D. Mitochondrial DNA mutations in human cancer. Oncogene. 2006;25(34):4663-74.
533. Lu J, Sharma LK, Bai Y. Implications of mitochondrial DNA mutations and mitochondrial dysfunction in tumorigenesis. Cell Res. 2009;19(7):802-15.
534. Ohta S. Contribution of somatic mutations in the mitochondrial genome to the development of cancer and tolerance against anticancer drugs. Oncogene. 2006;25(34):4768-76.
535. Tseng L-M, Yin P-H, Chi C-W, Hsu C-Y, Wu C-W, Lee L-M, et al. Mitochondrial DNA mutations and mitochondrial DNA depletion in breast cancer. Genes Chromosomes Cancer. 2006;45(7):629-38.

536. Petros JA, Baumann AK, Ruiz-Pesini E, Amin MB, Sun CQ, Hall J, et al. mtDNA mutations increase tumorigenicity in prostate cancer. Proc Natl Acad Sci U S A. 2005;102(3):719-24.
537. Horton TM, Petros JA, Heddi A, Shoffner J, Kaufman AE, Graham SD, et al. Novel mitochondrial DNA deletion found in a renal cell carcinoma. Genes Chromosomes Cancer. 1996;15(2):95-101.
538. Ishikawa K, Takenaga K, Akimoto M, Koshikawa N, Yamaguchi A, Imanishi H, et al. ROS-generating mitochondrial DNA mutations can regulate tumor cell metastasis. Science. 2008;320(5876):661-4.
539. Costello L, and, Franklin R. The intermediary metabolism of the prostate: a key to understanding the pathogenesis and progression of prostate malignancy. Oncology. 2000;59(4):269-82.
540. Sharma LK, Lu J, Bai Y. Mitochondrial respiratory complex I: structure, function and implication in human diseases. Curr Med Chem. 2009;16(10):1266-77.
541. Sharma LK, Fang H, Liu J, Vartak R, Deng J, Bai Y. Mitochondrial respiratory complex I dysfunction promotes tumorigenesis through ROS alteration and AKT activation. Hum Mol Genet. 2011;20(23): 4605-16.
542. Dohi T, Beltrami E, Wall NR, Plescia J, Altieri DC. Mitochondrial survivin inhibits apoptosis and promotes tumorigenesis. J Clin Invest. 2004;114(8):1117-27.
543. Hagenbuchner J, Kuznetsov A, Obexer P, Ausserlechner M. BIRC5/Survivin enhances aerobic glycolysis and drug resistance by altered regulation of the mitochondrial fusion/fission machinery. Oncogene. 2013;32(40):4748-57.
544. Manteifel V, Bakeeva L, Karu T. Ultrastructural changes in chondriome of human lymphocytes after irradiation with He-Ne laser: Appearance of giant mitochondria. J Photochem Photobiol. 1997;38(1): 25-30.
545. Maguire P, Mothersill C, Seymour C, Lyng FM. Medium from irradiated cells induces dose-dependent mitochondrial changes and BCL2 responses in unirradiated human keratinocytes. Radiat Res. 2005;163 (4):384-90.
546. Ambrosini-Spaltro A, Salvi F, Betts CM, Frezza GP, Piemontese A, Del Prete P, et al. Oncocytic modifications in rectal adenocarcinomas after radio and chemotherapy. Virchows Archiv. 2006;448(4): 442-8.
547. Aggarwal BB, Sethi G, Baladandayuthapani V, Krishnan S, Shishodia S. Targeting cell signaling pathways for drug discovery: an old lock needs a new key. J Cell Biochem. 2007;102(3):580-92.
548. Rodríguez-Enríquez S, Marín-Hernández A, Gallardo-Pérez JC, Carreño-Fuentes L, Moreno-Sánchez R. Targeting of cancer energy metabolism. Mol Nutr Food Res. 2009;53(1):29-48.
549. Ralph SJ, Rodriguez-Enriquez S, Neuzil J, Moreno-Sanchez R. Bioenergetic pathways in tumor mitochondria as targets for cancer therapy and the importance of the ROS-induced apoptotic trigger. Mol Aspects Med. 2010;31(1):29-59.
550. Moreira PI, Custódio J, Moreno A, Oliveira CR, Santos MS. Tamoxifen and estradiol interact with the flavin mononucleotide site of complex I leading to mitochondrial failure. J Biol Chem. 2006;281(15):10143-52.
551. Dong L-F, Freeman R, Liu J, Zobalova R, Marin-Hernandez A, Stantic M, et al. Suppression of Tumor Growth In vivo by the Mitocan α-tocopheryl Succinate Requires Respiratory Complex II. Clin Cancer Res. 2009;15(5):1593-600.
552. Bernal SD, Lampidis TJ, McIsaac RM, Chen LB. Anticarcinoma activity in vivo of rhodamine 123, a mitochondrial-specific dye. Science. 1983;222(4620):169-72.
553. Bonnet S, Archer SL, Allalunis-Turner J, Haromy A, Beaulieu C, Thompson R, et al. A mitochondria-K+ channel axis is suppressed in cancer and its normalization promotes apoptosis and inhibits cancer growth. Cancer Cell. 2007;11(1):37-51.
554. Huth ME, Ricci AJ, Cheng AG. Mechanisms of aminoglycoside ototoxicity and targets of hair cell protection. Int J Otolaryngol. 2011;2011:937861.
555. Guan M-X. Mitochondrial 12S rRNA mutations associated with aminoglycoside ototoxicity. Mitochondrion. 2011;11(2):237-45.
556. Prezant TR, Agapian JV, Bohlman MC, Bu X, Öztas S, Qiu W-Q, et al. Mitochondrial ribosomal RNA mutation associated with both antibiotic–induced and non–syndromic deafness. Nat Genet. 1993;4(3): 289-94.

557. Neuzil J, Wang X-F, Dong L-F, Low P, Ralph SJ. Molecular mechanism of 'mitocan'-induced apoptosis in cancer cells epitomizes the multiple roles of reactive oxygen species and Bcl-2 family proteins. FEBS Lett. 2006;580(22):5125-9.
558. Lopez-Gonzalez MA, Delgado F, Lucas M. Aminoglycosides activate oxygen metabolites production in the cochlea of mature and developing rats. Hear Res. 1999;136(1–2):165-8.
559. Cassidy-Stone A, Chipuk JE, Ingerman E, Song C, Yoo C, Kuwana T, et al. Chemical inhibition of the mitochondrial division dynamin reveals its role in Bax/Bak-dependent mitochondrial outer membrane permeabilization. Dev Cell. 2008;14(2):193-204.
560. Kushnareva Y, Andreyev AY, Kuwana T, Newmeyer DD. Bax activation initiates the assembly of a multimeric catalyst that facilitates Bax pore formation in mitochondrial outer membranes. PLoS Biol. 2012;10(9):1717.
561. Koseoglu S, Dilks JR, Peters CG, Fitch-Tewfik JL, Fadel NA, Jasuja R, et al. Dynamin-related protein-1 controls fusion pore dynamics during platelet granule exocytosis. Arterioscler Thromb Vasc Biol. 2013; 33(3):481-8.
562. Cereghetti GM, Stangherlin A, Martins de Brito O, Chang CR, Blackstone C, Bernardi P, et al. Dephosphorylation by calcineurin regulates translocation of Drp1 to mitochondria. Proc Natl Acad Sci U S A. 2008;105(41):15803-8.
563. Cribbs JT, Strack S. Reversible phosphorylation of Drp1 by cyclic AMP-dependent protein kinase and calcineurin regulates mitochondrial fission and cell death. EMBO Rep. 2007;8(10):939-44.
564. Wan YY, Zhang JF, Yang ZJ, Jiang LP, Wei YF, Lai QN, et al. Involvement of Drp1 in hypoxia-induced migration of human glioblastoma U251 cells. Oncol Rep. 2014;32(2):619-26.
565. McCarron JG, Wilson C, Sandison ME, Olson ML, Girkin JM, Saunter C, et al. From structure to function: mitochondrial morphology, motion and shaping in vascular smooth muscle. J Vasc Res. 2013;50(5): 357-71.
566. Galloway CA, Lee H, Yoon Y. Mitochondrial morphology-emerging role in bioenergetics. Free Radic Biol Med. 2012;53(12):2218-28.
567. Liu X, Hajnoczky G. Altered fusion dynamics underlie unique morphological changes in mitochondria during hypoxia-reoxygenation stress. Cell Death Differ. 2011;18(10):1561-72.
568. Sauvanet C, Duvezin-Caubet S, di Rago JP, Rojo M. Energetic requirements and bioenergetic modulation of mitochondrial morphology and dynamics. Semin Cell Dev Biol. 2010;21(6):558-65.
569. Lim S, Lee SY, Seo HH, Ham O, Lee C, Park JH, et al. Regulation of mitochondrial morphology by positive feedback interaction between PKCdelta and Drp1 in vascular smooth muscle cell. J Cell Biochem. 2015; 116(4):648-60.
570. Maimaitijiang A, Zhuang X, Jiang X, Li Y. Dynamin-related protein inhibitor downregulates reactive oxygen species levels to indirectly suppress high glucose-induced hyperproliferation of vascular smooth muscle cells. Biochem Biophys Res Commun. 2016;471(4):474-8.
571. Marsboom G, Toth PT, Ryan JJ, Hong Z, Wu X, Fang YH, et al. Dynamin-related protein 1-mediated mitochondrial mitotic fission permits hyperproliferation of vascular smooth muscle cells and offers a novel therapeutic target in pulmonary hypertension. Circ Res. 2012;110(11):1484-97.
572. Qian W, Choi S, Gibson GA, Watkins SC, Bakkenist CJ, Van Houten B. Mitochondrial hyperfusion induced by loss of the fission protein Drp1 causes ATM-dependent G2/M arrest and aneuploidy through DNA replication stress. J Cell Sci. 2012;125(Pt 23):5745-57.
573. Wang J, Li J, Santana-Santos L, Shuda M, Sobol RW, Van Houten B, et al. A novel strategy for targeted killing of tumor cells: Induction of multipolar acentrosomal mitotic spindles with a quinazolinone derivative mdivi-1. Mol Oncol. 2015;9(2):488-502.
574. Lindqvist A, Rodríguez-Bravo V, Medema RH. The decision to enter mitosis: feedback and redundancy in the mitotic entry network. J Cell Biol. 2009;185(2):193-202.
575. Gavet O, Pines J. Progressive activation of CyclinB1-Cdk1 coordinates entry to mitosis. Dev Cell. 2010; 18(4):533-43.
576. Hochegger H, Dejsuphong D, Sonoda E, Saberi A, Rajendra E, Kirk J, et al. An essential role for Cdk1 in S phase control is revealed via chemical genetics in vertebrate cells. J Cell Biol. 2007;178(2):257-68.
577. Crasta K, Huang P, Morgan G, Winey M, Surana U. Cdk1 regulates centrosome separation by restraining proteolysis of microtubule-associated proteins. EMBO J. 2006;25(11):2551-63.

578. Mori Y, Inoue Y, Taniyama Y, Tanaka S, Terada Y. Phosphorylation of the centrosomal protein, Cep169, by Cdk1 promotes its dissociation from centrosomes in mitosis. Biochem Biophys Res Commun. 2015; 468(4):642-6.
579. Abe S, Nagasaka K, Hirayama Y, Kozuka-Hata H, Oyama M, Aoyagi Y, et al. The initial phase of chromosome condensation requires Cdk1-mediated phosphorylation of the CAP-D3 subunit of condensin II. Genes Dev. 2011;25(8):863-74.
580. Robellet X, Thattikota Y, Wang F, Wee T-L, Pascariu M, Shankar S, et al. A high-sensitivity phospho-switch triggered by Cdk1 governs chromosome morphogenesis during cell division. Genes Dev. 2015;29(4): 426-39.
581. Fourest-Lieuvin A, Peris L, Gache V, Garcia-Saez I, Juillan-Binard C, Lantez V, et al. Microtubule regulation in mitosis: tubulin phosphorylation by the cyclin-dependent kinase Cdk1. Mol Biol Cell. 2006;17(3): 1041-50.
582. Qian W, Wang J, Roginskaya V, McDermott LA, Edwards RP, Stolz DB, et al. Novel combination of mitochondrial division inhibitor 1 (mdivi-1) and platinum agents produces synergistic pro-apoptotic effect in drug resistant tumor cells. Oncotarget. 2014;5(12):4180-94.
583. Wang J, Hansen K, Edwards R, Van Houten B, Qian W. Mitochondrial division inhibitor 1 (Mdivi-1) enhances death receptor-mediated apoptosis in human ovarian cancer cells. Biochem Biophys Res Commun. 2015;456(1):7-12.
584. Gharanei M, Hussain A, Janneh O, Maddock H. Attenuation of doxorubicin-induced cardiotoxicity by mdivi-1: a mitochondrial division/mitophagy inhibitor. PLoS One. 2013;8(10):e77713.
585. Shroff EH, Snyder CM, Budinger GR, Jain M, Chew TL, Khuon S, et al. BH3 peptides induce mitochondrial fission and cell death independent of BAX/BAK. PLoS One. 2009;4(5):e5646.
586. Salabei JK, Hill BG. Mitochondrial fission induced by platelet-derived growth factor regulates vascular smooth muscle cell bioenergetics and cell proliferation. Redox Biol. 2013;1:542-51.
587. Zhao YX, Cui M, Chen SF, Dong Q, Liu XY. Amelioration of ischemic mitochondrial injury and Bax-dependent outer membrane permeabilization by Mdivi-1. CNS Neurosci Ther. 2014;20(6):528-38.
588. Xie N, Wang C, Lian Y, Wu C, Zhang H, Zhang Q. Inhibition of mitochondrial fission attenuates Abeta-induced microglia apoptosis. Neuroscience. 2014;256:36-42.
589. Liu JM, Yi Z, Liu SZ, Chang JH, Dang XB, Li QY, et al. The mitochondrial division inhibitor mdivi-1 attenuates spinal cord ischemia-reperfusion injury both in vitro and in vivo: Involvement of BK channels. Brain Res. 2015;1619:155-65.
590. Park JH, Ko J, Hwang J, Koh HC. Dynamin-related protein 1 mediates mitochondria-dependent apoptosis in chlorpyrifos-treated SH-SY5Y cells. Neurotoxicology. 2015;51:145-57.
591. Twaroski DM, Yan Y, Zaja I, Clark E, Bosnjak ZJ, Bai X. Altered mitochondrial dynamics contributes to propofol-induced cell death in human stem cell-derived neurons. Anesthesiology. 2015;123(5):1067-83.
592. Wu Q, Xia SX, Li QQ, Gao Y, Shen X, Ma L, et al. Mitochondrial division inhibitor 1 (Mdivi-1) offers neuroprotection through diminishing cell death and improving functional outcome in a mouse model of traumatic brain injury. Brain Res. 2016;1630:134-43.
593. Zhao J, Zhang J, Yu M, Xie Y, Huang Y, Wolff DW, et al. Mitochondrial dynamics regulates migration and invasion of breast cancer cells. Oncogene. 2012;32(40):4814-24.
594. Farrand L, Byun S, Kim JY, Im-Aram A, Lee J, Lim S, et al. Piceatannol enhances cisplatin sensitivity in ovarian cancer via modulation of p53, X-linked inhibitor of apoptosis protein (XIAP), and mitochondrial fission. J Biol Chem. 2013;288(33):23740-50.
595. Kong B, Tsuyoshi H, Orisaka M, Shieh D-B, Yoshida Y, Tsang BK. Mitochondrial dynamics regulating chemoresistance in gynecological cancers. Annals of the New York Academy of Sciences. 2015;1350 (1):1-16.
596. Savry A, Carre M, Berges R, Rovini A, Pobel I, Chacon C, et al. Bcl-2—enhanced efficacy of microtubule-targeting chemotherapy through bim overexpression: implications for cancer treatment. Neoplasia. 2013;15(1):49-60.
597. Han XJ, Yang ZJ, Jiang LP, Wei YF, Liao MF, Qian Y, et al. Mitochondrial dynamics regulates hypoxia-induced migration and antineoplastic activity of cisplatin in breast cancer cells. Int J Oncol. 2015;46 (2):691-700.

598. Alaimo A, Gorojod RM, Beauquis J, Munoz MJ, Saravia F, Kotler ML. Deregulation of mitochondria-shaping proteins Opa-1 and Drp-1 in manganese-induced apoptosis. PLoS One. 2014;9(3):e91848.
599. Xie Q, Wu Q, Horbinski CM, Flavahan WA, Yang K, Zhou W, et al. Mitochondrial control by DRP1 in brain tumor initiating cells. Nat Neurosci. 2015;18(4):501-10.
600. Sharp WW, Beiser DG, Fang YH, Han M, Piao L, Varughese J, et al. Inhibition of the mitochondrial fission protein dynamin-related protein 1 improves survival in a murine cardiac arrest model. Crit Care Med. 2015;43(2):e38-47.
601. Din S, Mason M, Völkers M, Johnson B, Cottage CT, Wang Z, et al. Pim-1 preserves mitochondrial morphology by inhibiting dynamin-related protein 1 translocation. Proc Natl Acad Sci. 2013;110(15): 5969-74.
602. Ong SB, Subrayan S, Lim SY, Yellon DM, Davidson SM, Hausenloy DJ. Inhibiting mitochondrial fission protects the heart against ischemia/reperfusion injury. Circulation. 2010;121(18):2012-22.
603. Givvimani S, Munjal C, Tyagi N, Sen U, Metreveli N, Tyagi SC. Mitochondrial division/mitophagy inhibitor (Mdivi) ameliorates pressure overload induced heart failure. PLoS One. 2012;7(3):e32388.
604. Iglewski M, Hill JA, Lavandero S, Rothermel BA. Mitochondrial fission and autophagy in the normal and diseased heart. Curr Hypertens Rep. 2010;12(6):418-25.
605. Mattiolo P, Barbero-Farran A, Amigo J, Ripamonti M, Ribas J, Boix J. Cell death induced by 2-phenyl-ethynesulfonamide uncovers a pro-survival function of BAX. Cancer Lett. 2014;354(1):115-21.
606. Xie N, Wang C, Lian Y, Zhang H, Wu C, Zhang Q. A selective inhibitor of Drp1, mdivi-1, protects against cell death of hippocampal neurons in pilocarpine-induced seizures in rats. Neurosci Lett. 2013;545:64-8.
607. Qiu X, Cao L, Yang X, Zhao X, Liu X, Han Y, et al. Role of mitochondrial fission in neuronal injury in pilocarpine-induced epileptic rats. Neuroscience. 2013;245:157-65.
608. Ferrari LF, Chum A, Bogen O, Reichling DB, Levine JD. Role of Drp1, a key mitochondrial fission protein, in neuropathic pain. J Neurosci. 2011;31(31):11404-10.
609. Brooks C, Wei Q, Cho SG, Dong Z. Regulation of mitochondrial dynamics in acute kidney injury in cell culture and rodent models. J Clin Invest. 2009;119(5):1275-85.
610. Park SW, Kim KY, Lindsey JD, Dai Y, Heo H, Nguyen DH, et al. A selective inhibitor of Drp1, Mdivi-1, increases retinal ganglion cell survival in acute ischemic mouse retina. Invest Ophthalmol Vis Sci. 2011; 52(5):2837-43.
611. Zhang N, Wang S, Li Y, Che L, Zhao Q. A selective inhibitor of Drp1, Mdivi-1, acts against cerebral ischemia/reperfusion injury via an anti-apoptotic pathway in rats. Neurosci Lett. 2013;535:104-9.
612. Cui M, Ding H, Chen F, Zhao Y, Yang Q, Dong Q. Mdivi-1 protects against ischemic brain injury via elevating extracellular adenosine in a cAMP/CREB-CD39-dependent manner. Mol Neurobiol. 2016; 53(1):240-53.
613. Li Y, Wang P, Wei J, Fan R, Zuo Y, Shi M, et al. Inhibition of Drp1 by Mdivi-1 attenuates cerebral ischemic injury via inhibition of the mitochondria-dependent apoptotic pathway after cardiac arrest. Neuroscience. 2015;311:67-74.
614. Li G, Jia Z, Cao Y, Wang Y, Li H, Zhang Z, et al. Mitochondrial division inhibitor 1 ameliorates mitochondrial injury, apoptosis, and motor dysfunction after acute spinal cord injury in rats. Neurochem Res. 2015;40 (7):1379-92.
615. Wang J, Wang P, Li S, Wang S, Li Y, Liang N, et al. Mdivi-1 prevents apoptosis induced by ischemia-reperfusion injury in primary hippocampal cells via inhibition of reactive oxygen species-activated mitochondrial pathway. J Stroke Cerebrovasc Dis. 2014;23(6):1491-9.
616. Xie N, Wang C, Wu C, Cheng X, Gao Y, Zhang H, et al. Mdivi-1 protects epileptic hippocampal neurons from apoptosis via inhibiting oxidative stress and endoplasmic reticulum stress in vitro. Neurochem Res. 2016; 41(6):1335-42.
617. van Vugt MA, Gardino AK, Linding R, Ostheimer GJ, Reinhardt HC, Ong S-E, et al. A mitotic phosphorylation feedback network connects Cdk1, Plk1, 53BP1, and Chk2 to inactivate the G2/M DNA damage checkpoint. PLoS Biol. 2010;8(1):e1000287.
618. Nantajit D, Fan M, Duru N, Wen Y, Reed JC, Li JJ. Cyclin B1/Cdk1 phosphorylation of mitochondrial p53 induces anti-apoptotic response. PLoS One. 2010;5(8):e12341-e.
619. Krajewska M, Heijink A, Bisselink Y, Seinstra R, Silljé H, de Vries E, et al. Forced activation of Cdk1 via wee1 inhibition impairs homologous recombination. Oncogene. 2013;32(24):3001-8.

620. Benada J, Burdova K, Lidak T, von Morgen P, Macurek L. Polo-like kinase 1 inhibits DNA damage response during mitosis. Cell Cycle. 2015;14(2):219-31.
621. Candas D, Fan M, Nantajit D, Vaughan AT, Murley JS, Woloschak GE, et al. CyclinB1/Cdk1 phosphorylates mitochondrial antioxidant MnSOD in cell adaptive response to radiation stress. J Mol Cell Biol. 2013;5(3): 166-75.
622. Abdelwahid E, Yokokura T, Krieser RJ, Balasundaram S, Fowle WH, White K. Mitochondrial disruption in *Drosophila* apoptosis. Dev Cell. 2007;12(5):793-806.
623. Brooks C, Wei Q, Feng L, Dong G, Tao Y, Mei L, et al. Bak regulates mitochondrial morphology and pathology during apoptosis by interacting with mitofusins. Proc Natl Acad Sci U S A. 2007;104(28): 11649-54.
624. Brooks C, Cho SG, Wang CY, Yang T, Dong Z. Fragmented mitochondria are sensitized to Bax insertion and activation during apoptosis. Am J Physiol Cell Physiol. 2011;300(3):C447-55.
625. Margineantu DH, Cox WG, Sundell L, Sherwood SW, Beechem JM, Capaldi RA. Cell cycle dependent morphology changes and associated mitochondrial DNA redistribution in mitochondria of human cell lines. Mitochondrion. 2002;1(5):425-35.
626. Lutz AK, Exner N, Fett ME, Schlehe JS, Kloos K, Lammermann K, et al. Loss of parkin or PINK1 function increases Drp1-dependent mitochondrial fragmentation. J Biol Chem. 2009;284(34):22938-51.
627. Das S, Hajnoczky N, Antony AN, Csordas G, Gaspers LD, Clemens DL, et al. Mitochondrial morphology and dynamics in hepatocytes from normal and ethanol-fed rats. Pflugers Arch. 2012;464(1):101-9.
628. Barni S, Sciola L, Spano A, Pippia P. Static cytofluorometry and fluorescence morphology of mitochondria and DNA in proliferating fibroblasts. Biotech Histochem. 1996;71(2):66-70.
629. Ishihara N, Fujita Y, Oka T, Mihara K. Regulation of mitochondrial morphology through proteolytic cleavage of OPA1. EMBO J. 2006;25(13):2966-77.
630. Park K-S, Wiederkehr A, Kirkpatrick C, Mattenberger Y, Martinou J-C, Marchetti P, et al. Selective actions of mitochondrial fission/fusion genes on metabolism-secretion coupling in insulin-releasing cells. J Biol Chem. 2008;283(48):33347-56.
631. Jendrach M, Mai S, Pohl S, Vöth M, Bereiter-Hahn J. Short- and long-term alterations of mitochondrial morphology, dynamics and mtDNA after transient oxidative stress. Mitochondrion. 2008;8(4):293-304.
632. Winter L, Abrahamsberg C, Wiche G. Plectin isoform 1b mediates mitochondrion–intermediate filament network linkage and controls organelle shape. J Cell Biol. 2008;181(6):903-11.
633. Yu T, Fox RJ, Burwell LS, Yoon Y. Regulation of mitochondrial fission and apoptosis by the mitochondrial outer membrane protein hFis1. J Cell Sci. 2005;118(18):4141-51.
634. Schneider CA, Rasband WS, Eliceiri KW. NIH Image to ImageJ: 25 years of image analysis. Nat Methods. 2012;9(7):671-5.
635. Bortoletto R, Silva NS, Zangaro RA, Pacheco MT, Da Matta RA, Pacheco-Soares C. Mitochondrial membrane potential after low-power laser irradiation. Lasers Med Sci. 2004;18(4):204-6.
636. Ludovico P, Sansonetty F, Corte-Real M. Assessment of mitochondrial membrane potential in yeast cell populations by flow cytometry. Microbiology. 2001;147(Pt 12):3335-43.
637. Safiulina D, Veksler V, Zharkovsky A, Kaasik A. Loss of mitochondrial membrane potential is associated with increase in mitochondrial volume: physiological role in neurones. J Cell Physiol. 2006;206(2):347-53.
638. Deacon J, Peckham MJ, Steel GG. The radioresponsiveness of human tumours and the initial slope of the cell survival curve. Radiother Oncol. 1984;2(4):317-23.
639. Bjork-Eriksson T, West C, Karlsson E, Mercke C. Discrimination of human tumor radioresponsiveness using low-dose rate irradiation. Int J Radiat Oncol Biol Phys. 1998;42(5):1147-53.
640. Dwarakanath BS, Adhikari JS, Jain V. Hematoporphyrin derivatives potentiate the radiosensitizing effects of 2-deoxy-D-glucose in cancer cells. Int J Radiat Oncol Biol Phys. 1999;43(5):1125-33.
641. Deschavanne PJ, Debieu D, Fertil B, Malaise EP. Re-evaluation of in vitro radiosensitivity of human fibroblasts of different genetic origins. Int J Radiat Biol Relat Stud Phys Chem Med. 1986;50(2):279-93.
642. Fertil B, Deschavanne PJ, Debieu D, Malaise EP. Correlation between PLD repair capacity and the survival curve of human fibroblasts in exponential growth phase: analysis in terms of several parameters. Radiat Res. 1988;116(1):74-88.
643. Yin ZJ, Jin FG, Liu TG, Fu EQ, Xie YH, Sun RL. Overexpression of STAT3 potentiates growth, survival, and radioresistance of non-small-cell lung cancer (NSCLC) cells. J Surg Res. 2011;171(2):675-83.

644. Yang HJ, Kim N, Seong KM, Youn H, Youn B. Investigation of radiation-induced transcriptome profile of radioresistant non-small cell lung cancer a549 cells using rna-seq. PLoS ONE. 2013;8(3):e59319.
645. Zheng M, Morgan-Lappe SE, Yang J, Bockbrader KM, Pamarthy D, Thomas D, et al. Growth inhibition and radiosensitization of glioblastoma and lung cancer cells by small interfering rna silencing of tumor necrosis factor receptor-associated factor 2. Cancer Res. 2008;68(18):7570-8.
646. Brognard J, Clark AS, Ni Y, Dennis PA. Akt/Protein Kinase B is constitutively active in non-small cell lung cancer cells and promotes cellular survival and resistance to chemotherapy and radiation. Cancer Res. 2001;61(10):3986-97.
647. Balsara BR, Pei J, Mitsuuchi Y, Page R, Klein-Szanto A, Wang H, et al. Frequent activation of AKT in non-small cell lung carcinomas and preneoplastic bronchial lesions. Carcinogenesis. 2004;25(11):2053-9.
648. Guo W-F, Lin R-X, Huang J, Zhou Z, Yang J, Guo-Zheng G, et al. Identification of differentially expressed genes contributing to radioresistance in lung cancer cells using microarray analysis. Radiat Res. 2005;164 (1):27-35.
649. Lee YS, Oh J-H, Yoon S, Kwon M-S, Song C-W, Kim K-H, et al. Differential gene expression profiles of radioresistant non–small-cell lung cancer cell lines established by fractionated irradiation: tumor protein p53-inducible protein 3 confers sensitivity to ionizing radiation. Int J Radiat Oncol Biol Phys. 2010;77(3): 858-66.
650. Cao C, Mu Y, Hallahan DE, Lu B. XIAP and survivin as therapeutic targets for radiation sensitization in preclinical models of lung cancer. Oncogene. 2004;23(42):7047-52.
651. Kim Y-S, Jin H-O, Seo S-K, Woo SH, Choe T-B, An S, et al. Sorafenib induces apoptotic cell death in human non-small cell lung cancer cells by down-regulating mammalian target of rapamycin (mTOR)-dependent survivin expression. Biochem Pharmacol. 2011;82(3):216-26.
652. Lovey J, Nie D, Tovari J, Kenessey I, Timar J, Kandouz M, et al. Radiosensitivity of human prostate cancer cells can be modulated by inhibition of 12-lipoxygenase. Cancer Lett. 2013;335(2):495-501.
653. Koh SJ, Tak JK, Kim ST, Nam WS, Kim SY, Park KM, et al. Sensitization of ionizing radiation-induced apoptosis by ursolic acid. Free Radic Res. 2012;46(3):339-45.
654. Ryu S, Brown SL, Kim SH, Khil MS, Kim JH. Preferential radiosensitization of human prostatic carcinoma cells by mild hyperthermia. Int J Radiat Oncol Biol Phys. 1996;34(1):133-8.
655. Jayakumar S, Kunwar A, Sandur SK, Pandey BN, Chaubey RC. Differential response of DU145 and PC3 prostate cancer cells to ionizing radiation: role of reactive oxygen species, GSH and Nrf2 in radiosensitivity. Biochim Biophys Acta. 2014;1840(1):485-94.
656. Fitzgerald TJ, Wang T, Goel HL, Huang J, Stein G, Lian J, et al. Prostate carcinoma and radiation therapy: therapeutic treatment resistance and strategies for targeted therapeutic intervention. Expert Rev Anticancer Ther. 2008;8(6):967-74.
657. Fowler J, Chappell R, Ritter M. Is alpha/beta for prostate tumors really low? Int J Radiat Oncol Biol Phys. 2001;50(4):1021-31.
658. Chen Y, Wang J, Fraig MM, Metcalf J, Turner WR, Bissada NK, et al. Defects of DNA mismatch repair in human prostate cancer. Cancer Res. 2001;61(10):4112-21.
659. Brown KD, Rathi A, Kamath R, Beardsley DI, Zhan Q, Mannino JL, et al. The mismatch repair system is required for S-phase checkpoint activation. Nat Genet. 2003;33(1):80-4.
660. Cejka P, Stojic L, Marra G, Jiricny J. Is mismatch repair really required for ionizing radiation-induced DNA damage signaling? Nat Genet. 2004;36(5):432-3.
661. Yan T, Schupp JE, Hwang H-s, Wagner MW, Berry SE, Strickfaden S, et al. Loss of DNA mismatch repair imparts defective cdc2 signaling and G2 arrest responses without altering survival after ionizing radiation. Cancer Res. 2001;61(22):8290-7.
662. Halliwell B. Oxidative stress and cancer: have we moved forward? Biochem J. 2007;401(1):1-11.
663. Lynam-Lennon N, Maher SG, Maguire A, Phelan J, Muldoon C, Reynolds JV, et al. Altered mitochondrial function and energy metabolism is associated with a radioresistant phenotype in oesophageal adenocarcinoma. PLoS One. 2014;9(6):e100738.
664. Janssen AM, Bosman CB, van Duijn W, Oostendorp-van de Ruit MM, Kubben FJ, Griffioen G, et al. Superoxide dismutases in gastric and esophageal cancer and the prognostic impact in gastric cancer. Clin Cancer Res. 2000;6(8):3183-92.

665. Gear AR. Rhodamine 6G. A potent inhibitor of mitochondrial oxidative phosphorylation. J Biol Chem. 1974;249(11):3628-37.
666. Keil VC, Funke F, Zeug A, Schild D, Muller M. Ratiometric high-resolution imaging of JC-1 fluorescence reveals the subcellular heterogeneity of astrocytic mitochondria. Pflugers Arch. 2011;462(5):693-708.
667. Houston MA, Augenlicht LH, Heerdt BG. Stable differences in intrinsic mitochondrial membrane potential of tumor cell subpopulations reflect phenotypic heterogeneity. Int J Cell Biol. 2011;2011: 978583.
668. Truksa J, Dong LF, Rohlena J, Stursa J, Vondrusova M, Goodwin J, et al. Mitochondrially targeted vitamin E succinate modulates expression of mitochondrial DNA transcripts and mitochondrial biogenesis. Antioxid Redox Signal. 2015;22(11):883-900.
669. Richter U, Lahtinen T, Marttinen P, Suomi F, Battersby BJ. Quality control of mitochondrial protein synthesis is required for membrane integrity and cell fitness. J Cell Biol. 2015;211(2):373-89.
670. Panov A, Orynbayeva Z. Bioenergetic and antiapoptotic properties of mitochondria from cultured human prostate cancer cell lines PC-3, DU145 and LNCaP. PLoS One. 2013;8(8):e72078.
671. Mourier A, Devin A, Rigoulet M. Active proton leak in mitochondria: A new way to regulate substrate oxidation. Biochimica et Biophysica Acta (BBA) - Bioenergetics. 2010;1797(2):255-61.
672. Navet R, Mouithys-Mickalad A, Douette P, Sluse-Goffart CM, Jarmuszkiewicz W, Sluse FE. Proton leak induced by reactive oxygen species produced during in vitro anoxia/reoxygenation in rat skeletal muscle mitochondria. J Bioenerg Biomembr. 2006;38(1):23-32.
673. Horimoto M, Resnick MB, Konkin TA, Routhier J, Wands JR, Baffy G. Expression of uncoupling protein-2 in human colon cancer. Clin Cancer Res. 2004;10(18):6203-7.
674. Loiseau D, Chevrollier A, Verny C, Guillet V, Gueguen N, Pou De Crescenzo MA, et al. Mitochondrial coupling defect in Charcot–Marie–Tooth type 2A disease. Ann Neurol. 2007;61(4):315-23.
675. Wolken GG, Arriaga EA. Simultaneous measurement of individual mitochondrial membrane potential and electrophoretic mobility by capillary electrophoresis. Anal Chem. 2014;86(9):4217-26.
676. Labajova A, Vojtiskova A, Krivakova P, Kofranek J, Drahota Z, Houstek J. Evaluation of mitochondrial membrane potential using a computerized device with a tetraphenylphosphonium-selective electrode. Anal Biochem. 2006;353(1):37-42.
677. Dey R, Moraes CT. Lack of oxidative phosphorylation and low mitochondrial membrane potential decrease susceptibility to apoptosis and do not modulate the protective effect of Bcl-xl in osteosarcoma cells. J Biol Chem. 2000;275(10):7087-94.
678. Solaini G, Sgarbi G, Lenaz G, Baracca A. Evaluating mitochondrial membrane potential in cells. Biosci Rep. 2007;27(1-3):11-21.
679. Hitosugi T, Fan J, Chung TW, Lythgoe K, Wang X, Xie J, et al. Tyrosine phosphorylation of mitochondrial pyruvate dehydrogenase kinase 1 is important for cancer metabolism. Mol Cell. 2011;44(6):864-77.
680. Shavit R, Ilouze M, Feinberg T, Lawrence Y, Tzur Y, Peled N. Mitochondrial induction as a potential radio-sensitizer in lung cancer cells - a short report. Cell Oncol. 2015;38(3):247-52.
681. Biaglow J, Varnes M, Jacobson B, Koch C. Oxygen Transport to Tissue—IV. In: Bicher H, Bruley D, editor; Advances in experimental medicine and biology vol 159. New York: Plenum Press; 1983. p. 348-9.
682. Hess B, Chance B. Phosphorylation efficiency of the intact cell. I. Glucose-oxygen titrations in ascites tumor cells. J Biol Chem. 1959;234:3031-5.
683. Illingworth, JA. Bioenergetics: oxygraph. School of Biochemistry and Molecular Biology, Leeds University [Internet]. 2017. Available from: http://www.bmb.leeds.ac.uk/illingworth/oxphos/oxygraph.htm.
684. Herst PM, Berridge MV. Cell surface oxygen consumption: A major contributor to cellular oxygen consumption in glycolytic cancer cell lines. Biochim Biophys Acta. 2007;1767(2):170-7.
685. Brar SS, Corbin Z, Kennedy TP, Hemendinger R, Thornton L, Bommarius B, et al. NOX5 NAD(P)H oxidase regulates growth and apoptosis in DU 145 prostate cancer cells. Am J Physiol Cell Physiol. 2003;285(2): C353-69.
686. Kumar B, Koul S, Khandrika L, Meacham RB, Koul HK. Oxidative stress is inherent in prostate cancer cells and is required for aggressive phenotype. Cancer Res. 2008;68(6):1777-85.
687. Park M-T, Kim M-J, Kang Y-H, Choi S-Y, Lee J-H, Choi J-A, et al. Phytosphingosine in combination with ionizing radiation enhances apoptotic cell death in radiation-resistant cancer cells through ROS-dependent and-independent AIF release. Blood. 2005;105(4):1724-33.

688. Spitz DR, Azzam EI, Li JJ, Gius D. Metabolic oxidation/reduction reactions and cellular responses to ionizing radiation: a unifying concept in stress response biology. Cancer Metastasis Rev. 2004;23 (3-4):311-22.
689. Farrand L, Kim JY, Im-Aram A, Suh JY, Lee HJ, Tsang BK. An improved quantitative approach for the assessment of mitochondrial fragmentation in chemoresistant ovarian cancer cells. PLoS One. 2013; 8(9):e74008.
690. Youle RJ, van der Bliek AM. Mitochondrial fission, fusion, and stress. Science. 2012;337(6098):1062-5.
691. Rambold AS, Kostelecky B, Elia N, Lippincott-Schwartz J. Tubular network formation protects mitochondria from autophagosomal degradation during nutrient starvation. Proc Natl Acad Sci. 2011; 108(25):10190-5.
692. Mopert K, Hajek P, Frank S, Chen C, Kaufmann J, Santel A. Loss of Drp1 function alters OPA1 processing and changes mitochondrial membrane organization. Exp Cell Res. 2009;315(13):2165-80.
693. Lackner LL, Nunnari J. Small molecule inhibitors of mitochondrial division: tools that translate basic biological research into medicine. Chem Biol. 2010;17(6):578-83.
694. Solesio ME, Saez-Atienzar S, Jordan J, Galindo MF. Characterization of mitophagy in the 6-hydoxy-dopamine Parkinson's disease model. Toxicol Sci. 2012;129(2):411-20.
695. Chlystun M, Campanella M, Law AL, Duchen MR, Fatimathas L, Levine TP, et al. Regulation of mitochondrial morphogenesis by annexin A6. PLoS One. 2013;8(1):e53774.
696. Cunniff B, Wozniak AN, Sweeney P, DeCosta K, Heintz NH. Peroxiredoxin 3 levels regulate a mitochondrial redox setpoint in malignant mesothelioma cells. Redox Biol. 2014;3:79-87.
697. Bras M, Yuste VJ, Roue G, Barbier S, Sancho P, Virely C, et al. Drp1 mediates caspase-independent type III cell death in normal and leukemic cells. Mol Cell Biol. 2007;27(20):7073-88.
698. Cunniff B, Benson K, Stumpff J, Newick K, Held P, Taatjes D, et al. Mitochondrial-targeted nitroxides disrupt mitochondrial architecture and inhibit expression of peroxiredoxin 3 and FOXM1 in malignant mesothelioma cells. J Cell Physiol. 2013;228(4):835-45.
699. Cui M, Tang X, Christian WV, Yoon Y, Tieu K. Perturbations in mitochondrial dynamics induced by human mutant PINK1 can be rescued by the mitochondrial division inhibitor Mdivi-1. J Biol Chem. 2010;285(15): 11740-52.
700. Clerc P, Ge SX, Hwang H, Waddell J, Roelofs BA, Karbowski M, et al. Drp1 is dispensable for apoptotic cytochrome c release in primed MCF10A and fibroblast cells but affects Bcl-2 antagonist-induced respiratory changes. Br J Pharmacol. 2014;171(8):1988-99.
701. So EC, Hsing C-H, Liang C-H, Wu S-N. The actions of mdivi-1, an inhibitor of mitochondrial fission, on rapidly activating delayed-rectifier K+ current and membrane potential in HL-1 murine atrial cardiomyocytes. Eur J Pharmacol. 2012;683(1–3):1-9.
702. Westrate LM, Drocco JA, Martin KR, Hlavacek WS, MacKeigan JP. Mitochondrial morphological features are associated with fission and fusion events. PLoS One. 2014;9(4):e95265.
703. Khacho M, Tarabay M, Patten D, Khacho P, MacLaurin JG, Guadagno J, et al. Acidosis overrides oxygen deprivation to maintain mitochondrial function and cell survival. Nat Commun. 2014;5:3550.
704. Rajagopalan MS, Gupta K, Epperly MW, Franicola D, Zhang X, Wang H, et al. The mitochondria-targeted nitroxide JP4-039 augments potentially lethal irradiation damage repair. In Vivo. 2009;23(5):717-26.
705. Matthews J, Meeker B, Chapman J. Response of human tumor cell lines in vitro to fractionated irradiation. Int J Radiat Oncol Biol Phys. 1989;16(1):133-8.
706. Sivakumar S, Daum JR, Gorbsky GJ. Live cell fluorescence imaging for phenotypic analysis of mitosis. Methods Mol Biol. 2014;1170:549-62.
707. Hendzel MJ, Wei Y, Mancini MA, Van Hooser A, Ranalli T, Brinkley B, et al. Mitosis-specific phosphorylation of histone H3 initiates primarily within pericentromeric heterochromatin during G2 and spreads in an ordered fashion coincident with mitotic chromosome condensation. Chromosoma. 1997; 106(6):348-60.
708. Fenech M. The in vitro micronucleus technique. Mutat Res. 2000;455(1-2):81-95.
709. Fenech M, Chang WP, Kirsch-Volders M, Holland N, Bonassi S, Zeiger E, et al. HUMN project: detailed description of the scoring criteria for the cytokinesis-block micronucleus assay using isolated human lymphocyte cultures. Mutat Res. 2003;534(1-2):65-75.
710. Thery M, Bornens M. Get round and stiff for mitosis. HFSP J. 2008;2(2):65-71.

711. Stewart MP, Helenius J, Toyoda Y, Ramanathan SP, Muller DJ, Hyman AA. Hydrostatic pressure and the actomyosin cortex drive mitotic cell rounding. Nature. 2011;469(7329):226-30.
712. Marchesi S, Montani F, Deflorian G, D'Antuono R, Cuomo A, Bologna S, et al. DEPDC1B coordinates de-adhesion events and cell-cycle progression at mitosis. Dev Cell. 2014;31(4):420-33.
713. Cramer L, Mitchison T. Myosin is involved in postmitotic cell spreading. J Cell Biol. 1995;131(1):179-89.
714. Théry M, Bornens M. Cell shape and cell division. Curr Opin Cell Biol. 2006;18(6):648-57.
715. Palayoor ST, Bump EA, Teicher BA, Coleman CN. Apoptosis and clonogenic cell death in PC3 human prostate cancer cells after treatment with gamma radiation and suramin. Radiat Res. 1997;148(2):105-14.
716. Petersen C, Petersen S, Milas L, Lang FF, Tofilon PJ. Enhancement of intrinsic tumor cell radiosensitivity induced by a selective cyclooxygenase-2 inhibitor. Clin Cancer Res. 2000;6(6):2513-20.
717. Darzynkiewicz Z, Juan G, Li X, Gorczyca W, Murakami T, Traganos F. Cytometry in cell necrobiology: analysis of apoptosis and accidental cell death (necrosis). Cytometry. 1997;27(1):1-20.
718. Kyjacova L, Hubackova S, Krejcikova K, Strauss R, Hanzlikova H, Dzijak R, et al. Radiotherapy-induced plasticity of prostate cancer mobilizes stem-like non-adherent, Erk signaling-dependent cells. Cell Death Differ. 2015;22(6):898-911.
719. Listovsky T, Oren YS, Yudkovsky Y, Mahbubani HM, Weiss AM, Lebendiker M, et al. Mammalian Cdh1/Fzr mediates its own degradation. EMBO J. 2004;23(7):1619-26.
720. Norbury C, Blow J, Nurse P. Regulatory phosphorylation of the p34cdc2 protein kinase in vertebrates. EMBO J. 1991;10(11):3321.
721. Bartkova J, Rezaei N, Liontos M, Karakaidos P, Kletsas D, Issaeva N, et al. Oncogene-induced senescence is part of the tumorigenesis barrier imposed by DNA damage checkpoints. Nature. 2006;444(7119):633-7.
722. Mazouzi A, Velimezi G, Loizou JI. DNA replication stress: Causes, resolution and disease. Exp Cell Res. 2014;329(1):85-93.
723. Trachootham D, Lu W, Ogasawara MA, Nilsa RD, Huang P. Redox regulation of cell survival. Antioxid Redox Signal. 2008;10(8):1343-74.
724. Guidarelli A, Brambilla L, Cattabeni F, Cantoni O. Pyruvate enhances DNA single-strand break formation while abolishing cytotoxicity in U937 cells exposed to tert-butylhydroperoxide. Biochem Biophys Res Commun. 1996;226(1):70-4.
725. Iliakis G, Wang Y, Guan J, Wang H. DNA damage checkpoint control in cells exposed to ionizing radiation. Oncogene. 2003;22(37):5834-47.
726. Hoeferlin LA, Oleinik NV, Krupenko NI, Krupenko SA. Activation of p21-Dependent G1/G2 Arrest in the Absence of DNA Damage as an Antiapoptotic Response to Metabolic Stress. Genes Cancer. 2011;2(9): 889-99.
727. Benhar M, Engelberg D, Levitzki A. ROS, stress-activated kinases and stress signaling in cancer. EMBO Rep. 2002;3(5):420-5.
728. Martindale JL, Holbrook NJ. Cellular response to oxidative stress: Signaling for suicide and survival. J Cell Physiol. 2002;192(1):1-15.
729. Abal M, Andreu J, Barasoain I. Taxanes: microtubule and centrosome targets, and cell cycle dependent mechanisms of action. Curr Cancer Drug Targets. 2003;3(3):193-203.
730. Moudi M, Go R, Yien CYS, Nazre M. Vinca Alkaloids. Int J Prev Med. 2013;4(11):1231-5.
731. Chan KS, Koh CG, Li HY. Mitosis-targeted anti-cancer therapies: where they stand. Cell Death Dis. 2012; 3(10):e411.
732. Dong Y, Undyala VVR, Przyklenk K. Inhibition of mitochondrial fission as a molecular target for cardioprotection: critical importance of the timing of treatment. Basic Res Cardiol. 2016;111(5):1-17.
733. Sugimoto K, Toyoshima H, Sakai R, Miyagawa K, Hagiwara K, Ishikawa F, et al. Frequent mutations in the p53 gene in human myeloid leukemia cell lines. Blood. 1992;79(9):2378-83.
734. Zhang L, Zhang J, Hu C, Cao J, Zhou X, Hu Y, et al. Efficient activation of p53 pathway in A549 cells exposed to L2, a novel compound targeting p53-MDM2 interaction. Anticancer Drugs. 2009;20(6):416-24.
735. Mattes MJ. Apoptosis assays with lymphoma cell lines: problems and pitfalls. Br J Cancer. 2007;96(6): 928-36.
736. Balcer-Kubiczek EK. Apoptosis in radiation therapy: a double-edged sword. Exp Oncol. 2012;34(3):277-85.

737. Suetens A, Konings K, Moreels M, Quintens R, Verslegers M, Soors E, et al. Higher initial dna damage and persistent cell cycle arrest after carbon ion irradiation compared to x-irradiation in prostate and colon cancer cells. Front Oncol. 2016;6:87.
738. Xu B, Kim ST, Lim DS, Kastan MB. Two molecularly distinct G2/M checkpoints are induced by ionizing irradiation. Mol Cell Biol. 2002;22(4):1049-59.
739. Brian Dalton W, Nandan MO, Moore RT, Yang VW. Human cancer cells commonly acquire dna damage during mitotic arrest. Cancer Res. 2007;67(24):11487-92.
740. Hayashi MT, Cesare AJ, Fitzpatrick JA, Lazzerini-Denchi E, Karlseder J. A telomere-dependent DNA damage checkpoint induced by prolonged mitotic arrest. Nat Struct Mol Biol. 2012;19(4):387-94.
741. Hagting A, Den Elzen N, Vodermaier HC, Waizenegger IC, Peters J-M, Pines J. Human securin proteolysis is controlled by the spindle checkpoint and reveals when the APC/C switches from activation by Cdc20 to Cdh1. J Cell Biol. 2002;157(7):1125-37.
742. Hayashi MT, Karlseder J. DNA damage associated with mitosis and cytokinesis failure. Oncogene. 2013; 32(39):4593-601.
743. Colin DJ, Hain KO, Allan LA, Clarke PR. Cellular responses to a prolonged delay in mitosis are determined by a DNA damage response controlled by Bcl-2 family proteins. Open Biol. 2015;5(3):140156.
744. Agarwal ML, Agarwal A, Taylor WR, Stark GR. p53 controls both the G2/M and the G1 cell cycle checkpoints and mediates reversible growth arrest in human fibroblasts. Proc Natl Acad Sci U S A. 1995; 92(18):8493-7.
745. Lyamzaev KG, Nepryakhina OK, Saprunova VB, Bakeeva LE, Pletjushkina OY, Chernyak BV, et al. Novel mechanism of elimination of malfunctioning mitochondria (mitoptosis): formation of mitoptotic bodies and extrusion of mitochondrial material from the cell. Biochim Biophys Acta. 2008;1777(7-8):817-25.
746. McLelland GL, Soubannier V, Chen CX, McBride HM, Fon EA. Parkin and PINK1 function in a vesicular trafficking pathway regulating mitochondrial quality control. EMBO J. 2014;33(4):282-95.